University of Strathclyde
Department of
Electronic and Electrical Engineering

Stability and Control of Network with High Penetration of Small Scale Embedded Generation

Adel Hamad Rafa
B.Sc., MSc

A thesis presented in fulfilment of the requirements for the degree of
Doctor of Philosophy

April 2010

Copyright statement

Dedication

To my mother and my wife and my children Ahmed, Thuraya, Rima, Khalid, Doaa and Shiamaa

Acknowledgements

First I would like to express my sincere appreciation to my supervisor, Dr Olimpo Anaya-Lara, for his invaluable guidance, help, encouragement and patience throughout my research so far.

Thanks are also due to all research students in the Institute for Energy and Environment, for their helpful advice and discussions.

Finally, I would like to give my special thanks to my dear family members, who provide unceasing understanding, support and encouragement.

Abstract

Small scale embedded generation (SSEG) connected to low voltage (LV) distribution networks offer the potential to make major contributions to energy security and reductions in carbon emissions. SSEG technologies include non-renewable ones such as internal combustion engines, micro turbines, fuel cells and Stirling engines, but also renewables, such as small-scale wind turbines and photovoltaic arrays. If managed properly SSEG can benefit utility companies. These benefits can be realised by improving network efficiency and reliability, but also by gaining an increased understanding of the economies involved and opportunities for reductions in environmental costs. However there are issues and challenges associated with the interconnection between SSEG and the LV distribution networks; these should be carefully examined before incorporating SSEG in the power system. The issues of interconnection include: voltage and frequency control; increase in network fault levels; stability of the network; protection methodologies and power quality.

This work focuses on exploring the stability and control of the network with many small scale embedded generators (SSEGs) attached during steady state and disturbance situations. SSEG should be able to deliver a pre-set amount of real and reactive power to the grid, or be able to follow a time varying load profile. Therefore, proper controllers need to be designed for SSEG to enhance performance characteristics.

Control schemes for SSEG are proposed to enable proper system operation during steady state and disturbance situations, whilst maintaining system voltage and frequency within appropriate limits. A robust control method within a multi small scale embedded generation networks (SSEG networks) has been implemented to ensure fault ride through of distribution network. A centralized controller for the system with multi SSEG networks during grid and islanded modes has been applied and a primary frequency controller has been designed to contribute to power system frequency regulation.

Table of Contents

List of Tables

List of Figures

Abbreviations and nomenclature

List of Abbreviations

AC	Alternating Current
A_r	Sinusoidal reference signal
Ac	Amplitude of the Carrier triangle wave
CCT	Critical Clearance Time
CERTS	Consortium for Electric Reliability Technology Solutions
DC	Direct Current
DGSEE	The centre for Distributed Generation and Sustainable Electrical Energy
DG	Distributed Generation
DFIG	doubly fed induction generator
DNO	Distribution Network Operator
DTI	Department for Trade and Industry
DVR	Dynamic Voltage Restorer
EQSR	Electricity Quality of Supply Regulations
EPRSC	Engineering and Physical Sciences Research Council
EU	the European Union
FACTS	flexible ac transmission system
FCL	fault current limiter
HTS	high temperature superconducting
HDPS	Highly Distributed Power Systems
HP	Horse Power (746W)
HV	High Voltage
I	Current
ICE	Internal Combustion Engine
IEEE	Institute of Electrical and Electronic Engineers.
IGBT	Isolated-Gate Bipolar Transistor
k	Kilo
LV	Low Voltage

M	Mega
Micro CHP	Micro Combined Heat and Power
MS	Micro source
MT	Micro turbine
MVAr.	Mega Volt-Ampere Reactive
NEDO	New Energy and Industrial Technology Development Organization
NTUA	the National Technical University of Athens
PLL	Phase Locked Loop
PI	Proportional integral
PQ	active and reactive power controller
PSCAD	Power System Computer-Aided Design
pu	Per Unit
PV	Photovoltaic
P-V	active power-voltage controller
P	active power
PWM	Pulse-Width Modulation
Q	Reactive power
R	Resistance
RMS	Root Mean Square
RMU	Ring Main Unit
ROCOF,	Rate of change of frequency
SSEG	Small Scale Embedded Generation
SSEGs	Small scale embedded generators
SSEG network	Small scale embedded generation network
SSWT	Small Scale Wind Turbine
SSC	Static series compensator
STATCOM	STATic synchronous COMpensator
V	Voltage
VAR	Volt-Ampere Reactive
VSI	Voltage Source Inverter
UK	United Kingdom

UPFC	Unified power-flow controller
USSC	Unified series-shunt compensator
X	Interconnecting reactance
W	Watt

List of symbols

CMC	Central Management Controller
CESC	Central energy storage devices controller
EMAX	Maximum Field Voltage [pu]
EMIN	Minimum Field Voltage [pu]
E_{system}	the total stored energy of all generators and loads [MW.s].
f_{error}	the frequency error [Hz]
f_{gt}	measured grid frequency
f_{meas}	measured frequency
f_{mg}	measured SSEG networks frequency[Hz],
f_0	The steady state system frequency [Hz]
GPO	Real Power (MW.)
CLE	The length of the branch in kilometres.
CR1	Positive and Negative Sequence Resistance
CX1	Positive and Negative Sequence Reactance
CB1	Positive and Negative Sequence Susceptance
CR0	Zero Sequence Resistance
CX0	Zero Sequence Reactance
CB0	Zero Sequence Susceptance
GX0	Zero Sequence Reactance
GPX	Maximum Real Power
GPN	Minimum Real Power
GQA	Reactive Power (MVAr)
GQX	Maximum Reactive Power
GQN	Minimum Reactive Power GMB= Generator MVA Base
$H_{system,}$	inertia constant of all generators and loads in the system
K	Exciter Gain [pu]
K_p	Proportional gain of PI controller
K_{iA}	Integral gain
$K_{p\beta}$	proportional gain of PI controller

LOMDC	Loss of main detection controller
I_0	Inverter output current
I_s	average DC current
I_{se}	series current
M_a	Modulation index
M_f	Frequency Modulation index
MGCC	Micro grid Central Controller
mi	modulation index
Ph_{error}	The phase angle difference between grid and SSEG networks voltages
P_{av}	the average value of total actual generation of SSEG units
P_{dif}	the power that can be provided by SSEG units when under frequency occurs
P_g	main grid active power flow;
$P_{i\text{-}rat}$	rated power of SSEG unit (i) in [MW]
$P_{i\text{-}ac}$	actual power of SSEG unit (i) in [MW]
$P_{i\text{-}pu}$	Rated power of SSEG (i) in [pu] based on the rating of the unit.
P_{ir-par}	the participation of SSEG unit i at rated power based on total rated power generation of all SSEGs
P_{SN}	the total active power flow from the SSEG networks to the main grid
P_{se}	actual active power control for series inverter
P_{sh}	actual active power control for shunt inverter
P_{sh-ref}	active power control reference signal for shunt inverter
P_{sh}	shunt inverter output active power ,
P_{se}	series inverter output active power ,
P_{se}	active power before the series inverter,
P_{TEG}	total rated power of all SSEGs units in [MW].
Q	Servo gain [pu]
Q_{sh-ref}	reactive power control reference signal for shunt inverter

Q_{SN-g}	the reactive power flow between SSEG networks and the grid
SC	Synchronization controller
S_{se}	The complex power injection of the series inverter
SV	apparent power-voltage
Tm0	Mechanical torque from the machine [pu]
Tm	Mechanical torque output [pu].
T_p	Pilot valve and servo motor time constant [s]
T_R	Reset or Dashpot Time Constant [s]
T_1	Rectifier Smoothing Time Constant[s]
T_A	Controller Lead Time Constant[s]
T_B	Controller Lag Time Constant[s]
T_E	Exciter Time Constant [s]
V_1	inverter AC voltage
V_0	11 KV grid bus voltage
Vc	Carrier triangle wave
VF	voltage and frequency controller
V_g	RMS measured 33 KV grid voltage [kV],
V_{SN}	RMS measured SSEG networks voltage [kV]
V_{error}	the difference between grid and SSEG networks RMS voltages
VF	voltage and frequency control
Vp	positive sequence
Vn	negative sequence
V0	zero sequence
V_s	DC voltage
V_{sag}	the magnitude of voltage sag
Vse	series voltage magnitude inserted by SSES
V_{sh}	shunt voltage magnitude
X_{se}:	series injected reactance
w	Machine rotor speed [rad/s].
$\tau_{i\beta}$	integral time constant of PI controller
τ_{iA}	integral time constant of PI controller

$K_{i\beta}$	is the integral gain
θ_{se}	series voltage angle
θ_{sh}	shunt voltage angle
δ_p	The phase angle difference between V_0. and V_1
ϕ	phase angle between $.V_0$ and I_0
β	power angle of the SSEG networks bus voltage V_{mg} ;

CHAPTER 1

Introduction

1.1 Background

Rising public awareness for environmental protection and our continuously increasing energy consumption has created a greater interest in distributed generation (DG) systems connected directly to the distribution network rather than through the high voltage transmission network. Small scale embedded generation (SSEG) follows the concept of DG but is typically at the point of use and is of smaller generation capacity. This effectively eliminates the need to transport electricity from the supplier to the customer. Additionally SSEG may refer to small-scale installations that generate heat or electricity or both in the case of Micro Combined Heat and Power systems. The introduction of SSEGs in power system results in changes in operation of the electrical power system. These changes are mainly caused by the differences in location and operation principles compared to conventional generators and loads. The most important differences are:

- Connection of SSEGs to the distribution network introduces generators to the distribution network, which historically only contained loads.
- Many SSEG technologies do not use a conventional grid coupled synchronous generators to convert primary energy into electricity. Instead SSEG technologies tend to generate DC or high frequency AC power for output. This power can then be grid-connected through the use of power electronic converters [1]. The power electronic converters behave in a fundamentally different manner from that of conventional synchronous machine based generators.
- Several types of SSEG such as photovoltaic (PV) and wind are based on uncontrollable energy sources (sun and wind).

- Most SSEG units behave as 'negative loads' and do not participate in the conventional control of the network [2].

1.2 Problem Definition

Before introducing SSEGs in large quantities there are a number of issues related to their connection to the distribution network that need to be resolve. These issues include stability, voltage and frequency control, maintaining power quality, protection, reliability and safety. The problems investigated in this thesis are described below, and suitable control strategies were designed to handle them and to improve the dynamic performance of the network:

Transient behaviour – transient behaviour concerns the response of the SSEGs to network disturbances such as voltage dips and short-circuits [3]. The SSEGs can be based on synchronous generators, induction generators and power electronic interfaced SSEGs, all of which have different responses to fault disturbances.

Fault-ride through - There are two meaning of fault ride-through. The first one is for short circuit faults of up to 140ms in duration. In this case, each generating unit shall remain transiently stable and connected to the system without tripping for a close-up solid three-phase short circuit fault or any unbalanced short circuit fault on the GB transmission system operating at supergrid voltages. The second meaning is for voltage dips greater than 140ms in duration. In this case, each generating unit remains transiently stable and connected to the system without tripping of any generating unit for balanced supergrid voltage dips [4]. Most distribution network operators (DNOs) require that SSEGs are disconnected from the grid during fault conditions. Disconnection may become undesirable, however, when the penetration level of SSEGs in a network is significant, as it can result in a large unbalance between load and generation.

Islanded operation mode – Safe and stable operation of SSEGs in islanded mode under fault conditions could offer significant benefits in improving the security of supply to customers [5].

Voltage control – The objective of voltage control is to maintain the RMS value of the voltage within specified limits. The introduction of SSEGs in the distribution network changes the power flow in part of the network. As a result the changing in magnitude and direction of the power will change system voltages[6].

Voltage sags - Faults that occur in the main grid may lead to reduction in the RMS voltage magnitude of the scale embedded generation networks (SSEG networks). As result the SSEG networks may lose their stability depending on the severity of the voltage sag [7].

Voltage unbalance- As most of the SSEGs are single-phase sources adding generation to just one phase gives unbalanced voltages. This unbalance has a negative impact on the quality of the power supplied to the load as well as on the performance of the rotating machines [8].

Frequency control – The function of the frequency control is to maintain the balance between generation and demand as well as the synchronism between the synchronous generators in the system [3]. When an unbalance occurs between generation and demand, the system inertia would limit the rate of change of frequency. Therefore the inertia of the generators plays an important role in maintaining the stability of the power system during a transient (e.g. during and after a disturbance). With an increasing level of the SSEG penetration, the power system inertia would decrease [9].This is due to the power electronic interfaces between SSEGs and the grid which leads to the loss of direct relationship between power and frequency [1] .As a result, maintaining system stability can become increasingly difficult and disturbances might result in larger frequency deviations.

1.3 Research Motivation

The presence of SSEGs connected to the power distribution network is rapidly increasing. Scenarios developed by the EPSRC Supergen III Consortia [10] estimate that by the year 2020, SSEGs will produce about 6GW of online generation in the UK. As a result in the last few years, investments in SSEGs manufacturing and research into SSEGs integration with the distribution network has increased exponentially.

Currently there are many problems with integrating SSEGs into power distribution networks. These problems mainly arise from the design of the power distribution network; where during its design it was assumed that only loads, and not generators, would be connected to it. In addition to this: the power sources for SSEGs, such as solar and wind, are not consistent and therefore not guaranteed to realise their full benefit. The introduction of high penetration levels of SSEGs can also have adverse impacts on the utilities, especially on distribution system operation schemes. In addition, distribution network operators refer to Engineering Recommendations; these define industry-wide technical standards relating to the connection of embedded generators. In accordance with these recommendations operators disconnect the SSEGs from the network during fault conditions: if a loss-of-mains is detected, or the voltage, or frequency deviates outside set limits. Solving these identified problems is essential for seamlessly integrating SSEGs into the distribution networks. The motivation of this research lies in the following points:

- The introduction of SSEGs into the power system benefits not only the power companies and the customers, but also the whole society. However, before introducing SSEGs in large quantities a number of issues should be resolved in terms of connection to the distribution network, power quality, stability, voltage and frequency control, protection, reliability and safety.

- To develop a better understanding of the impact of the SSEGs on the voltage regulation, stability, frequency regulation, power quality and protection of distribution networks.

- To investigate the dynamic behaviour of different types of SSEGs (induction generator, synchronous generator and power electronic converter based SSEG). This is important since the design of control systems requires an understanding of how the different SSEGs technologies behave.

- To permit the stable operation of a network with many SSEGs attached during steady state and disturbance situations. The main challenge related to the integration of SSEGs is to do with their control.

- To permit the stable operation of SSEGs networks during islanded mode. In islanded mode how the voltage and frequency can be maintained using suitable control schemes.

- To design and develop frequency control, voltage control and fault-ride-through techniques that can address some of the challenges related to SSEGs integration with the distribution networks

1.4 Objectives of the Research

Most of the problems discussed in the problem definition section occur in the medium and low voltage networks, where generally no control is available. Therefore the general objectives can be summarised as follows:

(1) Exploring and identifying the main issues associated with the stability and control of distribution networks with a high penetration of SSEGs.

(2) Modelling the components of SSEGs and their corresponding control schemes to provide dynamic voltage and frequency control.

(3) Implementing a robust control scheme to ensure fault ride-through of a system with high penetration of SSEGs.

(4) Designing a centralized controller for an operating system with multi SSEG networks during grid and islanded modes.

(5) Designing a load–frequency controller for a system with large number of SSEGs.

(6) Assessing the dynamic performance characteristics of the proposed controllers in a network during steady state, small system disturbances and network faults.

(7) Demonstrating the performance of the controllers with case study simulations conducted in PSCAD/EMTDC [11].

1.5 Research Questions

Based on this objective and the problem definition given above, this research aims at answering the following questions:

- What are the main issues that can limit the installed capacity of SSEGs in a distribution network?
- What is the impact on distribution network stability when the network has a high penetration of SSEGs?
- How can distribution systems consisting of multi SSEG networks be controlled efficiently whilst providing required security levels?
- How can the frequency of the network be regulated by SSEGs?
- How can the fault ride through of a system with high penetration of SSEGs be guaranteed?

1.6 Research Contributions

The original contributions of this research can be summarised as:

- ❖ The development of enhanced controllers to facilitate the large–scale integration of SSEGs.
- ❖ The design of flexible controllers of converter-interfaced SSEG that

facilitate independent control of each phase in a three-phase converter addressing voltage rise and imbalance issues.

- ❖ The design of a control system that allows SSEGs to participate in the frequency stability of the distribution network.
- ❖ The design of a control system that ensures fault ride through for a system with a high penetration of SSEGs.
- ❖ A thorough evaluation of the dynamic performance characteristic of various control strategies aimed to improve the stability and security levels of LV network with SSEGs.

1.7 Software Evaluation

Power Systems Computer Aided Design (PSCAD) is a power system simulator and was the software chosen for the power system studies. PSCAD was first developed in 1988 by the Manitoba HVDC Research Centre and is a graphical front end to EMTDC [11]. In PSCAD, models of power networks can be created by connecting blocks, which represent items of plant. These models can then be executed, and results of the simulations analysed. The blocks are implemented in FORTRAN, and call an EMTDC code library to combine into executable files. Executing these files runs the simulations, and the results can be picked up by PSCAD during runtime. PSCAD is suitable for SSEG integration studies for several reasons:

- PSCAD has fully developed models of various devices used in the SSEG studies. The code library includes models of conventional synchronous, permanent magnet and induction machines, transformers, three-phase converters, turbine models including wind turbines, steam turbine and governor, relays, breakers, cables, and transmission lines.
- PSCAD offers tools to simulate various faults on the power system.
- The PSCAD code library provides a complete set of basic linear and nonlinear control components. These components can then be combined into larger, more elaborate systems. Outputs from these control components can

be used to control voltage and current sources, switching signals, and firing pulses for thyristors, gate turn-off thyristors, and insulated gate bipolar transistors (IGBTs). The control components can also be used for signal analysis, and the outputs may be directed to online plots or meters.

- PSCAD has an inbuilt model for a six-pulse SCR converter. Converter models with other switching devices and firing circuits can be built using the control systems modelling function library.
- Devices not available in PSCAD, such as models of micro turbines, fuel cells or pulse-width modulated inverters, can be written by the user in FORTRAN, C or C++.
- The graphing, plotting, and exporting of results is easy.

For the above reasons PSCAD is suitable software to use for the required power system studies as it has the tools to model the power systems and implement the proposed control algorithms.

1.8 List of Publications

During this research the following publications and reports were generated:

1. Adel H Rafa O Anaya-Lara, J R McDonald, "Stability Assessment of Micro generation Systems", paper presented at the RVP07 IEEE Conference, 8-14 July 2007, México.
2. R. Tumilty, Adel. H Rafa, A. Emhemed, O. Anaya-Lara, G.M. Burt, DTI/UGEN/TR/2007-001 "Micro generation Transient Stability Investigation Report". July 2007.
3. Adel H Rafa, O Anaya-Lara, J R McDonald," Stability Assessment of Induction Generator-Based Micro generation", paper presented at PEMD 2008, 2 April 2008, York, UK.
4. Adel H Rafa, O Anaya-Lara, J R McDonald, " Flexible Control of Converter-Interfaced Micro generation", paper presented at 2008 PES General Meeting,

20 - 24 July 2008,Pittsburgh, PA USA

5. Adel H Rafa, O Anaya-Lara, J R McDonald, "Power Factor Control for Inverter-Interfaced Micro generation", paper presented at UPEC 2008 43rd International Conference, 1-4 September, 2008. University of Padova, Italy
6. Adel H Rafa, O Anaya-Lara, J R McDonald, " Voltage Regulation of Small-Scale Distributed Generation through Voltage-Phase Angle Droop", IET Renewable Power Generation (Under review).
7. Adel H Rafa, O Anaya-Lara, J R McDonald, "Centralised Controller for Grid Connected and Islanded Small Scale Embedded Generation Networks", IEEE Transactions on Power Delivery (Under review).
8. Adel H Rafa, O Anaya-Lara, J R McDonald," Fault Ride-Through of Systems with High Penetration of Small-Scale Embedded Generation", Electric Power Systems Research (Under review).
9. Adel H Rafa, O Anaya-Lara, J R McDonald," Small-Scale Distributed Generation Contribution to the Primary frequency control", Journal of Renewable and Sustainable Energy (Under review).

1.9 Thesis Organization

The work carried out in this thesis has been organized in eight chapters. The present chapter provides a brief introduction to SSEG. It presents the motivation behind this work, the main research questions and the contributions made.

Chapter 2 introduces a literature review on SSEG technologies, benefits of using SSEGs, the technical impact of SSEGs on the distribution network and issues that can limit installation capacity of SSEGs in distribution networks. This information can be helpful to understand the remaining part of the thesis.

Chapter 3 investigates the transient behaviour of SSEG based on synchronous generators, SSEG based on induction generators and SSEG based power electronic inverters. The response of these different technologies to symmetrical and unsymmetrical faults has been investigated in this chapter. Also the impact of

reconnection of a large number of SSEGs on MV distribution network has been investigated. The comparison between simulation results and a theoretical analysis for the calculation of critical clearing time of the generators is also done.

Chapter 4 presents different control schemes that are applied to SSEG based on power electronic converter during different operating conditions: when the SSEG is isolated from the grid, and when the SSEG is connected to the grid. These control schemes are: active and reactive power control (PQ), voltage and frequency (VF) control, DC current control, power factor control, voltage/phase angle droop control, active power-voltage (PV) controller and apparent power-voltage (SV) controller. The test results to show the effectiveness of the controller.

Chapter 5 proposes a central storage device combined with a central controller located on the bus between the SSEG networks and the main grid. The central storage device compensates the difference between the generation and the load demand during islanded mode. The central controller coordinates between the central storage device, multi SSEG networks and the main grid. The presented control system maintains the voltage and frequency of the SSEG networks within acceptable operating limits when the SSEG networks are islanded, and synchronises them before connection with the distribution network.

Chapter 6 proposes a fault ride-through technique that prevents the flow of large fault currents and maintains the terminal voltages of networks with SSEGs during voltage sags or network disturbances within appropriate limits. This technique employs a unified series-shunt compensator (USSC) connected between networks with SSEGs and the utility grid. The test results to show the effectiveness of the controller for fault ride-through and improving the voltage quality have been presented in this chapter.

Chapter 7 investigates how the mix of types of SSEG networks can contribute to frequency control. It starts with testing the response of MV network with and without SSEG networks to load unbalances and frequency deviations. It then designs and

implements a control technique for load-frequency control for a system with a high penetration of SSEGs. The impact of SSEGs with load and frequency control on frequency stability is studied with the following different SSEG technologies: photovoltaic, reciprocating engine driven synchronous generator, stirling engine driven induction generator, small wind turbine driven induction generator, microCHP connected to permanent magnet synchronous generator. Case studies to show that system frequency control is possible with the proposed load-frequency control for the SSEG networks are presented.

In chapter 8 conclusions derived from the work are presented and possible future work outlined.

CHAPTER 2

Literature Review

2.1 Introduction

This chapter presents a literature review on various issues associated with the integration of small scale embedded generation (SSEG) in low-voltage distribution networks. The last decade showed a large increase in the literature on distributed generation, but only the publications that treat the electrical aspects of DG units and their interaction with the grid are included in this work. In this chapter a more general overview is presented. Later, in each chapter, more specific literature related to the respective chapter topic is discussed.

2.2 Micro grid (MG)

A micro grid is a cluster of interconnected micro sources (micro turbines, fuel cells, PV, diesel, etc.), loads and intermediate energy storage devices (flywheel, batteries, super capacitor, etc.), that is formed to provide reliable electricity and heat within a small area. Generally, this combination of devices is connected to the distribution network through a single Point of Common Coupling (PCC) and appears to the grid as a single controllable unit (load & source) [1]**.** Most of the micro source and micro storage equipment is connected through power electronic devices providing the required flexibility to ensure controlled operation as a single aggregated system [12,13]**.** The main objective of its conception is to facilitate the high penetration of SSEGs without requiring re-design of the distribution system and causing power system stability and power quality problems to the distribution network [14, 15]. The micro grid could be operated, either interconnected to the main grid or either isolated from it, by means of a local management system with a communication infrastructure allowing control actions to be taken following any given strategy and objective [16]**.** Figure 2.1 shows a micro grid architecture. Micro grids can be considered as a network architecture which supports the realisation of a Smart Grid – a concept

which was conceived in 2005 to enable the delivery of energy in a manner fit for the 21st century [15].

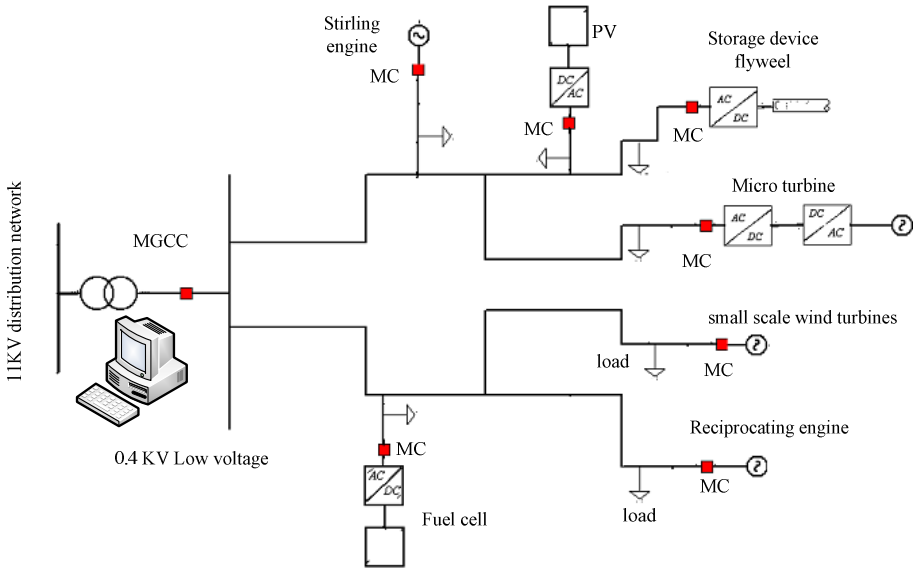

Figure 2.1: Micro grid architecture [1]

2.2.1 Micro grid Research Projects

Micro grids have been studied in several research projects, especially in Europe, the United State of America, Japan and Canada [17]. In the European Union (EU), two Micro grid projects were started, namely Micro grids: Large Scale Integration of Micro-Generation to Low Voltage Grids (1998–2002) and More Micro grids (2002–2006). The projects were led by the National Technical University of Athens (NTUA) together with research institutions and universities. EU demonstration sites are taking place in Greece, Netherlands, Germany, Denmark and Spain[17]. In the USA, the R&D activities on the micro grids research programme were supported both by the US Department of Energy & the Californian Energy Commission. The most well-known US micro grid R&D effort has been pursued under the Consortium for Electric Reliability Technology Solutions (CERTS) which was established in 1999 [18]. In Japan the NEDO (New Energy and Industrial Technology Development Organization) started three research projects, which deal with new energy integration to local power system field test in 2004 and also in 2008. The Japanese started a new research framework called TIPS {Triple I *(Intelligent,*

Interactive and Integrated) Power Systems} that focuses on large penetration of DG using renewable energy sources [19]. In Canada the micro grid R&D activities focused on medium voltage networks and are mostly carried out in collaboration with the electric utility industry, manufacturers and other stakeholders in distributed energy resources integration and utilization [20].

2.3 Highly Distributed Power Systems

The Highly Distributed Power Systems (HDPS) concept is based around the future vision that large numbers of small scale embedded generators (SSEGs), many (perhaps mostly) independently owned and operated, are connected across all voltage levels within the distribution network [21].

There are currently (2010) over 100,000 SSEG installations in the UK – generating heat and/or electricity [22]. However, this is set to increase with the backing of supportive governmental policies expected over the coming decade. A number of scenarios have recently been created by academic consortia, government agencies and trade associations to give an estimate for future capacity by considering the range of externalities that may impact on the electricity supply industry in the UK (examples include [10, 22,23]) As an illustration, the four scenarios developed jointly by the EPSRC Supergen III consortia [23] provide a projection of 6GW of SSEG by 2020 within their 'Environmental Awakening' scenario. Given the support for these technologies within the 2007 UK government energy white paper [24] and the wider scenario-based projections, the issue of SSEG is expected to be of growing interest within the industry as generation technologies mature and become more affordable. The HDPS concept can be summarised by the statement "many loads – many sources", in contrast to the traditional "many loads – few sources".

2.4 SSEG Technologies

SSEGs are currently based on several different technologies: reciprocating engines, Stirling engines, micro gas turbines, steam engines (Organic Rankine Cycle – ORC) and fuel cells.

2.4.1 Reciprocating Engines

Reciprocating engines are conventional internal combustion engines coupled with a generator and heat exchangers to recover the heat from the exhaust gas and the cooling cycle. Figure 2.2 shows the operation process of reciprocating engines that begins with fuel/air mixture is introduced into the combustion cylinder, and then compressed while the piston moves toward the top of the cylinder [25]. The heat from the engine exhaust, cooling water and oil jackets is used for respective heat demand. For micro combined heat and power (Micro CHP) applications, reciprocating engines offer low costs and good efficiency. However maintenance requirements are high and diesel-fuelled units have high emissions. Micro CHP products based on reciprocating engines are commercially available and are produced in large numbers by a variety of companies worldwide. The market leader is the Germany based company Senertec (The Senertec model – called Dachs – generates around 5.5 kWel and a thermal power of 14 kW). Other companies offering micro CHP products based on reciprocating engines include Power Plus, Spilling Energie Systeme, Buderus, Oberdorfer and GE Jenbacher. Other companies from the Asian region offering micro CHP products are Honda (1 kWel system – named Ecowill), Yanmar, Aisin and Sanyo. From the United States Victor Cogen is also developing a micro CHP system [26].

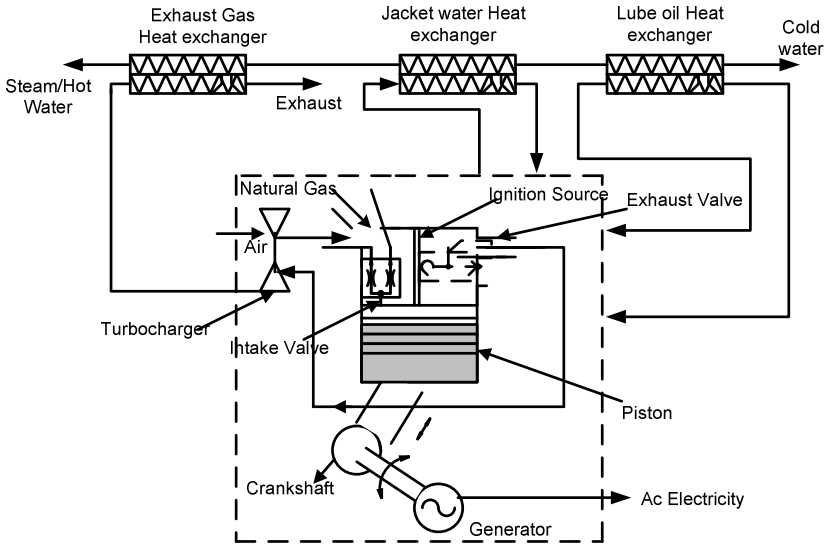

Figure 2.2: Process of Reciprocating Engines [25].

2.4.2 Stirling Engines

Stirling engines are closed-cycle engines characterized by an external heat supply that allows the use of any heat source operating at a sufficient temperature level. As shown in Figure 2.3 stirling engine is external combustion engine which, operates without a valve gear, an ignition system and no air or fuel is taken into or out of the cylinder from the atmosphere [27]. These allow continuous, controlled combustion resulting in very low pollutant emissions, long service intervals, low running costs and high combustion efficiency. The widely known companies that produce micro CHP products, based on stirling engines, are WhisperTech (New Zealand) and Solo (Germany). The New Zealand-based company WhisperTech is developing a Stirling engine called WhisperGen, with a capacity of up to 1.2 kW electric power and 8 kW_{th} of heat. Other companies developing micro CHP systems based on stirling engines are: MicroGen (UK), Sun Machine (Germany), EnAtEC micro-cogen B.V. (Netherlands), Stirling Systems (CH) [26].

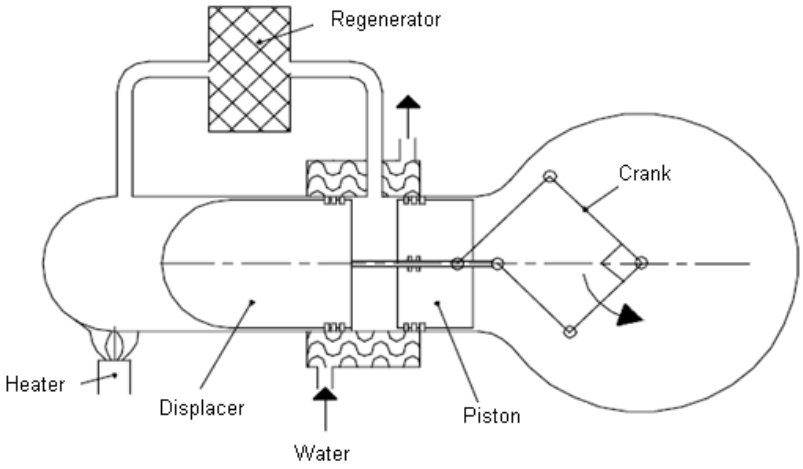

Figure 2.3: Example of a Stirling Engine [27].

2.4.3 Organic Rankine Cycle–ORC

The steam engine technology that is used in a MicroCHP system is the Organic Rankine Cycle (ORC). As shown in Figure 2.4 the operation of the ORC unit is similar to close cycle of a conventional steam turbine, except for the fluid that drives the turbine, which is a high molecular mass organic fluid [28]. The high molecular

mass organic fluid drives the turbine instead of water that allows for exploiting efficiently low temperature heat sources to produce electricity in a wide range of power outputs (from a few kW_{el} up to 3 MW_{el} per unit). Also, the ORC system has many advantages, such as high-cycle efficiency, simple start-stop procedures, low speed (which allows the direct-drive operation of the electric generator without reduction gearbox), quiet operation, minimum maintenance requirements and good part-load performance. The European market leader in ORC product development is the Italian company Turboden, which has developed a standard range of turbo generators using silicone oil as the working fluid. The biomass fuelled ORC systems have been mainly applied in the wood processing industry and in local district heating systems [26].

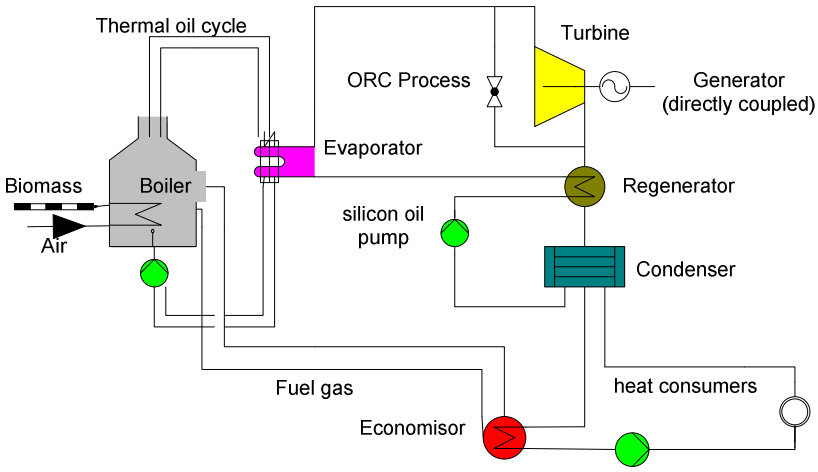

Figure 2.4: Working principle of a biomass-fired ORC process [28].

2.4.4 Micro Turbines

Micro turbines are the newest type of combustion turbine (small gas turbines), with outputs ranging between 25-500 kW, which are used in Micro CHP systems. As shown in Figure 2.5 a simple micro turbine consists of a compressor, combustor, turbine, and generator. Compressed air is mixed with fuel and burned in a combustor under constant pressure [26]. Then the resulting hot gas expands through a turbine

that turns connected generator to producing electricity. Microturbines have many advantages, such as their small number of moving parts, compact size, lightweight, low emissions, low electricity costs and they have the ability to use waste fuels. Moreover they can be located on sites with space limitations for the production of power. On the other hand micro turbines are still more expensive than internal combustion engines; because of the few moving parts of the device, lower operation and maintenance costs are possible to be compared to combustion engines. There are many manufacturers, which have made commitments to enter the micro turbine market. For example in the USA Honeywell, (AlliedSignal), Capstone and Elliott, in Europe, Volvo and ABB, in Japan, Toyota is a company that is developing micro turbine products [26].

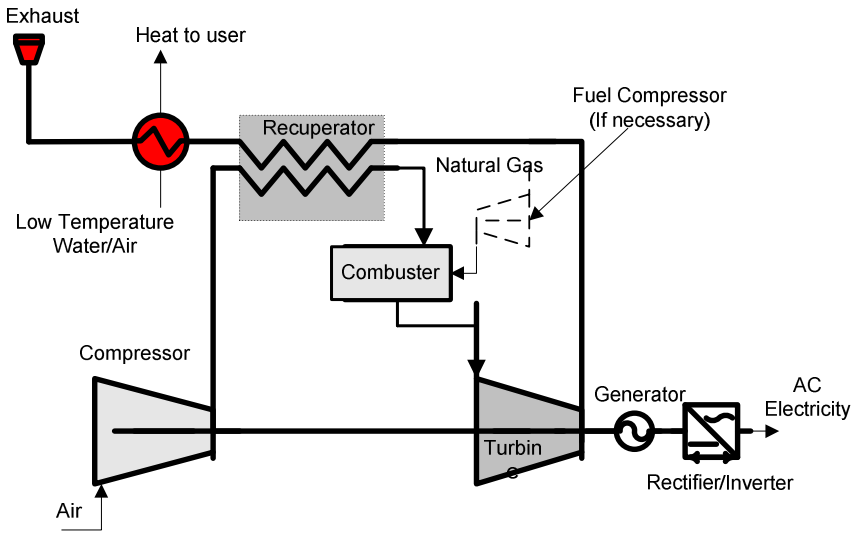

Figure 2.5: Operation Process of Micro turbine [26].

2.4.5 Fuel Cells (FCs)

Fuel cells are similar to batteries. They convert the chemical energy of a fuel into electrical energy without the use of a thermal cycle or rotating equipment. In contrast to most electrical generating devices that are used in MicroCHP systems (e.g. steam and gas turbine cycles and reciprocating engines) FCs first convert chemical energy

into thermal energy and then into mechanical energy before finally generating electricity. Physically a FC plant consists of three parts, as shown in Figure 2.6 a fuel processor, a Power section and a Power conditioner [29]. Compared with conventional power plants, the FCs have many advantages, such as high efficiency, zero or low emission (of pollutant gases) and have a flexible modular structure. Moreover, compared with other green DG technologies such as wind and photovoltaic, FCs have the advantage that they can be placed within any site in a distribution system, without geographic limitations, to provide optimal benefits. Also they show great promise for use as DG sources [29] FC systems are still in the research and development phase. Vaillant are developing a 5 kWel/7 kWth polymer electrolyte fuel cells (PEFC) system and Sulzer Hexis are developing a 1 kWel/3 kWth solid oxide fuel cells (SOFC) system. In the USA, International Fuel Cells/ONSI Company currently manufactures a 200 kW phosphoric acid fuel cell for use in commercial and industrial applications. The products of other companies such as DAIS Analytic, A Vista Corp, Ballard Power Systems, Plug Power and Fuel Cell Energy, are still at the test stage [25].

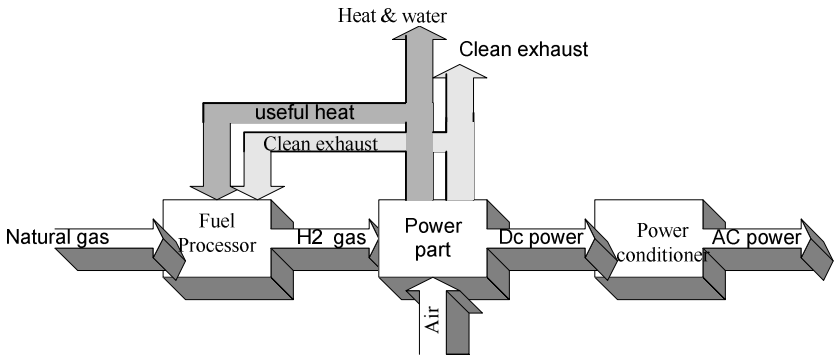

Figure 2.6: Block diagram of a fuel cell plant [29].

2.4.6 Small-Scale Wind Turbines

Wind turbines capture energy from the wind and transform this energy into electrical energy by conventional rotating generators. As shown in,Figure 2.7 the mechanism of power generation by a wind turbine starts with the wind blowing over the blades,

causing the blades to rotate; the rotating blades then keep the shaft turning. The function of the gearbox is to increase the rotational speed of the shaft and to drive the generator to produce electricity [30].

Wind is a highly variable resource that cannot be stored and wind energy conversion systems must be operated accordingly. Individual units can range in size from a few kilowatts to ratings approaching 4MW [31]. Previously the majority of small wind turbines were installed at schools or environment centres with very few domestic systems in existence, especially in urban areas. Installations were dominated by Horizontal Axis Wind Turbines in the 2.5–20 kW range. Products like the Skystream and Iskra are ideal for rural domestic applications, whereas the Gaia and Westwind are more suited to farm and commercial requirements or larger domestic installations with significant energy need [32]. However more recently the small wind turbine industry has started to focus on developing smaller (<1.5 kW) building- integrated wind turbines. In particular there has been a push to develop rooftop installations that are suitable for domestic properties in the urban environment. For example Segen offers a range of tower mounted small wind turbines suitable for rural domestic installations [33, 34].

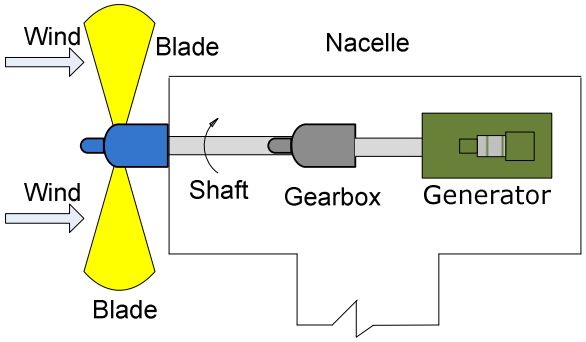

Figure 2.7: Mechanics of electricity generation by wind turbine [30].

2.4.7 Photovoltaic (PVs)

Photovoltaic (PV) technology is one of several promising energy generation technologies. Nowadays PV systems are available from major manufacturers in a number of standard sizes (from 5 W to 300W) of PV panels, and may be stand alone or grid connected. PV systems may be ground or roof mounted, or on the side of a

building. As shown in Figure 2.8 a PV system consists of a PV generator, maximum power point tracker (MPPT), energy storage (for example a battery) and a power conditioning system [35]. A PV generator can contain several PV arrays. Each array is comprised of several modules and each module is built up of several solar cells. Photovoltaic (PV) units, with the help of solar cells, convert the sun light directly into electrical energy. The MPPT is used to assure that the PV Array generates the maximum power for all irradiance and temperature values. The battery bank stores energy when the power supplied by the PV modules exceeds load demand and releases it back to the system when the PV supply is insufficient. The power conditioning system contains a DC to DC converter and DC/AC inverter, isolation transformer and filter. Its function is to provide an interface between all the elements of a PV system and the grid, as well as to protect and control the system [35]. There are many companies that produce, supply and install solar panel systems such as SolarUK Ltd and [36] the Green Electrician Ltd [37].

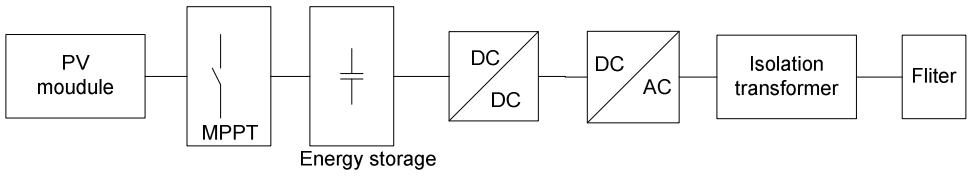

Figure 2.8: PV schematic diagram [35].

2.5 Storage Devices

Energy storage devices are essential for proper micro grids operation [8, 38]. An energy storage device is an inverter interfaced battery bank or flywheel. The storage devices in the micro grid are analogous to the spinning reserve of large generators in the conventional grid. They are needed to overcome differences in demand and generation during islanded mode. Therefore they are used for system stability (voltage and frequency) during post grid disconnection. Another method of integrating energy storage to the micro grid is to install battery banks or super capacitors in the DC links of the inverters of the SSEGs [39]. Papers [40, 41] assume

that an ultra-capacitor is used for energy storage on the DC bus of the inverter interfaced SSEG.

The different storage types that are available are:

- Batteries such as lead acid batteries, a flow battery, lithium ion batteries and metal-air batteries.
- A flywheel is a heavy rotating disk used as a storage device for kinetic energy
- Capacitors used to store electrical energy.

2.6 Communication Facilities

In the case of a micro grid, an advanced communication system is needed [16]**.** The storage devices and SSEGs with islanding detection capability can automatically transfer from grid-connected control mode to islanded control mode and vice versa. However, if the SSEGs rely on the central controller in determining the state of the micro grid, a fast communication line should be installed between the controller and the SSEGs. Moreover during islanded mode the communication between the central controller and loads is required if load shedding is implemented especially when the connected load exceeds the generation capacity or the frequency drops to excessively low levels immediately after grid disconnection. If the communication system is required for control of the micro grids, the delay within communication network should not present problems unless it exceeds the critical clearing time (CCT) of the SSEG which would lead to the instability of the generators. In micro grid applications an adapted communication environment based on internet and XML-RPC has been used in order to allow the micro grid supervisory controller to send control set points to the local generator controllers (Remote Terminal Units) of the different power units [42].

2.7 Benefits of SSEG Applications

The introduction of SSEG into the power system benefits not only the power companies and the customers, but also the whole society [43, 44].

a) Customer Benefits:

- Reduced fuel bills,
- Superior environmental performance and fuel flexibility,
- Offers using of both electricity and heat,
- Provides a stand-alone power option for areas where transmission and distribution infrastructure does not exist or is too expensive to build and
- New opportunities to replace old boilers without finance.

b) Supplier Benefits:

- Voltage support and improved power quality,
- Loss reduction,
- It is environmentally friendly and a fuel flexible system,
- Avoids unnecessary capital expenditure by closely matching capacity increases to growth in demand,
- Avoids major investments in transmission and distribution system upgrades by sitting new generation near the customer and
- Offers a relatively low-cost entry point into a competitive market and opens markets in remote areas without transmission and distribution systems

c) National Benefits:

- Reduces greenhouse gas emissions,
- Contribute to a reduction of the fuel poverty,
- Establishes a new industry to solve unemployment problem,
- Enhances productivity through improved reliability and quality of power delivered and
- Responds to increasing energy demands.

2.8 Technical Impacts of SSEG on the Distribution System

A number of previous studies in the public domain have investigated the technical issues surrounding the connection of a large number of SSEGs in small areas of the electrical network such as a new build housing development. The studies are

extensive in scope and cover issues such as those concerning fault level management voltage regulation, power flow management, protection systems and stability.

2.8.1 Power Flow

Traditionally, the distribution network was designed as a passive network, which delivered power flows from transmission to distribution network [2]. The effect of DG on the distribution network is largely dependent on the power flow into the network [6]. Consider the configuration shown in Figure 2.9 adding DG to distribution network, the power flows are in the reverse direction. Reverse flows of real or reactive power may cause problems for the DNO's voltage control and protection systems as well as metering systems. Transformer tap changers may not be adequately rated to accept significant flows of reverse real power. The voltage control schemes for tap changers may also be affected by the flows of reverse real and reactive power [45]. Installation of active systems in the distribution network requires new procedures and equipments to isolate such issues [46].

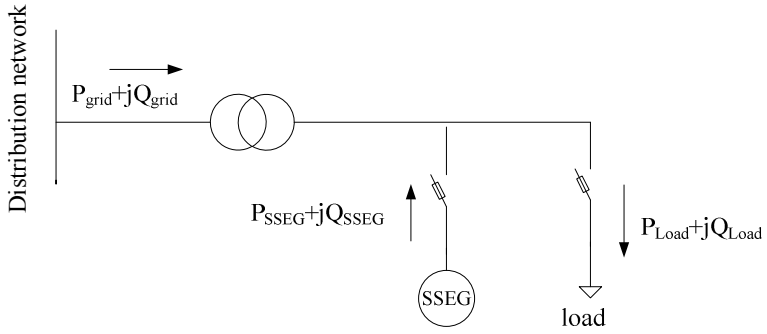

Figure 2.9: SSEG power flow to utility grid.

2.8.2 Voltage and Frequency Control

In the electricity system active and reactive power generated has to be balanced with the power consumed by the loads including the losses in the lines and plant. The unbalance condition happens when power generated is not equal to the power demand [3]. A significant unbalance between generation and load, results in a

deviation of the system frequency from its set point value (50/60Hz) [3]. The SSEGs can either be synchronous, asynchronous machines or inverter connected. When synchronous machines are used the voltage and frequency of the machine can be controlled by automatic voltage regulators (AVR) and speed regulators. However, when induction machines are used, the voltage cannot be controlled. The machine imports reactive power from the network, which depress the network voltage. On the other hand the inverters do not behave as rotational synchronous generators and require different control philosophies [47, 48]. The purpose of voltage and frequency control is to ensure that both voltage and frequency remain within predefined limits around the set point values by adjusting the active and reactive power generated or consumed.

Papers [18, 20, 39, 49-52] mention that the basic issue for micro grids is the technical difficulties related to the control of a significant number of micro sources. The possible control strategies for the micro sources (MS) and the storage devices may be: (a) PQ control (fixed power control) (b) Droop control and (c) Frequency/Voltage control. Papers [53-57] proposed controllers based on droop lines (frequency-active power and voltage-reactive power). These droop controls do not require any communication at all between the converters. Another method is the master/slave method, which strongly relies on fast communication between the micro sources and the micro grid central controller MGCC [8, 58]. In this method all micro sources remain in PQ control (slave) while the storage device shifts to droop control or voltage/frequency control (master). Therefore the storage device will control the voltage and frequency of the micro grid [59]. In addition the approach proposed by Lasseter and Piagi [39] is called autonomous control of micro sources. They avoided the installation of MGCC and dedicated storage units, so the micro sources have integrated storage (a battery bank in the dc bus of the inverter).

Frequency control is essential for the secure and stable operation of a power system. System frequency is generally regulated through primary and secondary frequency controls. Primary frequency control (PFC) regulates the system frequency in a dynamic process whereas secondary frequency control (SFC) regulates the frequency

as close as its nominal value by adjusting the loads of units participating in system frequency control [60, 61]. The next paragraphs present the publications that treat frequency stability of the electrical networks with DG connections.

One of the books on DG is [62], which attempts to provide a solid grounding in all significant aspects of wind power integration. It defines the time scales of categories of reserve (primary, secondary, tertiary and replacement). Primary reserve is the most critical and is required in the period immediately following an incident (5-15 sec). Secondary reserve is required to return the system towards 50 Hz (15-90 sec). The role of tertiary and/or replacement is to replace the lost unit, that is, generation outputs should be maintained (minutes to hours) until such time as a replacement plant can be brought online.

Paper [63], mentions that wind farms do not have to participate in network frequency control but in the future they will have to because of the high amount of wind energy integrated in the grid.

Paper [64] examines the impact on frequency control of increasing wind generation on the Ireland electricity system. It concludes that at high levels of wind generation, either the largest in feed needs to be reduced or wind generation needs to be curtailed or wind turbines should be required to provide an inertial response.

Paper [65] describes a control approach applied to doubly fed induction generators (DFIG) to provide a frequency regulation capability. The control approach adopted consists of an additional frequency control loop that is integrated into the rotor-side active power controller of a DFIG. In this control scheme a small de-load regarding the maximum power extraction curve of the wind generator is implemented to allow its participation in frequency control during an eventual decrease of system frequency.

Paper [66] addresses the design and implementation of a control scheme for a doubly fed induction generator (DFIG). This controller provides a DFIG-based wind farm

with operational and control compatibility with conventional power stations, giving the ability to contribute to frequency and voltage support and recovery following network faults as well as to provide a power system stabilizer capability that improves overall system damping.

Paper [67] focuses on the contribution of wind farms to ancillary services and more specifically to frequency regulation. In this paper the frequency droop strategy that is normally applied in classical generation units was applied to wind turbines whilst considering the wind conditions.

In paper [68] the impact of DG on safety of the transmission system is studied in detail with different DG technologies of various penetration levels. This study shows that large penetration of DG has a significant impact on the transient stability of the system. The impact depends on the DG technology used. In most cases, the induction generator has a larger influence compared to that of synchronous machines.

2.8.3 Voltage Regulation

The operation of SSEG results in an increase in LV system voltages. This increase is due to generators, which supply local loads and due to the excess in generators real power output flowing back through a mainly resistive network to the distribution transformer [69]. Large single SSEG units may violate the voltage profile or the constraints of maximum voltage rise even if the aggregated power in the grid is low [6]. The statutory voltage limits are currently (+10%/-6%) for LV-systems (0.4kV) in accordance with the Electrical Safety, Quality and Continuity Regulations 2002 [70]. Studies conducted by PB Power [71] indicated that, the remote end voltage level would exceed the upper limit level due to connection of SSEGs. This occurs regardless of customer loading conditions, where the customer installed SSEG produces 0.4kW or 1.5kW for minimum and maximum loading conditions respectively.

2.8.4 Voltage Step Changes

Voltage step changes can be caused by a sudden loss or tripping of generation in response to a system disturbance. Engineering Recommendation P28 provides a general limit of ±3% for the magnitude of the voltage step change occurring from switching operations [72].

2.8.5 Voltage Unbalance

Adding generation to just one phase, as expected, gives unbalanced voltages. The main effect of voltage imbalance in electrical equipments is the overheating of the stator and rotor windings of three-phase rotating machines. Also, power electronic converters tend to generate more harmonics when subject to an unbalanced supply voltage [2, 8]. The recommended limits for voltage unbalance are defined in the Engineering Recommendation P29. The maximum percentage difference between the average of all three phase voltages and the individual phase voltages has a design limit of 1.3%. In the studies conducted by PB Power [71], the limits will be exceeded when 1.6kW is connected at each customer on one phase. In some cases the connection of single phase sources can help to correct existing imbalance voltages, as the generation can behave like negative load. Figure 2.10 shows a voltage waveform during a voltage unbalance event.

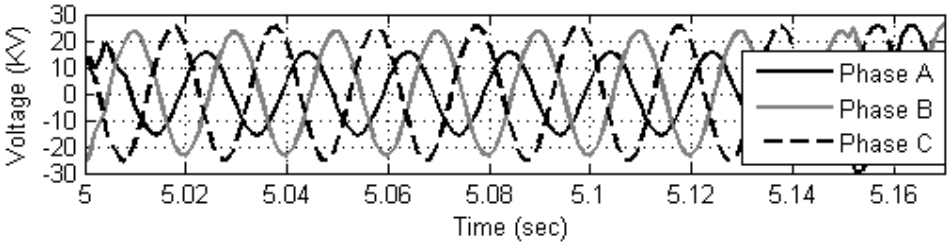

Figure 2.10: Voltage waveform during a voltage unbalance event.

The three-phase set of unbalanced voltage (Va, Vb and Vc) can be resolved into three–phase balanced positive sequence (Vp), negative sequence (Vn) and zero sequence (V0). The degree of voltage imbalance is expressed by equation (2.1) [73]:

$$Voltage\ unbalance\ (\%) = \frac{Negative\ \ phase\ se\ quence\ \ component\ x\ 100\%}{Positive\ phase\ sequence\ component} \quad (2.1)$$

This standard implies that if the magnitude of the negative phase sequence component is within 2% of the positive phase sequence component then the unbalance is acceptable [73].

2.8.6 Voltage Sags

Voltage sags are short duration reductions in the rms voltage magnitude caused by motors starting, transformer energizing or faults in the main grid. The voltage sags can occur at any instant of time with amplitudes ranging from 10–90% and a duration lasting for half a cycle to one minute [7]. In particular, during utility voltage sags, large line currents can flow along distribution feeders connecting the micro and utility grids. This leads to instability of SSEGs. Figure 2.11 shows a voltage waveform during a typical voltage sag event.

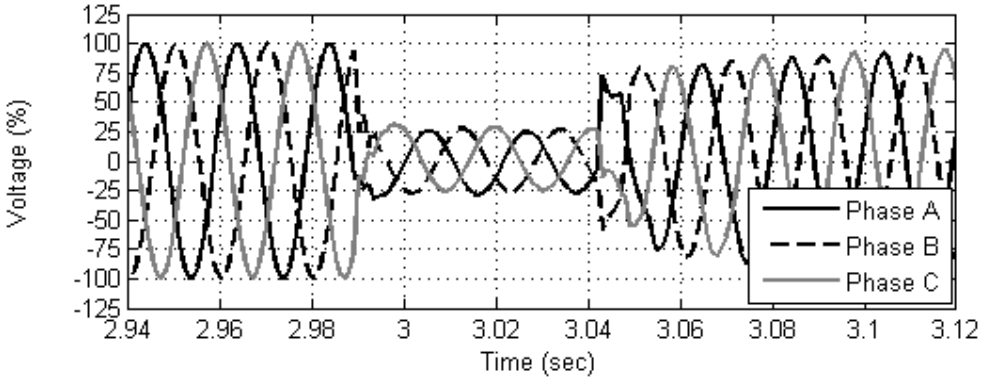

Figure 2.11: Voltage waveform during voltage sag event.

2.8.6.1 Voltage Sag Compensation

Previous research studies show that power electronic devices such as flexible ac transmission systems (FACTS) and custom power devices provide the power system with new control capabilities. In general, FACTS devices are used in transmission control whereas custom power devices are used for distribution control. The studies

related to distribution networks show that there are many different types of custom power devices that have been used to provide ride-through for voltage sags in distribution networks such as the distribution static compensator (D-STATCOM), Dynamic Voltage Restorer (DVR), unified power-flow controller (UPFC) and the solid-state fault current limiter. Some of the recent studies in this area that focus on voltage sags compensation, on the distribution network with distribution generation, are discussed in the next paragraphs.

Papers [74-76] use the UPFC for voltage sags compensation in distribution networks with distributed generation. Paper [74] presents an algorithm that functions by controlling a series inverter connected between the micro- and utility grids, to insert a large virtual RL impedance along the distribution feeder to limit the line currents and damp transient oscillations with a finite amount of active power circulating through the series (and shunt) inverter. Paper [75] proposes a topology that consists of a combination of shunt and series inverters connected to a common Z-source impedance network. The shunt inverter is controlled to maintain a quality voltage waveform at the load bus. Whereas the series inverter enhances the ride-through capability during grid faults, protects the shunt inverter by limiting the current and controls the power delivered to the grid. Paper [76] deals with the simulation of a unified series-shunt compensator (USSC) aimed at examining its capability in improving power quality in a power distribution system.

Paper [77] shows the analysis of custom power controllers, a new generation of power electronics based equipment aimed at enhancing the reliability and quality of power flows in low voltage distribution networks and the static VAr compensator (SVC) as an example of FACTS.

Paper [78] presents a detailed PSCAD/EMTDC simulation model of the distributed static series compensator (DSSC). The concept of Distributed Static Series Compensator (DSSC) uses a low-power, single-phase inverter that attaches to the transmission conductor and dynamically controls the impedance of the transmission line allowing control of active power flow on the line.

Papers [79-83] use the STATCOM for voltage sag compensation in distribution networks with distributed generation. Paper [79] illustrated and discussed the stability improvement of a wind farm consisting of 83 fixed speed induction generators with additional STATCOM. Paper [80] presents a study scenario composed of a fixed speed wind turbine and a D-STATCOM with battery storage connected to the distribution grid as an isolated system. The aim of the study is to demonstrate by means of simulation results, how the D-STATCOM with storage can be a solution for a larger and better integration of the intermittent energy produced by DG in the electrical grid. In paper [81], wind farm and STATCOM usage are studied to increase the upper limits of induction generators dynamic stability in various distortion conditions in the grid. In paper [82] the stability of wind generators are improved using STATCOM, limiting the generator speed by controlling the torque, with pitch control or dynamic slip control and reducing the reactive power consumption by disconnecting some induction generators. Paper [83] has assessed the performance of the electromagnetic transient models of custom power equipment, namely DSTATCOM and Dynamic Voltage Restorer (DVR) aimed at enhancing the reliability and quality of power flows in low voltage distribution networks.

Papers [84, 85] use the fault current limiter for voltage sags compensation in distribution networks with distributed generation. Paper [84] proposes a superconducting fault current limiter in the distribution system with dispersed generators to solve increases in fault current and voltage sag issues due to short circuits. In paper [85] a high temperature superconducting (HTS) fault current limiter (FCL) is inserted at the terminals of the 12 KVA synchronous generator to improve the dynamic stability of this generator.

Other papers [86, 87] introduce control methods for the voltage-dip ride-through capability of inverter connected distributed generators. Paper [86] has presented an asymmetrical grid-fault ride through control algorithm for modern wind turbines with a fully rated direct-in-line three-phase converter arrangement. The control enables the wind turbine to retain its connection to the grid during asymmetrical grid faults without having to derate the hardware, in particular the semiconductor devices

and the dc-link capacitors. Paper [87] describes the improvement of the voltage-dip ride-through capability of a full-bridge bidirectional converter by means of the implementation of an alternative current-control strategy. The current-control strategy with a programmable damping resistance has been compared to the classical sine wave control strategy.

2.8.7 Increase in Network Fault Levels

Increasing levels of SSEG tends to increase the fault current. For a distribution network fault, as shown in Figure 2.12, if the contribution of SSEGs is high compared to the utility supply, then the fault current will be the summation of the SSEGs and utility current. For each 48kVA generation (AC machine) connected to the network, the fault level will rise by approximately 0.3MVA at the secondary of the substation (0.4kV side) and by approximately 0.5MVA at the primary of the substation (11kV side) [71]. Also the fault levels at the primary 33kV busbar will be exceeded first since all generation feeds back through this busbar [88]. The increase in system fault levels may cause switchgear fault ratings to be exceeded. Therefore there is a need to look at ways of limiting the fault current to prevent up rating of the switchgear.

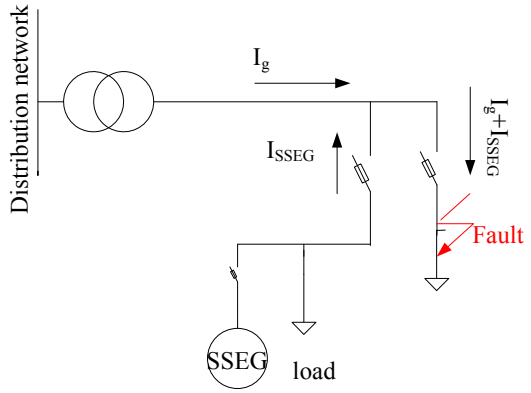

Figure 2.12: The contribution of SSEGs and the grid to fault.

2.8.8 Stability

Traditional distribution network design did not need to consider issues of stability as the network was passive and remained stable under most circumstances. Paper [89] mentions that DG can improve the stability of power systems if suitable types and appropriate locations are selected. The transient stability analysis shows that the maximum power angle deviations between the generators are decreased with the increase of DG penetration levels. With more power from the DG units, the absolute reserve power from generators and the network inertia constant are smaller due to the lower rated power of the rotating generators. As a result, the frequency response shows faster behaviour with higher maximum frequency deviations when more DG units are employed. The voltage profiles at load terminals are also improved due to the use of active DG sources near end-user terminals.

As the number of SSEGs connected to the main grid is rapidly increasing, the simultaneous disconnection of these SSEGs under fault conditions leads to local loads not being supplied by the SSEGs. This results in a decrease in system stability (i.e. angle and voltage stability) as hidden loads previously supplied by SSEGs, appears on the network. Therefore, it is essential that the SSEGs are kept connected during disturbances. This behaviour is called fault ride-through capability [90, 91].

2.8.9 Harmonics

The electronic devices that couple SSEG with the distribution network, for example AC-to-AC converter used in micro turbines and the DC-to-AC converter used in fuel cells and PV, produce several kinds of harmonics, because they inject currents that are not perfectly sinusoidal to the distribution system. The resulting harmonic distortion, if not properly contained and filtered, can bring serious operational difficulties to the loads connected on the same distribution system [69].

The quality of the inverter output waveform is defined by the total harmonic distortion (THD). In parallel processing mode of distributed generation systems as

per IEEE standard 1159 the total harmonic distortion is less than 5% (THD<5%) [92].

The total harmonic distortion (THD) is the square root of the sum of the squares of the harmonic voltages divided by the fundamental voltage:

$$\text{THD}= \frac{\sqrt{V_2^2 + V_3^2 + ... + V_n^2}}{V1} \qquad (2.2)$$

2.9 Conclusions

From the discussions on the recent studies in the field of distributed generation, it can be concluded that:

- Some of the SSEG technologies produce electrical energy in DC form such as fuel cells and photovoltaic arrays. Others generate at variable AC frequency such as wind turbines, or at a high AC frequency, such as micro gas turbines. Although some generators can be connected directly to the electric power grid such as wind power driven asynchronous induction generators, there is a trend to adopt power electronics based interfaces which convert the power first to DC and then use an inverter to export power to the 50Hz (or 60Hz) AC grid. Therefore most SSEGs do not have an inherent inertial response.

- A number of previous studies in the pubic domain have investigated the technical issues surrounding the connection of a large number of SSEGs in small areas of network such as a new build housing development. However, the studies were primarily aimed at addressing steady-state conditions and did not explore the transient response to be expected from SSEGs and any impact this may have on network performance or customer reaction.

- The integration of large numbers of SSEGs into LV networks may violate the voltage profile or constraints of maximum voltage rise even if the aggregated

power in the grid is low as they use constant power factor (unity power factor) controls. Thus in this work the power factor of SSEGs would be variable according to the voltage at the connection point. The advantage of this type of control that the local generation of reactive power by SSEGs reduces losses, and improves the voltage profile. As a consequence, the voltage security is also improved. This control scheme is useful during grid connected mode and islanded mode.

- Several research studies focus on a single micro grid connected to LV networks. In this work the connection of multiple small-scale distribution networks connected to the MV network (33kV) have been studied and will be discussed in the following chapters. Maintaining the stability of these small networks requires control strategies during grid connected mode and islanded mode. Therefore in this work the control schemes have been devolped to detect the loss of mains and to transfer the operation of these small networks from grid connected mode to islanded mode and vice versa.

- The tripping time of protection systems may be long such that they may not be possible to ensure system stability for all faults on the distribution network, due to the low or zero inertia of SSEGs. Then more care is required to try to ensure that SSEGs does not trip for remote network faults. Although previous research studies introduced solutions for voltage sags, the fault-ride through of a system with high penetration of SSEGs have not been considered and analyzed so far especially when there are mixed technologies of SSEGs connected together. In this case a comprehensive fault-ride through technique must be used.

- Even though previous research studied the contribution of DG to system frequency control, they concentrated on wind turbine especially for DFIG types. Thus the contribution of SSEGs in system frequency control would be investigated in this work. Also the frequency control scheme has to consider the different technologies of SSEGs.

CHAPTER 3

Transient Stability of Small-Scale Embedded Generation

3.1 Introduction

This chapter firstly presents the results of studies concerning the transient behaviour of small scale embedded generators (SSEGs) in response to network transients. The study uses small rotating AC machines and power electronic converter interfaced SSEG. The rotor angle and slip behaviour of a number of machine (synchronous and asynchronous) and prime mover technology combinations have been considered during and after the clearing of both local LV and remote HV faults. The results of case studies developed to examine the impact of fault locations, typical clearance times, type of fault (symmetrical or asymmetrical), type of SSEG (synchronous machine, asynchronous machine or inverter interfaced SSEG) or combinations of these types on the critical clearance times of SSEG are presented. A further study concerning the voltage step response due to the reconnection of a large number of power electronic converters is also considered in this chapter, specifically for the case of three single-phase inverters used to interface photovoltaic (PV) modules within a small area of the network. The step voltages that occur may be of a magnitude that is outside the limits (-6%, +10%) recommended in the Engineering Recommendation P28 [72]. All of these studies have been undertaken with simple control systems for active and reactive power control and no fault ride-through techniques were employed, aiming to understand nature behaviour of SSEG in transient conditions.

3.2 Fault Studies

The purpose of the following studies was to investigate the response of SSEG to a range of network faults and thereby ascertain the range of conditions under which SSEG might be expected to trip. Many of these may be regarded as nuisance trips when the action of network protection does not isolate the SSEG from a mains

supply. Any protection associated with the SSEG has not been included in order to demonstrate inherent capability and response. The critical clearing time (CCT) is used to indicate the stability of the SSEG. In this investigation the CCT of the SSEG is calculated from simulations conducted in PSCAD/EMTDC as well as from the mathematical calculations.

In this section difference types of studies are presented:

- The first study presents the transient behaviour of synchronous generator based SSEG in response to network faults.
- The second study presents the transient behaviour of induction generator based SSEG in response to network faults.
- The third study presents the dynamic performance of mixed SSEGs, three-phase induction generator powered by a small wind turbine, three-phase synchronous generator powered by small diesel and three–phase inverter interfaced fuel cell.
- The fourth study investigates the effect of unbalance voltage on transient performance of SSEGs when a fault occurs on a single-phase inverter interfaced PV.

These studies are complemented by finding the relationship between the inertia of the SSEG, fault location and CCT.

3.2.1 LV Network Model for Fault studies

The network model used for the transient studies is shown as a single line diagram in Figure 3.1 and is based on an assumption of customers representing a suburban mix of residential dwellings and small commercial premises. The high voltage (HV) 11kV network has been characterised using an ideal voltage source and impedance scaled to provide a fault level of 150MVA at the ring main unit (RMU) supplying the secondary substation (Appendix A provides the description of the infinite bus PSCAD model). An impedance of 4.5% and rating of 0.5MVA have been taken for

the secondary substation transformer. The demand on the secondary substation has been modelled as one detailed circuit and two equivalent unbalanced loads (the load model is provided in Appendix A) with the values as shown (a uniform power factor of 0.95 lagging has been assumed) and short lengths of connecting cable. SSEG has been connected at the location indicated depending on the particular study (e.g. synchronous generator, asynchronous generator, converter-connected source or all of them).

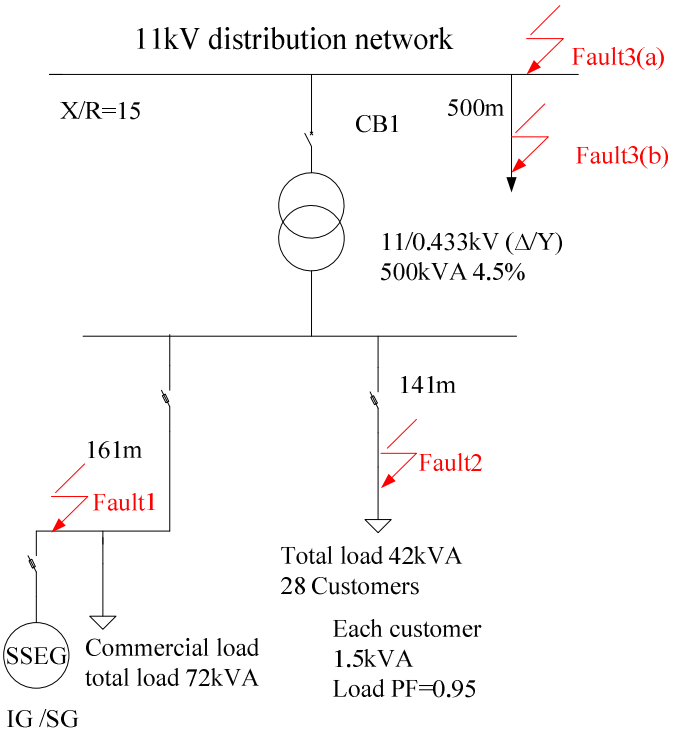

Figure 3.1: LV network model [71].

3.2.2 Three-Phase Synchronous Machine (11kVA)

The following studies present the investigation of the transient stability of a small diesel powered 11kVA three-phase synchronous generator (model, impedance and time constants are available in Appendix B) connected to the LV cable network described previously. A number of electrically local and remote three-phase faults have been applied and the critical clearance time (CCT) calculated. The studies are performed for two values of inertia constant (H = 1 s and 1.7s) and simulation results

are shown for fault clearance times in excess of the CCT to illustrate the impact of generator pole slipping. The figures in these studies illustrate the responses of the speed, load angle, and active and reactive powers of the machine, and also the voltage profile at the generator terminal and at the 0.433 kV and 11 kV bus bars.

3.2.2.1 Fault 1: Within LV Commercial Premises

The CCT for a three-phase fault applied within the same commercial premises as the generator (Fault 1 in Figure 3.1) was found to be 90ms and 115ms for the inertia constant values of 1s and 1.7s respectively. As shown in Figure 3.2(b) to (c), the duration of the fault is 110 ms applied at 3s (the complete collapse of voltage can be observed), in this case the generator (H=1.7s) recovers stability once the fault is cleared and returns to the pre-fault operating condition. If the duration of the fault is larger than the CCT=110 ms the generator will not recover stability after fault clearance.

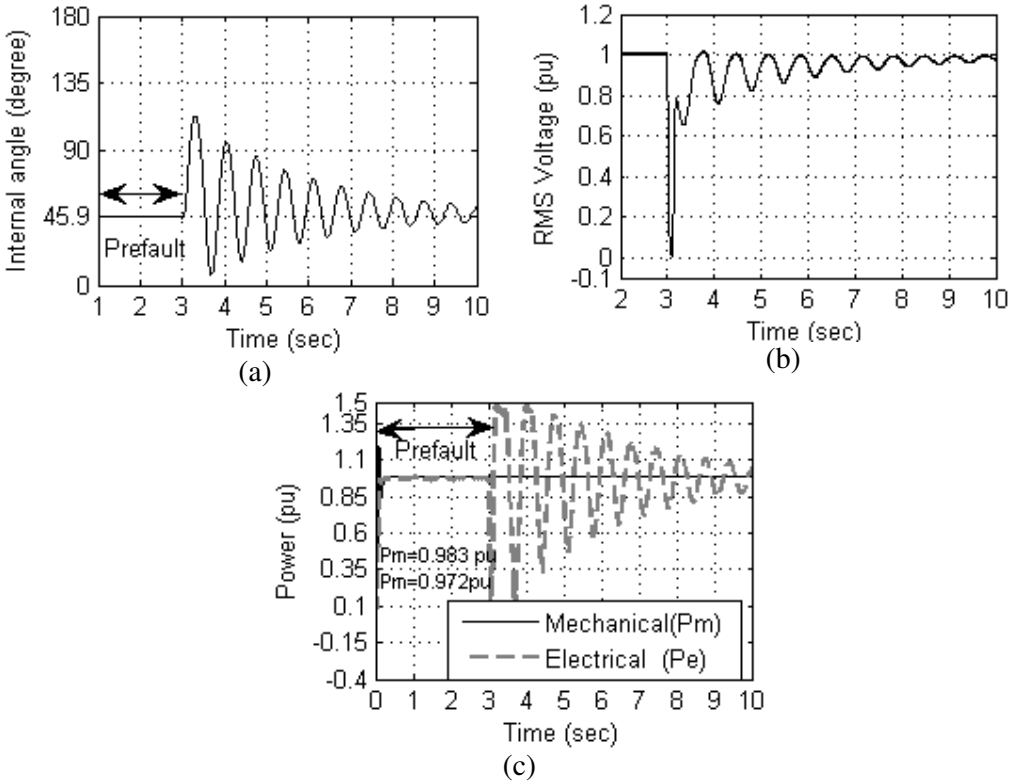

Figure 3.2: Performance of (SG) during LV local three-phase fault (tc =110 ms): (a) Machine internal angle, (b) Terminal voltage& (b) Mechanical and electrical power.

Figure 3.3 illustrates the instability of the generator (H=1.7s) by showing the machine internal angle, load angle and shaft speed responses for a fault duration of 116 ms applied at 3s. During the fault the speed increases to high speed and, depending on the mechanical design, could cause damage if the generator is not quickly tripped. The onset of instability can be observed after the continual increase in machine angle after the fault clearance the generator pole-slips. However, as faults within the commercial premises will be quickly cleared by the substantial fault current contribution from the mains supply, instability arising from these events is not deemed to be of concern.

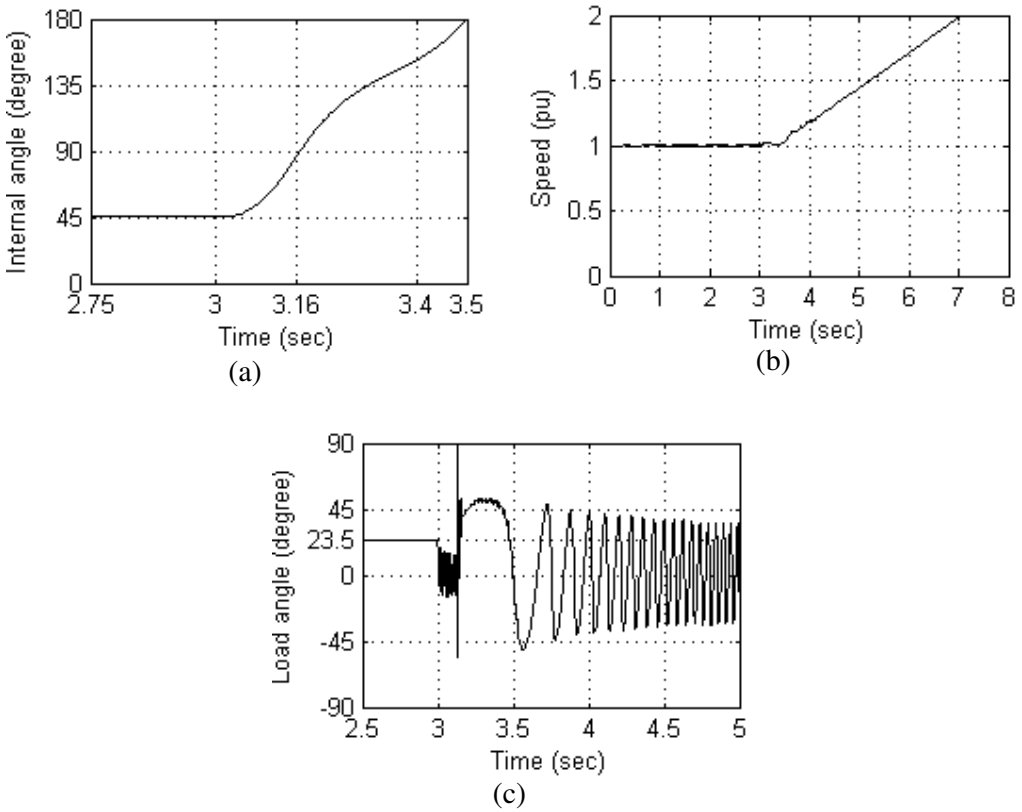

Figure 3.3: Performance of (SG) during LV local three-phase fault (t_f=116ms): (a) machine angle, (b) shaft speed& (c) Load angle.

3.2.2.2 Fault 2: Adjacent LV Circuit

The fault was applied on an adjacent LV circuit (Fault 2 in Figure 3.1) and it was observed that instability did not occur due to the relatively high retained voltage at the generator terminals. As an example, Figure 3.4 shows the machine angle, shaft

speed, terminal voltage responses and active and reactive powers of the machine for a fault duration of 500ms applied at 3s (H =1.7s). The power angle returned to the prefault value and the speed increased to 1.009 pu, but the voltages at the generator terminals and the load terminals decreased to 0.85 pu and 0.77 pu respectively (voltage sag). As shown in the results this voltage sag has an effect on the active and reactive power of the generator. The purpose of applying such a long-duration fault was to explore the performance of the generator during a permanent fault (assuming protection system failure). It also can be observed that when the fault is located further away from the generator it will evidently have the capability of withstanding faults of larger duration.

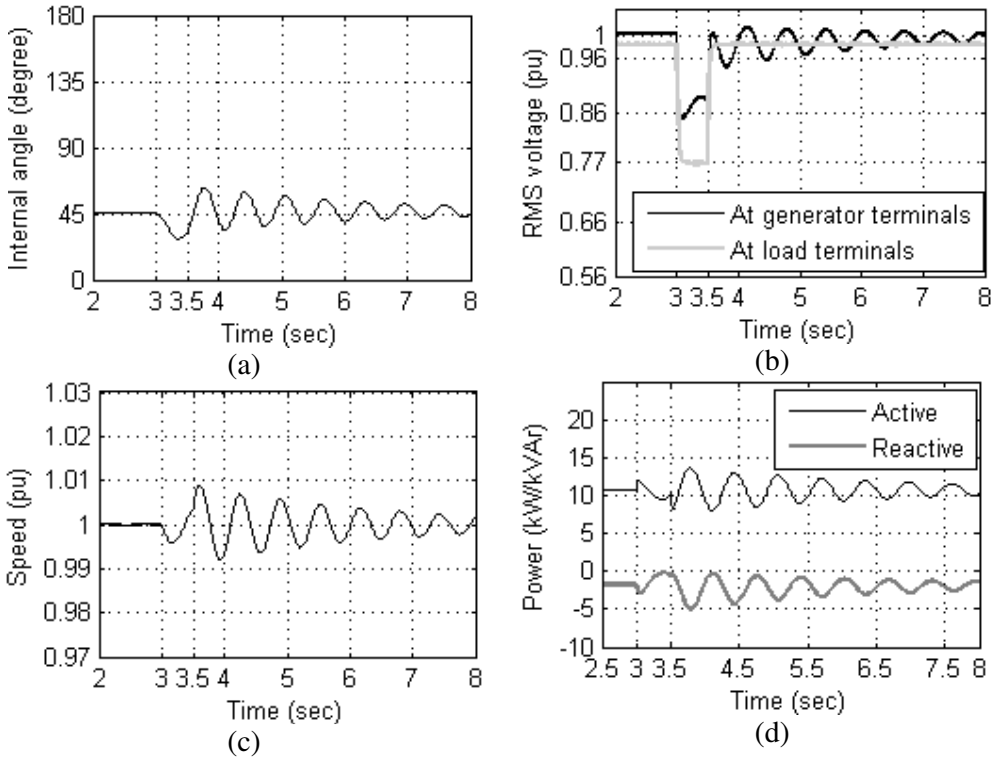

Figure 3.4: Performance of (SG) during adjacent LV circuit fault: (a) machine angle, (b) Generator and load terminal voltages (c) shaft speed & (d) Active and reactive power.

3.2.2.3 Fault 3: Electrically Remote on HV Distribution Network

Two specific fault conditions were applied on the HV side of the secondary substation and the CCT of the machine was found for both cases with different

inertia constants. The first fault condition was when a three-phase fault occurred adjacent to the HV terminals of the secondary substation transformer and the second when the same fault occurred at a remote location on the HV cable circuit.

For the first condition the CCTs were calculated as being 82ms and 110ms for the inertia constant values of 1s and 1.7s respectively. For the second condition the fault was placed 500m along a length of cable and the CCTs were found to be equal to 91ms and 121ms. Figure 3.5(a) and (b) illustrate the instability of the machine for a fault adjacent to the HV terminals with the drop in terminal voltage again evident. Figure 3.5 (a) shows the internal machine angle as function of time, for the three values of fault clearing time (tc): 100ms, 110 ms (critical clearing time) and 112 ms. The critical clearing angle (δ_{cr}) is about 70º. The results show that, when the fault duration is larger than the CCT the generator losses stability.

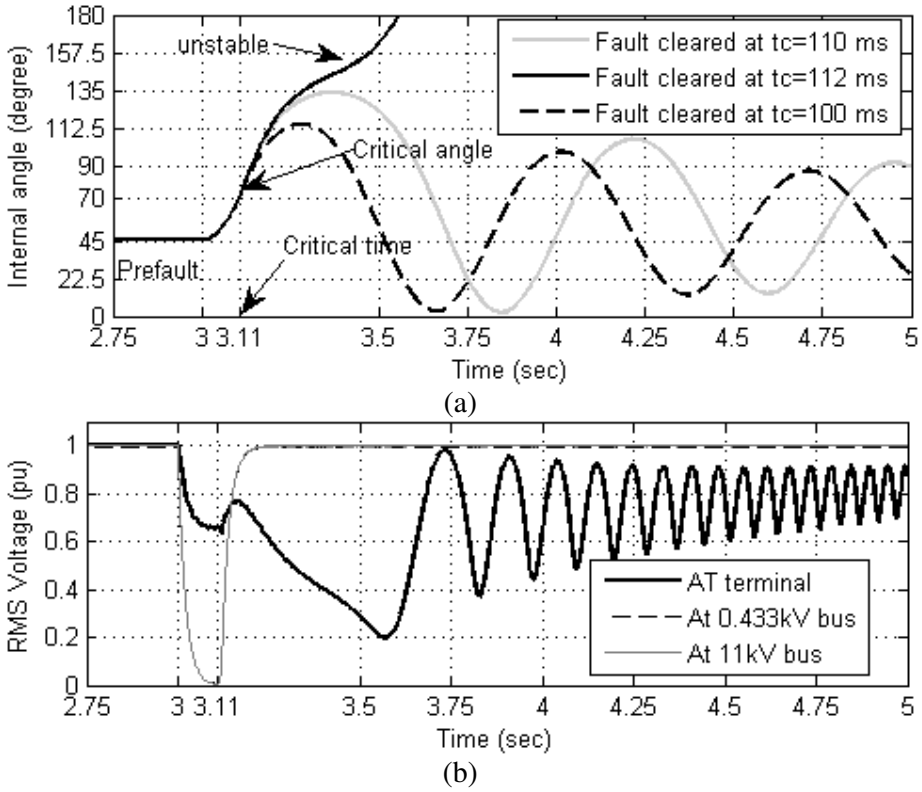

Figure 3.5: Performance of (SG) during remote HV fault: (a) machine internal angle response for different values of fault clearing time & (b) Terminal, 11kVbus and 0.433 kV bus voltages.

3.2.3 Three-Phase Asynchronous Machine (11kVA)

The following studies present the investigation of the transient stability of a three-phase induction generator 11kW (impedance and time constants are listed in Appendix B) driven by a small wind turbine connected to the LV cable network under different fault scenarios as shown in Figure 3.1.

3.2.3.1 Fault 1: Within LV Commercial Premises

A three-phase fault is applied within the same commercial premises as the generator (Fault 1) as shown in Figure 3.1. In this case the CCT was found to be 93ms and the critical speed ω_{cr} =1.232 pu (critical slip $s_{cr}=\omega_{cr}-1=0.232$ pu) as shown in Figure 3.6(a). Figure 3.6(a) to (d) illustrates the stability of the generator by showing the machine shaft speed, the output active and reactive power, electrical and mechanical torques and terminal voltage when fault 1 is applied at 3s lasting 80ms. During the prefault time the steady state operating slip is s_0=0.011pu. It can be seen that during the fault duration, the terminal voltage collapses completely, the output power and the electrical torque of the machine fall to zero and as a consequence the generator over-speeds and reaches the critical speed (ω_{cr}) if the fault duration increased to tc=93ms (CCT). However, it should be observed that the generator absorbs a significant amount of reactive power once the fault is cleared. This leads to depress the voltage of the system that may lead to voltage instability.

Figure 3.7 illustrates the instability of the generator if the fault duration is in excess of the CCT (93ms). In this case the fault duration is 94ms applied at 3s. The electrical torque developed by the machine falls to zero during the fault and as a consequence the machine quickly accelerates and reaches a high speed far over from the critical speed as shown in Figure 3.7(a). Therefore, when the fault is cleared insufficient electrical torque can be developed to reduce the machine speed causing instability. Due to the maximum torque the machine can develop at critical speed (1.232 pu). In this case over-speed protection would be required to operate to avoid damage to the machine and to avoid drawing a comparatively large amount of

reactive power from the network.

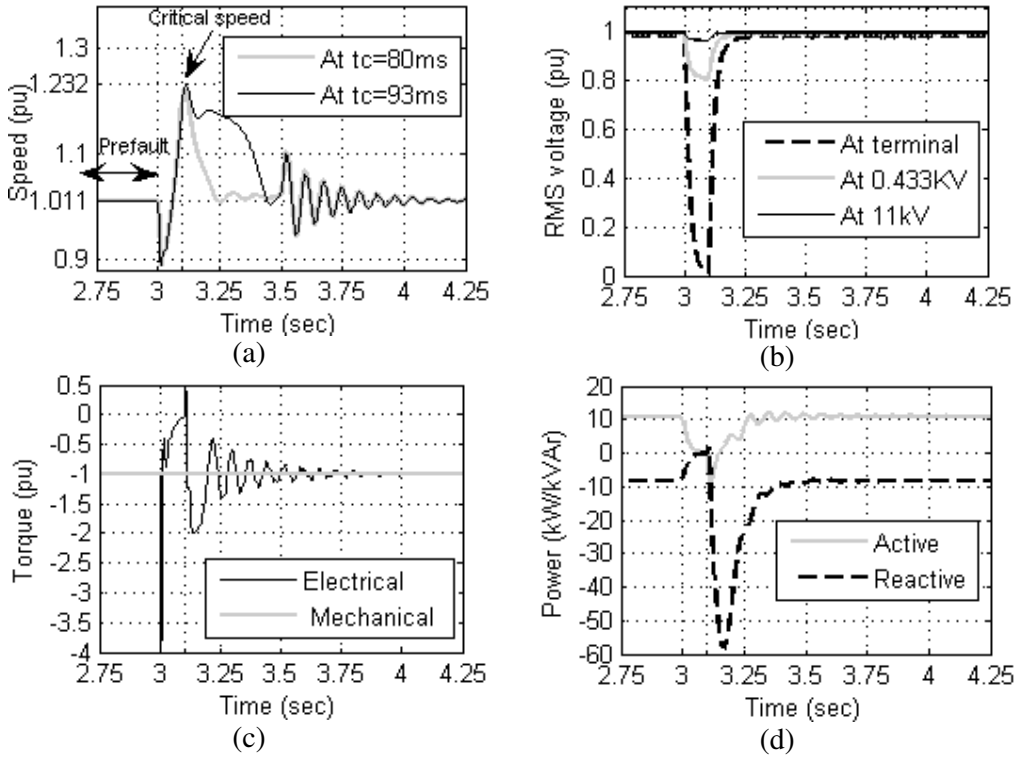

Figure 3.6: Performance of (IG) during LV local three-phase fault (t_c =80ms)**:** (a) Rotor speed, (b) Terminal, 11kV bus and 0.433 kV bus voltages, (c) Electrical and mechanical torques & (d) Active and reactive power.

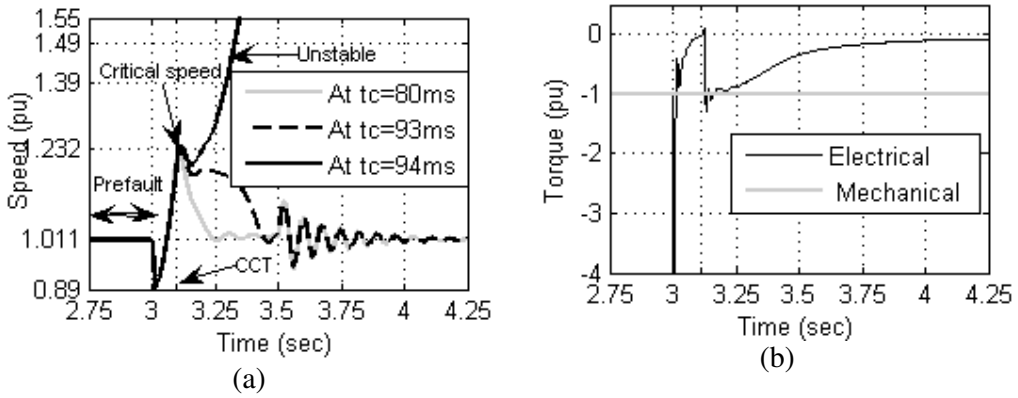

Figure 3.7: Performance of (IG) during LV local three-phase fault: (a) Rotor speed (tc=80ms, 93ms and 94ms) & (b) Electrical and mechanical torques (tc=94ms).

3.2.3.2 Fault 2: Adjacent LV Circuit

The fault was applied on an adjacent LV circuit (Fault 2) and it was observed that instability did not occur due to the relatively high retained voltage at the generator terminals. As an example Figure 3.8 shows the machine shaft speed and terminal voltage as well as the 11kV bus and 0.433kV bus voltages responses for a fault duration of 500ms applied at 3s. The generator terminal voltage decreased to 0.768 pu and the speed of the generator varied between 0.94 pu to 1.1 pu. The results also show that, although the generator is stable there are voltage sags in voltages at the different buses in the system.

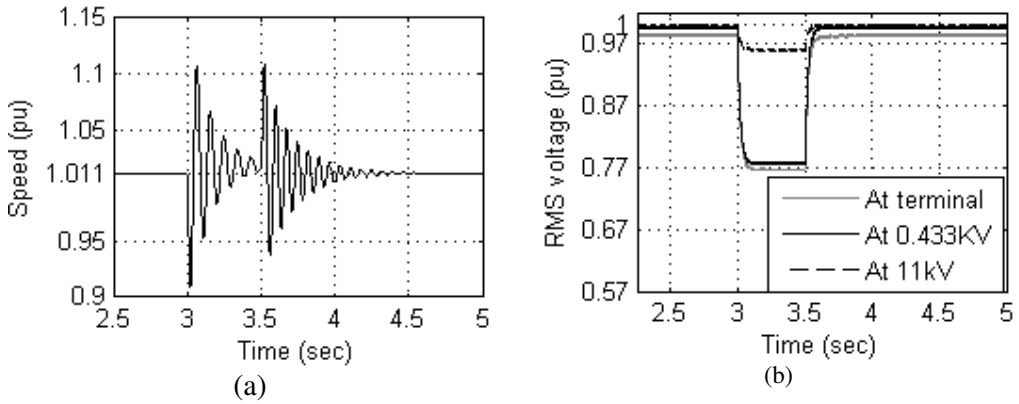

Figure 3.8: Performance of (IG) during adjacent LV circuit fault: (a) Rotor speed & (b) Terminal, 11kV bus and 0.433 kV bus voltages

3.2.3.3 Fault 3: Electrically Remote on HV Distribution Network

The fault was applied on the HV side of the secondary substation (Fault 3a). The CCT of the machine was found be equal to 87msec. Figure 3.9 illustrates the instability of the machine for a fault duration of 90ms. The results show that the machine quickly accelerates and reaches high speed far from critical speed and a complete collapse of system voltages (Terminal of the generator, 11kV bus and 0.433 kV bus voltages) can be clearly observed.

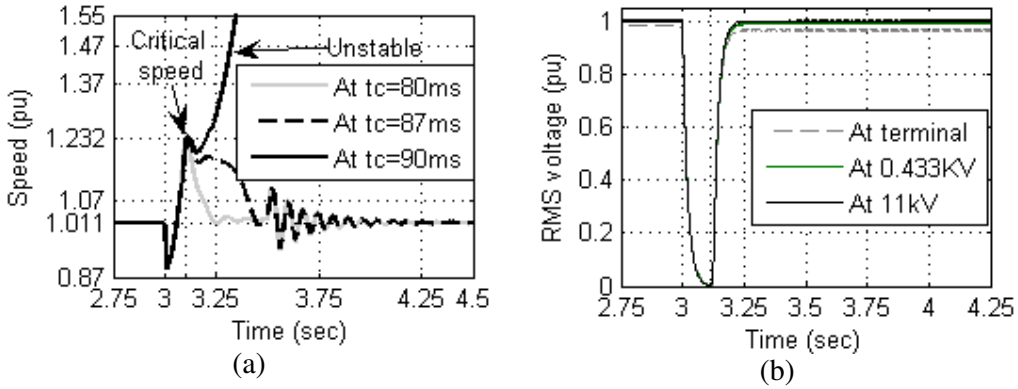

Figure 3.9: Performance of (IG) during HV transformer terminal fault (tc=119ms): (a) Rotor speed & (b) Terminal, 11kV bus and 0.433 kV bus voltages.

3.2.4 Mixed SSEGs

The following studies present the investigation of the transient stability of a three-phase induction generator powered by a small wind turbine, three-phase synchronous generator powered by small diesel engine generator and three–phase inverter interfaced fuel cell (Three-phase inverter parameters are listed in Appendix C) connected to the LV cable network of Figure 3.10. A number of electrically local and remote three-phase faults have been applied and the critical clearance time (CCT) calculated.

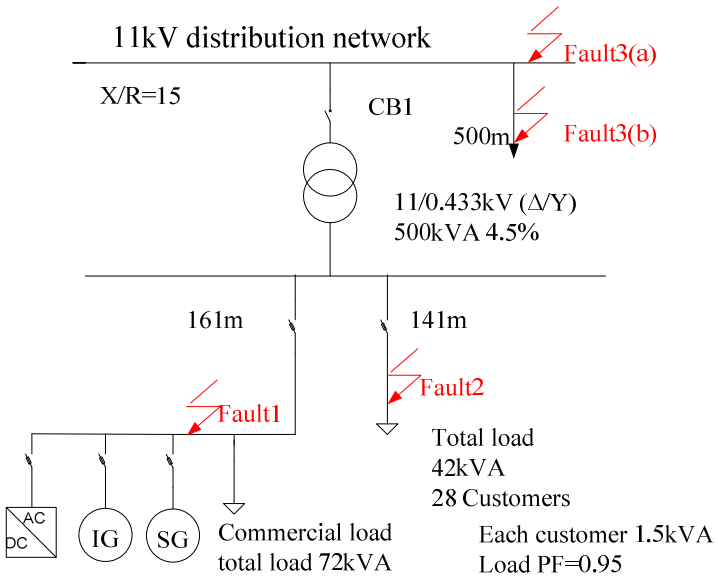

Figure 3.10: LV network model with mixed SSEGs

3.2.4.1 Fault 1: Within LV Commercial Premises

A three-phase fault is applied within the same commercial premises. The results show that the dynamic performance of the different types of SSEGs when connected together to the LV network is the same as the dynamic performance when every generator is connected alone to the network (Figures 3.2, 3.3 and 3.7) except that the CCT of the induction generator presented a minor improvement.

3.2.4.2 Fault 2: Adjacent LV Circuit

The fault was applied for 3s on an adjacent LV circuit (Fault 2) for duration of 500ms and it was observed that instability did not occur due to the relatively high retained voltage at the generator terminals. As an example, Figure 3.11 shows the terminal voltage response for cases containing only one SSEG compared with the case with mixed SSEGs. The results show that, when different SSEG types work in parallel with each other (a synchronous generator, induction generator and a converter-connected SSEG) the load terminal voltage changed slightly from 0.766 pu to 0.773 pu. This means that the connection of other type of SSEGs may have a positive impact on the power quality and voltage stability of the distribution network.

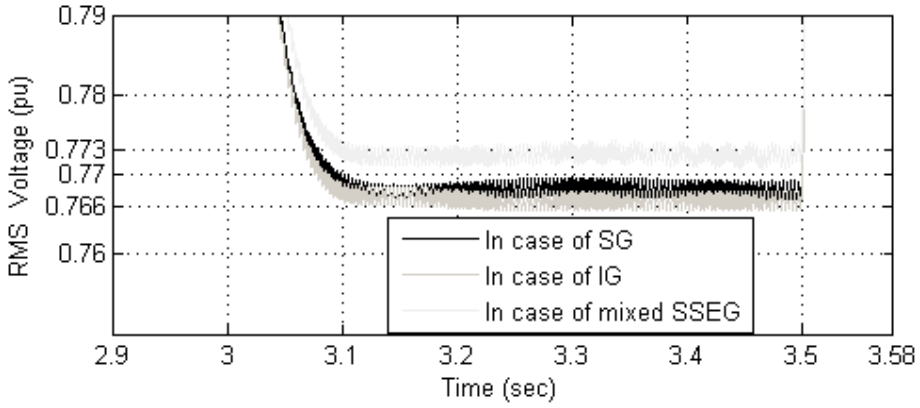

Figure 3.11: Load terminal voltage in case of mixed SSEG and only one generator.

3.2.4.3 Fault 3: Electrically Remote on HV Distribution Network

The fault was applied on the HV side of the secondary substation. The results show that the dynamic performances of the different types of SSEGs when connected

together to the LV network are the same as when every generator is connected alone to the network.

3.2.5 The Relationship between the Inertia, Fault Location and CCT

This study aims to show the relationship between the generator inertia, fault location and CCT (synchronous generator as an example). A number of electrically local and remote three-phase faults have been applied, and the critical clearance time (CCT) calculated. The studies are performed for different values of combined inertia constant (H) of the generator and prime mover (H = 1s, 1.35s and 1.7s). Figure 3.12 shows the relationship between the CCT, inertia constant of the machine and fault location. The results show that, the CCT increases as the inertia of the machine becomes larger showing a practically linear relationship. Also it was observed that the location of the fault (in the case of HV fault) significantly affected the CCT. The generator in case of the HV Distribution Network (500m) has longer CCT than in case of the HV transformer terminal fault.

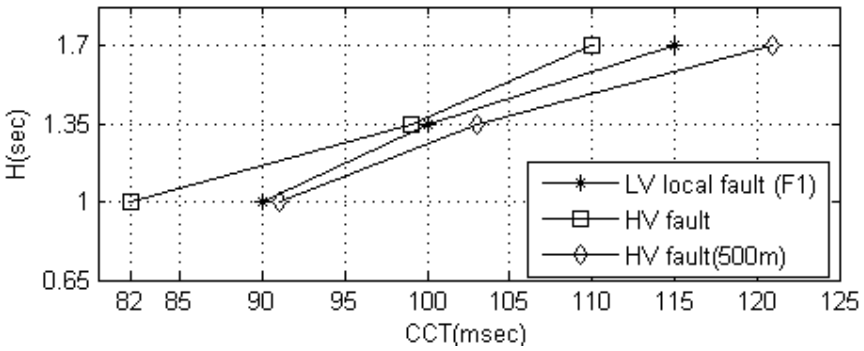

Figure 3.12: Relationship between inertia constant, fault location and CCT.

3.2.6 Single Line To Ground Fault with Single-Phase Inverter

In this section a single line to ground fault has been considered, as this fault type is more common and also some SSEG technologies like PVs are single–phase. Therefore, it is important to investigate the behaviour of SSEGs during this type of fault. In this study a single-phase inverter interfaced PV (single-phase inverter parameters are listed in Appendix C) was connected to the network as shown in

Figure 3.13. The inverter is connected to phase A of the bus 0.433kV with other SSEGs.

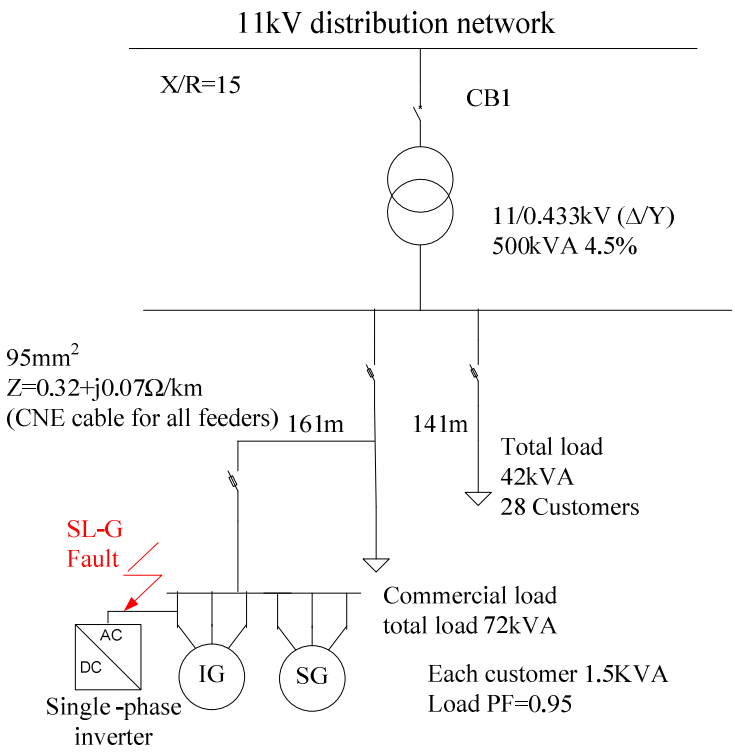

Figure 3.13: Induction generator and single-phase inverter connected to LV network

A single line to ground fault was applied at 3s for duration 400ms. This period has been chosen to explain the difference between performance of the generators during the single-phase-to-ground fault and during a three-phase fault. At this time the generators were unstable during the three-phase fault studies at the generator terminal in the previous sections. In this case, as shown in Figure 3.14 during an asymmetrical fault, the three-phase voltage of the system is unbalanced. Due to this unbalanced voltage, there are negative and positive torques and even the generators (induction and synchronous generators) are stable. However, these torques are pulsating with zero average values. The pulsating torque causes vibrations which reduce the life span of the machine and produces hum. Furthermore, this fault caused

unbalanced operation that leads to fluctuations in speed, load angle and output power.

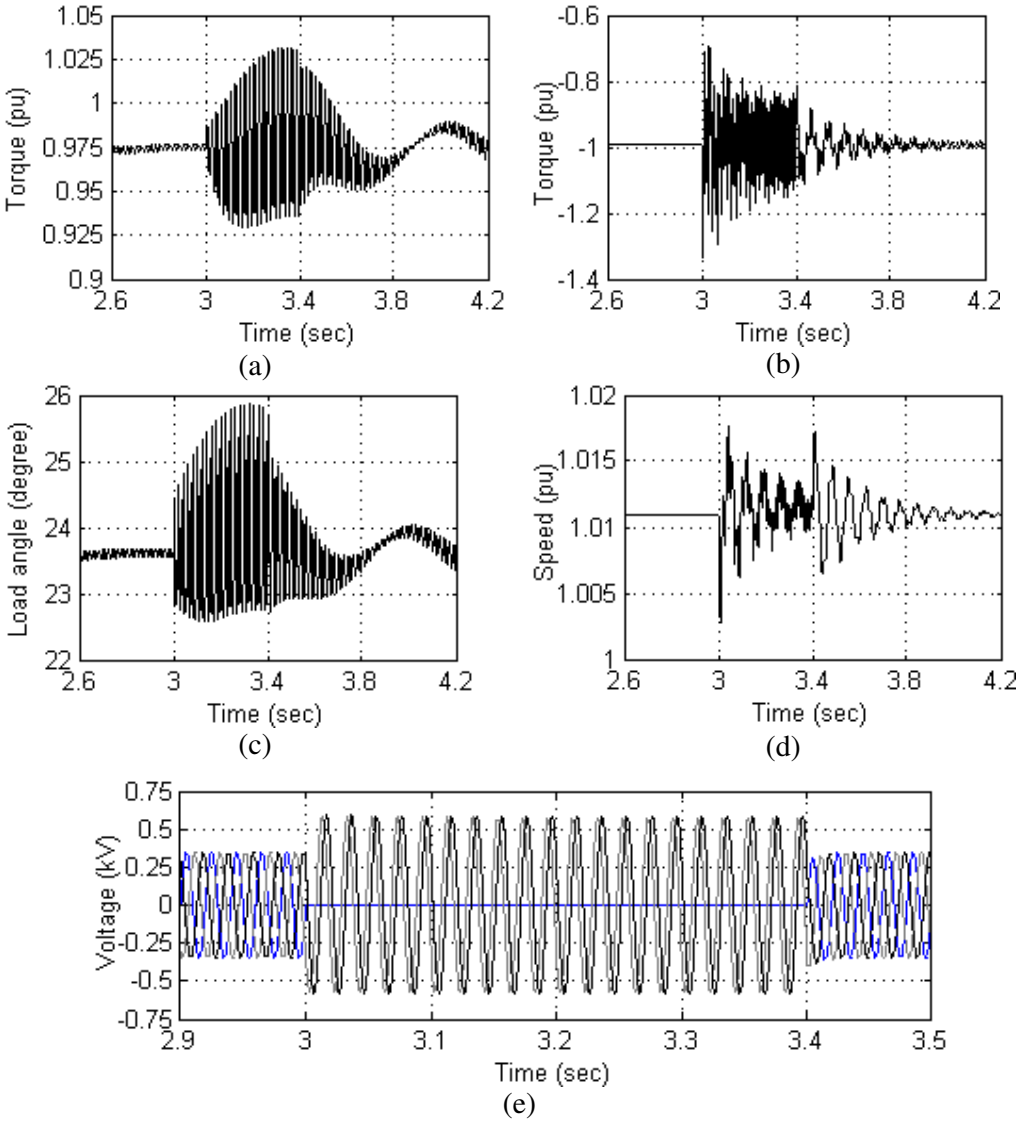

Figure 3.14: Single –phase inverter terminal fault: (a) SG electrical torque, (b) IG electrical torque, (c) SG load angle, (d) IG rotor speed and (e) Three-phase terminal voltage.

3.3 Reconnection Study

This study investigates the step changes in supply voltage experienced due to the simultaneous reconnection of a large number of SSEGs. The context for this event is

the reconnection of SSEG after a disturbance, once the system voltage and frequency have returned to within tolerance for a period of 3 minutes (G83/1) [93]. This study has been done with constant power factor operation.

3.3.1 33kV Network Model used for reconnection study

In this case the SSEG is assumed to be exclusively interfaced using power electronics and operates at a unity power factor. The SSEG is connected to the small rural 33kV network [94] through the sub-sea cable at bus 1115. Figure 3.15 shows that, the load connected at this bus is 2.85 MW and 0.58MVAr. This network is a basic power system model of the small rural network with a sub-sea cable and has been used to examine the effect of reconnection of a large number of SSEGs on the voltage of the distribution network. The EHV1 model is a 33kV rural network fed from a 132kV supply point. The network has long lines, including a sub-sea cable between buses 318 and 304, leading to voltage problems at the extremities of the network. The network includes a generator (G1) which represents the main 132kV system (system slack bus) connected to a 132kV bus (bus 100) and one interconnected generator which works as a PV bus 4MW connected to the network at bus 336. The full description of the 33kV rural network model is available in Appendix D.

3.3.1.1 Simulation Study

For this study it has been initially assumed that SSEG has been installed and meets 100% of the local peak demand if sufficient fuel is available. The units and loads are balanced across the phases. All SSEGs reconnect to the system at 10s and deliver real power at their rated value. Figure 3.16 shows both the instantaneous and calculated rms voltage as measured at the 11kV side of the secondary substation. A 7% step change can be observed based on the nominal value of 11kV.

Table 3.1 lists the step voltage changes for a number of levels of SSEG given as a percentage of peak demand and is in excess of the 3% recommendation within P28

[72]. However, the steady-state voltage is within statutory limits in all cases (-6%, +10%).

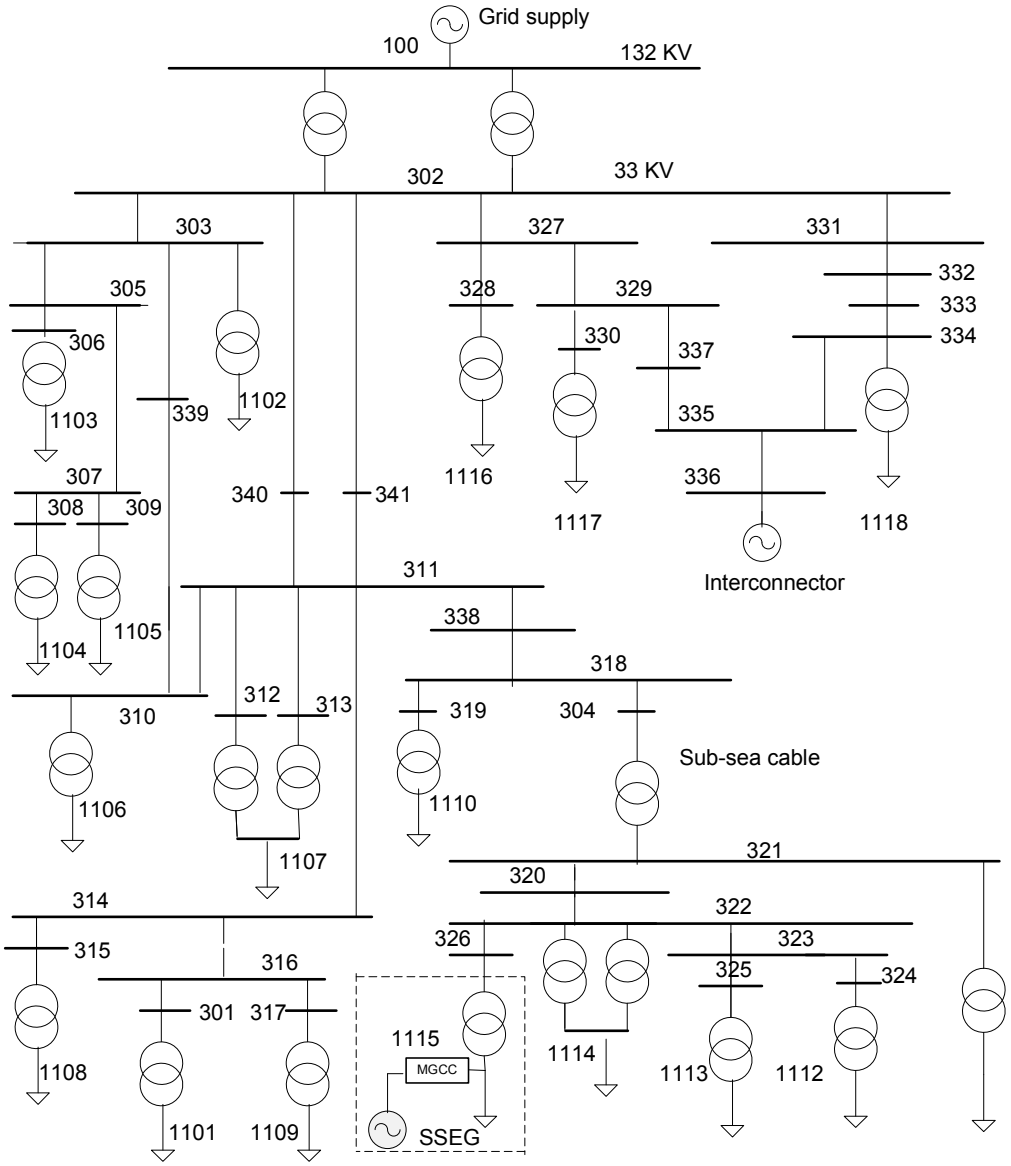

Figure 3.15: Network with small scale distributed generators [94].

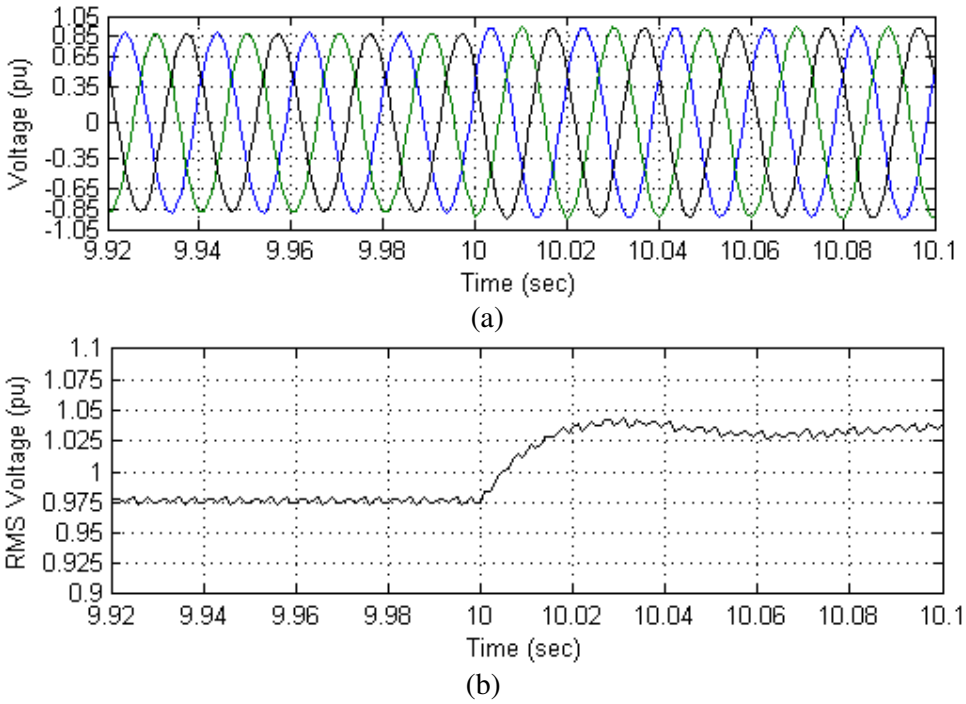

Figure 3.16: Secondary substation three-phase voltage at 10% step change: (a) Instantaneous & (b) RMS .

Table 3.1: Voltage step changes for various generation levels

SSEG as a % of Peak Demand	**% Voltage Step Change**
40	4.35
50	5.18
75	6.7
100	8
125	10.2

3.4 Theoretical Results

In this subsection the critical angle and critical time for the synchronous generator as well as the critical slip and critical clearing time for the induction generator

considered in this study have been calculated by using circuit analysis and machine theory.

3.4.1 The Equivalent Circuit of the Distribution Network

Calculating the critical angle and critical speed requires calculating the circuit impedance between the generator and the infinite bus, the voltage at the bus where the generator is connected to. Figure 3.17 shows the equivalent circuit of the low voltage network used in this study (Figure 3.1).

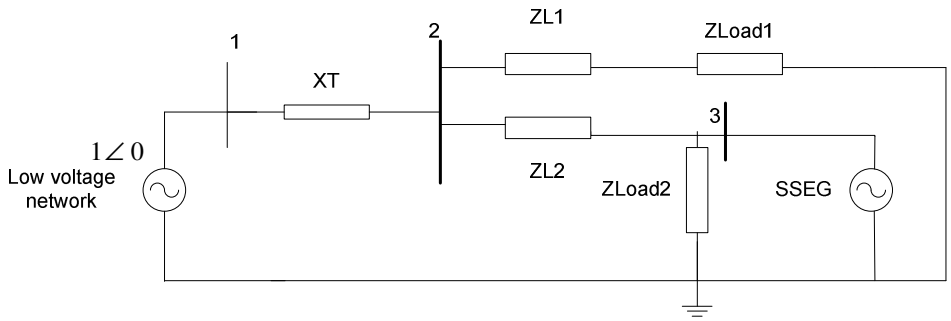

Figure 3.17: Network impedances diagram

Where Z_{L1} , Z_{Load1}, Z_{L2} and Z_{Load2} are the impedance of lines 1and 2 as well as load1 and 2 respectively. XT is transformer reactance.

The impedances values will be converted to per unit values on the system base. In general, the per unit value is the ratio of the actual value and the base value of the same quantity [95].

$$per\ unit\ value = \frac{actual\ value}{base\ value} \tag{3.1}$$

For the system the generator voltage and power have been taken as the system base (11kVA, 0.433kVA). The base impedance Z_{base} is given by:

$$Z_{base} = \frac{V_{base}^2}{S_{base}} \qquad [95] \qquad (3.2)$$

$$S_{base} = 11k\,VA$$

$$V_{base} = 433\,V$$

$$Z_{base} = \frac{V_{base}^2}{S_{base}} = \frac{433^2}{11000} = 17.044\,\Omega$$

The impedance of line 1(Z_{L1}) and load1 (Z_{Load1}) in per unit are:

$$Z_{L1\,p.u.} = \frac{Z_{L1}}{Z_{base}} = \frac{0.0323 + j0.0110929}{17.044} = 0.00194 + j0.00057\,p.u.$$

$$Z_{Load1\,p.u.} = \frac{Z_{Load\,1}}{Z_{base}} = \frac{4.067 + j1.268}{17.044} = 0.2387 + j0.0744\,p.u.$$

The impedance of line 2(Z_{L2}) and load2 ($Z_{Load\,2}$) in per unit are:

$$Z_{L2\,p.u.} = \frac{Z_{L\,2}}{Z_{base}} = \frac{0.0376 + j0.0097}{17.044} = 0.0022 + j0.00065\,p.u.$$

$$Z_{Load2\,p.u.} = \frac{Z_{Load\,2}}{Z_{base}} = \frac{2.474 + j0.813}{17.044} = 0.1451 + j0.0477\,p.u.$$

Converting the transformer reactance from the transformer per unit to the system per unit is given by:

$$Z_{N\ p.u.} = Z_{M\ p.u.} \frac{MVA_{N\ base}}{MVA_{M\ base}} \cdot \frac{(kV_{M\ base})^2}{(kV_{N\ base})^2} \qquad [95] \qquad (3.3)$$

Where the old base and per unit values of the transformer are denoted by subscript M, the base values of the system are denoted by subscript N. Thus the new per unit value is:

$$Z_{N\ p.u.} = 0.045 \times \frac{0.011}{0.5} \cdot \frac{(0.433)^2}{(0.433)^2} = 9.9 \times 10^{-4}\ pu$$

The Thevenin equivalent of the network, as viewed from the generator terminals, is shown in Figure 3.18.

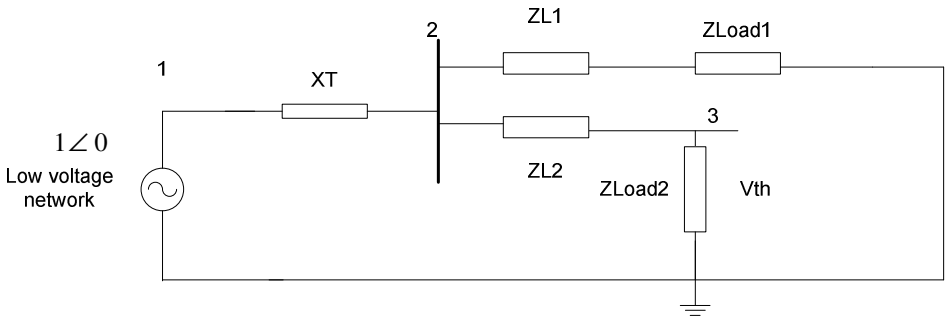

Figure 3.18: The network equivalent circuit after disconnected the generator

The Thevenin voltage is the voltage on bus 3 (V_{th}= V_3). The voltage at bus 3 can be calculated by using Kirchhoff current law as follow:

$$\begin{bmatrix} -\text{j}1010 & \text{j}1010 & 0 \\ \text{j}1010 & -421.8+j1134.8 & 418-\text{j}123.5 \\ 0 & 418-\text{j}123.51 & -424.2+j125.59 \end{bmatrix}\begin{bmatrix} V1 \\ V2 \\ V3 \end{bmatrix}=\begin{bmatrix} 0 \\ -j1010.1 \\ 0 \end{bmatrix}$$

The voltage at bus 1 is known then the first row and the first column are eliminated from the matrix.

$$\begin{bmatrix} -421.8+\text{j}1134.8 & 418-\text{j}123.5 \\ 418-\text{j}123.5 & -424.2+\text{j}125.59 \end{bmatrix}\begin{bmatrix} \text{V2} \\ \text{V3} \end{bmatrix}=\begin{bmatrix} -\text{j}1010.10 \\ 0 \end{bmatrix}$$

$$V3=\frac{\begin{bmatrix} -421.8+\text{j}1134.8 & -\text{j}1010.10 \\ 418-\text{j}123.5 & 0 \end{bmatrix}}{\begin{bmatrix} -421.8+\text{j}1134.8 & 418-\text{j}123.5 \\ 418-\text{j}123.51 & -424.2+\text{j}125.59 \end{bmatrix}}=\frac{1.2475\text{e}+005+4.2222\text{e}+\text{j}005}{-1.2306\text{e}+005-4.3111\text{e}+\text{j}005}$$

$$\text{V3}=0.9814\angle-0.53^\circ\,\text{pu}$$

Thevenin impedance is:

$$Z_{33} = [X_T \,//(Z_{L1} + Z_{Load1}) + Z_{L2}] // Z_{Load2} \tag{3.4}$$

Or it can be found from the Z bus (Z_{33}) of the network after the generator is disconnected from the circuit. The Z_{33} is the impedance of bus 3 where the generator is connected to the network which can be calculated by finding the Y bus first then the inverse of the Y bus is the Z bus.

The Y bus matrix of the system is:

$$Y = \begin{bmatrix} -421.8 + j1134.8 & 418 - j123.5 \\ 418 - j123.5 & -424.2 + j125.59 \end{bmatrix}$$

By taking the inverse of the Y bus the Z bus is:

$$Z = \begin{bmatrix} 0.0000 + j0.0010 & 0.0000 + j\,0.0010 \\ 0.0000 + j0.0010 & 0.0022 + j\,0.0016 \end{bmatrix}$$

From the Z matrix (Z_{33}) as well as from the parallel and series calculations the value of the Thevenin impedance of the network is:

$$Z_n = Z_{33} = R_{33} + jX_{33} = 0.0022 + j0.0016\,pu$$

Figure 3.19 shows the Thevenin equivalent of the distribution network.

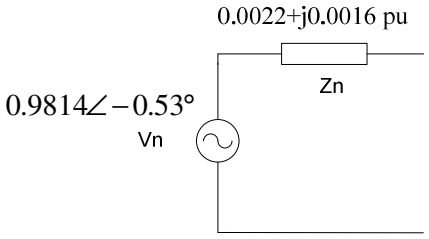

Figure 3.19: The thevenin equivalent of the network.

3.4.2 Calculation of Critical Clearing Angle/time for synchronous generator

In order to compare the simulation results with the mathematical result for finding the critical angle (δ_{cr}) and critical clearing time (CCT) for the synchronous generator considered in this study the equal-area criterion method has been used. Calculating the critical angle requires calculating the reactance between the generator internal voltage and the network, mechanical power (Pm) and electrical power (Pe). Figure 3.20 shows the generator equivalent circuit connected to the network.

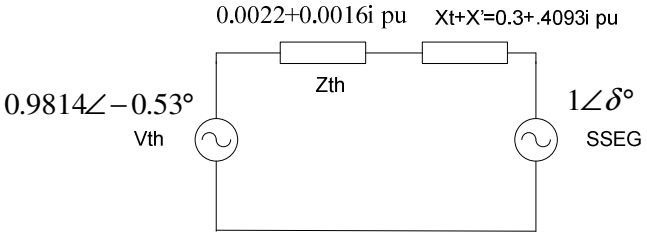

Figure 3.20: The equivalent circuit of the synchronous generator and the network

where

X' is the transient reactance of the generator which is equal to 0.3 pu.

X_t is reactance between the network and the generator 6.97Ω (22.2 mH). It is used for transmitting 11kW at corresponding phase angle difference equal to 23.3 deg (0.406 rad) as clearly satisfied from the simulation results as shown in Figure 3.3. This is entered as the initial machine angle for initialisation. The per unit reactance X_t is calculated by:

$$X_{tp.u.} = \frac{X_t}{Z_{base}} = \frac{6.97}{17.044} = 0.4093 \ p.u.$$

Figure 3.21 shows the p-δ plot. At steady state, the value of the electrical power of the generator is (Pe) 0.972 pu and the mechanical input torque of the generator (Pm) is 0.983 pu.

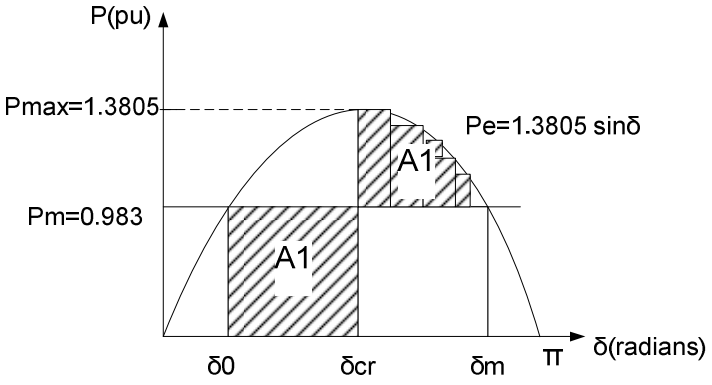

Figure 3.21: *p-δ* plot for case study [3].

The value of R_{33} and the Thevenin voltage angle are ignored to make this calculation easier. The power supplied by the generator is:

$$p_e = \frac{V_g V_{SE}}{X' + Xt + X_{33}} \sin \delta_0 \quad [3] \tag{3.5}$$

$$p_e = \frac{0.9814 \times 1}{0.3 + .4093 + .0.0016} \sin \delta_0$$

$$p_e = 1.3805 \sin \delta_0$$

The value of Pe=0.972 pu thus the steady state the internal phase angle δ_0 is 44.76° =0.7813 radians.

In this study the disturbance is a temporary three-phase fault on the grid side of the low voltage network. The power angle then increases to a maximum value δ_m =180- δ_0 =135.24° =2.3603 radians, which gives the maximum decelerating area. Equating the accelerating and decelerating areas in the *p-δ* plot:

A1=A2

$$A1 = \int_{\delta_0}^{\delta_{cr}} pm\, d\delta \quad = A2 = \int_{\delta_{cr}}^{\delta_m} (P_{\max} \sin\delta - p_m) d\delta \quad [3] \tag{3.6}$$

$$\int_{0.7813}^{\delta_{cr}} 0.983\, d\delta \quad = \int_{\delta_{cr}}^{2.3603} (1.3805 \sin\delta - 0.983) d\delta$$

Solving for δ_{cr}

$$0.983 \times (\delta_{cr} - 0.7813) = 1.3805[\cos\delta_{cr} - \cos(2.3603)] - 0.983 \times (2.3603 - \delta_{cr})$$

$$1.3805 \cos\delta_{cr} = 0.572$$

$$\delta_{cr} = 1.1435 \text{ radians} = 65.52^{\circ}$$

To calculate the critical clearing time (CCT) the swing equation is integrated twice with initial condition $\delta_{cr}(0) = \delta_0$ and $\frac{d\delta(0)}{dt} = 0$,

$$\frac{2H}{\omega_{syn}} \frac{d\delta(0)}{dt} = pm\ pu \qquad [96] \tag{3.7}$$

$$\frac{d\delta(t)}{dt} = \frac{(\omega_{syn})(pm.pu)}{2H} t + 0 \tag{3.8}$$

$$\delta(t) = \frac{(\omega_{syn})(pm.pu)}{4H} t^2 + \delta_0 \tag{3.9}$$

Solving

$$t = \sqrt{\frac{4H}{\omega_{syn}\, p_{mpu}} (\delta(t) - \delta_0)} \qquad [96] \tag{3.10}$$

Then the critical clearing time for inertia constant (H=1s and H=1.7s) is:

$$t = \sqrt{\frac{4(H)}{100\pi \times (.983)} (1.1435 - 0.7813)}$$

Table 3.2 shows the simulation and calculation results for different CCT for various inertial constants.

Table 3.2: Different CCT for various inertial constants

Method	**Steady state angle (δ_0) (degree)**	**Critical angle (δ_{cr}) (degree)**	**CCT (ms)**	
			H (s)=1	**H (s)=1.7**
Simulation Results	45.9º	70º	82	110
Calculation Results	44.76°	65.52º	69	90

3.4.2.1 Calculation of Critical Clearing Slip/time for Induction Generator

As the stability of an induction generator is related to the slip the critical clearing slip and the critical clearing time are calculated and compared with the simulation results in this study. The steady-state equivalent circuit for the system with induction generator is shown in Figure 3.22 [97].

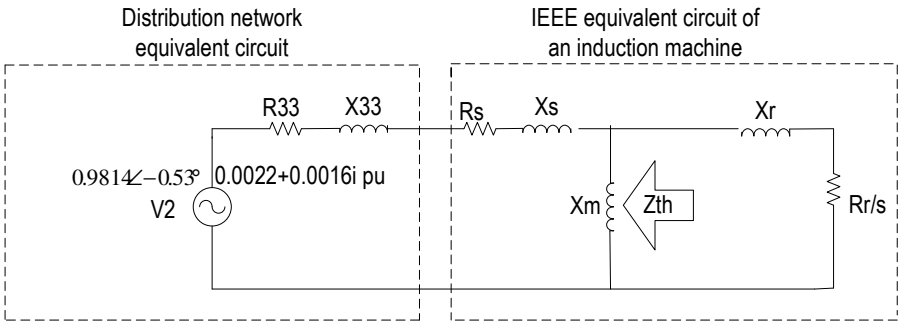

Figure 3.22: Induction generator connected to the network [97].

3.4.2.2 Calculation of critical slip

From the torque slip characteristic of the induction machine shown in Figure 3.23, for three-phase fault on the terminals of the generator the critical slip can be calculated as follows. Before the fault the electrical and mechanical torques are equal and the machine operates at s_0= -0.011pu. If the fault is cleared at a slip before

maximum/critical slip (s_m), where the electrical torque is higher than the mechanical torque the rotor decelerates and settles back to the steady-state slip. However if the fault is cleared at a slip higher than the critical slip then the mechanical torque is higher than the electrical torque the machine accelerates and goes unstable.

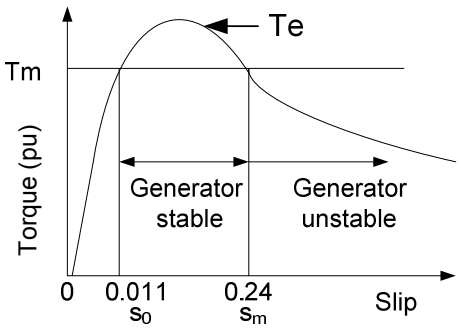

Figure 3.23: Torque slip characteristic [3] [97].

The developed torque of the induction generator is given by :

$$Te = \frac{\left|V_{th}^2\right| R'r / s}{(R_{th} + \frac{R'r}{s})^2 + (X_{th} + X'r)^2} \qquad [97] \qquad (3.11)$$

Where

R'r and Xr are the rotor resistance and reactance and equal to 0.0363 pu and 0.078 pu, respectively.

Rs and Xs are the stator resistance and reactance and equal to 0.05824 pu and 0.05824 pu, respectively.

Rth and Xth are the thevenin resistance and reactance which are calculated by finding the equivalent impedance of the stator circuit and the network by equation (3.12):

$$Z_{th} = jXm //[(Rs + R33) + j(Xs + X33)] \qquad (3.12)$$

Where *Xm* is the magnetising reactance and is equal to 2 pu.

$$Z_{th} = R_{th} + jX_{th} = j2//[(0.05824 + 0.0022) + j(0.0016s + 0.05824)] = 0.0569 + j0.0597\,pu$$

The developed torque is a function of slip. Therefore differentiating equation (3.11) with respect to slip (s) and equating the answer to zero gives the slip for maximum torque:

$$s_m = -\frac{R'r}{\sqrt{(R_{th})^2 + (X_{th} + X'r)^2}} \qquad [97] \qquad (3.13)$$

Thus from equation (3.13) the maximum slip is:

$$s_m = -\frac{0.0363}{\sqrt{(0.0569)^2 + (0.0597 + 0.078)^2}} = -0.243\,pu$$

The speed at which the torque is maximum $\omega_m = (1 - s_m) \times$ synchronous speed= (1+0.243) = 1.243pu. Stable operation is from synchronous speed to that at which the torque is maximum. Thus, the range of speed for safe operation will be from 1 to 1.243pu.

The critical clearing time of the induction generator can be calculated by integrating the equation of motion. The equation of motion in per unit is

$$2H\frac{d\omega_r}{dt} = T_m - T_e \qquad [3] \qquad (3.14)$$

Where ω_r is the angular velocity of the rotor in per unit, H inertia in seconds. T_m and T_e are the mechanical and electrical torques of the machine respectively in per unit. To calculate the critical clearing time (CCT) the equation of motion equation (3.14) is integrated from the steady-state speed ω_r to the maximum speed ω_m:

$$2H(\omega_m - \omega_0) = T_m(t_c - t_0) - \int_{\omega_0}^{\omega_r} Te\, dt \quad (3.15)$$

By assuming the integral of the Te during the transient is zero and initial time t_0=0. As the speed in per unit $(\omega_m - \omega_0) = \Delta s$ then the CCT (t_c) is:

$$t_c = \frac{2H}{T_m}\Delta s \quad (3.16)$$

For this study the CCT can be calculated using equation (3.15). The H=0.2s, T_m = 0.992 pu and normal steady state slip S_0=0.011 pu.

$$t_c = \frac{2\times 0.2}{0.992}(0.243 - 0.011) = 94\, pu$$

The CCT, critical slip and critical speed for the induction generator from the simulation results and calculations are shown in Table 3.3.

Table 3.3: CCT, critical slip and critical speed for induction generator

	Simulation results		**Calculation results**
	Terminal fault (F1)	**Network fault(F3a)**	
Critical slip (pu)	-0.2305	-0.232	-0.243
Maximum speed (pu)	1.2305	1.232	1.243
CCT (ms)	93	87	93

3.5 Conclusions

From the above results, we can conclude that:

- The stability of the induction generator during a disturbance depended on rotor speed stability which refers to the ability of the generator to remain connected to the network and running at a mechanical speed close to the speed corresponding to the actual system frequency. However the stability of the synchronous generator during a disturbance depended on the rotor angle stability which is concerned with the ability of the synchronous generator to remain in synchronism with the network. In contrast, the dynamic performance of the inverter based SSEG was different from the dynamic performance of rotating machines, as the inverter does not have inertia and the inverter current rating is set by the temperature rise of the semiconductors.

- The induction generator during the initial post-fault period absorbs high reactive power from the network that causes reduction in the network voltages. When the generator over-speed it also absorbs high reactive power.

- Connection of different types of SSEG together to the network (synchronous generator, induction generator and inverter interfaced SSEG) has a positive impact on the system voltage stability due to the above differences in the dynamic performance during disturbance.

- Concerning the type of fault, it was observed that the three-phase fault is more less severe on the generator than a single-phase to ground fault. Although the generator is stable during single-phase to ground fault (at the CCT of three phase fault), the resulting pulsating torque has an effect on the machine life span.

- The grid fault contribution at LV ensures fast fault clearance by operating the various fuses located on the network and consequently the tripping of SSEG

due to instability will not occur except in the cases where the fault is either at the terminals or in the service connection (sufficient terminal voltage remains for the electrically remote LV faults).

- The reconnection of a large group of SSEG at the same time has been shown to create relatively large voltage step changes of between 5% and 10% from nominal. The frequency of an occurrence of such step changes will be based on that of either originating HV faults causing the initial disconnection or the control strategy applied to the generators (e.g. heat led microCHP). Moreover, these figures represent the worst case as the impact of diversity in a population of SSEGs could result in a lower number being able to reconnect at a particular time due to variations in their primary energy source.

Based on the summary of findings given above, the following proposals are made for further study:

- An investigation of the potential solution to enhance the fault-ride-through capability for a large population of SSEGs.

- Design a control system to control the power flow in the grid-connected mode of operation, maintain voltage and frequency of the system with large population of SSEGs within acceptable operating limits when they island, and resynchronize them with the distribution network before reconnecting them.

- Addressing voltage rise and unbalance issues.

CHAPTER 4

Control Schemes for Converter-Interfaced Small Scale Embedded Generation

4.1 Introduction

This chapter presents the modelling, analysis and design of a power electronic converter (PEC) to be connected between a DC source and the AC grid. In this study a switching model and an ideal voltage source converter model are used. Different control schemes are applied to control the converter-interfaced SSEG in different operating conditions when the SSEG works with no connection to the grid and when the SSEG is connected to the grid. These control schemes are:

- Active and reactive power control (PQ),
- Voltage and frequency (VF) control,
- DC current control, power factor control,
- Voltage/phase angle droop control,
- Active power-voltage (PV) controller and
- Apparent power-voltage (SV) controller.

The objective is to show that with an adequate control the converter can transfer the DC energy from the SSEG and improve the power factor and voltage regulation of the electrical system. Some design considerations are also discussed. The feasibility of the proposed control schemes were verified by simulation studies conducted in PSCAD/EMTDC.

4.2 Converter-Interfaced SSEG

SSEG technologies include small-scale wind turbines, PV arrays, solar thermal collectors and micro combined heat and power (μCHP) connected to the electricity grid at the customer's side (residential) [98]. Unlike conventional synchronous

generation plant, many types of these new technologies are interfaced to the low-voltage distribution network through power electronic converters. Some SSEG technologies such as photovoltaic cells generate DC power whereas other technologies such as gas-fired micro turbines generate AC power at a frequency of a few kHz [92, 99]. The output power from these small sources must be first conditioned as required via DC/AC or AC/DC/AC converters before connecting to the system. The converter provides conversion of the source frequency to the conventional network frequency of 50/60 Hz, and controls the power exchange between the generator and the load/utility network playing thus a vital role to facilitate their integration to the network [99]. Most modern converters which are used for connection of SSEG use controlled power switches (e.g. MOSFETs or IGBTs), generally based on Pulse Width Modulation (PWM) control signals for producing an AC output. Single or three-phase voltage source converters (VSCs) are typically used for SSEG applications. Also, a VSC can be broadly classified as voltage-controlled or current-controlled VSC depending on its control mechanism. The most appropriate VSC should then be chosen based on the requirements of a particular application. Additionally, VSCs are suitable for those applications where voltage stabilization, unity power factor operation and active filtering are required [100].

4.2.1 Converter Characteristics

Power electronic converters have very different characteristics compared to electrical machines. Some of these are [18, 101, 102]:

- Converters do not present the inertia feature.
- Converters have no overloading capability; even slightly too high a current may permanently damage the power electronic components, while rotating machines can provide up to 9 pu of current during faults.
- Converters operate as voltage sources with near instantaneous and independent control of magnitude and angle in each phase.
- The switching action of the converter produces harmonics, which in some cases may only be addressed using filtering equipment.

4.2.2 Operation Principles of Single Phase Voltage Source Converter

Figure 4.1 shows a single-phase full-bridge converter consisting of four power switches (IGBTs), with anti-parallel diodes and a DC source. By turning ON and OFF these switches in a particular manner DC is converted into AC. Two transistors should be on at the same time (g_1 and g_2) or (g_3 and g_4) for a half cycle, which can be done by using a PWM technique.

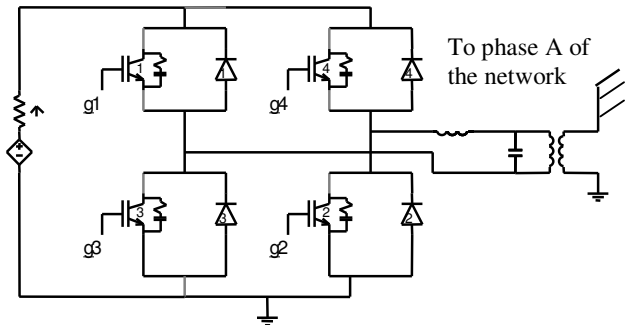

Figure 4.1: Single-phase full-bridge converter connected to the distribution network.

4.2.3 Operation Principles of Three-Phase Voltage Source Converter

A three-phase converter (Figure 4.2) may be considered as three single-phase converters where the output of each of these is shifted by 120º [103]. A carrier wave is compared with the reference signal corresponding to a phase to generate the gating signals for that phase.

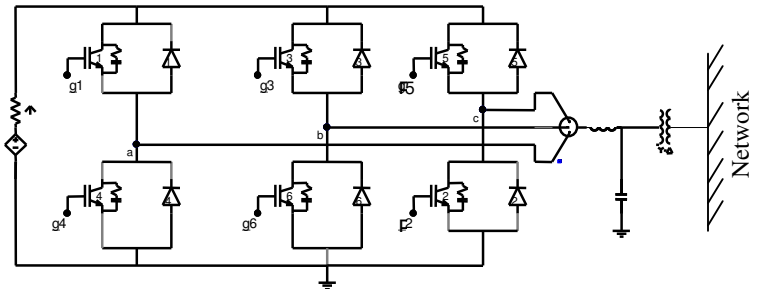

Figure 4.2: Three-phase converter connected to the distribution network.

In the studies conducted in this chapter the single-phase and three-phase converters were modelled and simulated in PSCAD/EMTDC. Appendix C provides further details of the principle of operation of single-phase and three-phase converters with SPWM technique.

4.3 Controller Design and Test for Single Source with no Connection to the Grid

This section focuses on controlling the power flow from a converter-connected single source to the load. In this case the source must supply the active and reactive power depending on load demand with suitable voltage and frequency values. In this case voltage and frequency should be kept constant; therefore a voltage and frequency (VF) control scheme was developed.

4.3.1 Basic Structure of the VF Controller

The basic structure of the VF controller is shown in Figure 4.3. The converter is controlled to maintain constant 220V and frequency 50 Hz by regulating the load terminal voltage using a PI controller. This PI controller generates the amplitude A_r for the SPWM. In order to keep the frequency constant, the reference frequency of a sinusoidal reference waveform is fixed at 50 Hz.

The transfer function of the PI controller is:

$$A_r(s) = \mathrm{K}_{pA}\left[1+\frac{1}{\tau_{iA}S}\right].E_V(s) \tag{4.1}$$

Where $E_V(s) = \left[V_{ref}(s) - V_{meas}(s)\right]$ (4.2)

Where V_{ref} and V_{meas} are the reference voltage and the RMS load terminal voltage respectively. K_{PA} is the proportional gain of the PI controller, τ_{iA} is the integral time

constant of the PI controller that equals $\frac{K_{pA}}{K_{iA}}$, where K_{iA} is the integral gain. All the PI controllers in this work were tuned using the Ziegler –Nichols Rules [104.

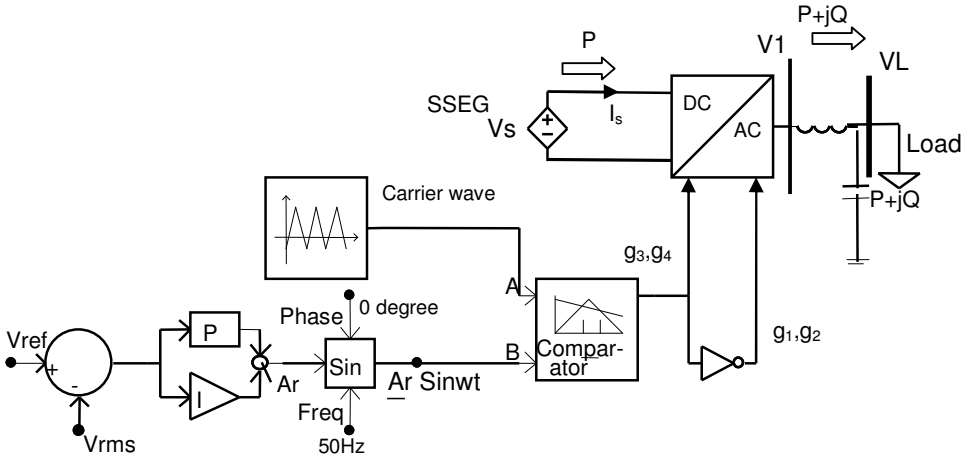

Figure 4.3:Single-phase converter with the SPWM and controller.

4.3.2 Simulation Study for a Single Source

As shown in Figure 4.3 a single–phase converter interfaced small source is connected to the RL load (10 ohm and 0.00265 H). The LC (120 μF and 0.003377 H) filter is added to mitigate the fifth harmonic. The source is controlled to supply the active and reactive power demanded by the load with constant voltage of 220V and frequency of 50 Hz. The output results in Figure 4.4 show the source supplying the power demanded by the load and maintaining the voltage and the frequency at the pre-defined values (220V, 50Hz). This study shows that the converter frequency can be controlled in a different way to that in rotating machine. For rotating machines there is a relationship between the speed and the frequency; in contrast, the frequency of the converter is controlled independently. Also, as shown in Figure 4.4 (c and d) by adding the LC filter the pure sinusoidal waveforms of current and voltage can be measured at the load terminal.

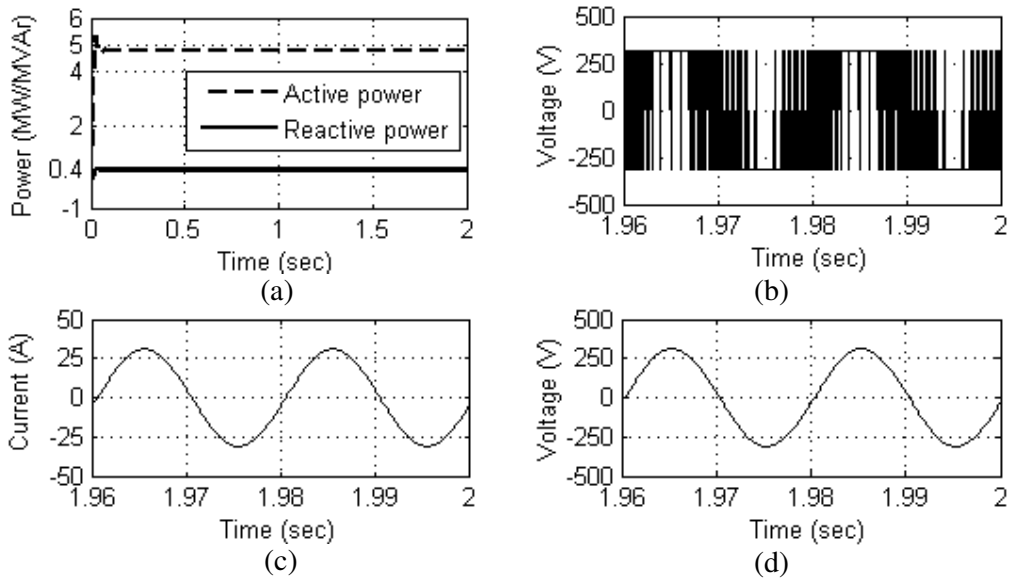

Figure 4.4: Single source with no connection to the grid: (a) Active power and reactive power, (b) Voltage, before LC filter (c) Current and (d) Voltage at load.

4.4 Flexible Control of Converter-Interfaced SSEG

This section focuses on controlling the power flow from converter-connected SSEG to the distribution network. A control scheme is presented which allows controlling independently each phase of the three-phase converter-interfaced SSEG. It is demonstrated that this technique provides additional control flexibility to balance voltages in a distribution network with high penetration of SSEGs. This controller is needed because SSEG installations may include a mix of SSEGs interfaced via single or three-phase converters, which may give rise to voltage unbalance problems. Some controllers used in SSEG applications are based on the synchronously referenced frame and have the disadvantage that the unbalance problem is more difficult to control. In this work a simple control scheme is provided that facilitates independent control of each phase in a three-phase converter. The performance of this controller is tested and explained using case studies implemented in PSCAD.

4.4.1 Small-Scale Embedded Generator Controller Design

The power output of the SSEG can be controlled by controlling the magnitude and angle of the converter output voltage. In this section the typical power angle and

voltage magnitude control method is improved by adding two PI blocks, one for power angle control, and another for voltage magnitude control where power factor is used as a reference value as opposed to reactive power. This is because an SSEG may be required to operate at different power factor conditions. Figure 4.5 illustrates the block diagram of the proposed controller of active power and power factor in a single-phase converter-interfaced SSEG.

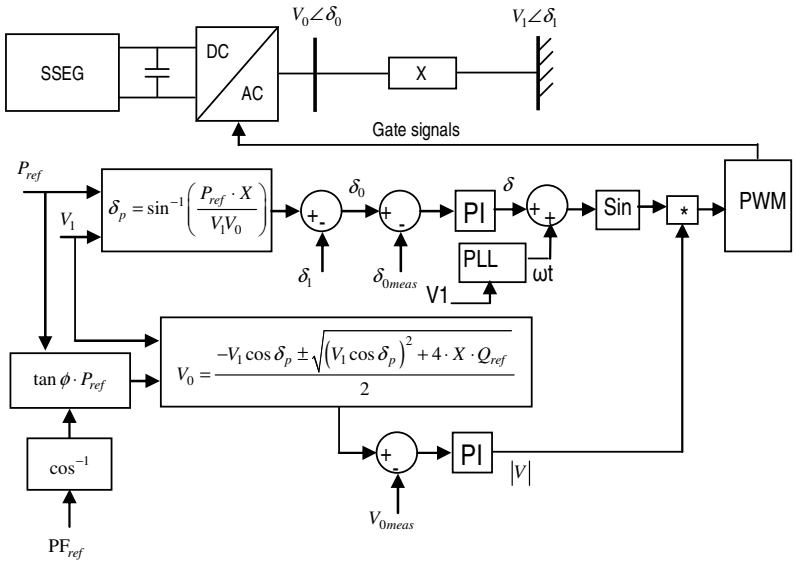

Figure 4.5: Control of active power and power factor for a single phase converter.

The dynamic performance and stability of the power angle control method can be improved by including the additional PI control blocks. The power angle control technique is based on the steady-state relationships given by Eqs. (4.3) and (4.4) [3]. The magnitude of the converter output voltage relative to the grid voltage is manipulated to control reactive power flow. The active power flow is controlled by adjusting the power angle δ_p .

$$P = \frac{V_0 V_1 \sin\delta_p}{X} \tag{4.3}$$

$$Q = \frac{\left(V_1^2 - V_0 V_1 \cos\delta_p\right)}{X} \tag{4.4}$$

$$P_{meas} = I_0 . V_0 \cos\phi \tag{4.5}$$

Where:

P : active power; Q : reactive power

V_1 : grid bus voltage; V_0 : converter terminal AC voltage

δ_1 : power angle of V_1 ; δ_0 : power angle of V_0

X : interconnecting reactance; δ_p : angle difference between V_0 and V_1

I_0 : converter output current

ϕ : phase angle between V_0 and I_0

From Eqs. (4.3) and (4.4), if $\delta_p = 0$ then the active power flow is zero, and the reactive power is determined by the magnitudes of V_0 and V_1. If $V_0 = V_1$ with $\delta_p \neq 0$, then the active power flow is determined by the angle δ_p and the reactive power flow is zero. The load angle δ_p and the converter AC voltage are calculated as:

$$\delta_p = \sin^{-1}\left(\frac{P_{ref} \cdot X}{V_1 V_0}\right) \tag{4.6}$$

$$V_0 = \frac{-V_1 \cos\delta_p \pm \sqrt{\left(V_1 \cos\delta_p\right)^2 + 4 \cdot X \cdot Q_{ref}}}{2} \tag{4.7}$$

Where P_{ref} is the reference value of the active power that needs to be transferred from the SSEG to the grid, and Q_{ref} is the reference value for the reactive power. Two PI control blocks are added to track the difference between the power angle and voltage reference values and their measured values. The maximum and minimum reactive powers depend on the power factor limitation to enhance the efficiency and stability of the system. Minimum reactive power ($Q_{\min}$) represents the minimum value the SSEG has when operating at lagging power factor. Maximum reactive power ($Q_{\max}$) represents the maximum value the SSEG has when operating at leading power factor. The maximum value of voltage ($V_{\max}$) is required when the SSEG operates at a threshold value of leading power factor. The minimum value of voltage ($V_{\min}$) is required when the SSEG operates at a threshold value of lagging power factor. These values are given by:

$$V_{\max} = \frac{V_1 \pm \sqrt{(V_1)^2 + 4 \cdot X \cdot Q_{\max}}}{2} \quad (4.8)$$

$$V_{\min} = \frac{V_1 \pm \sqrt{(V_1)^2 + 4 \cdot X \cdot Q_{\min}}}{2} \quad (4.9)$$

$$Q_{\max} = \frac{\left(V_{\max}^2 - V_{\max} V_1\right)}{X} \quad (4.10)$$

$$Q_{\min} = \frac{\left(V_{\min}^2 - V_{\min} V_1\right)}{X} \quad (4.11)$$

In order to detect the angular positions (ωt) of the voltages waveform, the measured three-phase voltages of the low voltage network are fed to a three-phase PI-controlled Phase Locked Loop (PLL) (the description of PLL is provided in Appendix E). Then this (ωt) is added to the load angle (δ_p) generated by the active power controller. Then the sin of (ωt +δ_p) is taken and multiplied by the output of the reactive power controller (V) to obtain a single phase sinusoidal voltage waveform as defined bellow [95]:

$$v = V \sin\left(\omega t + \delta_p\right) \quad (4.12)$$

This voltage is the input of the PWM unit to generate the gate signals for the converter.

For a SSEG interfaced through a three-phase converter this controller takes the form shown in Figure 4.6 which enables independent control of each phase of the converter. A second order LC filter is used for filtering the PWM switching harmonics of the converter. The LC filter used in this work is tuned to mitigate the third harmonic. The values used are C=30 μF and L=0.03753 H.

Similarly as with the single phase converter, the three phase converter controller generates three phase sinusoidal voltage waveforms as described below [95]:

$$v_a = V_1 \sin\left(\omega t + \delta_a\right) \quad ((4.13)$$

$$v_b = V_1 \sin\left(\omega t + \delta_b - 2\pi/3\right) \quad (4.14)$$

$$v_c = V_1 \sin\left(\omega t + \delta_c + 2\pi/3\right) \quad (4.15)$$

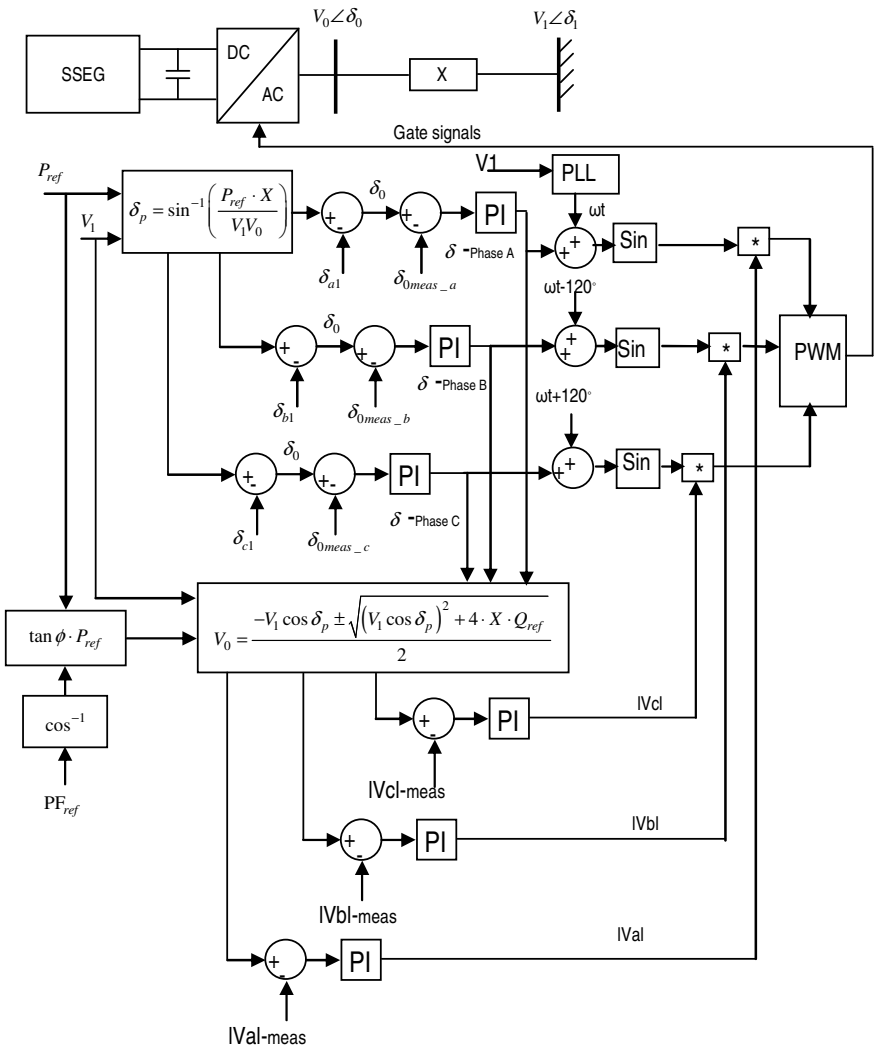

Figure 4.6: Control of active power and power factor for a three-phase converter.

4.4.2 Simulation Studies for Flexible Control

4.4.2.1 Single-Phase Converter -Connected SSEG

The study was conducted with a single–phase converter connected to the network of Figure 3.1 (described in chapter 3). The capacity of the converter is 2kW (connected to one customer). The rated active power P is 2kW, rated AC voltage is 250V, rated unity power factor and the power angle at full rating is 20 degrees. The converter is fed by a DC bus voltage source of 370V. The size of the inductance X is calculated

from the choice that the power angle at full power output is about 20 degrees. This choice guarantees operation in the linear region of the sinusoidal characteristic. The single-phase converter is connected to the network through a transformer (250/250 V) for isolation purpose.

The performance of the controller is tested by changing the active power set point with unity power (zero reactive power). As shown in Figure 4.7 the output active and reactive powers from the converter follow the reference values.

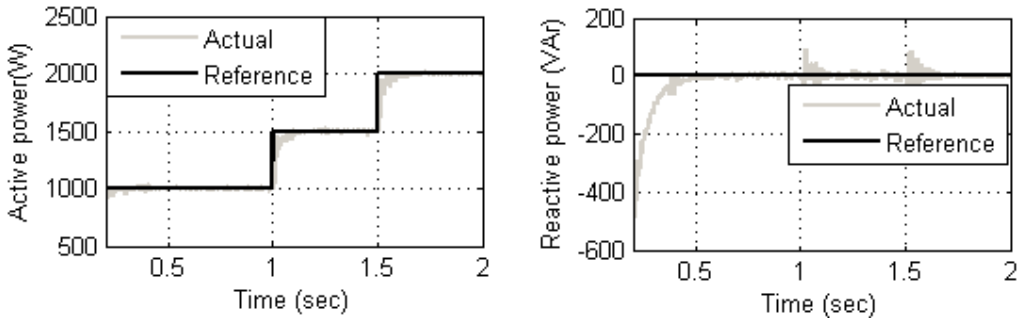

(a) (b)

Figure 4.7: Response of active and reactive powers to step-changes in demand

4.4.2.2 Three-Phase Converter-Connected SSEG

The study was conducted with a three–phase converter connected to the network of Figure 3.1. The capacity of the converter is 11kVA (connected to a commercial load 11kVA). Rated active power P =10kW, rated AC voltage 433V, rated power factor PF = 0.95 and power angle at full rating is 5.77 degrees. The converter is fed by a DC bus voltage source of 860 V. The size of the inductance X is calculated in such way as to get the power angle at full power output about 5.77 degrees. This choice guarantees operation in the linear region of the sinusoidal characteristic.

A Performance of Controller Different Demand Power among Phases

As shown in Figure 4.8(a) the desired power from phase A is 3.33kW, from phase B is 2.4kW and from phase C is 1.5kW all working at PF=0.909. It is observed that the

performance of the controller is correct with minimized steady-state error and no overshoot. As shown in Figure 4.8(b) the reactive power for every phase is different in order to maintain the power factor of all three phases at the desired value, PF=0.909. The controller sends the appropriate signals to the PWM generator to adjust the modulation index of every phase depending on the desired power factor as illustrated in Figure 4.8(c). Thus, by using this control approach the voltage imbalance problem may be solved. Also as illustrated in Figure 4.8(d) the sinusoidal phase currents present different amplitudes.

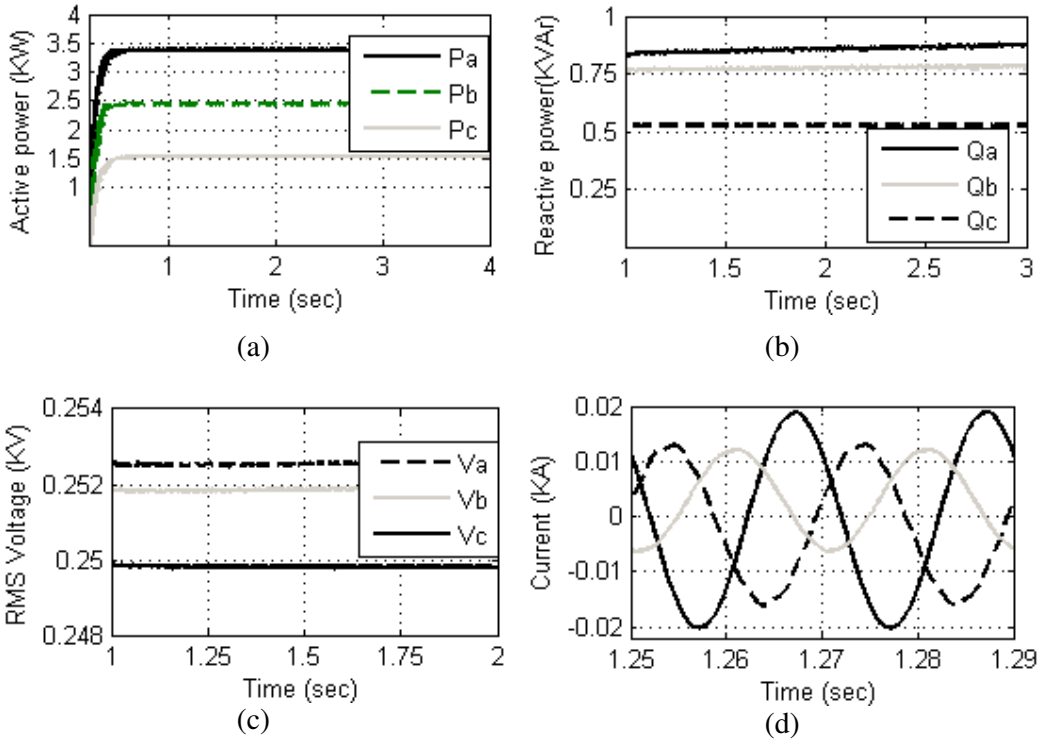

Figure 4.8: Performance of the three-phase converter controller with different power references among phases: (a) active power output (b) Reactive power output (c) output voltage at the desired power factor (d) Three-phase converter output currents at the desired power factor.

B Performance of Controller to Step-Changes in Demand

At time 1.75 sec the desired power from phase B is changed from 2.4 kW to 3.33 kW. Also the desired power from phase C is changed from 1.5 kW to 3.33 kW. As

shown in Figure 4.9(a) the output active power of every phase follows the desired values. The source operates at PF=0.909. As shown in Figure 4.9(b) and Figure 4.9(c) the controller changed the terminal phase voltages due to the change in desired reactive power. This is because the controller is designed to maintain fixed power factor in every phase. Also as shown in Figure 4.9(d) the phase currents are sinusoidal and have low harmonic distortion: THD= (phase A=0.267%, phase B=0.324% and phase C=0.46%).

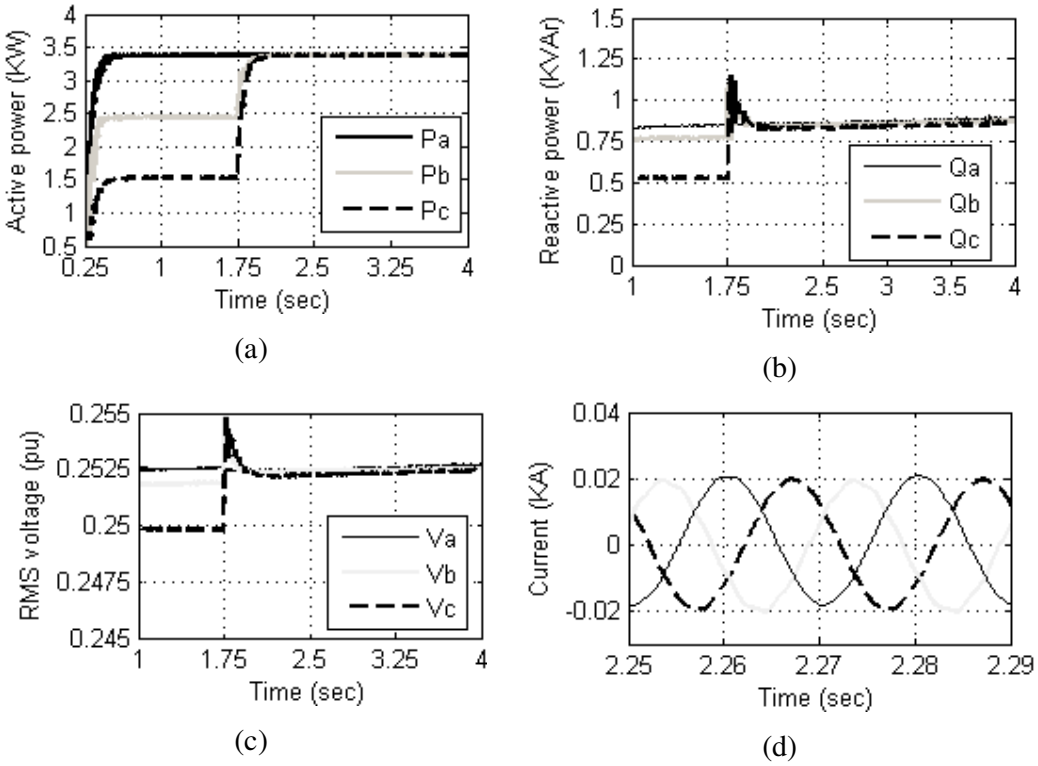

Figure 4.9: Response of the three phase-converter to step-changes in demand: (a) Active power (b) Reactive power, (c) Three-phase RMS output voltages & (d) Three-phase converter output voltages

4.5 DC Current Control for Converter -Interfaced SSEG

This section presents the analysis and design of a SSEG DC current control. As shown Figure 4.10 the DC source injects DC power to the AC system through the converter. In order to protect the converter from over current and the source from overload, such a controller is needed to keep the DC average current below the

maximum value. The study was conducted with a single–phase converter-interfaced SSEG connected to the network of Figure 3.1 (described in chapter 3). The capacity of the SSEG is 3 kVA (S_{rated}=3kVA). Rated AC voltage 250V and power angle at full rating and unity power factor is 8.5 degrees. This choice guarantees operation in the linear region of the sinusoidal characteristic. The single-phase converter is connected to the network through a single-phase transformer (250/250V), for isolation purposes. The size of the inductance X between the converter and the transformer is 1.885 ohm. Also a PLL is used for the same purpose as mentioned before.

4.5.1 Basic Structure of DC Current Controller

The basic structure of the DC current controller considering constant reactive power is shown in Figure 4.10. The first PI controller regulates the DC current by generating the proper reference active power for the active power controller, as described in the following equations:

With regard to Figure 4.10 the average DC current I_s when the losses are neglected is:

$$I_s = \frac{P}{V_s} \tag{4.16}$$

The transfer function of the PI controller is:

$$P_{ref}(s) = \mathrm{K}_{pI}\left[1 + \frac{1}{\tau_{iI} S}\right].E_{Is}(s) \tag{4.17}$$

Where $E_{Is}(s) = \left[I_{s-ref}(s) - I_{s-meas}(s)\right]$ (4.18)

where I_s,V_s and P are the instantaneous value of the average DC current from the source, the instantaneous value of the DC voltage and the converter active power output respectively. K_{PI} is the proportional gain of the PI controller, τ_{iI} is the integral time constant of the PI controller equals to $\frac{K_{pI}}{K_{iI}}$ where K_{iI} is the integral gain.

4.5.2 Basic structure of the Active Power (P)-Controller

After the DC current controller generates the proper reference active power (P_{ref}) the function of the active power (P) controller is to control the active power. As shown in Figure 4.10, the second PI controller would suffice to control the flow of active power by generating the proper values for δ_p, based on the instantaneous values of current and voltage taken from the converter output terminal, as described in the following equations:

From Eq. (4.18) the transfer function of the PI controller is:

$$\delta_p(s) = \mathrm{K}_{p\delta}\left[1 + \frac{1}{\tau_{i\delta} S}\right].E_P(s) \tag{4.19}$$

Where $E_P(s) = \left[P_{ref}(s) - P_{meas}(s)\right]$ (4.20)

$\mathrm{K}_{p\delta}$: proportional gain of the PI controller,

$\tau_{i\delta}$: integral time constant of the PI controller equal to $\frac{\mathrm{K}_{p\delta}}{\mathrm{K}_{i\delta}}$ where $\mathrm{K}_{i\delta}$ is the integral gain.

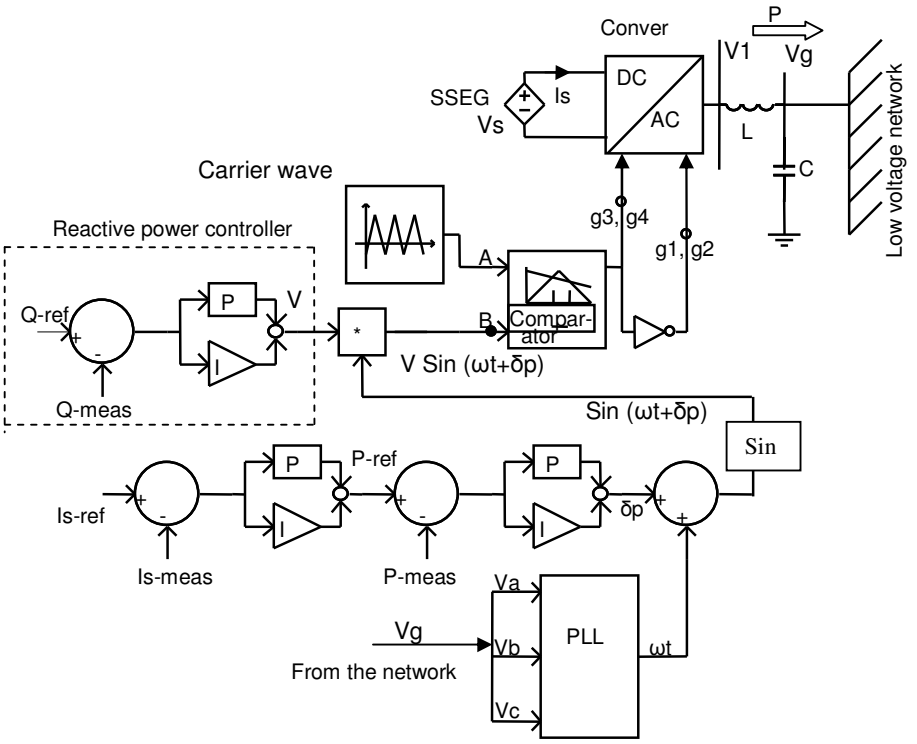

Figure 4.10: DC current controller considering constant Q.

4.5.3 Basic Structure of the Reactive Power (Q) - Controller

As shown in the dashed frame of Figure 4.10, the function of the PI controller is to control the flow of the reactive power (Q) by generating the proper values of the voltage magnitude (V), based on the reference reactive power required by the system, as described in the following equations:

The transfer function of the PI controller is:

$$V_{ref}(s) = \mathrm{K}_{PV}\left[1+\frac{1}{\tau_{iV} S}\right].E_Q(s) \tag{4.21}$$

Where $E_Q(s) = \left[Q_{ref}(s) - Q_{meas}(s)\right]$ (4.22)

K_{pV} : Proportional gain of the PI controller

τ_{iV} : Integral time constant of the PI controller which equals $\frac{K_{pV}}{K_{iV}}$ where K_{iV} is the integral gain, Q_{meas} : measured reactive power.

The reactive power is determined by the magnitudes of V_0 and V_1 as described in equation (4.4). If $V_0 = V_1$ then the reactive power flow is zero.

Also $Q_{meas} = I_0.V_0 \sin\phi$ (4.23)

For choosing the reactive power reference value, some careful consideration must be given. The reference reactive power must be selected within the limit of the source. Also the value of power factor must be higher than 0.75 as specified by the manufacturer [105]. The value of reactive power that the source can inject or absorb to or from the grid is given by:

$$Q_{ref} = \sqrt{\left(S^2_{rated} - (I_s V_s)^2\right)} \tag{4.24}$$

$$I_s V_s = P \tag{4. 25}$$

Minimum reactive power ($Q_{\min}$) represents the minimum value the source has when operating at lagging power factor. Maximum reactive power ($Q_{\max}$) represents the maximum value the source has when operating at leading power factor. The maximum value of voltage ($V_{\max}$) is required when the source operates at a threshold value of leading power factor. The minimum value of voltage ($V_{\min}$) is required when

the SSEG operates at a threshold value of lagging power factor. These values are given by equations (4.8, 4.9, 4.10 and 4.11).

To determine the maximum DC current that the SSEG can inject to the converter DC side we assume that the SSEG is operated at unity power factor (Q=0) at the AC side, that is, $P = S_{rated}$. Thus the value of the maximum DC current will be:

$$I_s = \frac{3000}{370} = 8.1\,\text{A}.$$

If the power factor assumed in this case is 0.95 leading then from equations (4.5) and (4.20) the reference values of active and reactive power are:

$$P_{ref} = 3000 \times 0.95 = 2.85\,\text{kW}$$

$$Q_{ref} = \sqrt{\left((3000)^2 - (2850)^2\right)} = 936.7\,\text{kVAr}$$

($Q_{\max} = 936.7\,\text{kVAr}$ capacitive or $Q_{\min} = -936.7\,\text{kVAr}$ inductive).

Then from equations (4.8, 4.9) the value of $V_{\max} = 256.87\,\text{V}$ and the value of $V_{\min} = 242.72\,\text{V}$ will be the limits of the Q controller.

4.5.4 DC Current Controller Considering Constant Power Factor

Instead of operating the source at constant reactive power, the source can be controlled to be operated at constant power factor. This can be achieved by adding a block on the DC current controller as shown in Figure 4.11. The basic structure of this controller is similar to the controller shown in Figure 4.10 the only difference is the part which is added to the controller according to the following equation:

$$Q_{ref} = P_{ref} \tan\phi \qquad (4.26)$$

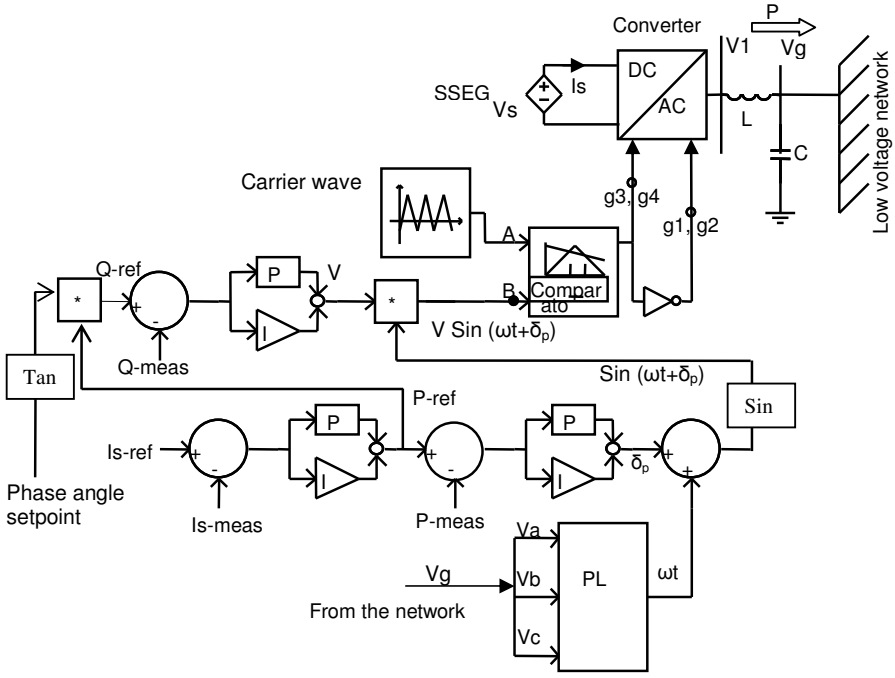

Figure 4.11: DC current controller considering constant power factor.

4.5.5 Response of the Controller to Load Variations

The aim of this study is to investigate the response of the controller when an additional load (18kW/5.9kVAr) is connected to the low-voltage network at t=1sec. This test was performed with the SSEG operating at a 0.95 leading power factor (reference reactive power is 0.986 kVAr). As illustrated in Figure 4.12 the performance of the controller has been evaluated, proving it to be stable against a load disturbance. However in this case the function of the controller is to maintain the constant DC current and constant reactive power output. Also there is a positive impact on the converter AC output current as it is also regulated by regulating the DC current.

.

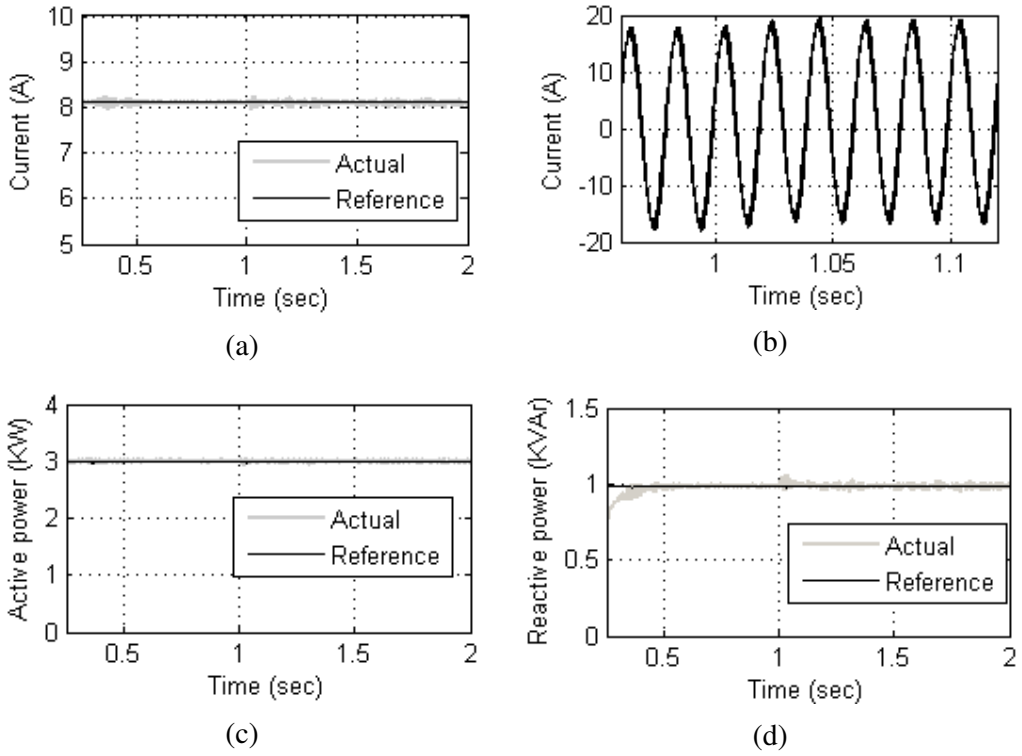

Figure 4.12: Performance of the controller during a load disturbance: (a) DC current (b) AC current waveform (c) and (d) output active and reactive powers.

4.5.6 Response of the Controller to Changes in the DC Current Set point

The aim of this study is to investigate the performance of the DC current controller with an additional loop to control power factor. The study was done when the DC current set point is changed due to a change in the operational conditions of the prime mover. In this case the current set point is changed from 0.6 pu to 0.75 pu at t=1 sec and to 1.0 pu (full load current) at t=1.5 sec. Concerning the results shown in Figure 4.13, some observations can be made. First the controller demonstrates a good response to a change in the set point. Second as shown in Figure 4.13(a) and (b) the DC current follows the reference value generated by the DC current controller and the AC output current transfers smoothly to the new operating condition. Third, as shown in Figure 4.13 (c) and (d) the active power output follows the reference output power generated by the controller and the reactive power changed depending on the reactive power and power factor reference values.

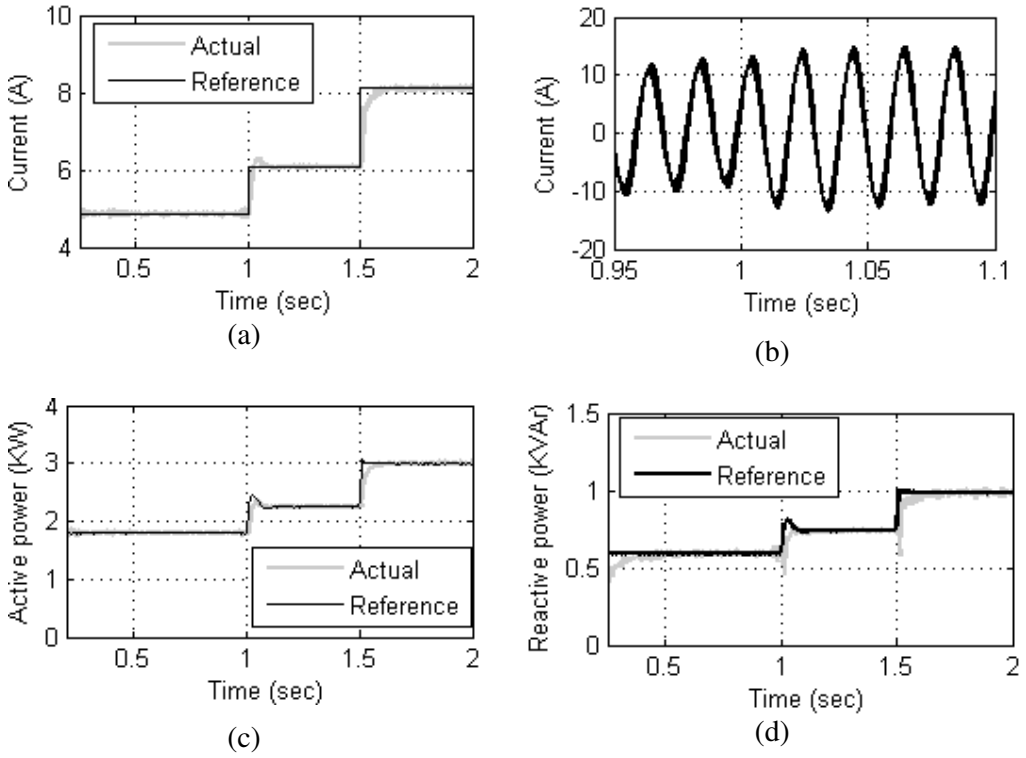

Figure 4.13: Performance of the controller during a change in the DC current set point: (a) DC current (b) AC current waveform (c) and (d) output reactive and active powers.

4.6 Voltage/Phase Angle Droop Control for SSEG

Voltage regulation is necessary for local reliability and stability. Without local voltage control, a system with high penetration of SSEG could experience voltage and/or reactive power oscillations [49]. In SSEG systems there is the problem of circulating reactive currents. With small errors in voltage set points, the circulating current can exceed the rating of the sources. Most research conducted to date uses a voltage/reactive power droop controller to solve this problem [49, 51, 53, 102, 106] However, little attention is given to operating the SSEG within the appropriate power factor range (0.95 lagging or leading). This range is mentioned in the Engineering Recommendation G83/1 that says that when the DG operates at rated power it should operate at a power factor within the range 0.95 lagging to 0.95 leading [107]. In order to satisfy this requirement the converter droop controller is modified in this work to become a voltage/phase angle droop controller. The controller manipulates

the terminal voltage of the converter at the required power factor whilst observing the specified limits. The function of the basic controller is shown in Figure 4.14. The phase angle limit (φ) shown in the figure is a function of the power factor limit.

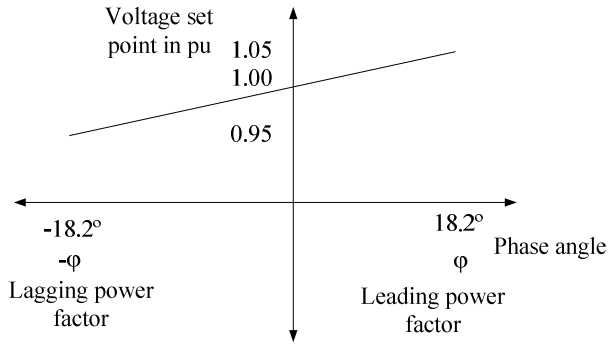

Figure 4.14: Voltage/phase angle droop.

4.6.1 Basic Structure of the Voltage/Phase Angle Droop Controller

Figure 4.15 shows a voltage/phase angle droop control block diagram based on specified set points for voltage control of SSEG. It consists of two PI controllers. RMS phase to ground voltages are measured in the bus where the source is connected. These values are compared with the reference value (for example the nominal value, 1pu). The error voltage is the input of the first PI controller to regulate the terminal voltage within the appropriate power factor range (0.95 lagging or leading) by generating a reference phase angle (limit $\varphi = \pm 18.2$). The reference reactive power is produced from the product of the tangent of this phase angle and the reference active power, as described in the following equation.

$$Q_{ref} = P_{ref} \tan\phi \qquad (4.27)$$

This reference reactive power is the set point of the second PI controller. The second PI controller would suffice to control the flow of reactive power by generating the proper values for V as described before (section 4.5.3). The SSEG injects reactive

power if the voltage falls below the nominal value and absorbs reactive power if the voltage rises above its nominal value.

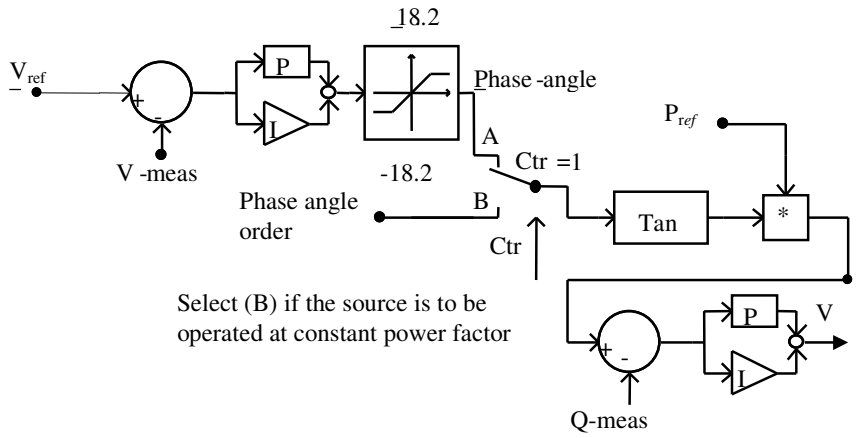

Figure 4.15: Voltage regulations through voltage-phase angle droop.

The following equations describe the transfer function of the controller.

$$\phi_{ref}(s) = \mathrm{K}_{pv}\left[1 + \frac{1}{\tau_{iv} S}\right].E_{vl}(s) \tag{4.28}$$

$$\text{Where } E_{vl}(s) = \left[V_{L-ref}(s) - V_{L-meas}(s)\right] \tag{4.29}$$

In addition, there is an additional switch that allows the controller to operate at constant power factor. For constant power factor operation, the input value to the controller is the phase angle that is related to the chosen power factor.

4.6.2 Simulation Results of the Controller

Studies were conducted to explore the performance of the controller in both steady state and transient operation for single-phase and three-phase converters. In the following plots the current and voltage waveforms are shown together. The three-phase voltages and currents are shown only for phase A in the bus where SSEG is connected to the network. Active and reactive powers measured and reference values, phase angle and load voltage are also shown.

4.6.2.1 Simulation Results for Single-Phase Converter Interfaced SSEG

In this subsection the study was conducted with a single–phase converter (switching model) connected to the network of (Figure 3.1). The capacity of the source is 3kVA**,** rated active power is 2850kW and rated AC voltage is 250V. The converter is fed by a DC bus voltage source of 370 V. The single-phase converter is connected to the network through a single-phase transformer (250/250 V) for isolation purposes.

A Output Results for the Controller during Steady State Conditions

The aim is to investigate the performance of the controller when the load terminal voltage is equal to the set point as shown in Figure 4.16 (the period between 0-1sec). In this case the controller has to generate unity power factor reference which means there is no reactive power absorbed from or injected to the network.

B Response of the Controller to Disturbance

The aim of this study is to investigate the response of the controller when an additional load (18kW/5.9kVAr) is connected to the low-voltage network at t=1sec. This test was performed when the SSEG is operating at unity power factor (the voltage set point at V=1pu) as illustrated in Figure 4.16. When the new load is connected the load voltage decreases but the controller responds rapidly to operate the source at leading power factor in order to inject reactive power to the network.

4.6.2.2 Simulation Results for Three-Phase Converter Interfaced SSEG

In this subsection the phase angle/voltage droop control technique has been used to control a three–phase converter-interfaced SSEG which is connected to supply a domestic load. The capacity of the SSEG is 15.1 kVA and it is connected to the low-voltage network (Figure 3.1) through a three-phase power transformer.

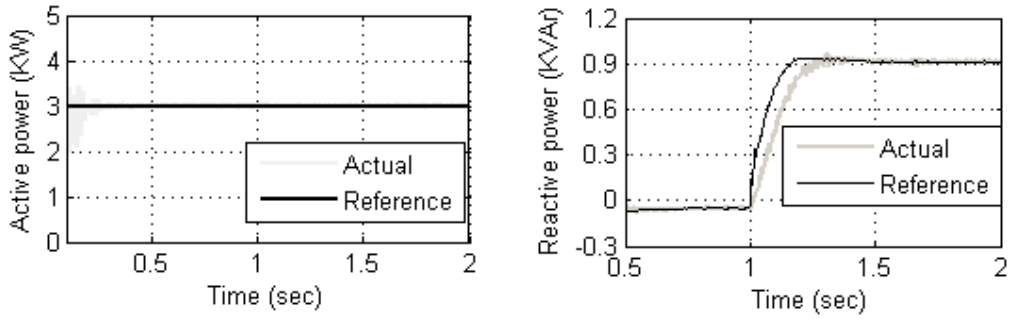

(a)

(b)

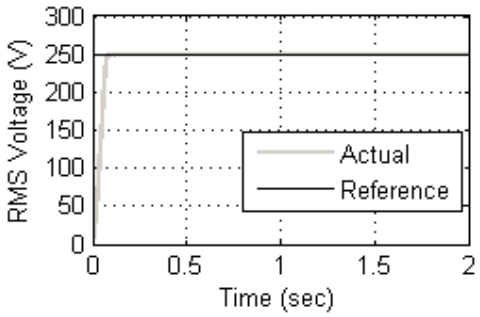

(c)

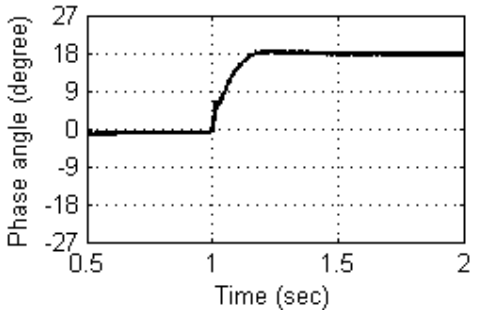

(d)

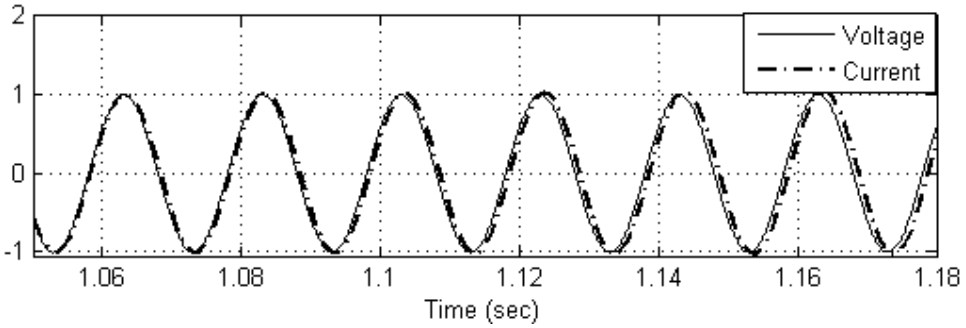

(e)

Figure 4.16: Response of a voltage/phase angle droop controller for single–phase converter to load increase: (a) Active power, (b) Reactive power response, (c) RMS load voltage, (d) phase angle response and (e) Transfer from unity power factor to leading power factor (Fundamental voltage and current waveforms).

A Results for the Controller during Steady State

To investigate the response of the controller the load terminal set point is changed to values over, under and at 1 pu. First the response of the controllers when the load terminal voltage is equal to the set point as shown in Figure 4.17 (the period between

0-5sec) is investigated. In this case the controller has to generate unity power factor reference which means there is no reactive power absorbed from or injected to the network. The response of the controller when the load terminal voltage is lower than the set point is shown in Figure 4.18 (the period between 0-5sec). In this case the controller has to generate a leading power factor reference to inject reactive power to the network. Figure 4.19 (the period between 0-5sec) shows the response of the controller when the load terminal voltage is higher than the set point. In this case the controller has to generate lagging power factor reference to absorb reactive power from the network.

B Response of the Controller to Load Variations

The aim of this study is to investigate the response of the controller when an additional load (15 kW/5kVAr) is connected to the low-voltage network at t=5sec. The first test when the voltage set point at (V=1pu, unity power factor), the second test when (V>1.00pu, leading power factor) and the third test when (V<1.00pu, lagging power factor).

In the first case the source is operating at unity power factor. However, as shown in Figure 4.17, when the new load is connected the load voltage decreases but the controller responds rapidly to operate the source at leading power factor in order to inject reactive power to the network to support the voltage.

In the second case the source is operated at 0.95 leading power factor when the load is connected at 5 sec. As shown in Figure 4.18 the voltage decreases but in this case the power factor controller does not modify the source operation because they are already operating at the threshold value of leading power factor.

In the third case the source is operated at 0.95 lagging power factor (absorbing reactive power from the network) when the new load is connected at 5 sec. As shown in Figure 4.19 the voltage decreases, however the power factor controller reacts to modify the operation of the source to leading power factor in order to inject reactive power into the network and compensate for the new load power demand.

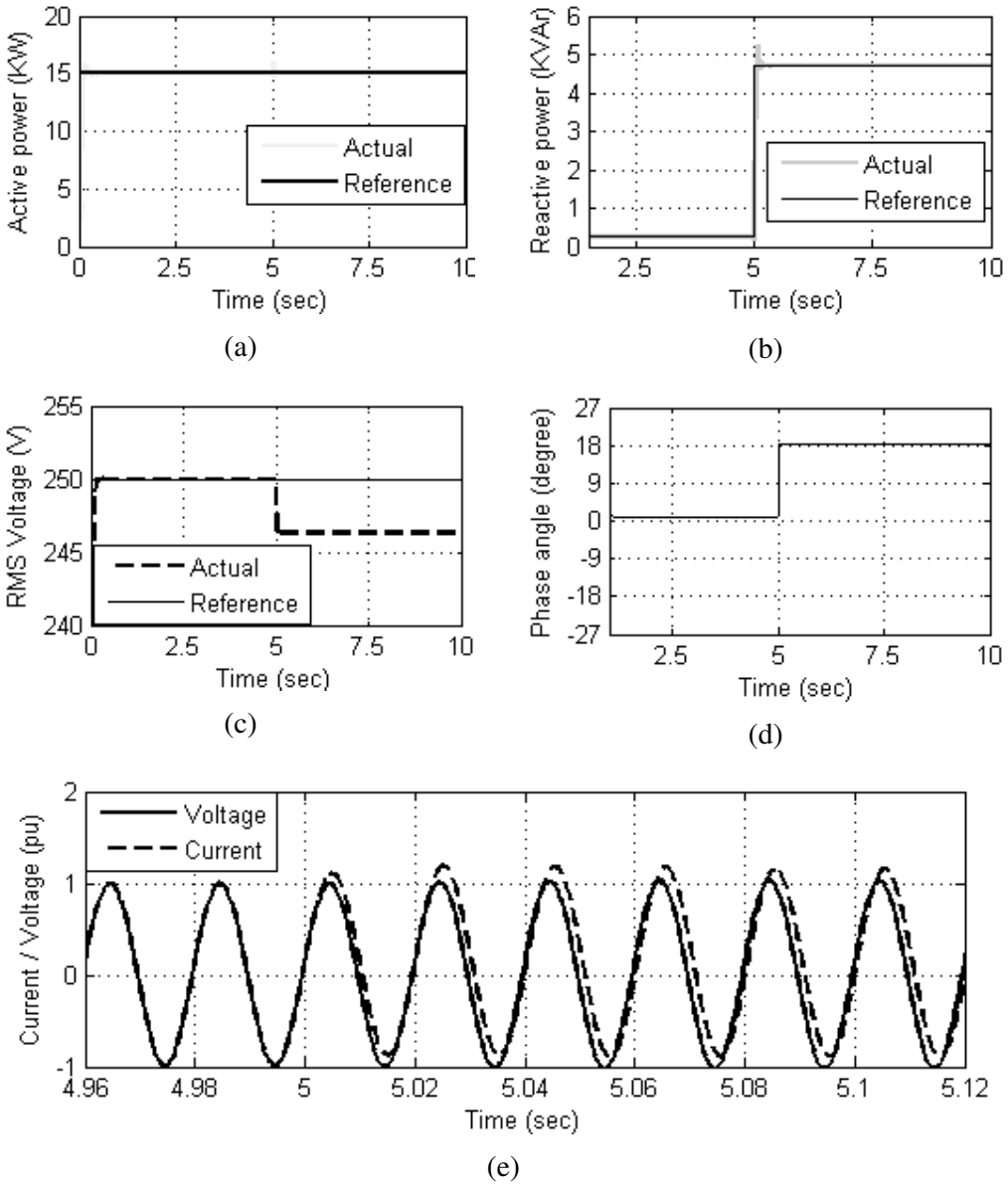

Figure 4.17: Response of a voltage/phase angle droop controller for three–phase converter to load increase (at unity power factor): (a) Active power, (b) Reactive power response, (c) RMS load voltage (d) phase angle response and (e) Transfer from unity power factor to leading power factor (voltage and current waveforms).

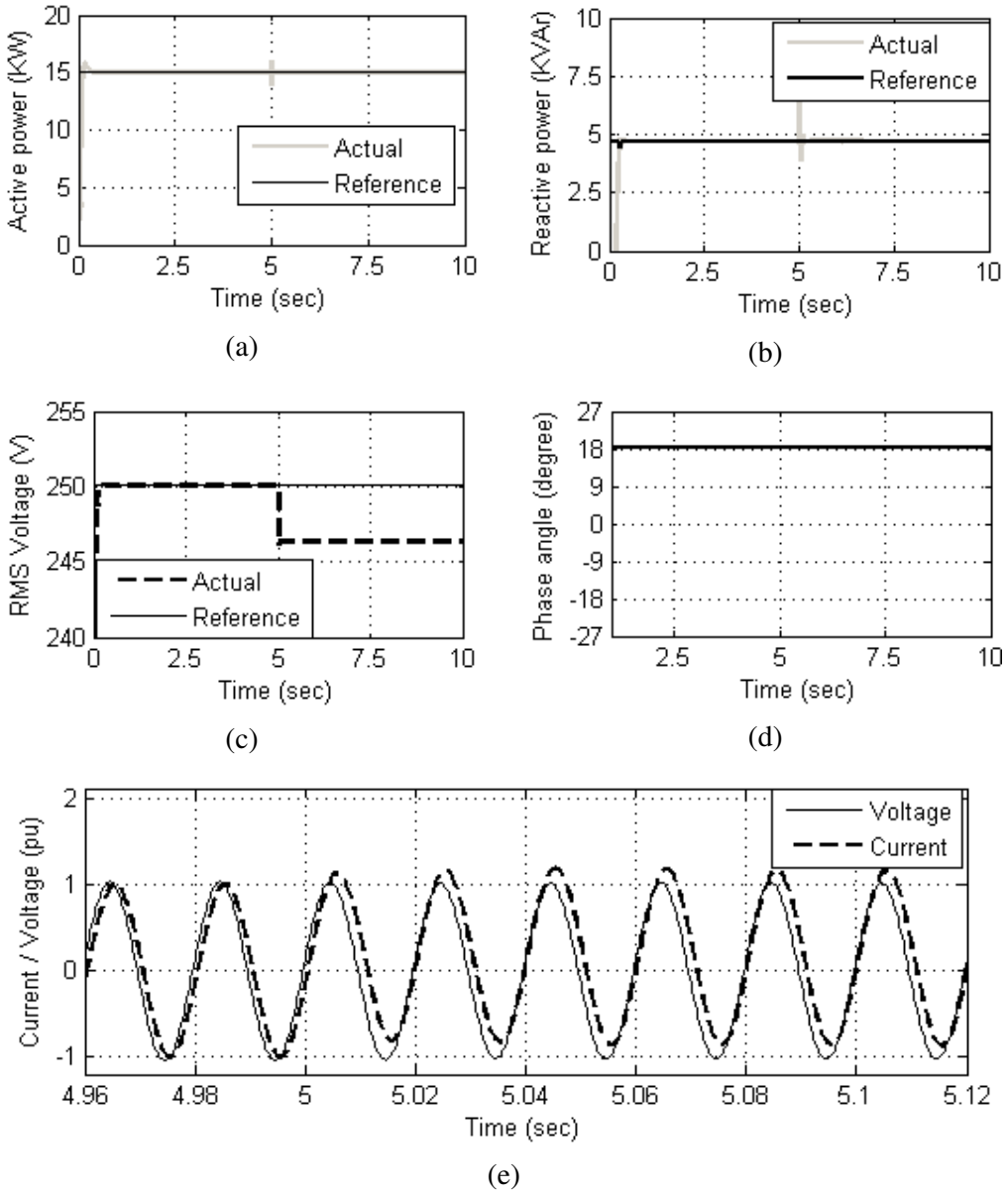

Figure 4.18: Response of a voltage/phase angle droop controller for three–phase converter to load increase (at 0.95 leading power factor): (a) Active power, (b) Reactive power response, (c) RMS load voltage (d) phase angle response and (e) Voltage and current waveforms.

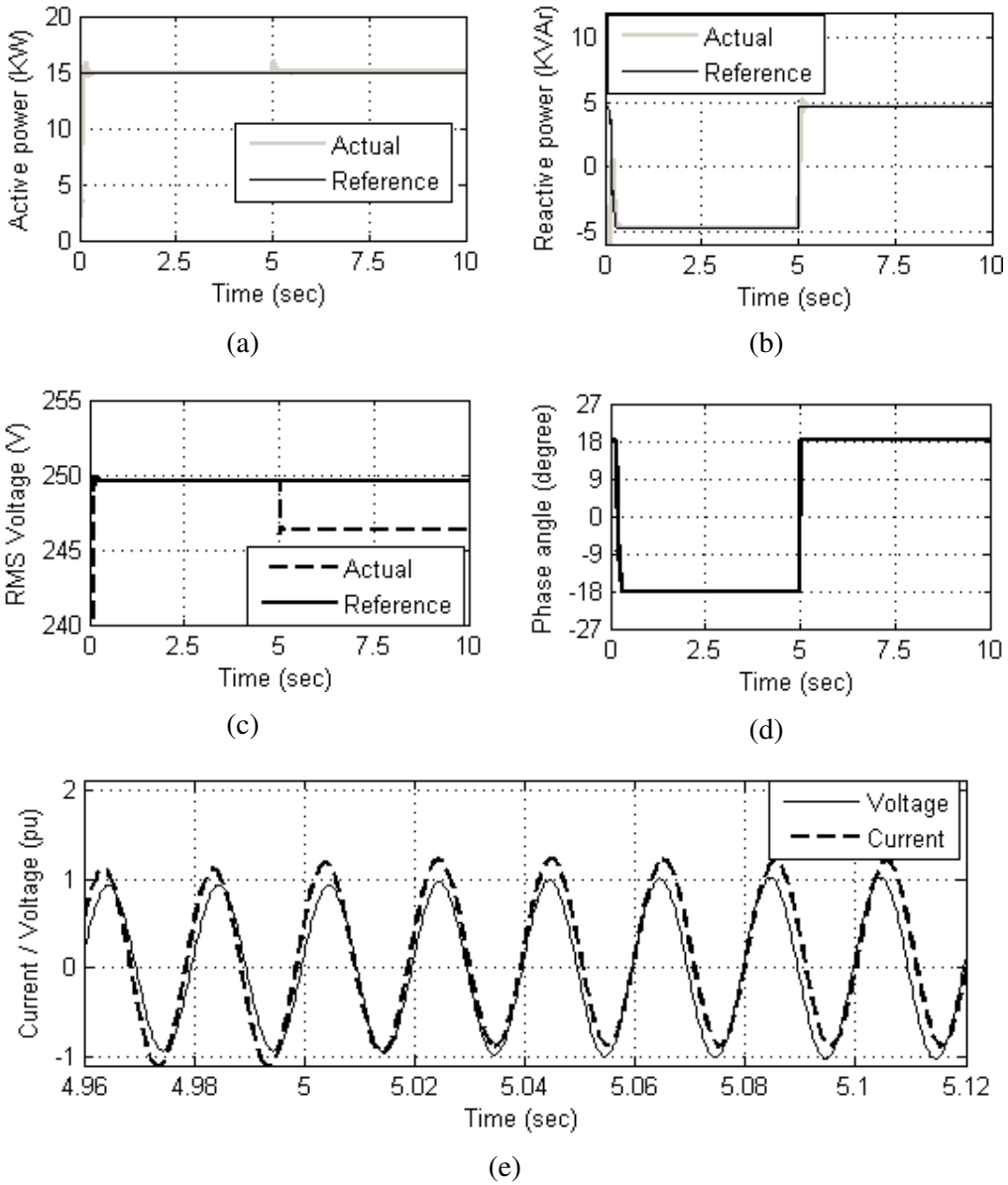

Figure 4.19: Response of a voltage/phase angle droop controller for three–phase converter to load increase (at 0.95 lagging power factor): (a) Active power, (b) Reactive power response, (c) RMS load voltage (d) phase angle response and (e) Transfer from lagging factor to leading power factor (voltage and current waveforms).

4.7 Relationship between Phase Angle and Converter Terminal Voltage

In this study the relationship between phase angle and converter terminal voltage and the performance of the controller was also investigated for different power factor

values (0.95 lagging to 0.95 leading) using the same network (Figure 3.1). As shown in Figure 4.20, the simulation results indicate that this relationship is essentially linear.

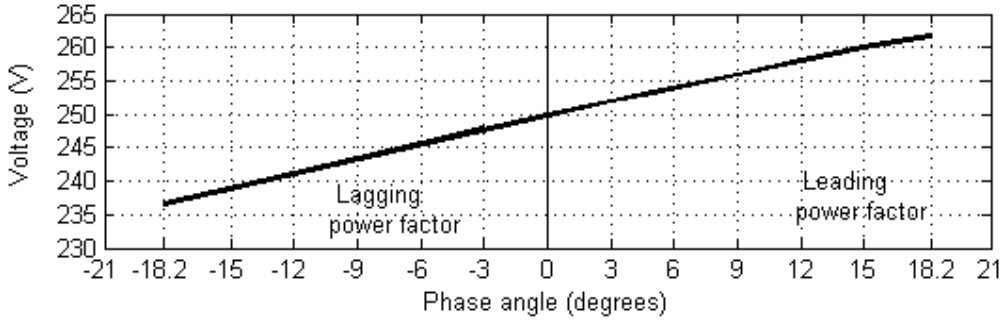

Figure 4.20: Relationship between phase angle and converter terminal voltage.

4.8 Active Power-Voltage and Apparent Power-Voltage Controllers

This section deals with SSEG connected to the network of (Figure 3.1) as a weak low voltage network with low fault level (1.14MVA). In order to support the voltage magnitude of this low voltage network, two control techniques namely active power-voltage (PV) controller and apparent power-voltage (SV) controller, have been used to achieve this task.

4.8.1 Active Power-Voltage (PV) Controller

This section focuses on controlling the active power flow from a converter-connected SSEG unit to the low voltage distribution network and supports the network voltage magnitude by generating the adequate voltage magnitude. The controller works similarly to a PQ controller but the reactive power is variable according to the network voltage need. This value of the reactive and active power should be within the VA capacity of the source. The maximum and minimum voltage values depend on the estimated reactive powers that the source needs to inject or absorb. When the voltage of the network at the converter connection point dips, the converter needs to inject reactive power by raising the value of its terminal voltage to more than 1pu.

On the other hand when the voltage swells the source absorbs reactive power by reducing the terminal voltage to a value lower than 1pu. The maximum and minimum values of voltage can be determined by equations (4.8) and (4.9). The maximum reactive power (leading or lagging) considering the rated apparent power of the converter is given by [95]:

$$Q = \sqrt{\left(VA_{rated}^2 - P_{ref}^2\right)} \tag{4.30}$$

$$Q_{\max} = \frac{P_{ref}}{PF} \tag{4.31}$$

In this case the source may inject reactive power to the system or absorbs reactive power from the system. The capacity of the source that is used in this study is 15.1kVA. If the power factor assumed in this case is 0.75 leading then from equations (4.2, 4.3) P_{ref} =11325 W and $Q_{\max}$ will be $Q_{\max} = \frac{P_{ref}}{0.75} = 9987.7$ VAr from equation (4.8) the value of $V_{\max}$ =467 V is obtained. For calculation of $V_{\min}$ the power factor is 0.75 lagging and from equation (4.9), then of $V_{\min}$ =377 V. $V_{\max}$ and $V_{\min}$ will be the limits of the V controller.

The basic structure of the PV controller is the combination of the previously described P and V controllers generating the proper values for voltage angle δ_p and magnitude V.

4.8.1.1 Simulation Results of the PV Controller

In this section some basic simulations have been performed based on models which were discussed in previous sections. Through these simulations two case studies were considered. One case study addresses the controller performance during steady state conditions and the other case study investigates the performance of the controller during disturbances.

4.8.1.2 Results of the PV Controller during Steady State Conditions

The PV controller is applied to control active power and support the grid voltage. The results are shown in Figure 4.21 (the period between 0-5sec). The results show the response of the controller during steady state operation which proves stable operation of the source.

4.8.1.3 Response of the PV Controller to An Increase in Load

The aim of this study is to investigate the response of the controller when an additional load of 28kW and 5kVAr is inserted to the network at t=5sec. As illustrated in Figure 4.21, the source maintains the same reference active power and injects reactive power to the system to support the voltage. This reactive power is within the capacity of the source.

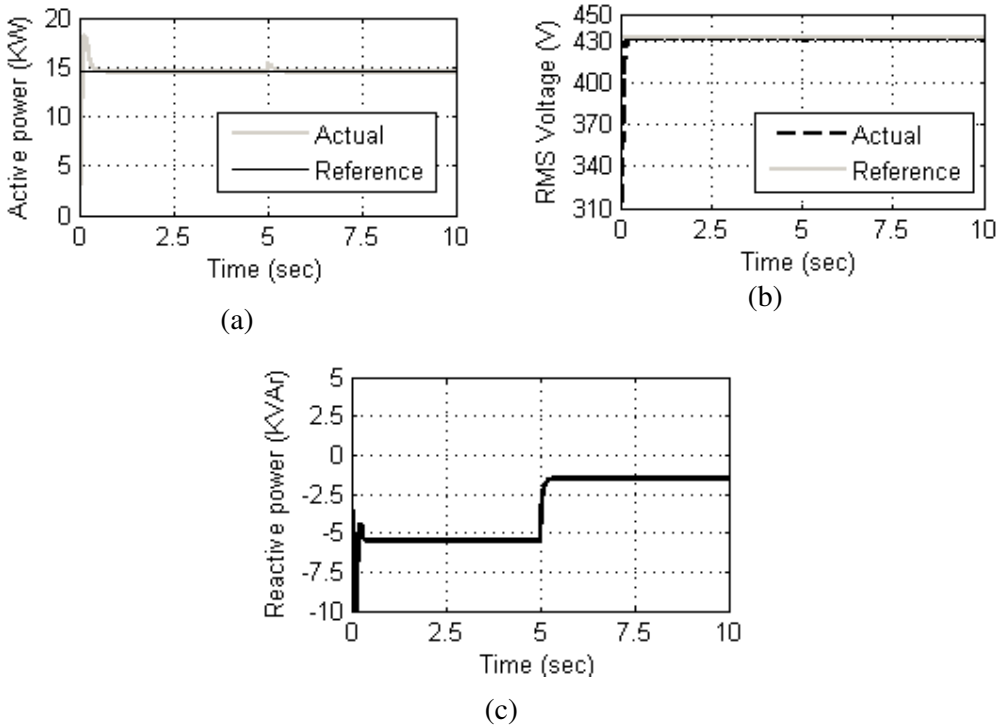

Figure 4.21: Performance of the PV controllers during steady state and disturbance conditions: (a) Active power output, (b) Terminal voltage and (c) Reactive power.

4.8.2 Apparent Power-Voltage (SV) Controller

This section focuses on controlling the apparent power flow from converter-connected SSEG units to the low-voltage distribution network and supporting the network voltage magnitude by generating adequate voltage magnitude. This technique is useful for converter interfaced storage devices or for custom power devices (DSTATCOM, DVR, USSC, etc). In this case the controller works in a similar way to the PV controller but the amount of active power is not constant. The difference here is that the values of the active power and the reactive power are determined by the converter apparent power rating and the phase angle required by the V controller described in section 4.6.

4.8.2.1 Basic Structure of the SV Controller

As shown in Figure 4.22, based on the reference apparent power S_{ref}, the first part of the controller calculates the reference active power by converting the reference phase angle ϕ required by the V controller and apparent power S_{ref} from polar form to rectangular form that generates *P* and *Q*, which are taken as input values to the PI controllers. Thus, these PI controllers would suffice to control the flow of active power and reactive power by generating the proper values for δ_p and V based on the instantaneous values of active and reactive power taken from the converter output terminal (*P* and *Q* controllers are described in 4.5.1 and 4.5.2). These values of *P* and *Q* are given by:

$$S = \sqrt{3} I.V \angle \phi \quad (4.32)$$

In polar form $S = |S| \angle \phi$ (4.33)

In rectangular form $S = P + jQ$ [95] (4.34)

Where $P_{ref} = S_{ref} \cos\phi$ (4.35)

$$Q_{ref} = S_{ref} \sin\phi \quad (4.36)$$

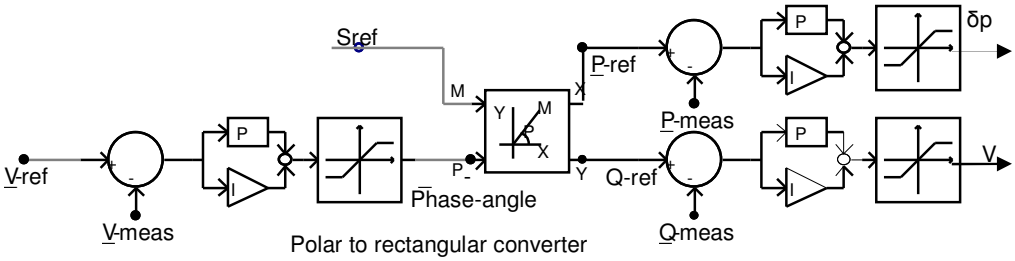

Figure 4.22: Basic structure of the S controller.

4.8.2.2 *Simulation Output* Results *of S*V *Controller*

In this section two case studies were performed. One case study during steady state conditions, the second case study investigating the performance of the controller during disturbances.

A Output Results of the SV Controller during Steady State Operation

In this study the source is connected to the 433V distribution network. The SV controller is applied to control apparent power and support the grid voltage. Figure 4.23 (the period between 0-5sec) shows the response of the controller during steady state operation which proves stable operation of the source.

B Response of the SV Controller to Disturbance

The aim of this study is to investigate the response of the controller when a disturbance load is inserted to the network at t=5sec. As illustrated in Figure 4.23, the performance of the controller has been evaluated and shown to be stable to load disturbance. However in this case the function of the controller is to maintain a constant apparent power and support the voltage magnitude at the connection point to the network. As shown in the figure the values of active and reactive powers change. The change in the reactive power is due to the source injecting more reactive power to the system to compensate for voltage sag caused by load increase. As a result, the controller decreases the active power flow from the source to the network to maintain the source apparent power at a constant level.

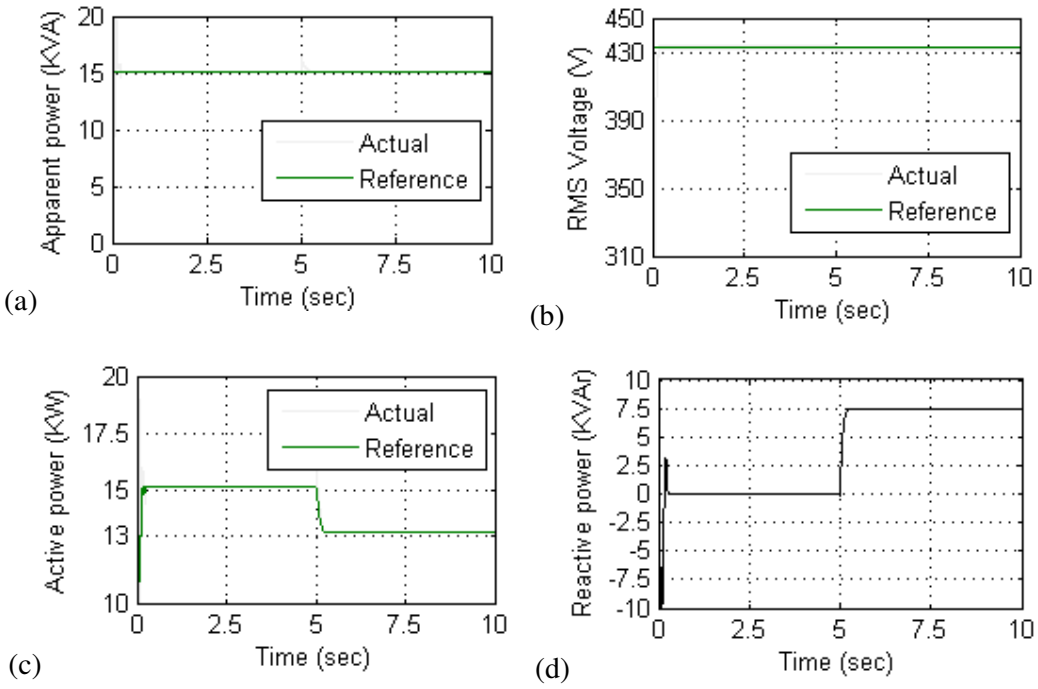

Figure 4.23: Performance of the SV controllers during steady state and disturbance: (a) Apparent power, (b) Terminal voltage, (c) Reactive power and (d) active power.

4.9 Summary

The main task of this chapter was to propose control schemes to control output power from a converter interfaced SSEG. These control schemes are VF control, PQ control, PV control, SV control, DC current control power factor control and a voltage/phase angle droop control. A low-voltage distribution network with embedded generation was modelled and simulated in PSCAD/EMTDC to assess the performance of the proposed control schemes for converter-interfaced SSEG under different operation conditions. The studies showed that the response of the SSEG controllers was satisfactory during steady state and disturbance conditions. It was also shown that each phase of a three-phase converter can be controlled independently in order to address voltage unbalance problems encountered in SSEG applications which use single and three-phase converters to interface SSEG. Therefore the controllers have a positive impact on the voltage stability and power quality of the network. Moreover the results show that there is a linear relationship between the phase angle and the SSEG terminal voltage.

CHAPTER 5

Centralised Controller for Grid Connected and Islanded Small Scale Embedded Generation Networks

5.1 Introduction

Small scale embedded generation networks are designed to be isolated from the distribution system during disturbances. They intentionally disconnect when the quality of power from the grid falls below certain standards, as an example the total harmonic distortion (THD) is more than 5% [58]**.** Once these problems are resolved they reconnect back to the grid. Normally, in grid-connected mode, the small sources act as constant power sources, which are controlled to inject the demanded power into the network. In islanded mode, small sources are controlled to supply all the power needed by the local loads while maintaining the voltage and frequency within acceptable operating limits [108]**.** Moreover, the existing power utility practice often does not allow islanded operation and automatic resynchronisation of a SSEG network. However, the high penetration of SSEGs potentially necessitates provisions for both islanded and grid-connected modes of operation and smooth transfer between the grid-connected mode and the islanded mode to enable the best utilisation of the SSEG network resources [109].

This work, proposes a control system for use with multiple SSEG networks connected to the 33kV distribution network. This control system employs a multilayered control approach where a combination of centralised and distributed controllers are used. Each SSEG will have its own distributed controller. Moreover, each SSEG network will deploy a centralised (EGCC, SSEG network Central Controller) controller which oversees the operation of the distributed SSEG controllers. There also exists a Central Management Controller (CMC) which coordinates the operation of the EGCCs. The proposed controller controls power flow in the grid-connected mode of operation, enables voltage and frequency control when the SSEG networks are islanded, and resynchronises the SSEG networks with the utility before reconnecting them. The proposed control system has a fast

response, allowing the controlled SSEG networks to transition smoothly between the grid-connected and islanded modes without disrupting critical loads connected to them. In addition the control system contains loss-of-mains and synchronising algorithms. The loss-of-mains detects the loss of grid connection and isolates the SSEG networks from the system. The synchronising algorithm synchronises the SSEG networks and grid voltages and reconnects the SSEG networks back to the grid. The performance of the proposed controller has been tested in simulations using PSCAD.

5.2 Control Approach for A System with Multiple SSEG Networks

A specific area with high levels of SSEGs, for example a city, could be divided into many areas, each of which is represented by one SSEG network. The interconnection of these individual SSEG networks forms multi-SSEG networks. This new concept is formed at the Medium Voltage (MV) level, consisting of LV SSEG networks connected on several adjacent MV feeders. SSEG networks under Demand Side Management control can be considered in this network as active cells, for control and management purposes [110]**.** These SSEG networks should be able to operate when they are in grid-connected or islanded modes, and should transition reliably through the connection/disconnection event [111]. Thus the technical operation of such a system requires the transposition of the SSEG network concept to the MV level, where all these active cells, as well as MV/LV passive substations, should be controlled by a Central Autonomous Management Controller (CAMC). This CAMC would be installed at the MV bus level of a HV/MV substation, serving as an interface to the Distribution Management System (DMS), and under the responsibility of the Distribution System Operator [112].

5.3 Network Used in the Study

The basic power system model of the small rural network as shown in Figure 5.1 (described in chapter 3)**,** has been used to evaluate the performance of the general control approach that this work proposes. As shown the Central Management Controller (CMC) is located between five SSEG networks and the grid.

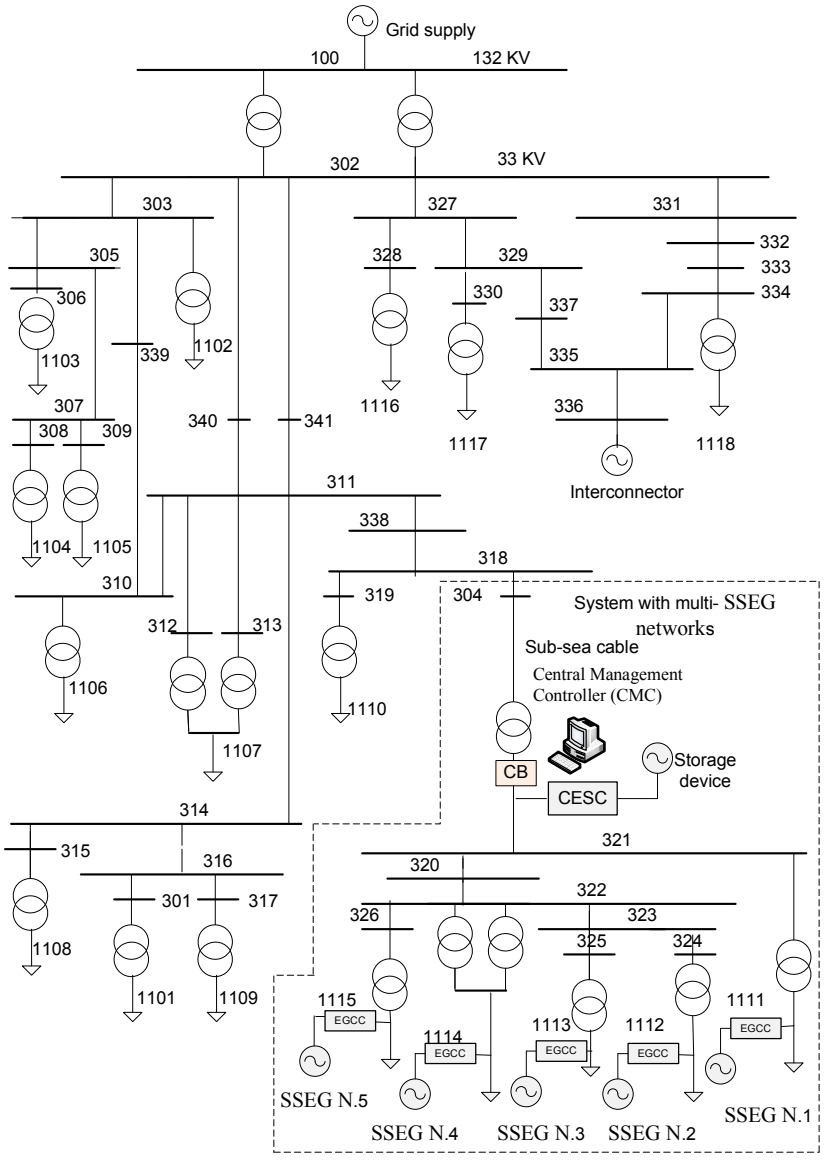

Figure 5.1: Network with multiple SSEG networks used in the analysis

The position of the controller has been chosen in this place to be close to the SSEG networks. Moreover, positioning this controller on the SSEG networks side of the sub-sea avoids the cable losses that may result if the controller and energy storage were placed on the other side. The SSEG networks are connected to this network through the sub-sea cable at buses 1111(0.55 MW), 1112(0.04 MW), 1113(0.77 MW), 1114(2.7 MW) and 1115 (2.85 MW) all of which operate within the appropriate power factor range (0.95 lagging or leading). The load connected at these

SSEG networks are 1111 (0.55MW, 0.11MVAr), 1112 (0.04MW, 0.01MVAr), 1113 (0.77MW, 0.15MVAr), 1114 (2.7 MW, 0.55MVAr) and 1115 (2.85 MW, 0.58MVAr). Every SSEG network has its own control system, named the SSEG network central controller (EGCC). The central energy storage device and the controller (CESC) are connected on bus 321.

5.4 Assumptions

A number of assumptions are made concerning SSEG networks modelling. The main assumptions are:

- Each LV SSEG network was considered as a single bus with an equivalent generator (sum of all SSEGs) and equivalent load (sum of all LV loads),
- There is a central storage device to compensate the difference between the generation and the load demand during islanded mode. The capacity of the inverter interfaced storage device is 1.25 MVA, which can be working at 0.8 power factor (leading or lagging).
- There is communication in place between the controller and storage device,
- There is a circuit breaker between the SSEG networks and utility ends,
- The models of the SSEG networks and storage device in this study are not concerned with the switching dynamics of the converter. The initial switched model was used as the basis of a functional model using a controlled voltage source to allow for the connection of a large number of modules whilst ensuring that simulations are completed in a reasonable time [14]. The validity of the functional model used for the studies in this work is demonstrated in **Figure 5.2** for the cases of a real power reference step change from 1kW to 1.5kW at 1s and from 1.5kW to 2kW at 1.5s.

Appendix F provides further details on the operation principle of the functional model and the full switched model.

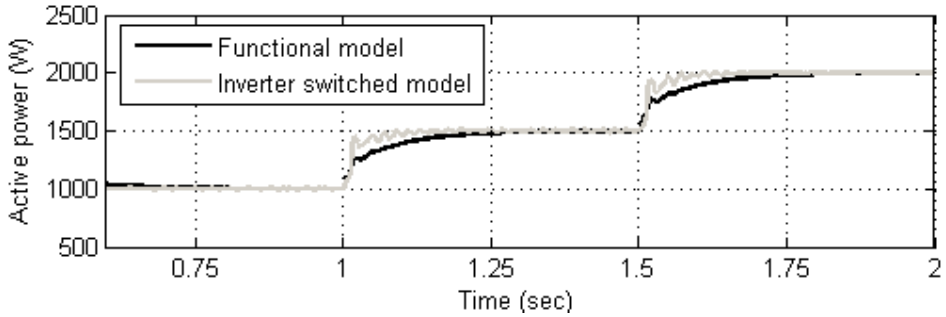

Figure 5.2: Power Response to Step Reference Change (+1kW)

5.5 Controller Design

In order to regulate the power flow of SSEG networks in the grid–connected mode and islanded mode, the SSEG networks should have a certain amount of control. This control system must fulfil a number of tasks. For this purpose several control elements are used. The objective of the control design for multiple SSEG networks is to offer a solution for power control along with voltage regulation in islanded as well as grid-connected modes.

5.5.1 Control Goals

This control system must fulfil a number of tasks:

- It needs to facilitate new SSEG connection to the system without disturbing the controller's operation.
- Keep the SSEG networks bus voltages within specified limits during grid-connected mode.
- Control the power factor.
- Control active power and reactive power.
- Detect loss-of- mains conditions.
- Connect to or isolate the SSEG networks from the main network in a rapid and seamless fashion.

- Maintain both voltage and frequency within the standard permissible levels during islanded operation of the SSEG networks.
- Synchronise the SSEG networks to the grid after islanding.

5.5.2 Control Elements

Three control elements are distinguished, as presented in **Figure 5.3**.

- Central Management Controller (CMC).
- Central Energy Storage Devices Controller (CESC).
- SSEG network Central Controller (EGCC).

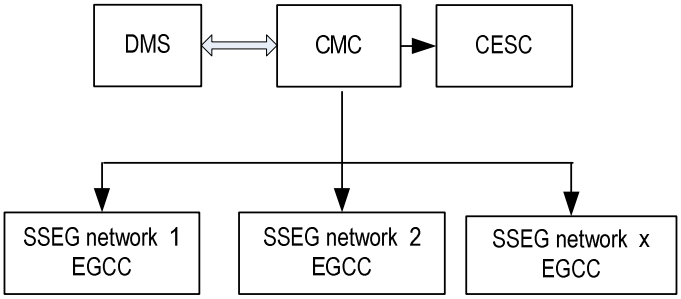

Figure 5.3: Control elements

5.5.2.1 Central Management Controller (CMC)

The Central Management Controller (CMC) is installed at the MV bus on the 33kV sub-sea cable between the SSEG networks and the main grid, serving as an interface to the Distribution Management System (DMS), and under the responsibility of the Distribution Network Operator (DNO). The block diagram of the CMC and the direction of the output signals can be seen in Figure 5.4. The CMC contains loss-of-mains detection controller (LOMDC) and synchronising controller (SC). The function of the LOMDC is to detect the loss-of-mains and isolate the SSEG networks from the system by sending a signal to the circuit breaker when the main generation

is lost. However, the function of the SC is to compensate for the difference in magnitude and angle of the SSEG networks and grid voltages and to verify the synchronisation conditions. Once the conditions are satisfied it sends a signal to the circuit breaker to reconnect the SSEG networks.

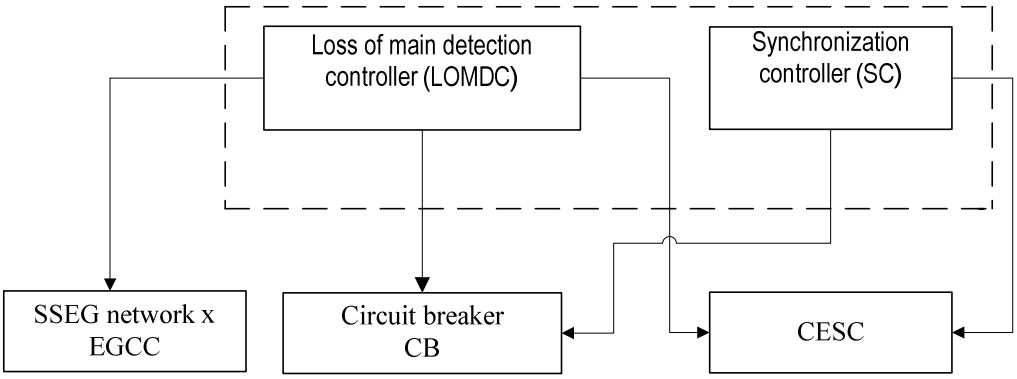

Figure 5.4: Block diagram of CMC and the direction of the output signals.

A. Loss-of-Main Detection Controller (LOMDC)

To effectively integrate SSEG networks into distribution networks, several requirements, such as voltage regulation, loss-of-mains protection and the sustainability of SSEG networks following disturbances on the associated network need to be satisfied [113]**.** The loss-of-mains protection may consist of one of the following protections: reverse power flow, neutral voltage displacement, directional over-current, directional under current, rate-of-change of frequency (ROCOF) and change of power factor. In this work an islanding detection algorithm was developed to be responsible for switching between the grid and islanded modes of operation. This is operated by sending signals to open the circuit breaker between the SSEG networks and the main grid and change the control mode of CESC.

In this work a loss-of-mains protection scheme depending on the ROCOF, has been implemented. As shown in **Figure 5.5** the relay block diagram consists of a derivative component, which determines the rate at which the frequency of the system is changing (df/dt). The output value of the derivative (ROCOF) is compared with a preset threshold value [-0.125 Hz/s] (this reference value has been taken from

[114]). During the initialisation the relay is deactivated**.** If the ROCOF exceeds the threshold value this means the main generation is lost and the output will be logic true (1), otherwise the output is logic false (0). This output will be the input of the OR logic gate, its output value is logic false (0), during steady state the output remains logic false (0). If the disturbance is detected the input of the OR gate becomes 1 and the output changes to logic true (1). This signal goes to the circuit breaker to open the circuit. Using the selector switch the circuit breaker B1 can be kept closed or controlled by the loss-of-mains protection scheme and synchronising relay. When a utility fault occurs, the main circuit breaker on the 33kV bus opens to isolate the SSEG and utility networks within one frequency cycle. At the same time it sends a signal to the central storage device to switch from PQ control to voltage and frequency control (VF).

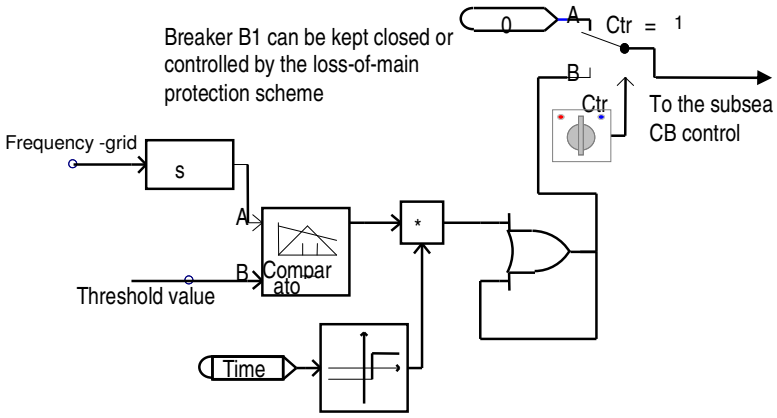

Figure 5.5: Loss of main relay block diagram

B. Synchronisation Controller (SC)

In order to reconnect the SSEG networks to the main grid it is necessary to synchronise the SSEG networks to the grid at the point of connection. Hence the following conditions must be fulfilled.

- The SSEG networks voltage must be the same as that of the main grid.
- The frequency of the SSEG network must be the same as that of the main grid.
- The SSEG networks voltage must be in phase with the main grid.

Figure 5.6 shows the block diagram of the synchronisation controller (SC).

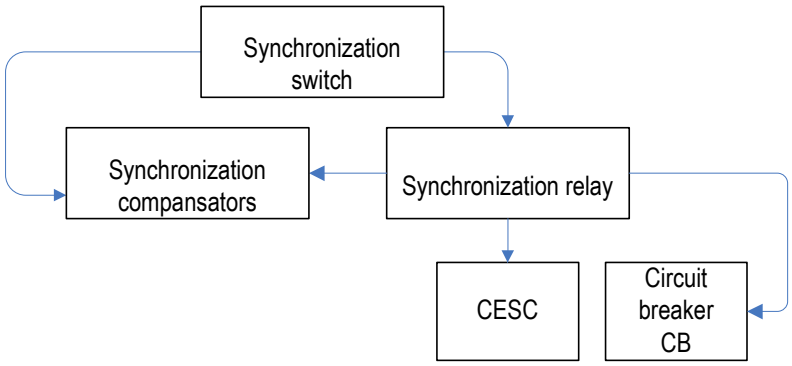

Figure 5.6: Synchronisation controller (SC).

i. Synchronising Procedure

When the utility grid returns back to normal operating conditions, the SSEG networks have to be resynchronised with the utility grid before the circuit breaker can be reclosed to smoothly return the system back to the grid-connected mode of operation. Synchronisation can be achieved by aligning the phase angle and magnitude of the three-phase voltages at the SSEG networks and utility ends of the circuit breaker shown in **Figure 5.1**. To align these voltages phase angles and magnitudes, two separate synchronisation compensators are added to the external voltage and frequency control loops of the central energy storage device. As shown in Figure 5.7 and Figure 5.8, the inputs to these synchronisation compensators are the magnitude and phase errors of the two voltage phasors at both ends of the circuit breaker. Their outputs are fed to the real and reactive power loops to make the voltage phasor at the SSEG networks end track the phasor at the main grid end closely (both in magnitude and frequency). Also during resynchronisation, the voltage and frequency references of the central energy storage device are changed to achieve the same voltage magnitude and frequency at the connection point as that of the grid voltage while the SSEG networks maintain the supply to the demand. When synchronisation criteria are acceptable the circuit breaker will be closed, thus the SSEG networks are reconnected to the main grid. Once the SSEG networks are

reconnected, the synchronisation compensators must be deactivated by setting their outputs to zero so as not to interfere with the proper operation of the real and reactive power control loops in the grid-connected mode.

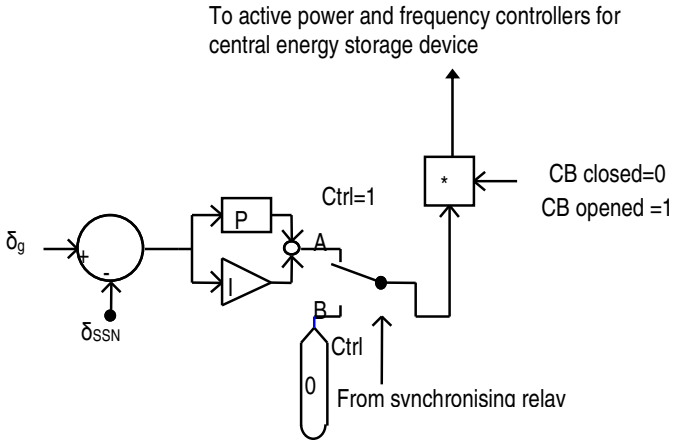

Figure 5.7: Voltage angle synchronising compensator

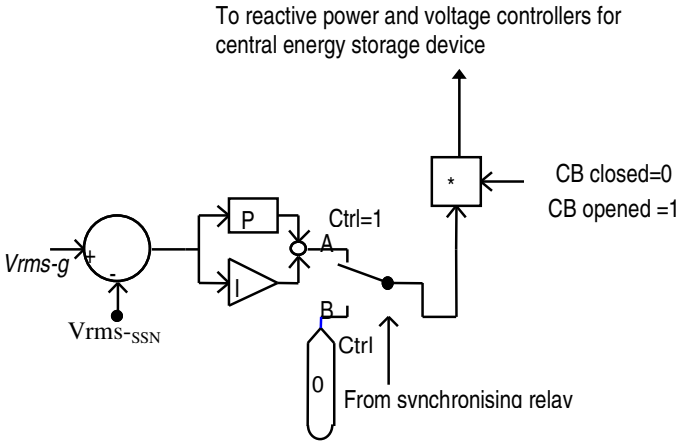

Figure 5.8: Voltage magnitude synchronising compensator

The transfer function of the voltage angle synchronising compensator is given by the equation below:

$$P_{com}(s) = \mathrm{K}_{pc\delta}\left[1+\frac{1}{\tau_{ic\delta}S}\right].E_{\delta}(s) \qquad (5.1)$$

Where $E_{\delta}(s) = \left[\delta_g(s) - \delta_{SSN}(s)\right]$ (5.2)

$K_{pc\delta}$: proportional gain of voltage angle synchronising compensator PI controller,

$\tau_{ic\delta}$: integral time constant of PI controller ($\tau_{ic\delta} = \frac{K_{pcop}}{K_{icop}}$ where $K_{ic\delta}$ is the integral gain).

Similarly the transfer function of the RMS voltage magnitude synchronising compensator is given by the equation below:

$$Q_{com}(s) = K_{pcv}\left[1 + \frac{1}{\tau_{icv} S}\right].E_V(s) \quad (5.3)$$

Where $E_V(s) = \left[Vrms_g(s) - Vrms_{SSN}(s)\right]$ (5.4)

K_{pcv}: proportional gain of RMS value of the voltage magnitude synchronising compensator PI controller,

τ_{icv}: integral time constant of PI controller ($\tau_{icv} = \frac{K_{pcv}}{K_{icv}}$ where K_{icv} is the integral gain).

ii. Synchronisation Relay

This controller performs a check synchronisation function which compares the voltage (angle and magnitude) on either side of the CB at the point of connection (SSEG networks and grid voltages) before issuing a reclose command. In addition it activates the synchronisation compensators to correct for the difference between the SSEG networks and the grid voltages (magnitude and angle) before reconnecting the SSEG networks to the main grid. **Figure 5.9** shows schematic diagram of the synchronisation relay block diagram.

The first selector switch and two-state switch (ON, OFF) form the synchronisation switch. The output of the selector switch component will be either the signal connected to A, or the signal connected to B, depending on the value of Ctrl. The Ctrl is changed by the two state switch (ON, OFF), if the switch is ON the Ctrl=1 then the output will be the signal connected to A which is logic true (1). This signal

will be one of the inputs to the logic gate AND, and also goes to the synchronisation compensators to activate them. On other hand if Ctrl=0 then the output will be the signal connected to B which is logic false (0). This synchronisation switch is switched ON by the distribution network operator (DNO) to start the synchronisation procedure (ON=1, OFF=0).

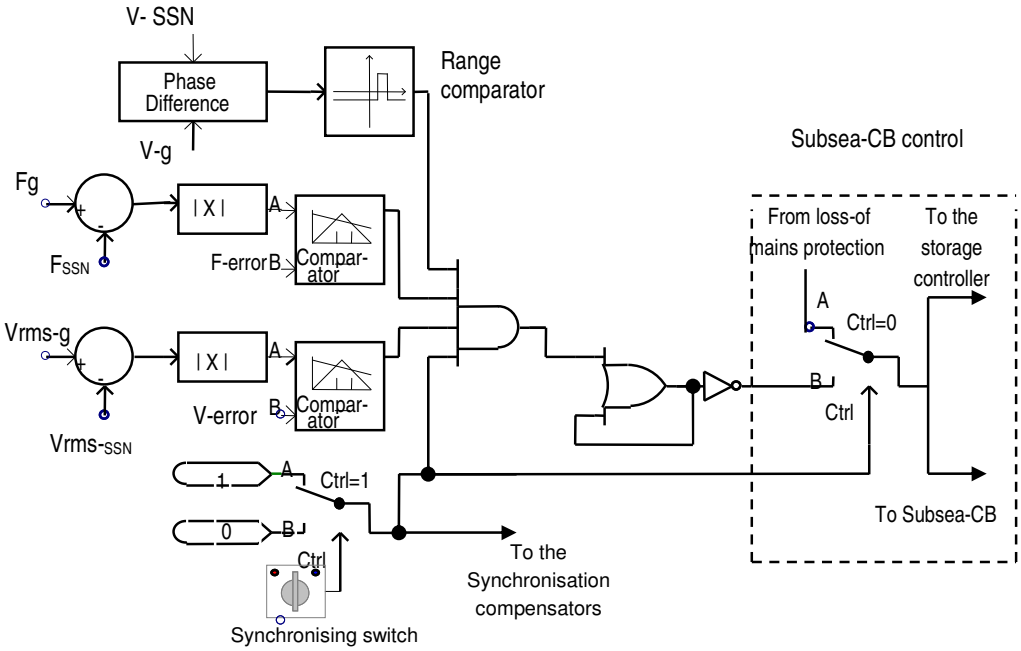

Figure 5.9: Synchronisation relay.

The voltage waveforms of the SSEG networks and the grid are the inputs of the phase difference component as shown in the upper part of **Figure 5.9**. The phase difference component determines the phase angle difference (Ph_{error}) between the voltages of the SSEG networks and the grid. The phase angle difference is positive if the SSEG networks side's voltage leads the grid voltage otherwise it is negative. The phase angle difference (Ph_{error}) is the input to the range comparator. The range comparator determines which of three ranges the input signal belongs to, and then outputs a value corresponding to that region. The regions are defined by a lower input limit $Ph_{error}<0$ and an upper input limit $Ph_{error}>0$. The first region is composed of values below the lower limit (the SSEG networks side's voltage lags the grid

voltage); the second region is Ph $_{error}$ = zero which is between the two limits (normal operation); and the third region is composed of values above the upper limit (the SSEG networks side's voltage leads the grid voltage). The output of the range comparator is logic true (1) for Ph $_{error}$ = 0 and logic false (0) for Ph $_{error}$ <0 or Ph $_{error}$ > 0.

The first difference junction subtracts the filtered measured frequency of the SSEG networks from the filtered measured frequency of the grid, the difference will be the frequency error f_{error} which is given by the equation below:

$$f_{error} = f_g - f_{SSN} \qquad \text{[Hz]} \qquad (5.5)$$

f_g is the measured grid frequency [Hz], f_{SSN} is the measured SSEG networks frequency [Hz].

The upper two input comparator component will output logic true (1) if the frequency error $|f_{error}| \geq 0.002$ otherwise the output is logic false (0).

The second difference junction subtracts the RMS value of the measured voltage of the SSEG networks side from the RMS value of the measured voltage of the grid. The difference will be the voltage V_{error} which is given by the equation (5.6).

$$V_{error} = V_{rms\,g} - V_{rms\,SSN} \qquad \text{[kV]} \qquad (5.6)$$

Where: V_g is RMS measured grid voltage [kV] and, V_{sn} is the RMS measured SSEG networks voltage [kV].

The output of the lower two input comparator component will be logic true (1) if the voltage error $|V_{error}| \geq 0.01$ otherwise the output is logic false (0).

The output of the AND gate is logic true (1) if all synchronisation conditions are satisfied, otherwise the output is logic false (0). The OR gate holds the output constant (logic false (0)) until the input signal is changed to logic true (1), then the

new output will be logic true (1). The function of the inverter is to invert the output of the relay, because the signal (0) here means close the circuit breaker. The function of the second selector is to change the source of the command signals that go to the subsea cable circuit breaker and the central energy storage device. If the synchronisation switch is ON the output signal will be the signal from the synchronisation relay, otherwise the output will be from the loss-of-mains protection or from the control panel by the distribution network operator (DNO).

5.5.2.2 Central Energy Storage Device Controller (CESC)

The control schemes of the storage device are PQ control or Frequency/Voltage control. The storage device provides voltage and frequency control of the SSEG networks when the SSEG networks are operated in islanded mode. During the grid-connected mode the control technique of the energy storage device is PQ control. When the main circuit breaker opens to isolate the SSEG networks from the utility grid, the system must immediately keep the balance between load and generation using the storage devices or by the load-shedding technique to continue supplying power to all critical loads within the SSEG networks adequately. In this case the storage device controller receives a signal from the main controller to switch from PQ control mode to voltage and frequency control modes.

A. PQ Control for Central Storage Device

The PQ concept was obtained from the active and reactive power equations (4.3), (4.4). The control of the active power is realised by controlling the load angle δ_{st} and reactive power is controlled by controlling the voltage magnitude V.

i. Active power controller for Central Storage Device

As shown in Figure 5.10, during grid–connected mode the central controller sends a signal to deactivate the two PI controllers. Thus only the first PI is activated, which would suffice to control the flow of active power by generating the proper values for δ_{st} as described in the following equations:

$$\delta_{st}(s) = \mathrm{K}_{pstp}\left[1 + \frac{1}{\tau_{ist\delta} S}\right].E_P(s) \tag{5.7}$$

Where $E_P(s) = \left[P_{st-ref}(s) - P_{st-meas}(s)\right]$ (5.8)

K_{pstp}: proportional gain of storage device PI controller,

τ_{istp}: integral time constant of PI controller ($\tau_{istp} = \frac{\mathrm{K}_{pstp}}{\mathrm{K}_{istp}}$ where $\mathrm{K}_{ist\,p}$ is the integral gain.

In this study during the grid–connected mode, the output active power of the storage device is kept zero. In islanded mode the active power reference value is received from the frequency controller. This will be discussed later in this chapter.

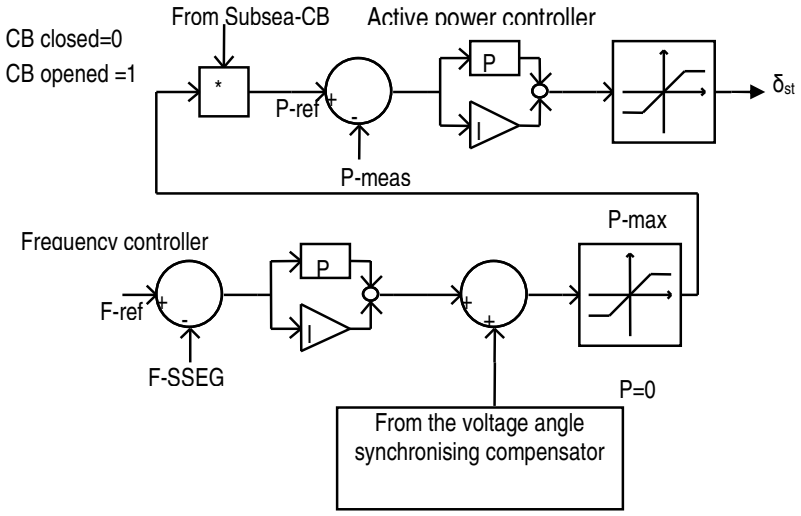

Figure 5.10: Active power and frequency controllers for central energy storage device.

ii. Reactive power controller for Central Storage Device

The first PI controller in **Figure 5.11** controls the reactive power injected or absorbed by the central storage device. During the grid-connected mode the controller maintains the output reactive power of the storage device at zero level. However during islanded mode the controller controls the flow of the reactive power according to the reference reactive power value issued by the voltage controller.

Controlling the reactive power is performed by generating the proper values for $V_{st,}$ as described in the following equations:

$$V_{st}(s) = \mathrm{K}_{PV}\left[1+\frac{1}{\tau_{iV} S}\right].E_Q(s) \tag{5.9}$$

Where $E_{Q-st}(s) = \left[Q_{st-ref}(s) - Q_{st-meas}(s)\right]$ (5.10)

K_{pV} : Proportional gain of PI controller.

τ_{iV} : Integral time constant of PI controller ($\tau_{iv} = \frac{K_{pV}}{K_{iV}}$ where K_{iV} is the integral gain).

$Q_{st-meas}$: Storage device measured reactive power.

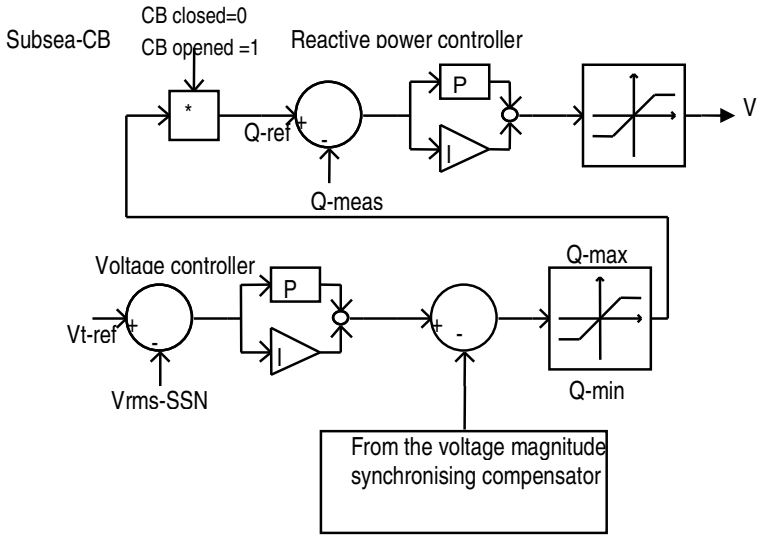

Figure 5.11: Reactive power and voltage controllers for the central energy storage device.

B. Frequency /Voltage Control using Central Storage Device

The voltage and frequency control concept was obtained from the active and reactive power equations (4.3), (4.4). Control of the frequency is realised by controlling the active power P, the control of the voltage is enabled by controlling the reactive power *Q*. At the instant of detection of the islanded operation by loss-of-mains protection, the central controller sends three signals at the same time, one signal to

open the circuit breaker and the other two signals to change the operation of the storage device from PQ control mode to frequency and voltage control mode.

i. Frequency Controller

The objective of the frequency controller is to restore the frequency to its normal value. This is accomplished by increasing or decreasing the required active power from the storage device to maintain the system frequency at a constant value. **Figure 5.12** shows the characteristics of the frequency controller of the storage device, which during islanded mode adjusts the output of the storage device (within its capacity) to restore the frequency of the system to normal (e.g. 50Hz). The system frequency is measured from a phase locked-loop (PLL), which operates based on the three-phase terminal voltage (the description of the PLL is provided in Appendix G). The implementation of frequency control is shown in Figure 5.10. When islanded operation is detected by the loss-of-mains protection, the controller receives a signal from the central controller to activate the frequency controller (second PI controller). The PI controller compares the system frequency with a reference value (50 Hz) and restores the frequency of the SSEG networks near the set value, by generating the proper value of active power. This value of active power becomes the input reference value of the active power controller. The frequency controller is described in the following equations:

$$P_{ref}(s) = \mathrm{K}_{pf}\left[1+\frac{1}{\tau_{iA}S}\right].E_f(s) \tag{5.11}$$

Where $E_f(s) = \left[f_{ref}(s) - f_{meas}(s)\right]$ (5.12)

Where f_{ref} and f_{meas} are reference frequency and the measured SSEG networks frequency respectively. K_{pf} is the proportional gain of the PI controller, τ_{if} is integral time constant of the PI controller that equals $\frac{\mathrm{K}_{pf}}{\mathrm{K}_{if}}$ where K_{if} is the integral gain.

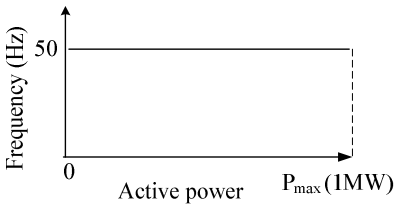

Figure 5.12: Frequency controller characteristic

ii. Voltage Controller

As shown in Figure 5.13 the voltage control increases or decreases the required reactive power from the storage device to maintain a constant voltage when the voltage of the SSEG networks is changed. Thus, the voltage of the SSEG networks is fixed at a desired value (e.g. 1.0 p.u). The implementation of the voltage control is shown in **Figure 5.11**. When islanded operation is detected by the loss-of-mains protection, the controller receives a signal from the central controller to activate the voltage controller (the second PI controller). The second PI controller compares the bus voltage at the point of connection with a reference value (e.g. 1.0 p.u) and restores the voltage at this point near the set value by generating the proper value of reactive power (inject or absorb). This value of reactive power becomes the input reference value of the Q controller of the storage device. The voltage controller of the storage device is described in the following equations:

$$Q_{ref}(s) = \mathrm{K}_{pv}\left[1+\frac{1}{\tau_{iv}S}\right].E_V(s) \tag{5.13}$$

Where $E_V(s) = \left[V_{ref}(s) - V_{meas}(s)\right]$ (5.14)

Where V_{ref} and V_{meas} are reference voltage and the RMS SSEG networks terminal voltage respectively. K_{pv} is the proportional gain of the PI controller, τ_{iv} is the integral time constant of the PI controller that equals $\frac{\mathrm{K}_{pv}}{\mathrm{K}_{iv}}$ where K_{iv} is the integral gain.

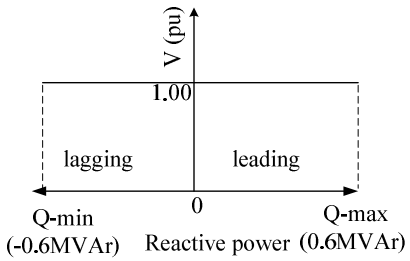

Figure 5.13: Voltage controller characteristic

5.5.2.3 SSEG Network Central Controller (EGCC)

The main interface between the central controller of the whole SSEG networks and each individual SSEG network is the SSEG network Central Controller (EGCC). The EGCC is the main component responsible for the optimisation of the SSEG network operation. Also the output power set points of the SSEGs are determined by the EGCC or by the owners. The problem is approached in this way because the assumption in this work is that each LV SSEG network is considered as a single bus with an equivalent generator (sum of all SSEGs) and an equivalent load (sum of all LV loads) connected to an 11kV bus. Thus the SSEG controller concept will transpose to EGCC.

Most of the SSEGs technologies that use renewable energy sources are often non-dispatchable units (photovoltaic and small wind turbine), for example a small-scale wind turbine is normally operated to extract the maximum possible power from the wind. Thus, its output power varies according to the wind conditions. Also photovoltaic panels depend on the weather conditions. Moreover the micro combined heat and power (μCHP) produces electrical power depending on the heat demand. Therefore the control strategy based upon maximum point of tracking (MPPT) is used to deliver the maximum power to the system. In this work active power and voltage regulation through voltage-phase angle droop strategies are used. This uses pre-specified reference values for real power and phase angle (limit $\Phi = \pm 18.2$).

A. Active Power Control for SSEG networks

Every SSEG network produces constant output active power during grid-connected and islanded modes. During grid-connected mode if the load increases in the system the extra power comes from the main grid. When the SSEG networks are islanded, the energy storage device compensates this difference between generation and demand. If energy storage is unable to match this demand then load shedding is implemented.

The active power controller described in section 4.5.2 is used to control the active power output from the SSEG networks, based on pre-specified set points (P_{ref}). The (P_{ref}) value can be set by the central controller or locally calculated according to a pre-specified power profile to optimise active power export from the SSEG network.

B. Voltage Control for SSEG networks

To maintain the voltage between acceptable limits, the SSEG network will adjust the reactive power in the network: it will inject reactive power if the voltage falls below the nominal value (for example the nominal value, 11kV) and will absorb reactive power if the voltage rises above its nominal value. This goal is achieved by using the voltage/phase angle droop control technique (described in section 4.6.1).

5.5.3 The Algorithm of the Controller to Smooth Transfer between Grid Connected and Islanded Mode

The sequence of control from a grid connected operation to islanded mode and then again back to grid connected is given in Figure 5.14. To summarise the operational principle of the proposed control system, the final block diagram representation of the proposed controller is shown in Figure 5.15.

5.5.3.1 Control of SSEG Networks in the Grid Connected Mode

In grid-connected mode, the SSEG networks supply pre-specified power to minimise power import from the grid, and each SSEG is controlled to represent a PV-bus. The

central storage device is controlled to represent a PQ-bus. Thus, the main grid is expected to accommodate the difference in real/reactive power supply and demand within the SSEG networks. In this mode, the voltage and frequency are established by the grid.

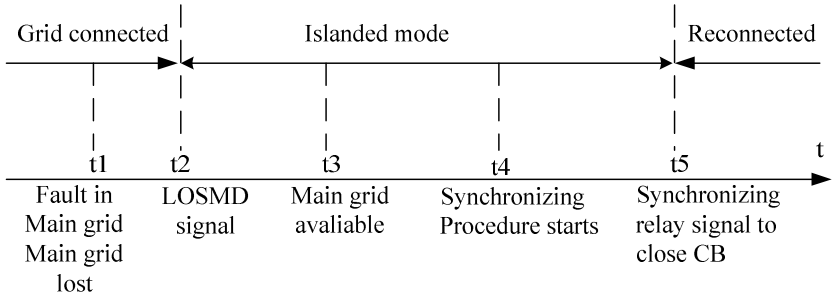

Figure 5.14: Control system time sequence.

5.5.3.2 Control of SSEG Networks to Transition from Grid-Connected to Islanding Mode of Operation

When an abnormal condition occurs in the main grid and the main generation is lost. The tasks of the control system are:

1. The loss-of-mains protection has to detect this event and send a signal to the circuit breaker between the SSEG networks and the main grid to disconnect the SSEG networks from the main grid [the SSEG networks are in islanded mode]. According to this condition $df/dt \leq -0.125$ Hz/s.

2. The control of the energy storage device shifts to islanded mode of operation (voltage and frequency control).

3. In this mode, the central energy storage device forms the grid by establishing its voltage and frequency; otherwise, the SSEG networks will collapse. Both voltage and frequency should be regulated within acceptable limits. If the frequency has dropped to excessively low levels, loads may be shed to hasten its recovery towards the nominal value.

4. Balance between supply and demand, if the SSEG networks are exporting or importing power to the grid before disconnection, then the control system takes actions to balance generation and consumption in island mode.

5. The SSEG networks control strategy is same as during grid connected mode (active power /voltage regulation through voltage-phase angle droop strategies).

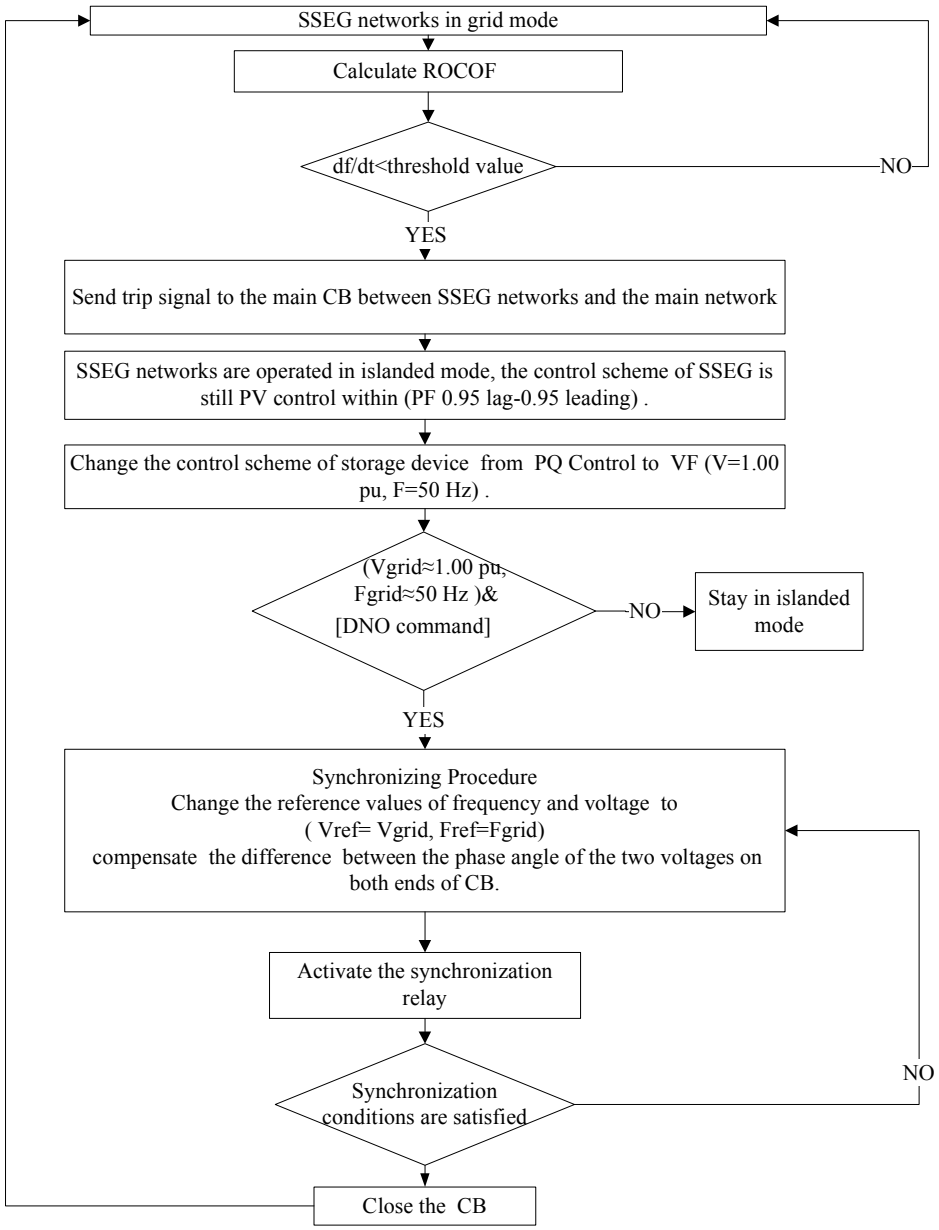

Figure 5.15: Flow diagram of overall control system.

5.5.3.3 Control of SSEG Networks to Transition from Islanding to Grid-Connected Mode of Operation

Finally, once service has been restored to the utility grid after an event has caused separation of the SSEG networks from the utility grid, the SSEG networks must be reconnected to the grid. In this case the controller matches the voltage sine wave of the SSEG networks with the voltage sine wave of the main grid at the point of connection and issues the command to close the breaker tying them together.

Sequence of actions during reconnection of SSEG networks:

1. When the MV network becomes available, check if the voltage and frequency are within acceptable limits, if yes close the synchronising switch (it is done automatically or by DNO) and go to the grid-connected mode.
2. Activate synchronisation compensators
3. Synchronisation conditions (phase sequence, frequency and voltage differences) should be verified to avoid large transient currents during reconnection.
4. If the synchronisation conditions are satisfied go to step 5 to close the circuit breaker otherwise wait until the conditions are satisfied.
5. Send signal to close the circuit breaker to reconnect the SSEG networks
6. Deactivate synchronisation compensators
7. Go to the grid-connected mode

5.6 Simulation Results

The performance of the proposed controller of the multiple SSEG networks connected to a 33 kV distribution power network through a subsea cable has been tested using PSCAD. This section introduces the results which display the operation of the controller under various operating conditions. The main quantities will be presented and an analysis of the results will be made.

5.6.1 Performance of SSEG Networks in Grid-Connected Mode

The test verifies the active power and voltage regulation control strategies of the SSEG networks when the system operates in grid-connected mode. First assume that the SSEG networks operate in grid-connected mode in steady state operation when there are no faults in the network (time 0-10 sec). Figure 5.16, Figure 5.17 and Figure 5.18 illustrate the performance of the overall system control, SSEG networks and central storage devices controllers. Each SSEG network central controller (EGCC) regulates the bus voltage of the SSEG network within standard limits and maintains constant real power output from each SSEG. Figure 5.16(a) shows that during grid-connected mode the SSEG networks import power from the main grid to accommodate the difference in real power demand within the SSEG networks. Also as shown in Figure 5.17, during grid-connected mode there is no participation from the storage device in the active and reactive power flow of the system. At the same time, Figure 5.16(b) shows that the SSEG networks inject reactive power to the system providing voltage support. Also Figure 5.18 (a), (b), (c), (d) and (e) show that the terminal voltage of every SSEG network bus is regulated by the SSEG network itself due to the phase angel/voltage droop control. Figure 5.18(f) shows the voltage of the SSEG networks and the grid at the two ends of the PCC circuit breaker, which are sinusoidal waveforms and synchronised.

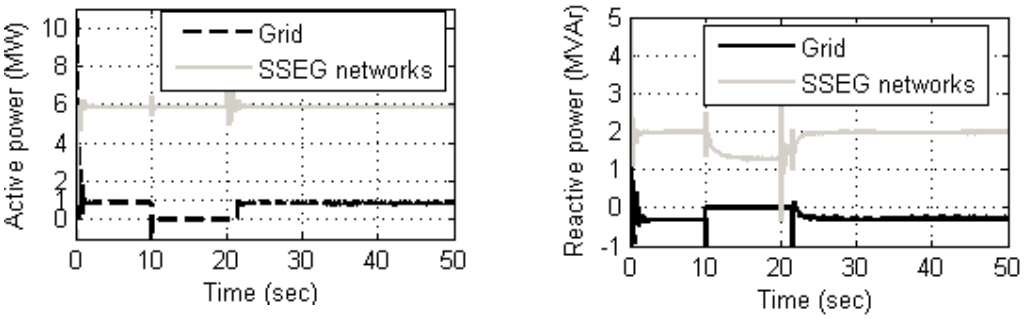

(a) (b)

Figure 5.16: Power output from the SSEG networks and the power flow between SSEG networks and the grid: (a) active power and (b) reactive power

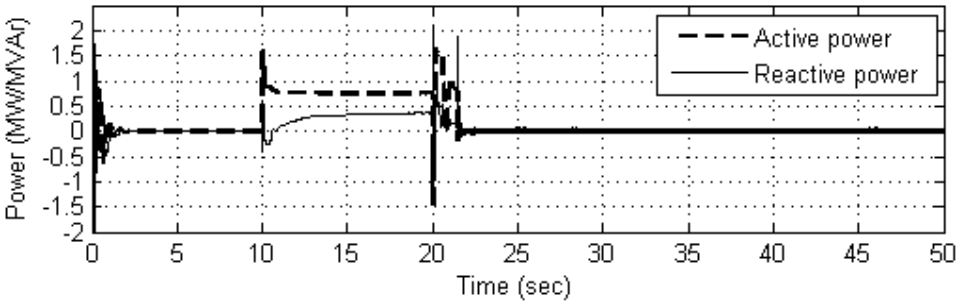

Figure 5.17: Output of the storage device

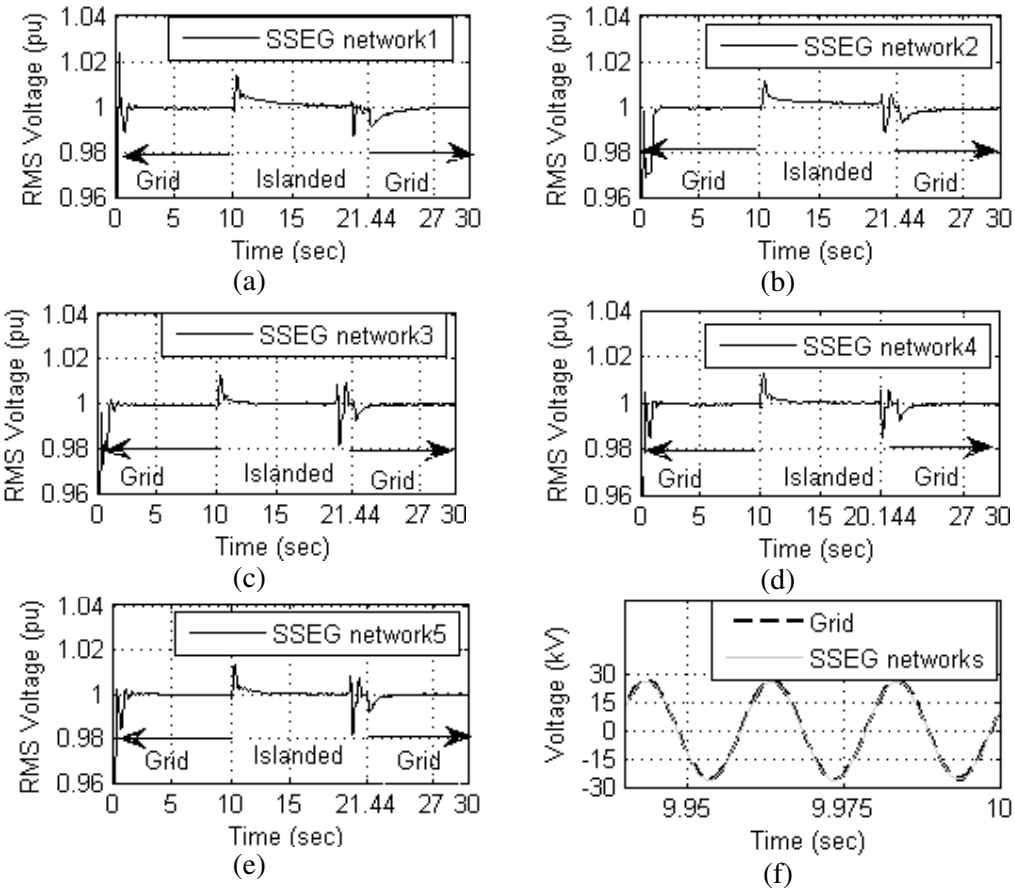

Figure 5.18: (a), (b), (c),(d) and (e) RMS per unit of three phase terminal voltage of SSEG networks (f) Grid and SSEG networks voltages waveform (kV) during grid mode phase a.

5.6.2 Performance of the SSEG Networks during Transition from Grid-Connected to Islanded Mode

The test verifies the frequency and voltage control strategies of the SSEG networks when the system operates in islanded mode. A set of simulation scenarios were performed in order to evaluate the dynamic behaviour of the SSEG networks during islanded mode. The evaluation includes disconnection from the upstream MV network (33kV) and load-following in islanded operation. Several scenarios were simulated. At the occurrence of a fault, the protection equipment disconnects the SSEG networks as a protective measure. In this case the assumption is that the fault in the main grid caused a loss-of-mains condition. This event was detected by the loss-of-mains protection algorithm which is part of the control system of the SSEG networks. Under this condition as shown in Figure 5.19 the loss-of-mains protection sends a signal to the circuit breaker in the subsea cable between the SSEG networks and the grid to open the circuit as well as a signal to the central storage device controller to change the operation mode from grid-connected mode to islanded mode (from PQ control to V/F control). The operation of the SSEG networks seamlessly shifts from grid connected to island mode. The following figures show simulation results when the SSEG networks were operated in islanded mode (time 10-20sec). Figure 5.16 (time 10-20sec) shows the constant active power output and the change in reactive power output (for local voltage control) of the SSEG networks when they transit from grid-connected to islanded mode. Figure 5.17 (time 10-20sec) shows simulation results with the voltage and frequency regulation control technique operating in response to an abrupt change in load when the SSEG networks were operated in islanded mode. The storage device injects active and reactive power to maintain the terminal voltage and the SSEG networks frequency within acceptable limits. Furthermore, the waveforms showing the load terminal voltage and the circuit breaker currents during transfer from grid-connection to islanded mode are illustrated in **Figure 5.20**. It is observed that no current passes through the circuit breaker between the SSEG networks and the main grid. However, the controller regulates voltage in all three phases and makes the transfer from grid-connection to island mode a seamless one.

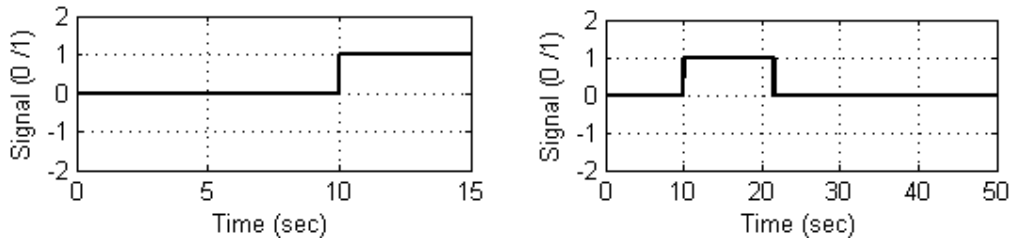

(a) (b)

Figure 5.19: (a) Control signals from LOMCD and (b) State of the circuit breaker.

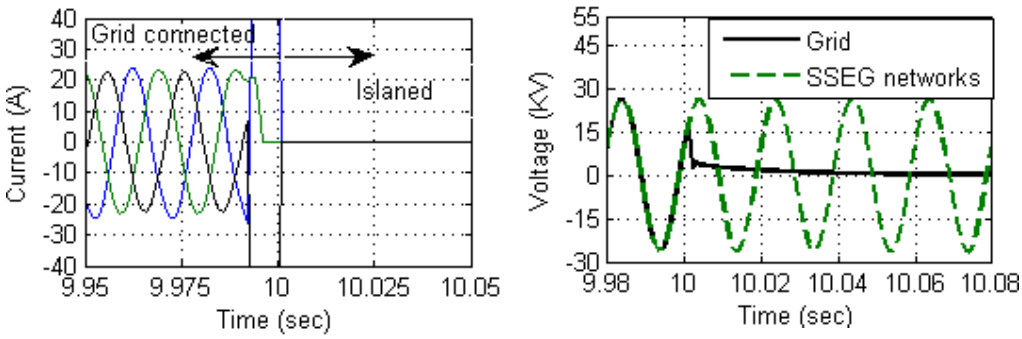

(a) (b)

Figure 5.20: (a) The circuit breaker currents and (b) The voltage at two ends of the circuit breaker during transfer from grid-connection to islanded mode (phase A).

5.6.3 Performance of the SSEG Networks during Transition from Islanded to Grid-Connected Mode of Operation

This test was held to investigate the synchronisation processes between the grid and the SSEG networks. At the start of the test the SSEG networks were disconnected from the main grid (islanded mode). The regulating process during which the voltage of SSEG networks is synchronised with the utility grid's voltage is observed in the following figures. Before transfer from islanded mode to grid-connection, the grid voltage is inspected and verified to be within the acceptable limits as shown in Figure 5.21. Then, the controller allows the SSEG networks voltage to synchronise with the grid voltage at the ends of circuit breaker (refer to Figure 5.22), the synchronising switch starts the synchronising procedure and sends a signal to activate the two synchronisation compensators at 20sec**.** The synchronisation is done by means of aligning the three-phase space vectors of the two voltages. The

synchronisation relay checks whether the voltages on both ends of the circuit breaker are locked in magnitude and phase angle before making the decision to send a signal to close the circuit breaker. Once the magnitude and phase angle of the terminal voltage are locked with that of the grid network, a signal is given to the circuit breaker.

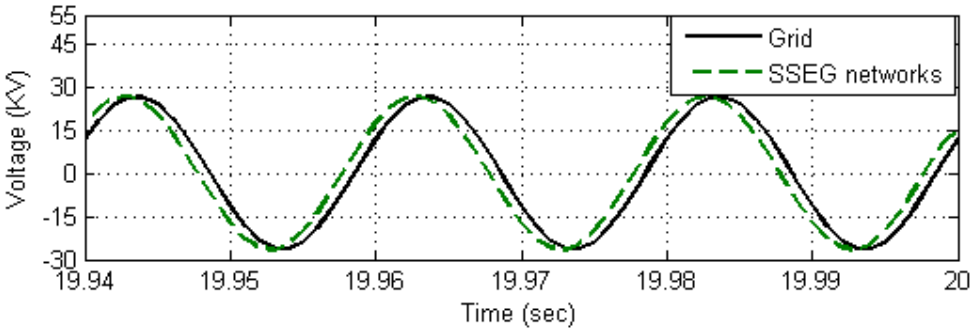

Figure 5.21: Grid and SSEG networks voltages waveform (kV) during islanded mode

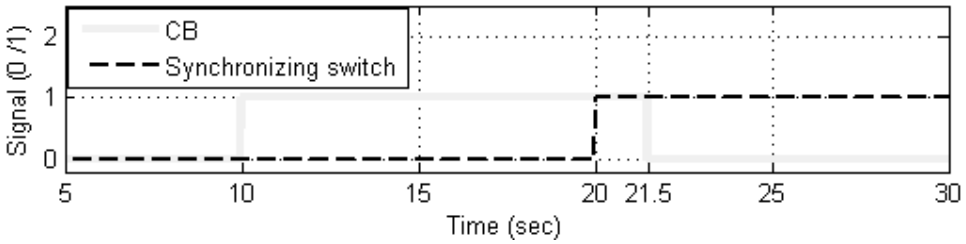

Figure 5.22: Control signals for (CB and synchronising switch).

The waveforms showing the synchronisation to the grid and transfer from islanded mode to grid-connection at both ends of the circuit breaker when the synchronisation algorithms start functioning in the islanded mode are illustrated in Figure 5.23. It was observed that there is a difference in voltage magnitudes and angles of the SSEG networks system and the grid network during islanded mode. It can be seen that the proposed controller successfully forces the voltage at the SSEG networks end to track that of the main grid end without any power oscillation between the SSEG networks. In the first 300ms the difference in phase and magnitude between the SSEG networks and grid voltages is gradually decreasing, until synchronisation conditions are fulfilled (at about 21.44 s as shown in Figure 5.22 the controller closes

the circuit breaker). Subsequently, the system operates at a single voltage and frequency.

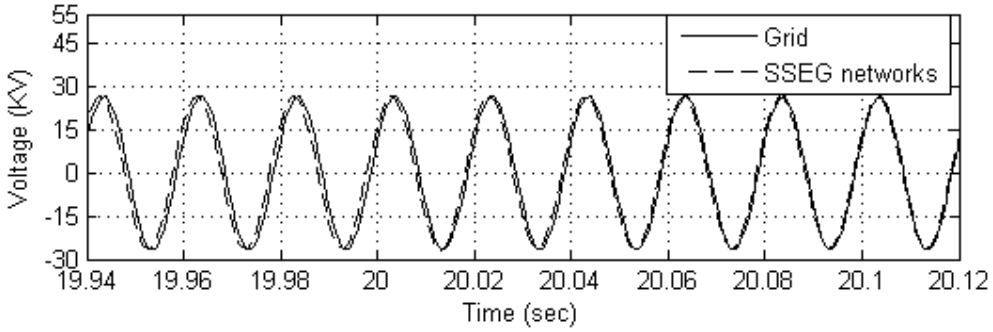

Figure 5.23: Grid and SSEG networks voltages waveform (kV) during islanded mode and during synchronisation.

Figure 5.24 shows how the RMS values of the SSEG networks and grid voltages are synchronised before the circuit breaker is closed. Figure 5.25 shows the frequency synchronisation, the different frequencies are observed during the islanded mode. After the alignment of the voltages, the frequencies are synchronised. It can be seen in Figure 5.26 that at the start of the test the phase angle values of the voltages of the main grid and the SSEG networks were different. However before the circuit breaker is closed as clearly seen in the results the phase shift and rms voltage values of the grid voltage match the SSEG networks voltage before the circuit breaker is closed. After 21.44sec the network was connected to the SSEG network.

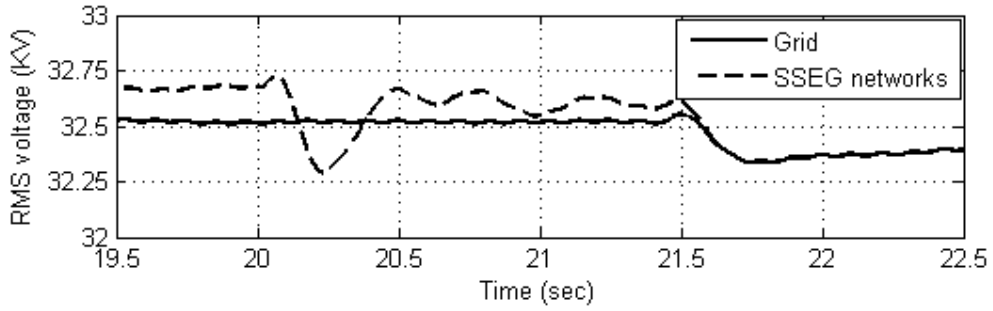

Figure 5.24: RMS voltage of grid and SSEG networks at point of connection (Phase A)

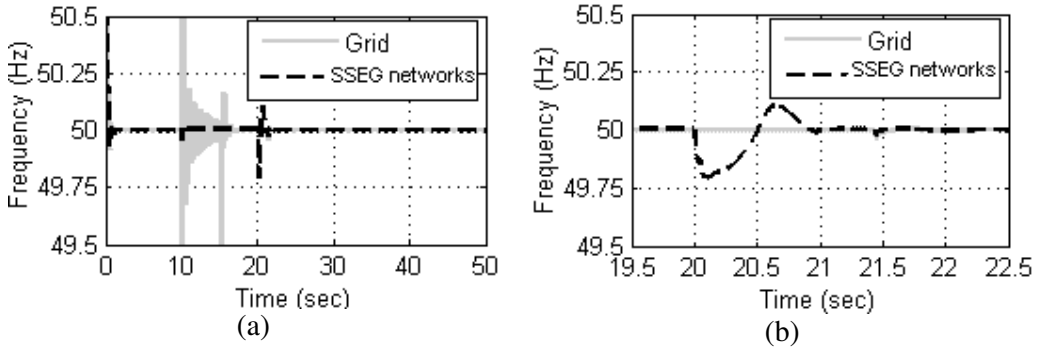

Figure 5.25: Frequency of grid and SSEG networks (a) during the three modes (b) before, during and after reconnection.

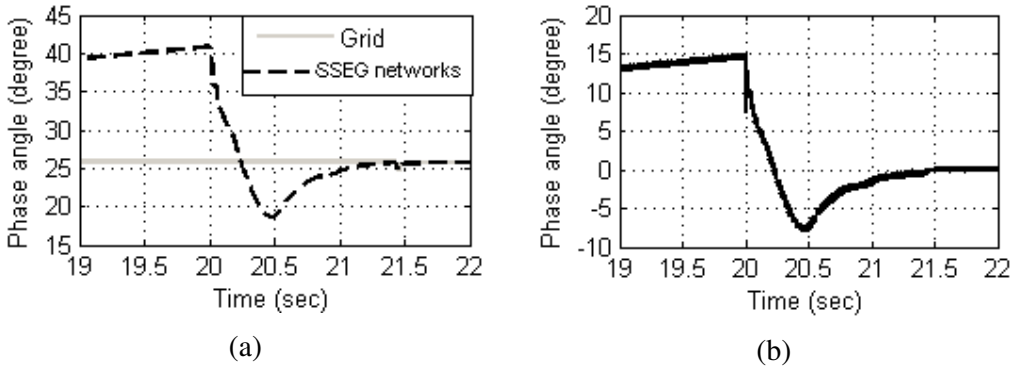

Figure 5.26: Voltage angle of the grid and SSEG networks voltages: (a) for phase A (b) Phase angle difference between grid and SSEG networks voltages for three phases.

Figure 5.27 illustrates the corresponding real and reactive power outputs of the storage device during the process of reconnection of the SSEG networks between 20-21.44 sec. This figure shows an increase in both real and reactive power outputs, which are expected due to the higher SSEG networks output voltages during synchronisation.

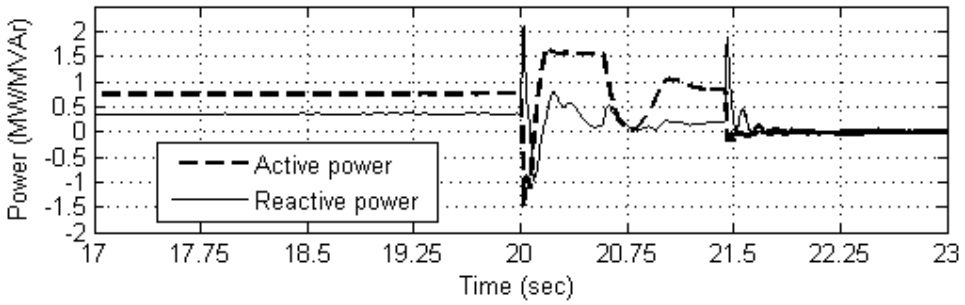

Figure 5.27: Output power of storage device before, during and after reconnection.

At approximately 21.44sec, the SSEG networks are synchronised to the grid and its frequency and voltage become equal to the values of the network ($f \approx 50$Hz, $V \approx 33$kV) as shown in Figure 5.28 (a). At the end of the synchronisation process the steady-state current from the main grid began feeding the SSEG networks as shown in Figure 5.28(b). The system returns to its initial operating state also as shown in Figure 5.18(a), (b), (c), (d) and (e) after reconnection (after 21.44sec) of the SSEG networks. There is no a step change in the SSEG networks terminal voltages as can be observed based on the nominal value of 33kV.

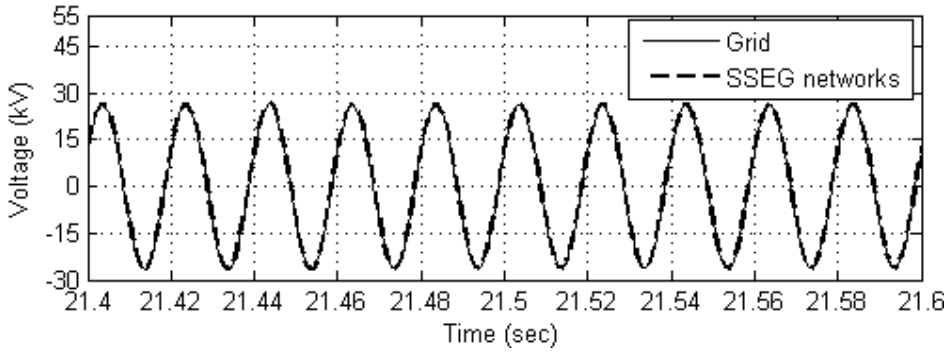

(a)

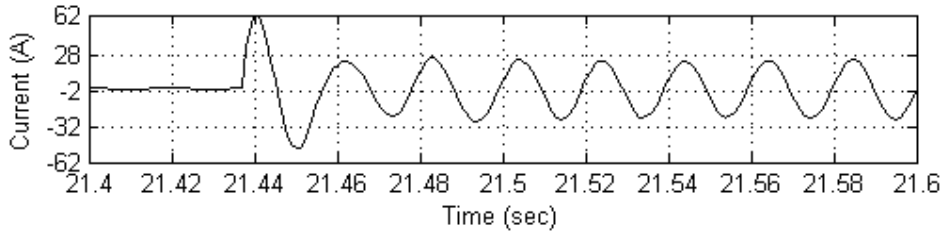

(b)

Figure 5.28: The circuit breaker currents and the voltages at two ends after the SSEG networks are reconnected (phase A).

Figure 5.29 shows the simulation results of the time sequence of the control system during grid connected mode, islanded mode and reconnection of the SSEG networks to the main grid.

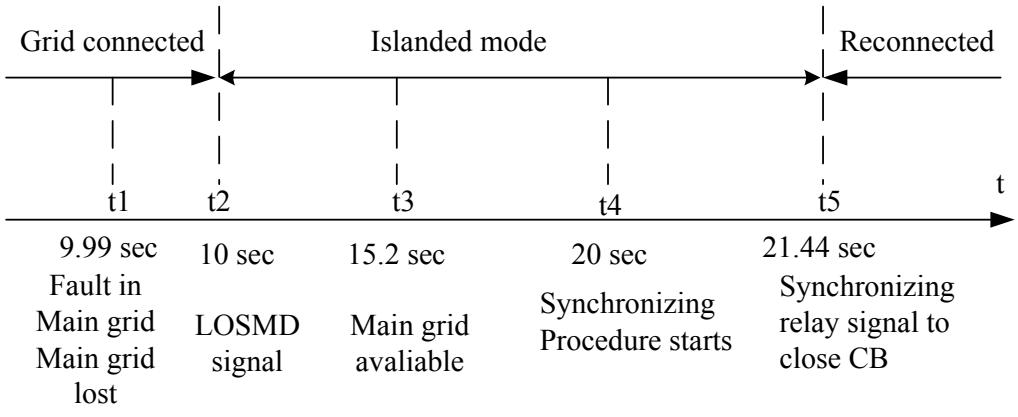

Figure 5.29: Control system time sequence from simulation results.

5.7 Review of Energy Storage Technologies

In this work, the SSEG networks in islanded mode require an energy storage device to balance the load and the generation. The storage device plays the role of the main grid to permit stable operation of SSEG networks by controlling the voltage and frequency of the system. This storage device is installed in the substation where the SSEG networks are connected to the main grid (bus 321). Thus the storage device should be chosen properly to meet the requirements of the operation of the SSEG networks in islanded mode. Then the capacity of the storage device has to be sufficient to compensate the difference between the demand and the generation. This is in addition to supporting an islanded mode of operation for an extended period of time.

5.7.1 Energy Storage Device Options

There are a variety of energy storage device options. They can be divided into two different categories depending on their application [115]. The first being short-term response energy storage devices that can be used for a few seconds or minutes to aid power systems during transient events such as line switching, load changes and fault clearance [115]. Their application prevents the collapse of the power system due to loss of synchronism or voltage instability, improving its reliability and power quality. The main short-term energy storage devices are: flywheels, super capacitors [39] and

ultra-capacitors [40, 41]. The second group is long-term response energy storage devices that can absorb and supply electrical energy for several hours. They can contribute in the energy management and frequency regulation of the power system [115]. Long-term response energy storage technologies are already available and in use today such as pumped hydro, redox flow batteries, compressed air and hydrogen fuel cells [116]. Long-term response energy storage devices are more suited to the application discussed in this chapter (SSEG networks during islanded mode of operation) due to their time response. Thus a suitable device has to be considered in this study among the others.

5.7.2 Available Long-Term Response Energy Storage Technologies

A brief description of these main devices is presented in this subsection except for fuel cells which has already been described in chapter 2. A summary of the main long-term response energy storage devices' characteristics is presented in **Table 5.1**.

5.7.1.1 Pumped- hydro

The operation principle of pumped-hydro units is the same as the operation principle of hydro-electric power plant. However during off peak hours the surplus water is pumped from a lower reservoir to a higher level reservoir by an electrical motor. Then during the times of high electrical demand the water is released from the higher reservoir to turn a turbine and rotate the motor to work as a generator to produce electrical energy [115, 116].

5.7.1.2 Compressed air

The operation principle of the compressed air energy storage is that during the off-peak hours the power is taken from the grid and used to pump and compress air into a sealed underground cavern to a high pressure. This compressed air is kept underground for use when it is needed during peak periods to drive turbines to generate electrical energy as the air in the cavern is released [115].

5.7.1.3 *Redox Flow Battery*

Redox flow battery (RFB) is a storage device that converts electrical energy into chemical potential energy by charging two liquid electrolyte solutions and subsequently releasing the stored energy on discharge [116]. The name redox flow battery is based on the redox reaction between the two electrolytes in the system [115].

Compared with other energy storage devices, the redox flow battery (RFB) has a number of advantages which makes its integration with SSEG networks very attractive. The RFB system has a high speed response and is not aged by frequent charging and discharging. The battery efficiency increases when the charging/discharging period becomes shorter unlike the classical batteries [117]. An RFB system is environmental friendly, it operates at ambient temperature, has a short duration overload capacity and a long service life [117]. The size and location of pumped hydro and compressed air depend on geological formations to provide adequate storage. Therefore the RFB technology is more suitable as energy storage for an SSEG network application as the storage units are more portable.

Table 5.1: Comparison of Long-term Response Energy Storage Technologies [115,116].

Characteristics	**Technology**			
	Pumped Hydro	**Redox Flow Batteries**	**Compressed Air**	**Hydrogen Fuel Cell**
Power (MW)	30-300	<100	100-3000	<50
Energy (MWh)	<10000	<500	50-5000	…..
Charge-Discharge Efficiency	80%	60-90%	75%	20-40%
Life-Time (cycles)	40 years	2-12 years	30 years	12 years
Price (€/kW)	35-70	65-100	10-70	…..

5.8 Summary

Much research has been carried out regarding the operation and control of small, low voltage networks. However the crucial difference between the research presented in this chapter and that which has been carried out previously, is the focus here on multiple small networks connected to MV voltage. This chapter proposed a control system for use with a system consisting of multiple SSEG networks connected to a 33kV distribution network. The proposed control system contains a central controller, local controller for every individual SSEG network and a controller of central energy storage devices. The proposed controller controls power flow in the grid-connected mode of operation, enables voltage and frequency control when the SSEG networks are islanded, and resynchronises the SSEG networks with the utility before reconnecting them. This control system can respond fast, allowing the controlled SSEG networks to transition smoothly between the grid-connected and islanded modes. In addition the central controller incorporates a loss-of-mains algorithm and synchronising algorithm. The function of the loss-of-mains algorithm is to detect the loss of mains conditions and isolate the SSEG networks from the system by sending a signal to the circuit breaker when the main generation is lost. The function of the synchronising algorithm is to compensate the difference in magnitude and angle of the SSEG networks and grid voltages and verifies the synchronisation conditions. Once the conditions are satisfied it sends a signal to the circuit breaker to reconnect the SSEG networks. Including the loss-of-mains algorithm and the synchronising algorithm in the controller made the difference from the controllers used in the literature review for a single small network. The performance of the proposed controller has been tested in simulations using PSCAD. The main goals of the proposed control system were achieved.

CHAPTER 6

Fault Ride-Through of Systems with High Penetration of Small-Scale Embedded Generation

6.1 Introduction

The fault-ride-through capability of SSEGs is the ability of the system with high penetration of SSEGs to maintain uninterrupted operation during and after grid faults. There are two meaning of fault ride-through. The first one is for short circuit faults of up to 140ms in duration. In this case, each generating unit shall remain transiently stable and connected to the system without tripping for a close-up solid three-phase short circuit fault or any unbalanced short circuit fault on the GB transmission system operating at supergrid voltages. The second meaning is for voltage dips greater than 140ms in duration. In this case, each generating unit remains transiently stable and connected to the system without tripping of any generating unit for balanced supergrid voltage dips[4]. This chapter proposes a fault ride-through technique that prevents the flow of large fault currents and maintains the terminal voltages of networks with SSEGs during voltage sags or network disturbances within appropriate limits. This technique employs a unified series-shunt compensator (USSC) connected between networks with SSEGs and the utility grid. This technique has been chosen as an alternative to other similar solutions described in the literature review such as DVR, DSTATCOM and FCL. The problem facing the application of DVR, DSTATCOM and FCL in networks with SSEGs is that these networks use a combination of different generation technologies (e.g. induction machines, synchronous machines and converter–connected generators) which have different transient performance. Thus the solution has to compensate the voltage sag, limit the fault current, mitigate the voltage unbalance and control the power flow, preventing the induction generator absorbing excessive reactive power from the system and reaching over-speed and balance the electrical power with the mechanical power of the synchronous generator, to avoid the pole slipping of the synchronous generator. It must also keep the fault current within the limit of the semiconductors devices capabilities of converter-connected generation. All of these requirements

cannot be provided by individual devices such as DVR, DSTATCOM or FCL but can be provided by the USSC as demonstrated in this chapter.

The USSC consists of a shunt converter and series converter connected together at the DC link side. The series-connected converter injects a voltage in series with the line between the SSEG networks and the main grid, thereby controlling the power flow between the grid and these networks. The shunt-connected converter also injects a reactive current, thereby controlling the voltage at the point of connection. Operating both series and shunt-connected converters together as a USSC, the series injected voltage can be at any angle with respect to the SSEG networks terminal voltage and the RMS value of the voltage magnitude would be less than 1pu. In addition the rating of the series converter is small compared to the converter used in the DVR [118]. The effectiveness of the USSC to enhance fault ride-through of SSEG networks is illustrated based on studies conducted in PSCAD/EMTDC.

6.2 Small-Scale Embedded Networks with the Proposed USSC based scheme

The aim of the study is to demonstrate by means of simulation results how the USSC can be a solution for a larger and better integration of SSEGs in the distribution network. The network used to evaluate the performance of the USSC is shown in Figure 6.1 (described in chapter 3). Five SSEG networks were connected to this network through a sub-sea cable at buses 1111, 1112, 1113, 1114 and 1115. Table 6.1 describes the rating and technology type of every SSEG networks.

The main function of a USSC is the protection of SSEG networks from voltage sags due to faults in the main grid. Therefore as shown in Figure 6.1, the USSC is located on the subsea cable between the SSEG networks and the main grid. If a fault occurs on the main grid, the USSC inserts a series voltage V_{se} and recovers the SSEG networks voltage to the pre-fault value. The three injected phase voltages are controlled such as to eliminate the effects of grid faults to the SSEG networks voltage.

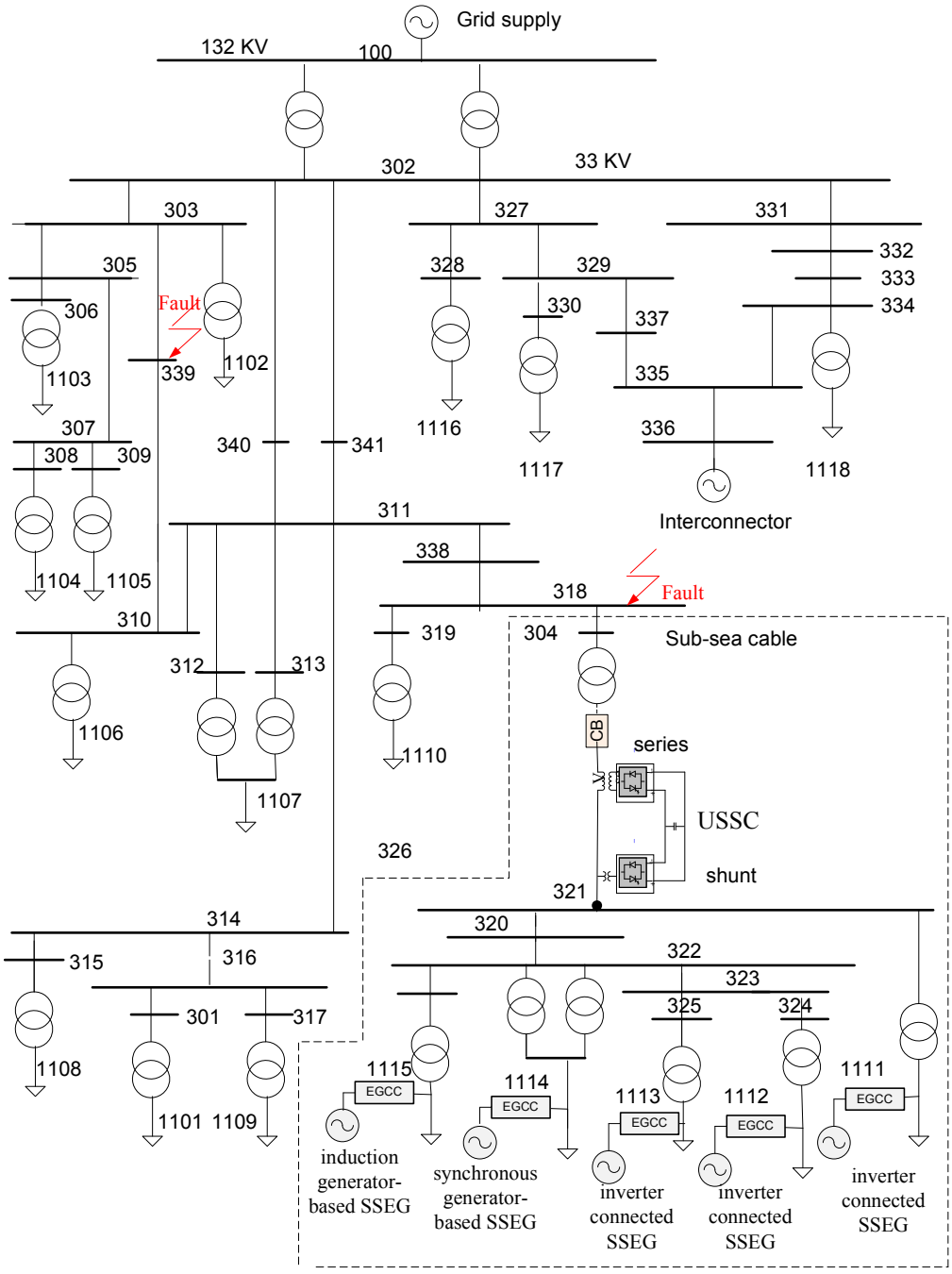

Figure 6.1: Network with multiple SSEG networks used in the analysis.

6.3 Operation Principle of the USSC

The basic components of the USSC are two voltage source converters (VSIs) sharing a common dc link, and connected to the power system through coupling transformers. One VSI is connected in shunt to the distribution system via a shunt

transformer, while the other VSI is connected in series through a series transformer. A basic USSC electrical diagram is shown in Figure 6.2. [119-121]. The USSC is almost similar to the UPFC, but the only differences are that the UPFC converters are in a shunt-series connection from the main grid side and it is used in transmission systems whereas the USSC converters are in shunt–series connection from the SSEG networks side and it is used in distribution systems between SSEGs and the main grid [122].

Table 6.1**:** Small scale distribution networks data.

SSEG network	**Bus no**	**Technology**	**Rating in (MW)**
1	1111	Converter connected (PV)	0.55 MW
2	1112	Converter connected (PV)	0.04 MW
3	1113	Converter connected (FC)	2 MW
4	1114	Synchronous generator (Reciprocating engine)	2.7 MW
5	1115	Squirrel cage induction generator (small scale wind turbine)	2.85 MW

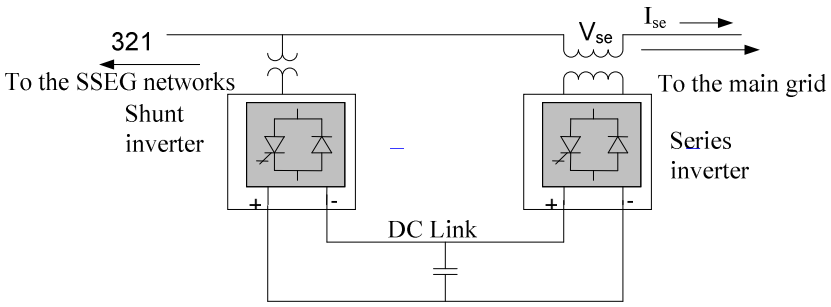

Figure 6.2: Basic Electrical diagram of USSC [119-121].

The operation principle of the USSC is that the shunt converter operates as a static synchronous compensator (STATCOM) to control the AC voltage at its terminal, while the series converter operates as a power flow controller to control the power

flow between the main grid and SSEG networks during steady state. Under fault conditions, the series converter injects a series voltage to balance the voltage difference between the grid and the shunt converter to avoid high fault currents flowing from the SSEGs. Thus the control system of the USSC can be divided into two parts, namely a shunt converter controller and a series converter controller, which control the shunt current and the voltage injected in series respectively. The two voltage source converters of the USSC, connected through a DC link can be modelled as two ideal voltage sources, one connected in series and the other in shunt between the two buses [123]. In this work the controlled voltage sources used simplify the model of the PWM converters. The two ideal voltage sources of the USSC can be mathematically represented as:

$$v_{se} = V_{se}\left(\cos\theta_{se} + j\sin\theta_{se}\right) \tag{6.1}$$

$$v_{sh} = V_{sh}\left(\cos\theta_{sh} + j\sin\theta_{sh}\right) \tag{6.2}$$

[96]

The output of the series voltage source V_{se} and θ_{se} and the shunt voltage source is V_{sh} and θ_{sh} are controllable in magnitude and angle.

6.3.1 Shunt Converter Control

The shunt converter works as a STATCOM, which compensates the reactive power needed by the system in order to keep the voltage at the point of connection of SSEG networks to the main grid at 1pu. Therefore the controller of the shunt converter is used to operate the voltage source converter in such a way that the voltage magnitude of the converter terminal is adjusted so that the shunt converter generates or absorbs reactive power at the point of connection to the SSEG networks. This controller consists of an active power control part and a reactive power control part. The reference signals Q_{sh-ref} and P_{sh-ref} can control the amplitude V_{sh} and phase angle θ_{sh} of the output voltage, respectively.

The reactive power control part can be controlled in two different modes:

- VAR Control Mode: The reference reactive power Q_{sh-ref} is an inductive or capacitive VAR request. The shunt converter control adjusts the converter terminal voltage to establish the desired reactive power.

- Automatic Voltage Control Mode: The shunt converter reactive current is automatically regulated to maintain the SSEG networks voltage at the point of connection to a reference value [124,125].

The active power control part supplies the active power that the series converter requires and compensates the losses of the shunt converter so that the DC link voltage V_{DC} remains constant. Figure 6.3 shows the overall control system of the shunt converter implemented in PSCAD/EMTDC. This consists of two parts; the AC voltage controller and the active power controller.

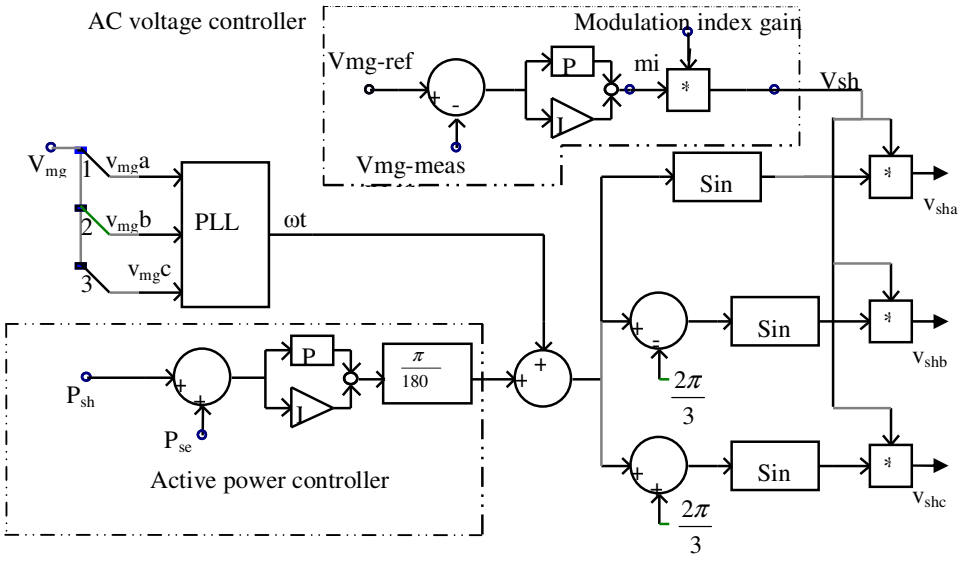

Figure 6.3: Block diagram representation of the overall controller of the shunt converter.

6.3.1.1 Basic Structure of Shunt Converter - the AC Voltage Controller

In this work, the shunt converter operates in automatic voltage control mode. The shunt converter simply generates or absorbs reactive power to maintain the SSEG networks voltage at the point of connection at 1pu. The upper dashed frame of Figure 6.3 illustrates the control design of the AC voltage controller of the shunt converter. In this controller the measured three-phase voltages of the SSEG networks connection point are compared with a reference voltage. A voltage error is fed to the proportional integral (PI) control block. The output of the PI controller is the proper value of voltage magnitude of the shunt converter (V_{sh}), which gives a value either higher or lower than the voltage at point of connection which results in the absorption or injection of reactive power.

The transfer function of the PI controller is:

$$V_{sh}(s) = \mathrm{K}_{PV}\left[1 + \frac{1}{\tau_{iV} S}\right].E_{SNV}(s) \tag{6.3}$$

$$E_{SNV}(s) = \left[V_{SN.-ref}(s) - V_{SN}(s)\right] \tag{6.4}$$

Where V_{SN-ref} and V_{SN} are the reference voltage and the RMS SSEG networks voltage respectively. K_{PV} is the proportional gain of PI controller, τ_{iV} is the integral time constant of PI controller that equals $\frac{K_{pV}}{K_{iV}}$ where K_{iV} is the integral gain.

6.3.1.2 Basic Structure of the Shunt Converter - Active Power Controller

The USSC's energy storing capacity is generally small therefore, the active power supplied to the shunt converter P_{sh} should be equal to the active power demanded by the series converter P_{se} at the DC link [122]. Thus the DC link voltage can be obtained from the power flow mismatch and the following equality constraint has to be guaranteed [122].

$$P_{se} + P_{sh} = 0 \text{ [125]} \tag{6.5}$$

The power flow equation at node (321) where the shunt converter is connected gives:

$$P_{sh} - P_{SN} + P_{bse} = 0 \tag{6.6}$$

$$P_{bse} = P_{SN} - P_{sh} \tag{6.7}$$

The power flow equation before and after the series converter is:

$$P_{se} = P_{bse} - P_g \tag{6.8}$$

$$P_{bse} = P_g + P_{se} \tag{6.9}$$

Combining equation (6.7) and equation (6.9):

$$P_{se} + P_{sh} = P_{SN} - P_g \tag{6.10}$$

The two converters are assumed lossless in this voltage sources model. This implies that there is no absorption or generation of active power by the two converters for their losses. According to equation (6.10), during steady state operation, the summation of active power absorbed or generated by the shunt and series converter from the system is equal to the difference in active power between the SSEG networks and the utility grid at bus 321. Another assumption is that during the disturbance, if the SSEG networks supply or absorb the power to or from the grid, the differences in demand and generation during the disturbance are accommodated by the storage devices available in each individual SSEG network or at the DC side of the SSEGs to maintain a stable operation of the SSEG networks. The advantages of these assumptions allow the series converter to control the active and reactive power flow between the SSEG networks and the grid without any predefined reference values for active and reactive power.

During the disturbance, the above condition must be satisfied even if there is no active power flow between the SSEG networks and the grid ($P_g = 0$). Thus the active power flow in the system is:

$$P_{se} + P_{sh} = P_{SN} \tag{6.11}$$

P_{SN} : the total active power flow from the SSEG networks to the main grid before the shunt converter;

P_{sh} : shunt converter output active power,

P_g : active power flow between the SSEG networks and the main grid after the series converter;

P_{se} : series converter output active power,

P_{bse} : active power before the series converter.

As shown in the lower dashed frame in Figure 6.3, the PI controller would suffice to control the active power of the shunt converter by generating the proper values for θ_{sh}. From equation (6.5) the transfer function of the PI controller is:

$$E_P(s) = \left[P_{sh}(s) + P_{se}(s)\right] \tag{6.12}$$

$$\theta_{sh}(s) = \mathrm{K}_{p\theta}\left[1 + \frac{1}{\tau_{i\theta} S}\right].E_P(s) \tag{6.13}$$

The angle order θ_{sh} represents the shift between the system voltage and the voltage generated by the shunt converter. The angle order is combined with the voltage synchronizing signal (ωt) which is provided by the phase-locked loop (PLL) fed by the measured three-phase voltages of the shunt converter. Finally, with the voltage order this signal becomes three phase sinusoidal voltage signals whose magnitude and phase are controlled as described below [95, 96]:

$$v_{sha} = V_{sh}\sin\left(\omega t + \theta_{sh}\right) \tag{6.14}$$

$$v_{shb} = V_{sh}\sin\left(\omega t + \theta_{sh} - 2\pi/3\right) \tag{6.15}$$

$$v_{shc} = V_{sh}\sin\left(\omega t + \theta_{sh} + 2\pi/3\right) \tag{6.16}$$

6.3.2 Series Converter Control

The series converter controls the magnitude and angle of the voltage injected in series with the line between the SSEG networks and the distribution network. The Main objective of this voltage injection is to control the power flow between the

SSEG networks and the distribution network. The actual value of the injected voltage can be obtained in several ways [126-128].

- Direct Voltage Injection Mode: In this control mode, the reference inputs are directly the magnitude and phase angle of the series voltage.
- Phase–shifting regulation mode: The reference input is the phase displacement between the SSEG networks bus voltage at the shunt converter terminal and the voltage at the point of connection to the distribution network after the series converter.
- Line Impedance Emulation mode: The reference input is an impedance value to insert in series with the line impedance between the SSEG networks and the distribution network.
- Active and reactive Power Flow Control Mode: The reference inputs are values of P and Q to be delivered or absorbed from the distribution network.

In this work, the series converter operates in the direct voltage injection mode. The series converter simply injects voltage as per the beta 'β' order. β is the value of phase angle shift β between the SSEG networks bus voltage V_{SN} and the main grid voltage V_g that follows the active power $P_{SN\text{-}g}$ and the reactive power $Q_{SN\text{-}g}$ flow between the SSEG networks and the main grid. As β varies, the magnitude V_{se} and phase angle θ_{se} of the series injected voltage also vary. The series-injected voltage of the series converter is given by:

$$V_{se}\angle\theta_{se} = V_{SN}\angle\theta_{SN} - V_g\angle\theta_g \tag{6.17}$$

Where θ_{se}, θ_{SN} and θ_g are the angle of V_{se}, V_{SN} and V_g, respectively. With the SSEG networks voltage V_{SN} taken as the reference, the phase difference between the SSEG networks and the main grid voltages is:

$$\beta = \theta_g - \theta_{SN} \tag{6.18}$$

From equation (6.17)

$$\underbrace{V_{se}\angle\theta_{se} = V_{SN}\angle 0 - V_g\angle\beta}_{polar} = \underbrace{V_{SN} - V_g\cos\beta - jV_g\sin\beta}_{rectangular} \tag{6.19}$$

From equation (6.19) the injected voltage magnitude and angle are:

$$\theta_{se} = \tan^{-1}\left(\frac{-V_g\sin\beta}{V_{SN} - V_g\cos\beta}\right) \tag{6.20}$$

$$\left|V_{se}\right| = \sqrt{\left(V_{SN} - V_g\cos\beta\right)^2 + \left(V_g\sin\beta\right)^2} \tag{6.21}$$

$$\left|V_{se}\right| = \sqrt{V_{SN}^2 - 2(V_{SN}V_g\cos\beta) + V_g^2\cos^2\beta + {V_g}^2\sin^2\beta} \tag{6.22}$$

$$\left|V_{se}\right| = \sqrt{V_{SN}^2 - 2(V_{SN}V_g\cos\beta) + V_g^2\left(\cos^2\beta + \sin^2\beta\right)} \tag{6.22'}$$

The term $\cos^2\beta + \sin^2\beta = 1$ [129], then the voltage magnitude will be:

$$\left|V_{se}\right| = \sqrt{V_{SN}^2 - 2(V_{SN}V_g\cos\beta) + V_g^2} \tag{6.23}$$

The equations of the active and reactive powers of the system are given as follows:

$$P_{SN-g} = \frac{V_gV_{SN}\sin\beta}{X_{se}} \quad [3] \tag{6.24}$$

$$Q_{SN-g} = \frac{V_{SN}^2 - V_gV_{SN}\cos\beta}{X_{se}} \quad [3] \tag{6.25}$$

$$P_{SN} = I_{SN}.V_{SN}\cos\phi_{SN} \tag{6.26}$$

$$P_g = I_{se}.V_g\cos(\phi_{SN} - \beta) \quad [96] \tag{6.27}$$

$$P_{bse} = I_{se}.V_{SN}\cos\phi_{SN} \tag{6.28}$$

P_{SN-g}: the active power flow between the SSEG networks and the main grid

Q_{SN-g}: the reactive power flow between the SSEG networks and the main grid

X_{se}: series injected reactance

From equations (6.8), (6.27) and (6.28) the series injected active power can be expressed as:

$$P_{se} = I_{se}.V_{SN}\left(\cos\phi_{SN} - \left(\frac{V_g}{V_{SN}}\right)\cos(\phi_{SN} - \beta)\right) \tag{6.29}$$

From the above equations when the grid voltage and the SSEG networks voltage are in phase ($\beta = 0^\circ$, ($\theta_g = \theta_{SN}$)), it is clear that the series injected voltage and the supply-side voltage are in phase ($\beta = \theta_{se}$), thus the magnitude of the series injected voltage attains its minimum value as in:

$$|V_{se}| = \sqrt{V_{mg}^2 - 2V_{SN}V_g + V_g^2} \tag{6.30}$$

$$|V_{se}| = \sqrt{(V_{SN} - V_g)}^2 \tag{6.31}$$

$$|V_{se}| = |V_{SN} - V_g| \tag{6.32}$$

For $V_{SN} = 1.0$ pu, the magnitude of a sag can be defined as:

$$V_{sag} = 1 - V_g \tag{6.33}$$

In steady state the SSEG networks bus voltage is regulated by the shunt converter to maintain $V_{SN} = 1.0$ pu. If the grid voltage is close to 1pu ($V_g \approx 1.0pu$) then the series injected voltage $V_{se} \approx 0pu$ and the sag is zero $V_{sag} \approx 0pu$.

The worst case during the disturbance is when $V_g \approx 0$ in this case the maximum sag that must be compensated is $V_{sag}\ \max = V_{se} = 1pu$

To compensate the maximum sag, the required series voltage magnitude injection is $V_{se} \approx 1pu$.

When the SSEG networks voltage and series current V_{SN} and I_{se} are used as base quantities (1pu), the injected active power and injected voltage magnitude and angle in equation (6.29), (6.20) and (6.21) respectively will be:

$$P_{se} = \cos\phi_{SN} - V_g \cos(\phi_{SN} - \beta) \tag{6.34}$$

$$\theta_{se} = \tan^{-1}\left(\frac{-V_g \sin\beta}{1 - V_g \cos\beta}\right)) \tag{6.35}$$

$$\left|V_{se}\right| = \sqrt{1 - 2(V_g \cos\beta) + V_g^2} \tag{6.36}$$

If $V_g = 1.00\,pu$ then the equations (6.34) and (6.36) will be

$$\left|V_{se}\right| = \sqrt{1 - 2\cos\beta + 1} \tag{6.37}$$

$$\left|V_{se}\right| = 1.414\sqrt{1 - \cos\beta} \tag{6.38}$$

$$\theta_{se} = \tan^{-1}\left(\frac{-\sin\beta}{1 - \cos\beta}\right) \tag{6.39}$$

6.3.2.1 Series Converter Controller Design

Figure 6.4 shows a schematic diagram of a series converter controller block. The function of this controller is to control the power flow between the SSEG networks and the main grid by determining the magnitude and angle of the series injected voltage for the series converter. These values of magnitude and angle are controlled by the angle β between the SSEG networks and the main grid. The angle β is

generated by the PI controller that controls the flow of active power at node (321) where the shunt converter is connected, as described in the following equations.

The transfer function of the PI controller is given by:

$$\beta(s) = \mathrm{K}_{p\beta}\left[1+\frac{1}{\tau_{i\beta}S}\right].E_P(s) \tag{6.40}$$

Where $E_{P_{sh}}(s) = \left[P_{SN}(s) - P_g(s)\right]$ (6.41)

$\mathrm{K}_{p\beta}$: proportional gain of the PI controller

$\tau_{i\beta}$: integral time constant of PI controller (equal to $\frac{K_{P\beta}}{k_{i\beta}}$ where $\mathrm{K}_{i\beta}$ is the integral gain).

β: power angle of V_{SN};

The angle β is the input of the second part of the controller which is equation (6.42) decomposed into its real and imaginary components (x and y) as described in the following equations:

If the grid voltage $V_g = 1pu$ and SSEG networks voltage $V_{SN} = 1pu$, the equations (6.1) and (6.19) can be written together as:

$$V_{se}\left(\cos\theta_{se} + j\sin\theta_{se}\right) = 1 - \cos\beta - j\sin\beta \tag{6.42}$$

Then x and y will be:

$$x = \left(1 - \cos\beta\right) \tag{6.43}$$

$$y = -\sin\beta \tag{6.44}$$

These two equations (6.43 and 6.44) are the input of the rectangular to polar form component to generate the modulation index, $\mathrm{m_i}$ and θ_{se}. The $\mathrm{m_i}$ and θ_{se} signals are

used to develop firing pulses for the PWM converter. Since a controlled voltage source is used instead of a PWM converter, the reference value m_i is converted from per unit to volts to get V_{se} in kV. Finally, the measured three-phase voltages of the grid are fed to the phase locked loop (PLL) in order to detect the angular positions (ωt) of the voltages as a saw tooth waveform. Then (ωt) is added to the series injected phase shift θ_{se} signals to represent the three phase sinusoidal voltage source converter as defined below [95]:

$$v_{sea} = V_{se}\sin(\omega t + \theta_{se}) \tag{6.45}$$

$$v_{seb} = V_{se}\sin(\omega t + \theta_{se} - 2\pi/3) \tag{6.46}$$

$$v_{sec} = V_{se}\sin(\omega t + \theta_{se} + 2\pi/3) \tag{6.47}$$

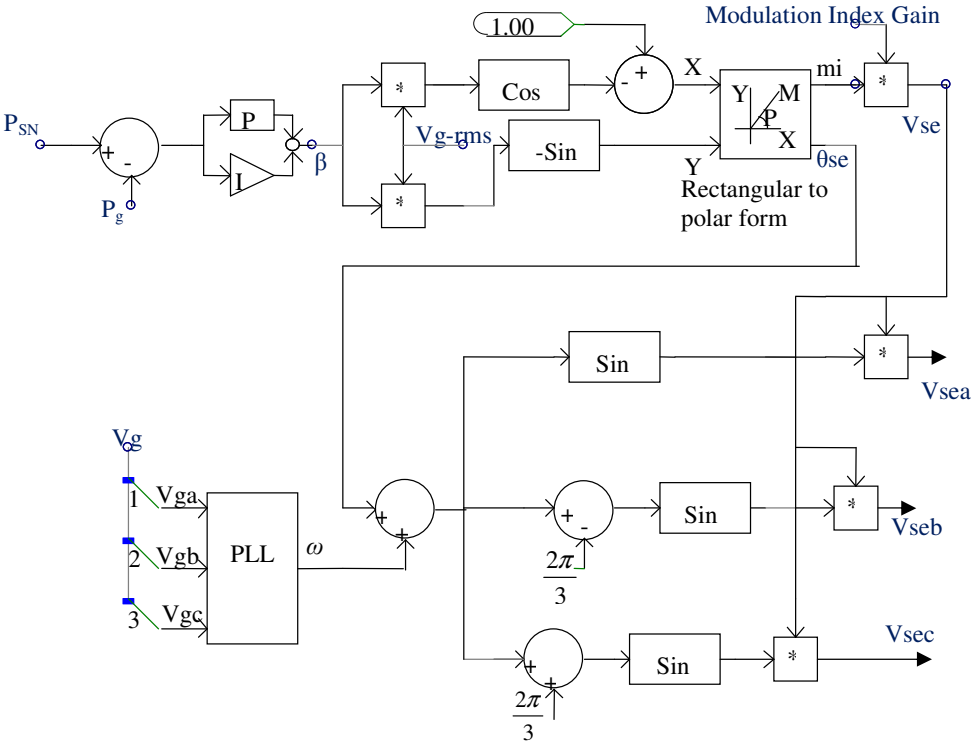

Figure 6.4: Block diagram representation of the controller of the series converter

6.4 USSC Rating

In this section the rating of USSC components; converters, transformers and capacitance of the DC Link capacitor has been calculated.

6.4.1 USSC Converter Ratings

Operation of the USSC demands a proper power rating of the series and shunt converters. The ratings should enable the USSC to carry out pre-defined regulation tasks without becoming overloaded. The shunt and series converters mutually exchange active power only, whereas reactive power is controlled independently at both sides. Thus the sizing of the converters depends upon the amount of reactive power needed by the system to achieve the appropriate response. This can be identified from the simulation results by assuming the USSC can deliver large amounts of reactive power at the connected bus. The amount of reactive power needed at the connected bus is the amount of reactive power needed by the system, which dictates the size of the USSC converters. This size of the USSC converters is required to alleviate over and under voltage fluctuations during steady state and disturbance conditions [130].

According to equation (6.5) the active power absorbed by the shunt converter from the system could be equal to the active power needed by the series converter if the losses in the shunt converter are neglected. Thus the apparent power rating of the shunt converter S_{sh} is given by:

$$S_{sh} = \sqrt{P_{se}^2 + Q_{sh}^2} \tag{6.48}$$

Or

$$S_{sh} = \sqrt{P_{sh}^2 + Q_{sh}^2} \tag{6.49}$$

Also the apparent power of the series converter S_{se} , given as:

$$S_{se} \approx Q_{se} \tag{6.50}$$

Thereby, the minimum apparent power rating (S_{sh}) of the shunt converter is given as a maximum active power demanded by the injected series voltage source.

$$S_{sh-\min} = P_{se-\max} \tag{6.51}$$

The maximum available reactive power from the shunt converter is given as:

$$Q_{sh-\max} = \sqrt{\left(S_{sh}^2 - \left(P_{se-\min}\right)^2\right)} \tag{6.52}$$

Therefore, based on the active power absorbed by the shunt converter from the system and reactive power injected by the shunt converter to the system during the network disturbance in the case studies performed in this work, the active power absorbed by the shunt converter is 0.5 MW and reactive power injected to the system by shunt converter is 2.7MVAr. Thus from equation (6.49) the rating of the shunt converter is 2.746MVA. Also from the results the reactive power injected by the series converter is 0.25MVAr, therefore according to equations (6.50) and (6.5) the rating of the series converter is 0.25MVA. Thus, the rating of the series converter need not be as high as the shunt converter.

6.4.2 Transformers Ratings

The shunt inverter is connected through 11/33 kV, 2.8 MVA Y-Δ transformer. The series inverter is connected through set of three single-phase series transformers (6.35/19.05 kV, 0.3 MVA).

6.4.3 Capacitance of the DC Link Capacitor

The total capacitance of the DC link in Farads, is related to the USSC converter ratings and to the DC link nominal voltage. The energy stored in the capacitance (in Joules) divided by the converter rated power (in VA) is a time duration which is usually a fraction of a cycle at nominal frequency as given:

$$t = \frac{c \times \left(V_{DC}\right)^2}{2 \times S_{sh}} \qquad [131] \tag{6.53}$$

The DC voltage can be calculated from the equation below:

$$V_{DC} = \frac{3 \times \sqrt{3}}{\pi} V_s \qquad [132] \tag{6.54}$$

V_s = peak phase voltage of the converter

The converter terminal voltage (Vs) used in this study is 6.35kV. From equation (6.54) the value of the V_{DC} is 10.5kV. Also in this study the time duration was assumed to be 400ms, which represents 20 cycles for a 50 Hz frequency. Thus from equation (6.53) the value of the capacitor is 19.9 mF.

6.5 Results and Discussions

In this section two types of fault studies are presented, in order to illustrate the effectiveness of the USSC as a compensator for voltage sag, fault ride-through of SSEG networks, power flow control and voltage unbalance mitigation. The first type of fault study investigates the transient performance of the USSC in response to symmetrical faults (three-phase fault) in the grid by compensating the voltage sag and controlling the power flow in the system for fault ride-through of SSEG networks. The second study presents the transient behaviour of the USSC in response to an asymmetrical fault (single-line to ground fault) in the grid by mitigating the voltage unbalance.

6.5.1 Three –Phase Fault Study

In this study, two specific three-phase fault conditions were applied on the grid side of the distribution network as shown in Figure 6.1. The first fault condition was when a three-phase fault occurred at a remote location on bus 339 to examine performance of the USSC as the voltage sag compensator. The second fault condition when the same fault occurred at the subsea cable connection to the grid (bus 318) to examine voltage-interruption compensation, the power flow control and fault ride-through capabilities of different types of SSEG networks with the proposed USSC-based method. The three-phase faults were applied at 5s for a duration of 400ms. This time has been chosen to determine the effective of the USSC to enhance the stability of the SSEGs. From Chapter 3, at this time the synchronous and induction generators were unstable for a fault in distribution network.

6.5.1.1 Voltage Sag Compensation

Figure 6.5(a) and (d) show the operating waveforms and rms voltage in per unit, respectively of the grid voltage when a three-phase voltage sag by 60% voltage drop occurred due to an electrically remote three-phase fault on distribution network (bus 339). As shown in Figure 6.5(b) during the voltage sag the series converter injects three-phase sinusoidal voltage across the line between the grid and SSEG networks which compensates the voltage drop. As a result, the SSEG networks voltage is compensated as shown in Figure 6.5 (c) and (d).

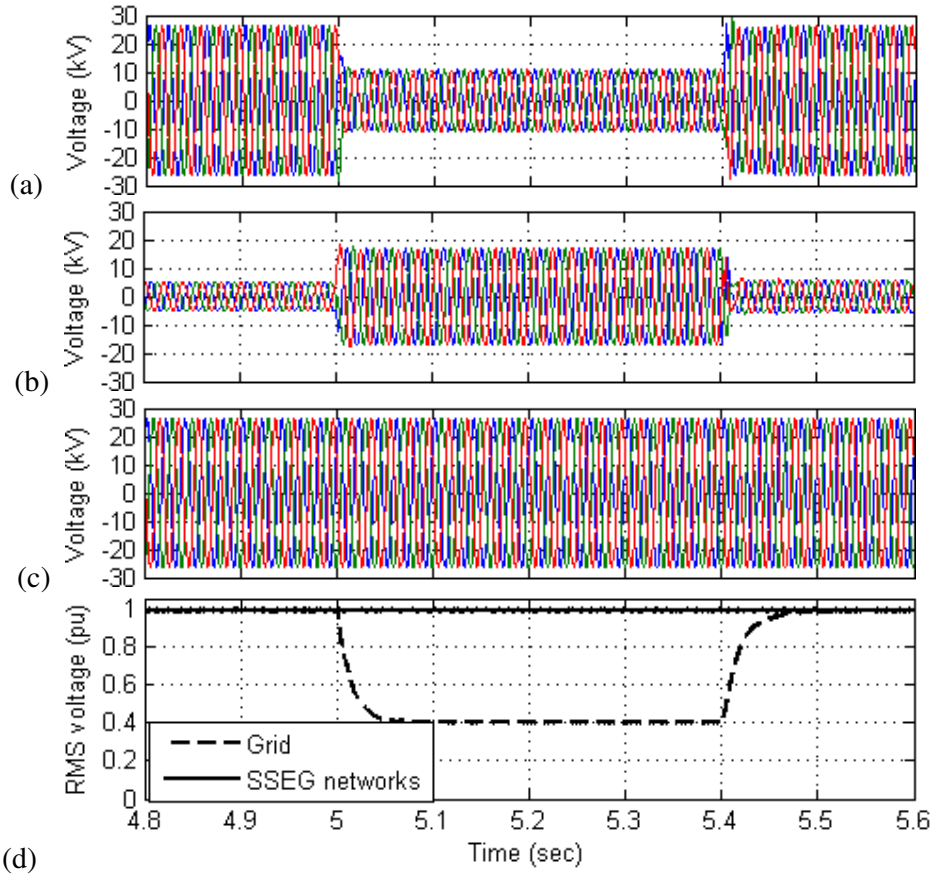

Figure 6.5: Operating waveforms and rms during three-phase voltage sag by 60% voltage drop at the main grid side: (a) Grid voltage in kV (b) Injected voltage in kV (c) SSEG networks voltage in kV (d) RMS value of grid& SSEG networks voltage in pu.

6.5.1.2 Voltage interruption Compensation

Figure 6.6 illustrates the use of the USSC in compensating voltage interruption due to the three-phase fault on bus 318 of distribution network. As shown in Figure 6.6 (a) and (d) during the fault duration, the collapse of the grid voltage can be observed. The grid voltage drops from 0.9987 to 0.025 pu. Figure 6.6 (b) and (c) show the voltage injected by the series converter and the corresponding SSEG networks voltage (at the shunt converter connection) with compensation. As a result of using the USSC, the voltage at the connection point of the SSEG networks to the subsea cable (bus 321) is kept at 1pu during the steady state and the disturbance.

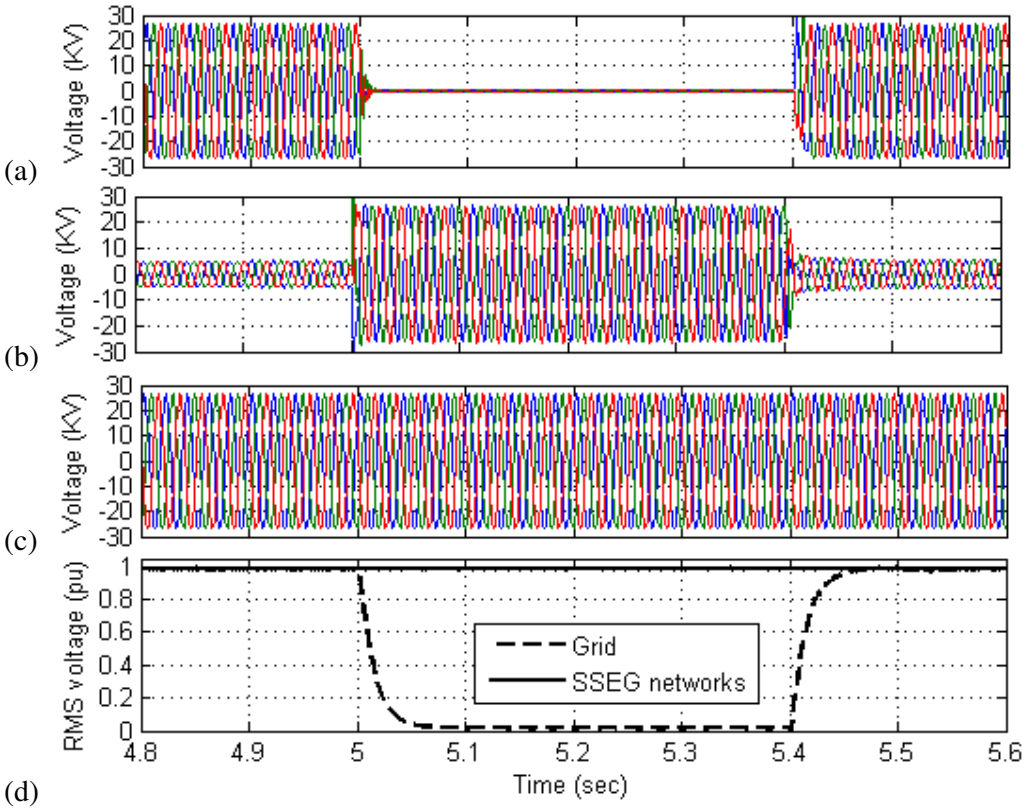

Figure 6.6: Simulation result of voltage interruption during three-phase fault study: (a) Grid voltage in kV (b) Injected voltage in kV (c) SSEG networks voltage in kV (d) RMS value of grid& SSEG networks voltage in pu.

6.5.1.3 Power Flow Control during Steady-State and Transient Conditions

The aim of the study is to evaluate the performance of the USSC for power flow control during steady-state and network disturbance. The flow of instantaneous active and reactive powers into or out of the USSC is shown in Figure 6.7(a and b), which illustrate the active and reactive power flow into the system at the SSEG networks and main grid sides of the USSC (before and after the USSC) during the steady state. The active and reactive power flows from the SSEG networks are constant, 0.126MW and 0.15MVAr. When a fault occurs at time 5 sec for a duration of 400s, the active and reactive power flows into the system dropped to zero. Figure 6.7 (c) shows that during the steady state the active powers from or into the series and shunt converters are zero and during the fault period, active power is absorbed by the shunt converter and also injected into the system from the series converter, the summation of these powers are approximately zero which satisfies equation (6.5) as shown in Figure 6.7 (e). The simulation result in Figure 6.7 (d) indicates that during the fault period, the reactive power of the shunt converter increases to 2.7MVAr to maintain the voltage of the SSEG networks at 1pu. Figure 6.7 (e) shows the active power flow mismatch in the system for the shunt and series converters and the SSEG networks and the grid. This result demonstrates the equation (6.10). Thus, by using the USSC the active and reactive power flows from the SSEG networks are controlled and maintained at constant levels during steady state and also under fault conditions. As a result the frequency of the system is maintained at 50Hz as shown in Figure 6.7 (f).

6.5.1.4 Fault Ride Through for Converters-Connected based SSEG Networks

When the fault occurs in the grid, high fault currents will flow through the converter; this must be constrained within the capability of the semiconductor devices. The converters are designed to supply a fault current that is typically only twice the nominal load value for microseconds [133]. But in this case study the USSC ensures the fault ride-through of the SSEG networks based on converters–connected (SSEG networks 1, 2 and 3). As shown in Figure 6.8(a) during the fault in the distribution network for period (5sec-5.4 sec) the SSEG networks do not experience the voltage

sag. Thus as shown in Figure 6.8 (b, c and d) the current output from the SSEG networks based on converters–connected (SSEG networks 1, 2 and 3 respectively) remain the same as the pre-fault values. Therefore the semiconductor devices of the converter connected to SSEG networks have been protected from over current. As a result the USSC works as fault current limiter which limits the current outputs of the converters at values equal to pre fault values.

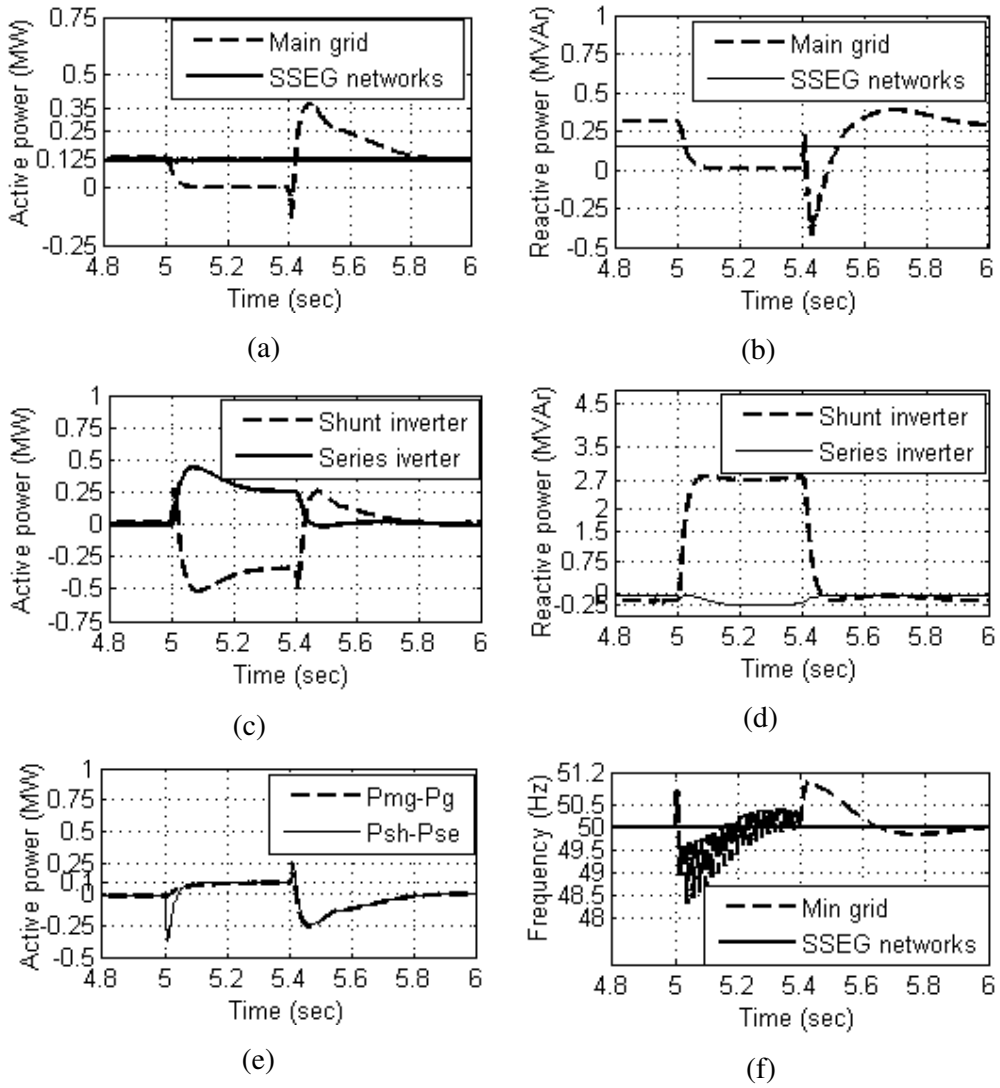

Figure 6.7: Simulation results with grid side three-phase fault: (a) and (b) Active and reactive power flow between SSEG networks and main grid, (c) and (d) Active and reactive power output to or from the system by the series and shunt converters, (e) Active power flow mismatch $(P_{se}+P_{sh})-(P_{mg}-P_g)=0$ (f) Grid and SSEG networks frequency.

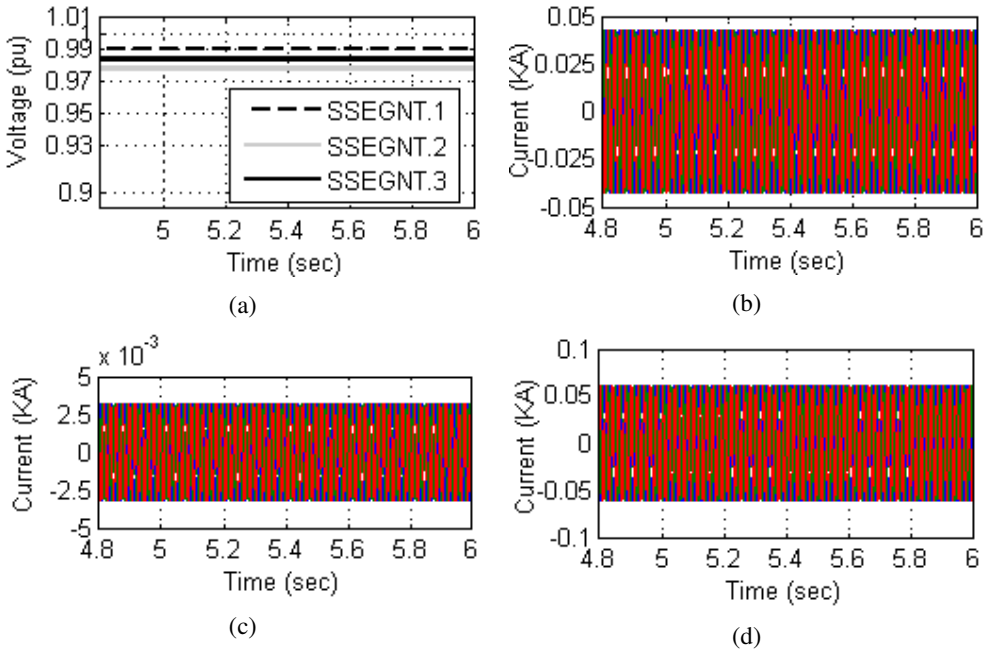

Figure 6.8: Simulation results of the SSEG networks currents and RMS terminal voltages with grid side ac fault with USSC: (a) RMS terminal voltages and (b, c &d) output currents of the SSEG networks (1,2&3) respectively.

6.5.1.5 Fault Ride-Through of SSEG Network Based on Induction Generator

Due to voltage sag under fault conditions, the induction generators tend to significantly increase their reactive power demand and the capability of an induction generator to deliver active power during the fault will reduce. The reduced delivery of active power during the fault causes acceleration of the rotor which reaches a high steady-state speed. This speed exceeds that corresponding to the frequency of the system and leads to instability. But by using the USSC the ensuring fault ride-through of the generator can be seen in Figure 6.9, for a three-phase fault in the distribution network at 5 sec lasting 400msec. As shown in Figure 6.9 (a), the reactive power demand of the generator remains the same as the pre-fault value. Thus, the generator does not experience the voltage sag (Figure 6.9(b)) and the over-speeding of the generator is avoided (Figure 6.9 (c)). Also as shown in Figure 6.9 (a) the ability of the generator to produce active power is not affected.

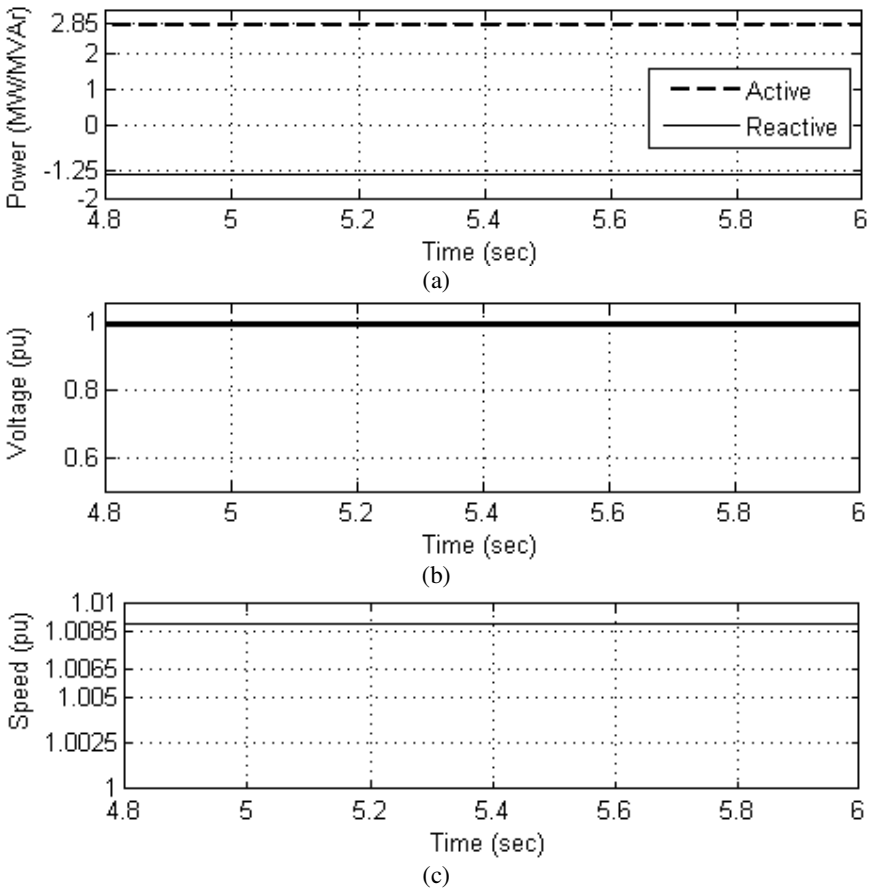

Figure 6.9: Dynamic performance of induction generator-based SSEG with USSC: (a) Active power output and reactive power, (b) RMS terminal voltage and (c) rotor speed

6.5.1.6 Fault Ride-Through of Synchronous Generator-based SSEG Network

During the fault, the mismatch between the mechanical power input and electrical power output causes rotor acceleration or deceleration with a corresponding variation of rotor angle. Therefore the synchronous generator will pole-slip and become unstable. However by using a USSC as shown in Figure 6.10 there would be no effect on the angle and the output active and reactive powers of the machine. As seen in Figure 6.10(a) during the fault in the distribution network at 5 sec lasts 400msec the terminal voltage of the generator is maintained at almost constant value. Thus, as shown in Figure 6.10(b) the active power generated by the generator remains the same

as the pre-fault value. As a result the fault ride-through of the generator is ensured because the generator does not experience pole slipping as shown in Figure 6.10(c).

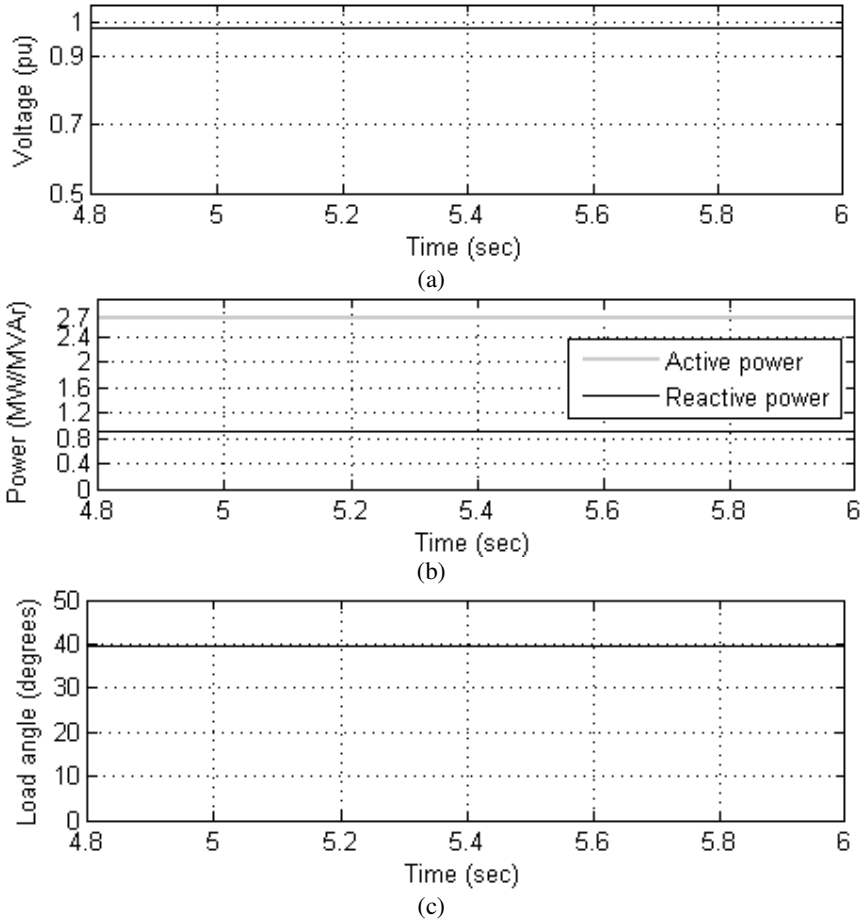

Figure 6.10: Dynamic performance of synchronous generator-based SSEG with USSC: (a) Active power output and reactive power, (b) RMS terminal voltage and (c) load angle.

6.5.2 An Asymmetrical Fault Study for Voltage Unbalance Mitigation

The aim of this study is to investigate whether the USSC can mitigate a voltage unbalance. An unbalanced voltage condition is created by applying a single phase to ground fault on phase A on the subsea cable connection to the main grid (bus 318) at time 5s for a duration of 400ms. Figure 6.11 (a, d and e) show the simulation results

of the three-phase unbalanced voltages for the grid system and the positive (Vp), negative (Vn) and zero (V0) sequence components.

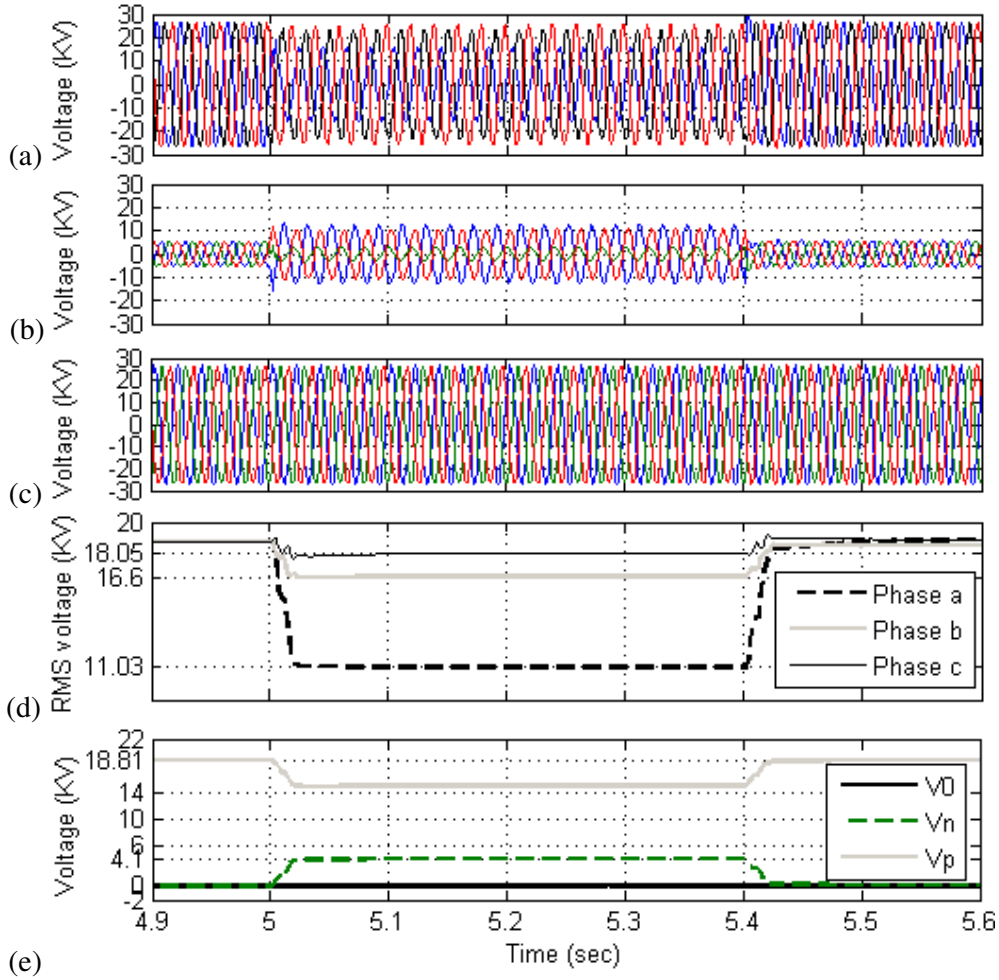

Figure 6.11: Three-phase voltages for unbalance mitigation study: (a) Grid voltage in kV (b) Injected voltage in kV (c) SSEG networks voltage in kV (d) RMS values of Phase (a, b and c) of grid voltage in kV (e) The positive (Vp), negative (Vn) and zero (V0) sequence components in kV for the voltage on the main grid side.

It can be seen that during fault conditions, the maximum RMS phase voltages are Va = 1.03kV, Vb = 16.639kV and Vc = 18.05kV and the Vp = 14.984kV, Vn = 4.1kV and V0 ≈ 0kV. The value of zero sequence is cancelled by the delta-delta transformer on the subsea cable between the measuring point and the fault.

The percentage of voltage unbalance is calculated according to the (2.1) and found to be 27.36%.

$$\text{Voltage unbalance}(\%) = \frac{\text{Negative phase sequence component x } 100\%}{\text{Positive phase sequence component}}$$

$$\text{Voltage unbalance}(\%) = \frac{(14.984 + 4.1 + 0) \text{ x } 100\%}{14.984} = 27.36\%$$

This value indicates that the voltage unbalance is severe during the fault as the limit of the voltage unbalance as mentioned in chapter 2 (section 2.8) is 2%. Also Figure 6.11 (b and d) show the voltage injected by the series converter and the corresponding SSEG networks voltage (at the connection of the shunt converter) with compensation. Therefore the USSC can reduce the voltage unbalance to value less than 2% as in the result the voltage unbalance is zero.

6.6 Justification of Choosing the USSC among other Compensation Devices

A fair comparison between using the USSC instead of other reactive power compensation devices used in the distribution system must include their cost and their impact on power system steady-state and dynamic issues.

6.6.1 Comparison between Custom Power Devices and Conventional Reactive Power Compensation Devices

The comparison between the costs along with the characteristics of some well known distribution system reactive power compensation devices are shown in Table 6.2 [132,134-138]. These are conventional devices (capacitors and SVCs) and custom power devices (DVR, STATCOM and USSC). It can be seen that the costs of producing reactive power by using fixed shunt and series capacitors are much lower than those of producing dynamic reactive power by using other types of equipment. If the cost is the only concern, fixed shunt and series capacitors would be the

preferred choice for obtaining reactive power. Although the capacitors are cheaper than others, they suffer from a few drawbacks: They are far less efficient due to their response time; they cannot adapt to rapid changes during power system disturbances; their reactive power production drops with the square of the voltage [135,137]; the mechanical switching reduces the life span of the load and distribution equipment especially rotating machines [137,138].

Table 6.2: Cost comparison and characteristics of main reactive power compensation devices [132,134-138].

Equipment Type	**Capital Cost ($/kVAr)**	**OperatingCost**	**Speed of Response**	**Ability to Support Voltage**	**Effect on Reliability of distribution system Equipments and loads**
Shunt Capacitor	8	low	Slow	Poor, drops with V^2	Reduced the life span of the equipment
Series Capacitor	20	low	Slow		
SVC	40	Moderate	Fast		Limited
DVR	50	Moderate	Fast	Fair, drops with V	Maximizing system reliability and availability.
D-STATCOM	50	Moderate	Fast		
USSC Series Part	50	Moderate	Fast		
USSC Shunt Part	50	Moderate			

The cost of SVCs that produce capacitive and inductive reactive power within timescales in the order of milliseconds is lower than the cost of custom power devices. The main disadvantage of SVCs is that they are similar to capacitors; their reactive power output varies according to the square of the voltage they are connected to [135,137]. Thus their impact on the distribution system reliability is limited during voltage sags. The more expensive reactive power sources (custom power devices) sometimes must be purchased even if the low-priced sources (capacitor banks and SVC) are available because of their relative advantages. Their response time (in the order of microseconds) and their reactive power output does not vary with the square of the voltage they are connected to [135,137]. Therefore they help the distribution system to provide highly reliable, high-quality power [77,132]. As the improved quality of power in the distribution network reduces the stress on installed equipment, their lifespan increase, thus lowering their maintenance and

replacement costs [138]. Moreover the reliability of high sensitivity equipment such as high-speed motors, computers, microprocessors and medical instruments would be maximized as they are less affected by power quality issues occurring in the system [132].

6.6.2 Comparison between USSC and other Custom Power Devices

From the comparison between the power electronics and conventional types of compensation devices, the compensation devices based on the application of power electronic controllers (custom power devices) are preferred over the conventional types. As the application of custom power provides high quality power, the reliability of the distribution network is improved [139]. However, in this work the required solution has to satisfy two goals, to aid SSEGs to provide high quality power and to enable them to have enhanced fault ride-through capability. Table 6.2 compares between the application of DVR, DSTATCOM, USSC and fault current limiter (FCL) for addressing some steady state and dynamic power system issues [76,134, 140-147]. In this compression the FCL is included which is used for limiting the short circuit current for aiding the fault ride-through capability [148]. According to the assessment presented in Table 6.3 the USSC has a better capability to mitigate various power quality problems and to enhance the stability of the distribution system compared to others. The referenced literature [76] concludes that the USSC show a better voltage sag compensation capability as compared to the DVR and the D-STATCOM in terms of the voltage magnitudes. For task related to voltage unbalance mitigation the USSC making the three phase voltages more balanced while for cases with the DVR and D-STATCOM connected the voltage unbalance can be reduced [76,119] but to value outside the limit of the percentages of voltage unbalance (2%). The unbalance can be reduced by DVR and D-STATCOM to value 5.02% and 2.2%, respectively [76,119]. For harmonics mitigation tasks the USSC can perform the current and voltage based harmonics mitigation [144]. However the DVR can mitigate apart from voltage harmonics [146] and the DSTATCOM can mitigates the current harmonics only [132,134,135]. For the voltage flicker mitigation task the only both the USSC and the D-STATCOM can be used for reducing voltage flicker [76,119,141]. The DVR and the DSTATCOM fail to

perform task related to power flow control [119]. In paper [137] the performance of the USSC is compared with that of a DSTATCOM to aid fault ride-through of the conventional fixed-speed induction generator (FSIG). The rating requirement of the STATCOM (1.72 pu) was found higher than the rating requirement of a USSC (1.47 pu) to aid fault ride-through of the FSIG. If the STATCOM rating is reduced further, the generator fails to ride through the fault. Thus the USSC proves to be a potential solution to the grid integration problems faced by the wind-driven FSIG. The task for limiting the fault current can be only performed by the USSC [147], the DVR [145] and the FCL [148]. In contrast to other devices, it is clearly seen that the USSC is a comprehensive solution for the mitigation all power quality problems, fault current limiting and enhancing voltage stability of the distribution network as well as aiding the fault ride through capability of the SSEGs.

Table 6.3: Power quality mitigation, fault ride through and voltage stability of USSC, D-STATCOM, DVR and FCL [76,134, 140-147].

Tasks	DVR	D-STATCOM	FCL	USSC
Sag compensation	yes	limited	limited	yes
Swell compensation	yes	limited	No	yes
Voltage unbalance mitigation	No-outside the limits	No-outside the limits	No	yes
Voltage flicker reduction	No	yes	No	yes
Current harmonics mitigation	No	yes	No	yes
Voltage harmonics mitigation	yes	No	No	yes
Power factor correction	yes	yes	No	yes
Reactive power compensation	yes	yes	No	yes
Power flow control	No	No	No	yes
Limiting the fault current	yes	No	yes	yes
Fault ride through	yes	Requires high rating	yes	yes
Voltage Stability	yes	yes	No	yes

6.6.3 USSC Cost and Benefits

Based on the reactive power required by the system during the network disturbance in the case studies considered in this chapter, the size of the USSC series part is 0.25MVAr and the size of the USSC shunt part is 2.7MVAr. However, active power

flows on the DC side through the shunt converter is about 0.5 MW. Thus the size of the shunt converter is 2.746MVA. As a result, the size of the USSC series part is small compared to the size of the USSC shunt part. Therefore, based on the calculated size of the USSC in these case studies, the capital cost of the USSC would be about $149,000 ($137,000 for USSC shunt part and $12,000 for USSC series part). These costs will have to be considered within the context of the benefits that would be gained from the USSC. Table 6.4 summarises the technical benefits that can be gained from employing a USSC compared to the DVR and DSTATCOM [139,149,150]. As shown in Table 6.4, in contrast to the USSC neither DVR nor DSTATCOM has a strong impact on load flow control, stability or voltage quality. Therefore the USSC has more impact on the reliability of the distribution system equipment. DSTATCOM is current-based problems compensation [144] and DVR is voltage-based problems compensation [144] whereas the USSC is a combination of voltage- and current-based problems compensation. Moreover the cost of USSC is less than the cost of DSTATCOM for fault ride through application due to the rating of the DSTACOM is higher than rating of the USSC to achieve the same target [137]. Thus the USSC (combination of active series with active shunt filters) [144] [147,118,119] is an ideal choice for such mixed compensation due to the benefits that can be derived from it.

Table 6.4: Technical benefits of the USSC compared with other custom power devices [139,149,150].

Devices	**Impact on System Performance**			**Reliability of the system with**
	Load Flow control	**Stability**	**Voltage Quality**	
DVR	No	Medium	Medium	Reliable
DSTATCOM	No	Medium	Strong	Reliable
USSC	Strong	Strong	Strong	More Reliable

6.7 Summary

The fault ride-through capability is an important issue when integrating large scale SSEGs. In this study, PSCAD is used to simulate the model of a USSC connected between SSEG networks and a 33kV distribution network. The simulation results show that the proposed technique (based on the USSC) can ensure the fault ride-through capability of SSEG networks and improve voltage quality at the SSEG networks bus during steady state and transients. During steady state, the USSC controls the power delivered to the grid and improves the voltage of the SSEG networks. During a disturbance, the controllers maintain the voltage and frequency of the SSEG networks at pre fault values. Therefore the speed of an induction generator and the load angle of a synchronous generator during and after fault conditions are kept constant. This is due to the balanced electrical and mechanical torque of the machines. Moreover, the results show that there is no effect on the output current for the SSEG networks based on converter–connected SSEGs. Thus the current levels remain within the capability of the semiconductor devices. Furthermore, the proposed technique can mitigate voltage unbalance due to asymmetrical grid faults. In addition this technique can reduce the increase in fault current levels in the electricity grid caused by the high penetration of SSEGs.

CHAPTER 7

Small-Scale Embedded Generation Contribution to Power System Frequency Regulation

7.1 Introduction

This chapter describes the design and implementation of a proposed control technique for load-frequency control (LFC) for systems with high penetration of SSEG. The control includes a facility for discrimination between normal operation and system disturbances. The controller can respond to disturbances such as load increase or load losses. During initialisation the controller does not operate. After the system reaches steady state, the controller starts to monitor the balance between the load and the generation in the system. This task can be performed by monitoring the system frequency as this indicates a balance or unbalance between the power generated and the load. Under normal operating conditions, this difference is zero, in this case the system frequency will be at nominal value 50 Hz. On other hand when the load is more than the active power generated the system frequency will be under 50 Hz, if the system frequency reaches a value below 50 Hz, the under frequency protection will operate to trip the generators. Also when the active power generated exceeds the load for values more than 50 Hz, the over frequency protection will operate to trip the generators. According to the G59/1 recommendation, the protection settings for under frequency is 49.5 Hz and for over frequency is 50.5Hz to trip the generator [151] . The system frequency has to be prevented from reaching the threshold values. Therefore frequency control is essential for secure and stable operation of a power system. This target has been achieved using the control technique proposed in this chapter.

7.2 Proposed Control Technique Design

A block diagram of the proposed controller is shown in Figure 7.1. The controller is mainly a set of mathematical instructions used to control and check system operating

conditions and it differentiates from conventional automatic generation by including control logic instructions. The controller consists of the following five subsystems:

- Measurement subsystem
- Actual power generation subsystem
- Control logic subsystem
- Change in active power calculation subsystem
- Power distributed controller subsystem

In this work the rate of change of frequency (ROCOF) has been used to calculate the change in the active power demand in the system. Also the frequency error has been used to check the system operating condition and made the decision to increase or decrease the output power from SSEGs, if a system frequency deviation occurs.

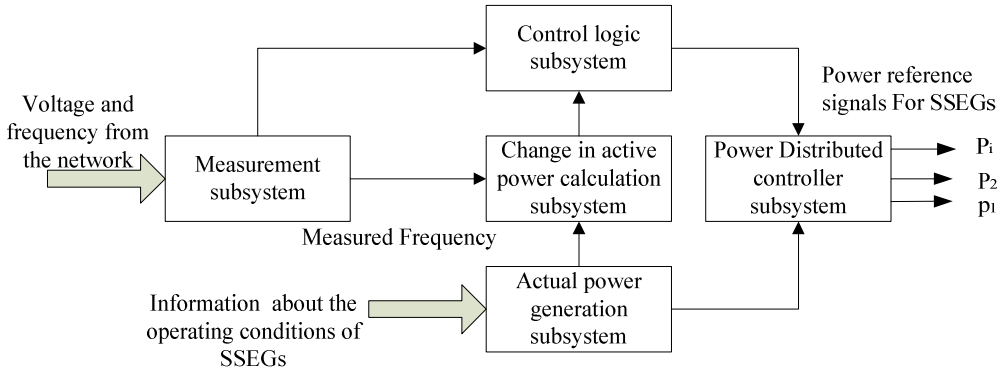

Figure 7.1: A block diagram of the load-frequency control system

7.2.1 Measurement Subsystem

Figure 7.2 shows the schematic diagram of the measurement subsystem. The measurement subsystem consists of two modules one for measuring the voltage and one module for measuring frequency. A module for measuring the voltage measures the three–phase voltage at bus 100 (main bus 132 kV bus in Figure 3.15). This

voltage is converted to three single-phase voltages measurements which become the input to the frequency measurement module. A module for measuring frequency measures the system frequency using a three-phase PI-controlled Phase Locked Loop (PLL) (the description of PLL is provided in Appendix G). The measured frequency is passed through a low pass filter to mitigate the harmonics from the measured frequency to be used by the control logic subsystem and required power calculation subsystem (the description of the low pass filter and its transfer function is provided in Appendix H).

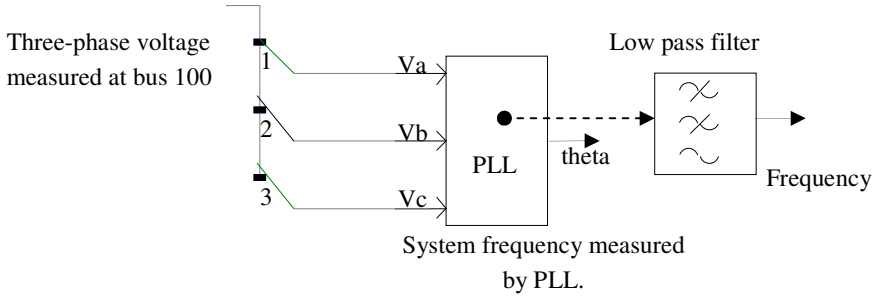

Figure 7.2: The schematic diagram of measurement subsystem

7.2.2 Actual Power Generation Subsystem

Figure 7.3 shows the schematic diagram of the actual power generation subsystem. The function of this subsystem is to calculate the total actual SSEG networks generation, actual output power for every SSEG network and the power of the SSEG network which can be provided in an emergency. These calculated values will be used in other subsystems of the controller.

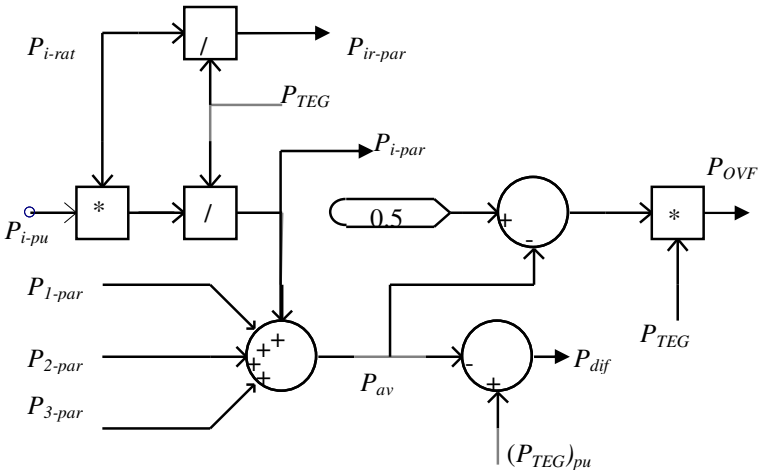

Figure 7.3: Actual power generation subsystem

The following steps explain how the actual power generation subsystem works:

1. The controller starts to calculate the actual power of the SSEG network (i) $P_{i\text{-}ac}$ in [MW] which can be described by the following equation:

$$P_{i-ac} = P_{i-rat} \cdot P_{i-pu} \quad \text{[MW]} \qquad (7.1)$$

Where i=1, 2…n, n= number of SSEG networks.

$P_{i\text{-}rat}$ = rated power of SSEG network (i) in [MW].

$P_{i\text{-}pu}$ = rated power of SSEG network (i) in [pu] based on the rating of the SSEG network.

2. Then the controller calculates the participation of the SSEG network (i) at rated power based on the total rated power generation of all SSEG networks P_{ir-par}.

$$P_{ir-par} = \frac{P_{i-rat}}{P_{TEG}} \cdot \quad \text{[pu]} \qquad (7.2)$$

Where $P_{TEG} = \sum_{i=1}^{i=n} P_{i-rat}$ [MW] (7.3)

P_{TEG} = total rated power of all SSEG networks in [MW].

Also the penetration level can be calculated as a function of the total SSEG networks power generation over the total load demand as given by:

$$\text{Penetration level}(\%) = \frac{\sum P_{TEG}}{\sum P_L} \times 100 \qquad (7.4)$$

3. After that the controller calculates the actual participation ($P_{i\text{-}par}$) of the SSEG network (i) based on the total rated power of all SSEG networks.

$$P_{i-par} = \frac{P_{i-ac}}{P_{TEG}} \quad [\text{pu}] \qquad (7.5)$$

4. Thus the average value of total actual generation of SSEG networks P_{av} can be calculated by the following equation:

$$P_{av} = \sum_{i=1}^{i=n} P_{i-par} \quad [\text{pu}] \qquad (7.6)$$

5. From the above equations the controller calculates the per unit power (P_{dif}) that can be provided by the SSEG networks in case of an under frequency event. Also it calculates the power (P_{OVF}) that can be reduced from the SSEG networks when over frequency occurs as described in the following equations.

$$P_{dif} = 1 - P_{av,} \quad [\text{pu}] \qquad (7.7)$$

$$P_{dif} = [1 - P_{av}] \times P_{TEG} \quad [\text{MW}] \qquad (7.8)$$

$$P_{OVF} = [0.5 - P_{av}] \times P_{TEG} \quad [\text{MW}] \qquad (7.9)$$

7.2.3 Control Logic Subsystem

Figure 7.4 shows the schematic diagram of the control logic subsystem. The function of the control logic subsystem is to check the system operating condition and made the decision to increase or decrease the output power from the SSEG networks if a system frequency deviation occurs. First the controller subtracts the filtered

measured frequency from the reference value of 50Hz. The difference will be the frequency error f_{error} which is given by the equation below:

$$f_{error} = f_{set} - f_{meas} \,. \qquad \text{[Hz]} \qquad (7.10)$$

Where f_{set}= 50 Hz, f_{meas} = measured frequency.

During the initialization period of the simulation the frequency error is multiplied by zero. Once the system reaches steady state the actual value of the frequency error will be the input of the range comparator. Then the range comparator determines which of three ranges the input signal is within, and then outputs a value corresponding to that region. The regions are defined by a lower input limit $f_{error} < zero$ and an upper input limit $f_{error} > zero$. The first region is composed of values below the lower limit (Over frequency); the second region is $f_{error} = zero$ which between the two limits (normal operation); and the third region is composed of values above the upper limit (under frequency).

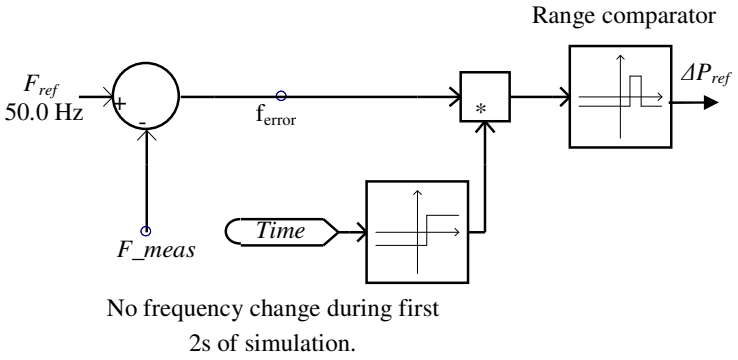

Figure 7.4: Schematic diagram of control logic subsystem.

7.2.4 Change in Active Power Calculation Subsystem

Figure 7.5 shows the schematic diagram of the subsystem to calculate the change in active power. The function of the change in active power calculation subsystem is to

calculate the change in active power in the system and to determine the change in the reference power setting for all SSEG networks, ΔP_{ref} according to the total full load capacity of all SSEG networks. The change in active power ΔP_{ref} can be positive or negative; positive meaning that the load is greater than generation (under frequency) or negative meaning that generation greater than the load (over frequency). In case of under frequency the ΔP_{ref} must be no more than the power (P_{dif}) that can be provided by the SSEG networks in an emergency ($0 \leq \Delta P_{ref} \leq P_{dif}$). This can be achieved by the lower limiter in this control block. Also in case of over frequency the change in active power ΔP_{ref} must be between the powers (P_{OVF}) that can be reduced from the SSEG networks when over frequency occurs in MW and zero ($P_{OVF} \leq \Delta P_{ref} \leq 0$). This can be achieved by the upper limiter in this control subsystem. The output of this subsystem, ΔP_{ref} will be the input value for the distributed power controller subsystem.

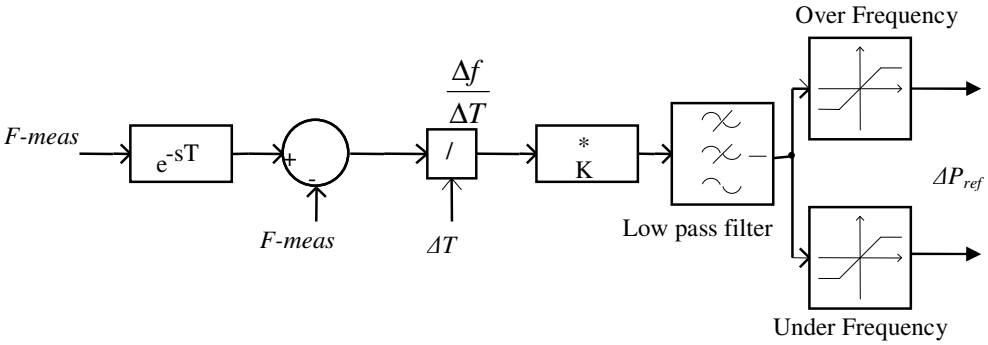

Figure 7.5: Schematic diagram of the change in active power calculation subsystem

During the initialization the ΔP_{ref} is set to be zero. After the system reaches steady state the calculated change in active power in the system ΔP_{ref} is passed through a low-pass filter (4Hz) to smooth any unwanted oscillation, Figure 7.6 shows that the calculated ΔP_{ref} is smooth using the low pass filter. The transfer function of the low pass filter is provided in Appendix F.

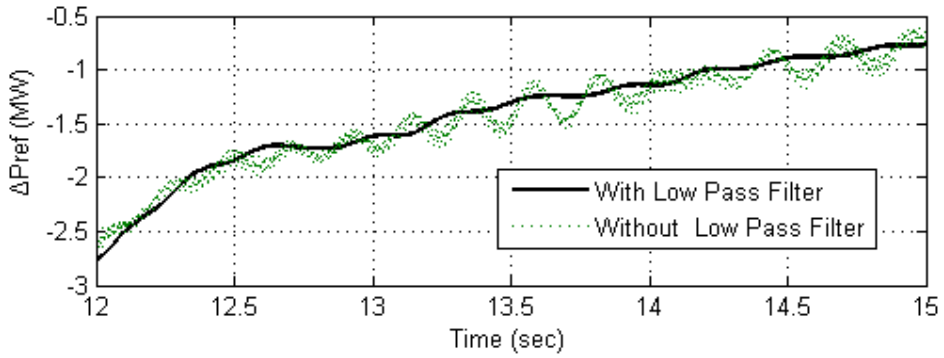

Figure 7.6:The effect of filtering on the calculated *ΔPref*

Calculation of (ΔP_{ref}) will be described in the following equations:

$$\frac{df}{dt}=\left(-\frac{f_0}{2.E_{system}}\times\Delta P\right) \quad \text{Hz/s} \quad [62] \tag{7.11}$$

$$\frac{df}{dt}=\left(-\frac{f_0}{2.H_{system}\ S_{\max}}.\times\Delta P\right) \tag{7.12}$$

$$\Delta P=\frac{df}{dt}\left(\frac{-2\ \ H_{system}\ \ S_{\max}}{f_0}\right) \tag{7.13}$$

Where

$\frac{df}{dt}$ is the rate of change of frequency (ROCOF) [Hz/s].

$f_{0,}$ is the steady state system frequency [Hz].

E_{system} encompasses the total stored energy of all generators and loads connected to the system at the nominal system frequency in [MW.s].

ΔP is the change in active power in the system during a disturbance [MW].

S_{max} represents the total generation rating of the system [MVA].

$H_{system,}$ is the inertia constant of all generators and loads in the system referred to the base S_{max} [s].

From the equations (7.12) and (7.13) the ΔP_{ref} can be calculated as function of a rate-of-change of frequency (ROCOF) $\frac{\Delta f}{\Delta t}$ multiplied by gain (K) as described in the following equation:

$$\Delta P_{ref} = -K \frac{\Delta f}{\Delta t} \tag{7.14}$$

Where K is a constant obtained from equation (7.13) and equal to

$$K = \left(\frac{2 \ H_{system} \ S_{\max}}{f_0} \right) \tag{7.15}$$

ΔP_{ref} is the change in the reference power setting for all SSEG networks [MW].Calculation of $\frac{\Delta f}{\Delta t}$ has been performed in this block by using the time delay and the difference junction components, the controller takes samples of the frequency measurements every T_s (the sampling time) which has been set at 0.5sec to give stable operation of the controller. Each sample f_{tn} is subtracted from the previous sampled frequency f_{tn-1}, the result will be:

$$\Delta f = f_{tn-1} - f_{tn} \tag{7.16}$$

f_{tn-1} is the measured frequency at time t_{n-1} and f_{tn} is the measured frequency at time t_n.

The controller then calculates the rate-of-change of the frequency.

$$\frac{\Delta f}{\Delta t} = \frac{f_{tn-1} - f_{tn}}{\Delta T_s} \tag{7.17}$$

Where

$$\Delta T_s = t_n - t_{n-1} \tag{7.18}$$

$$\Delta T_s = 0.5 \ sec$$

The calculated rate-of-change of frequency (ROCOF) $\frac{\Delta f}{\Delta t}$ will be multiplied by gain (K) to calculate the $\Delta P_{ref,}$ the gain (K) has been determined by simulation.

Figure 7.7 shows the calculated rate-of-change of frequency. When the system is operating at steady state the ROCOF is zero. But when there is a disturbance in the system the value of ROCOF changes, as an example in this case the type of disturbance is under frequency.

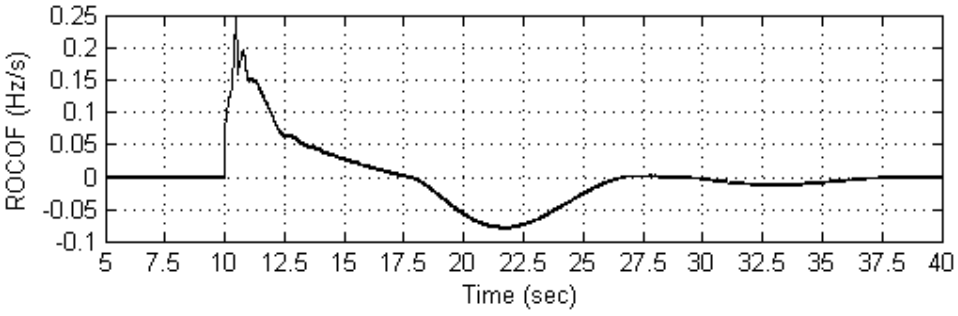

Figure 7.7: Calculated rate of change of frequency (ROCOF).

7.2.5 Power Distributed Controller Subsystem

This subsystem identifies how much should be produced by each SSEG network based on its capacity and sends appropriate signals for every SSEG network to increase or decrease its output. Figure 7.8 shows a schematic diagram of the power distributed controller subsystem. In steady state the outputs of this subsystem are predefined power set points values determined by the local controller fitted in each SSEG network. When a disturbance is detected this reference will be changed by the controller according to the type of disturbance (e.g. over frequency or under frequency) and based on the capacity of the unit.

During the disturbance (increasing or decreasing in the load) the function of this subsystem is to distribute this required power between the SSEG networks in the system according to the capacity of every unit. This will be described by the following equations:

The change in the reference power setting for all SSEG networks (ΔP_{ref}) is converted to per unit value based on total rated of SSEG networks.

$$\Delta P_{ref} = \left(\frac{(\Delta P_{ref})_{MW}}{(P_{dif})_{pu} \; (P_{TEG})_{MW}} \right) \quad \text{[pu]} \tag{7.19}$$

Then the new set point for one SSEG network i can be calculated as follows:

First calculate ΔP_i share for unit i

$$\Delta P_i = \left[\Delta P_{ref} \times (P_{ir-par} - P_{i-par}) \right] \quad \text{[pu]} \tag{7.20}$$

$$P_i = \left[\Delta Pi + P_{i-par} \right] \quad \text{[pu]} \tag{7.21}$$

From equations (7.20, 7.21) the new set point P_i for unit i is determined as:

$$P_i = \left[\Delta P_{ref} (P_{ir-par} - P_{i-par}) + P_{i-par} \right] \times P_{TEG} \tag{7.22}$$

This signal will be the reference power for unit i.

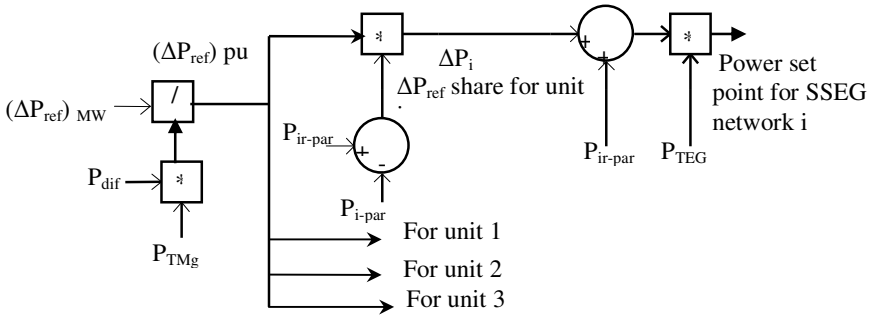

Figure 7.8: Schematic diagram of the distributed power controller subsystem.

7.3 Algorithm of the Load-Frequency Controller

Figure 7.9 shows the flowchart of the load-frequency controller. The function of the control logic is to detect whether there is a disturbance or not and if there is a disturbance, the type of disturbance that has to be defined; under frequency or over frequency, and then finally send appropriate control signals to the SSEG networks to increase or decrease their outputs according to the type of disturbance.

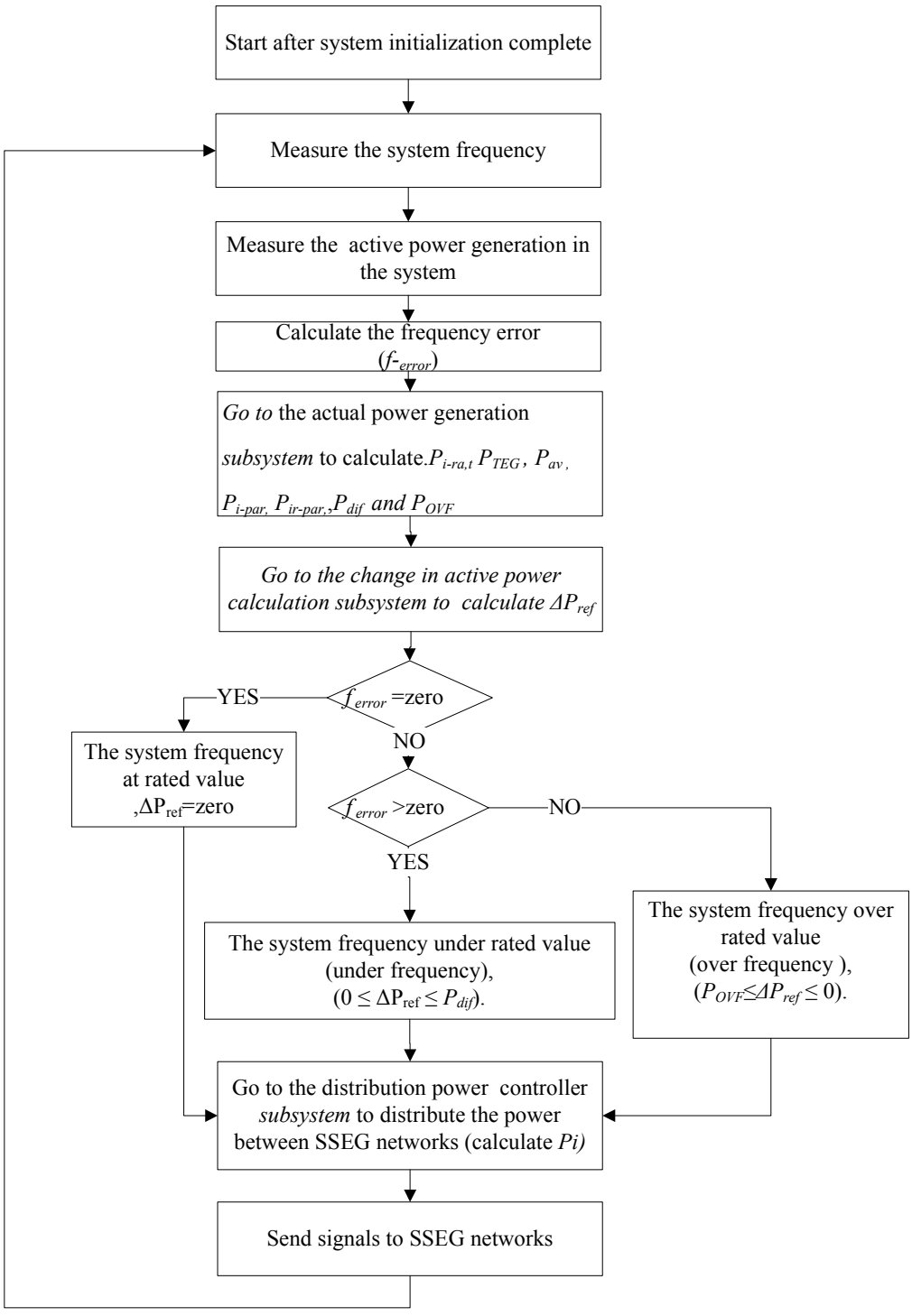

Figure 7.9: The flowchart of the load-frequency controller.

The algorithm of the controller starts with:

1. Start after system initialization completes.
2. Measure the system frequency.
3. Measure the power generation in the system.
4. Calculate the frequency error, $f_{error} = f_{set} - f_{meas}$.
5. Record the actual set points for every SSEG networks from the local controllers.
6. Calculate the total rated power of all SSEG networks (P_{TEG}) in MW.
7. Calculate the average value of total actual generation of SSEG networks P_{av}.
8. Calculate the power P_{dif} , that can be provided by SSEG networks when under frequency occurs in MW, $(P_{dif} = P_{TEG} - P_{av})$.
9. Calculate the power P_{OVF}, that can be reduced from the SSEG networks when over frequency occurs in MW, $P_{OVF} = [0.5 - P_{av}] \times P_{TEG}$.
10. Calculate the $\frac{\Delta f}{\Delta t}$ (ROCOF).
11. Calculate the change in the reference power setting for all SSEG networks ΔP_{ref} ($\Delta P_{ref} = -K \frac{\Delta f}{\Delta t}$).
12. If the frequency error is equal to zero (f_{error} =zero) go to next step, otherwise go to step 15.
13. The system in actual operating condition and ΔP_{ref}=zero (the SSEG networks power set points are equal to the actual set points).
14. Go to step 20.
15. If the frequency error more than zero (f_{error} >zero) go to next step, otherwise go to step 18.
16. The system suffers from under frequency problem then ΔP_{ref} will be in this range ($0 \leq \Delta P_{ref} \leq P_{dif}$).
17. Go to step 20.
18. If the frequency error is more than zero (f_{error} <zero) go to next step, otherwise go to step 2.

19. The system suffers from over frequency problem then the value of ΔP_{ref} in this range $P_{OVF} \leq \Delta P_{ref} \leq 0$.
20. Go to the distribution power controller block to distribute the power between SSEG networks.
21. Send signals to SSEG networks.
22. Go to the step 2.

7.4 Results and Discussions for the Load-Frequency Controller

The load-frequency controller has been successfully implemented and tested using PSCAD/EMTDC. The participation of the SSEG networks in the primary frequency control during different types of system disturbances, over frequency or under frequency using the proposed controller has been tested using different case studies.

7.4.1 Case Study Network

Figure 7.10 shows the EHV1 33kV rural network model (described in chapter 3) which has been used to evaluate the performance of the general control approach proposed in this work. It includes three synchronous generators (G1, G2 and G3) with similar ratings (impedances and time constants are listed in Appendix A and the descriptions of the governor and exciters are available in Appendices G and H) representing the main system (providing 34.2MW connected to the 132kV bus (bus 100). An additional interconnected generator is functioning as a PV bus (providing 4MW connected to the 33kV bus 336). The total load is 38.16MW and 7.74 MVAr. Five SSEG networks with different technologies were connected to this network at busses 1101, 1106, 1108, 1114 and 1115 (the models and parameters are available in Appendix B). Table 7.1describes the technology type, rating and actual output power of every SSEG networks. The penetration of these SSEG networks in the generated power of the network is 26.2% (10 MW) for 9090 customers (1.1 kW per customer), the rated active power of every unit is 2MW (1818 customers).

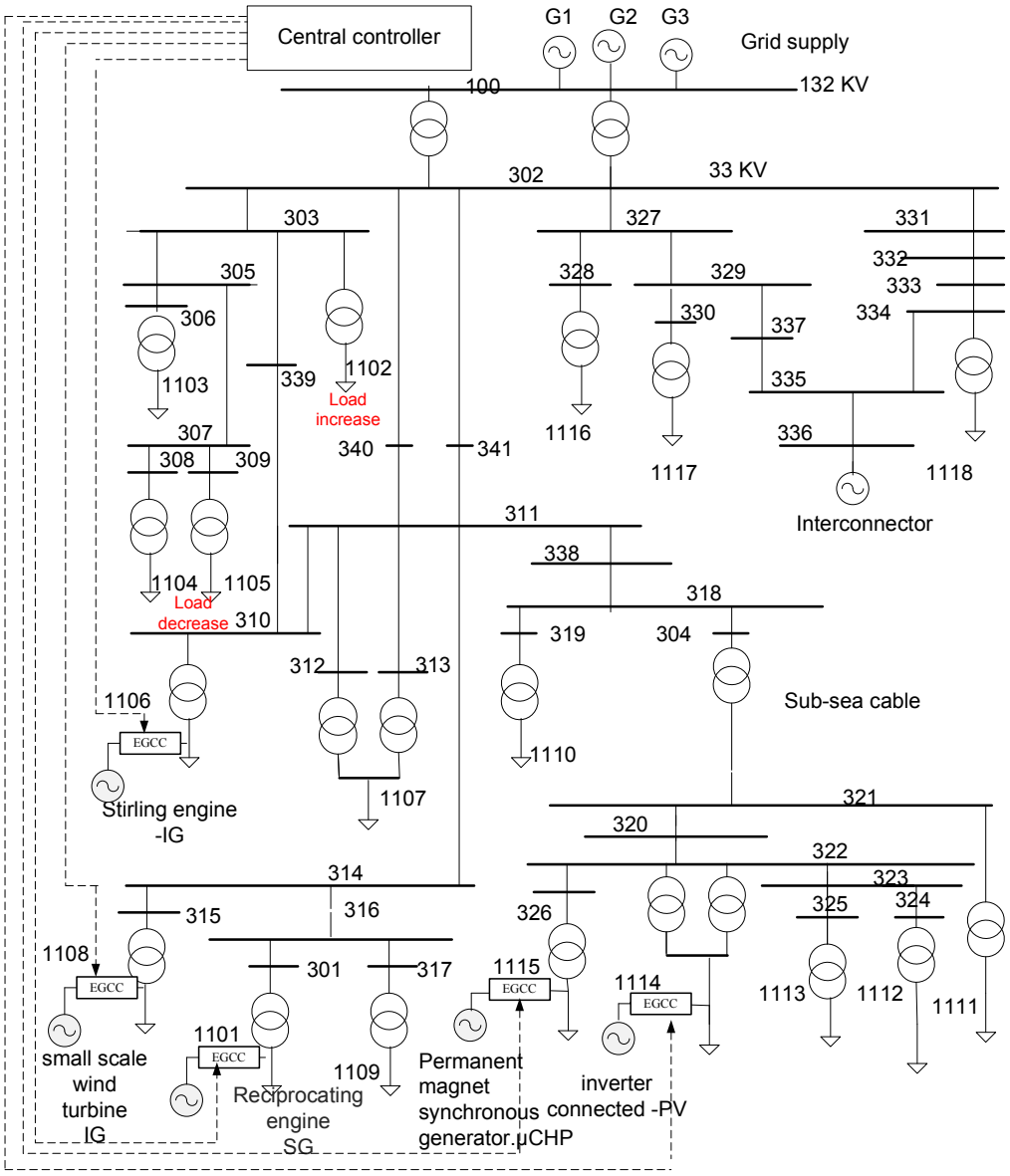

Figure 7.10: Network with mixed SSEG units used in the study.

7.4.2 SSEG Contribution to the Frequency Control Investigation

Regarding the participation of SSEG networks in frequency control, two types of system disturbances, load increase and loss of load have been considered. The assumption is the SSEG networks contribute only to the primary frequency control, so they have to increase or decrease their production when the generation unbalance

is detected, and they have to recover their previous state when the governors of the main generators take action in order to restore the frequency of the system to a new stable frequency.

Table 7.1: Small scale distribution networks data

SSEG network	**Bus no**	**Technology**	**Rating in (MW)**	**Actual output power**	
1	1101	Synchronous generator (Reciprocating engine)	2	**in (MW)**	**In (%)**
				1.6	80%
2	1106	Stirling engine (SE) driven induction generator (IG)	2	1.46	73%
3	1108	Squirrel cage induction generator (small scale wind turbine)	2	1.5	75%
4	1114	Converter connected (PV)	2	1.34	67%
5	1115	Reciprocating engine unit driven permanent magnet synchronous generator	2	1.4	70%

The scenarios for testing the performance of the proposed controller for contribution of SSEG to primary frequency control are:

- System with no participation of SSEG networks (base case).
- Simulation at 22.6% penetration for SSEG networks without Load–Frequency controller, in this case there is no participation on primary frequency control.
- Simulation at 22.6% penetration for SSEG networks with Load–Frequency controller.

- Each SSEG network was considered as a single bus with an equivalent generator (sum of all SSEGs) and equivalent load (sum of all loads) .
- Appendix I provides additional test results which have not been presented in this chapter.

7.4.2.1 *Scenario1: System with no Participation of SSEG networks*

In order to investigate the system frequency behaviour with no participation of SSEG networks, system disturbances have such as increase and decrease in load. These types of test are applied on the EHV1 33kV rural network as shown in Figure 7.10.

A Under Frequency Test (load increase)

During the test, at the beginning the balance between consumption and generation is ensured and maintained, then suddenly "load 1102" is increased by 3.816MW. The duration of the simulation is 70s. At t= 10s, the total load in the system is increased by 10% by adding 3.816MW to load 1102. Due to the sudden increase in load, the main generators (G1, G2 and G3) have to supply more power to the system. This results in deceleration of the generator speed at the beginning before the governor takes action. As illustrated in Figure 7.11 at the instant of load increasing at t= 10sec, the output power from the main system increased to supply the change in the load. This increasing of output power means an increase in the electrical torque of the main generators that leads to an unbalance between electrical and mechanical torque of the main generators, as illustrated in Figure 7.12 (G1 as an example), where the electrical torque is higher than the mechanical torque. Figure 7.13 shows the system frequency response due to the unbalance between electrical and mechanical torque, as observed the system frequency falls to 48.8 Hz. In this case the under frequency protection will operate to trip the main generators because the system frequency is 48.8 Hz which is out of the normal operation limits. If the protection of the system is assumed to not operate thus the speed of the main generators drops at the beginning due to the sudden increase in the load. Then the governor takes action in order to prevent the frequency of the system from dropping further. The system reacts fast and then slowly turns to a new stable frequency.

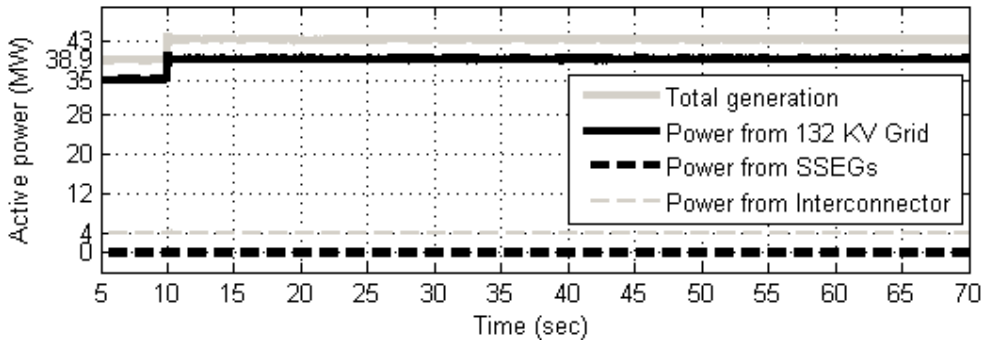

Figure 7.11: Active power generation in the system with no SSEG (load increase).

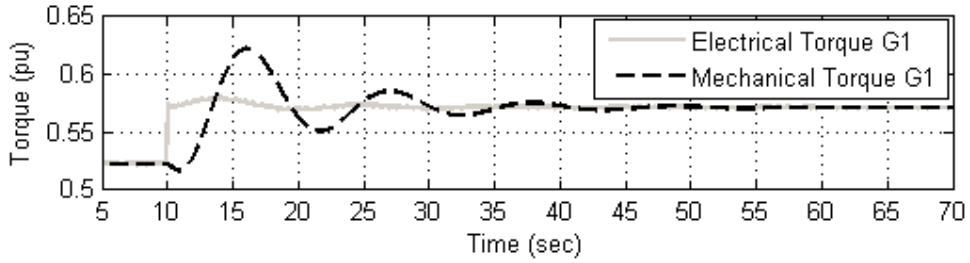

Figure 7.12: Torque for main synchronous generators with no SSEG (load increase)

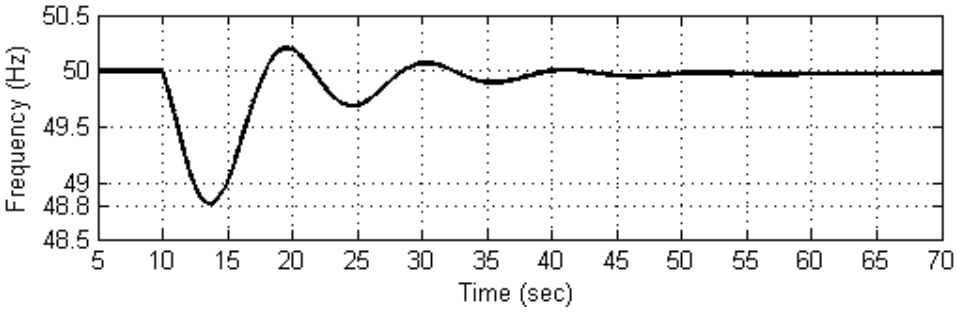

Figure 7.13: System frequency behaviour without participation of SSEG (load increase)

B Over Frequency Test (load decrease)

The test aims to show the effect of the disconnection of a part of the load on the system frequency. As shown in Figure 7.14 for this test the load " load 1105" is disconnected at t= 10 sec. Due to the loss of a part of the load, a part of power is temporarily not supplied to the system. Thus the mechanical torque of the main

generators is more than the electrical torque as illustrated in Figure 7.15 (G1 as an example). This unbalance between electrical and mechanical torques leads to an acceleration in the generator speed. As a result the system frequency rises to 50.9 Hz as shown in Figure 7.16. This frequency value is out of normal operation limits. Thus the over frequency protection will operate to trip the generators. However in this study the protection of the system is assumed to not operate. Thus the speed of the main generators rises at the beginning due to a sudden loss of part of the load. Then the governor takes action to balance the mechanical torque with electrical torque by reducing the mechanical torque. Once the balance is achieved the system frequency returns to the normal operating condition as before the disturbance.

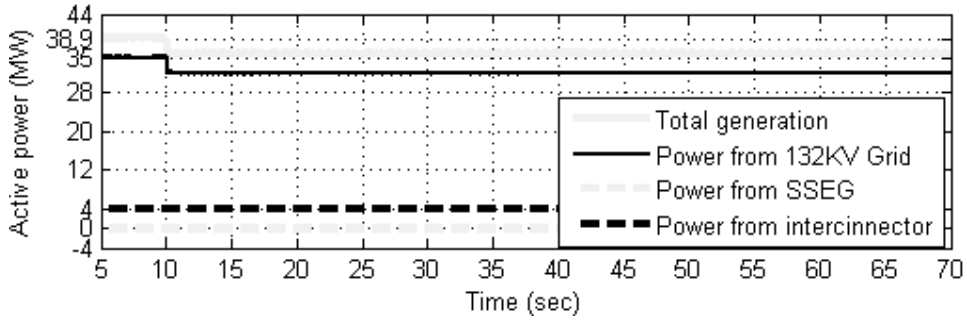

Figure 7.14: Active power generation in the system with no SSEG (load decrease)

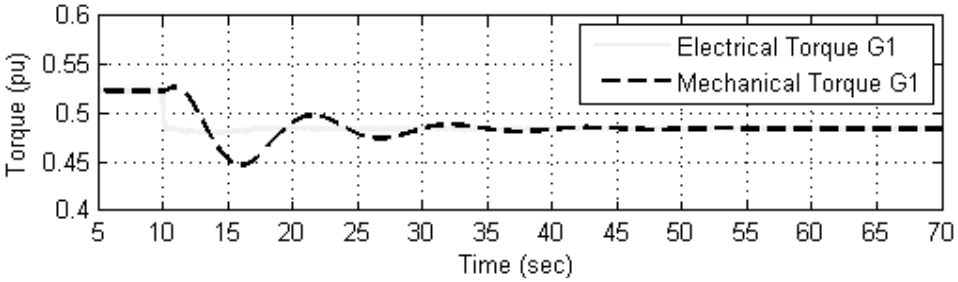

Figure 7.15: Torque for main synchronous generators with no SSEG (load decrease)

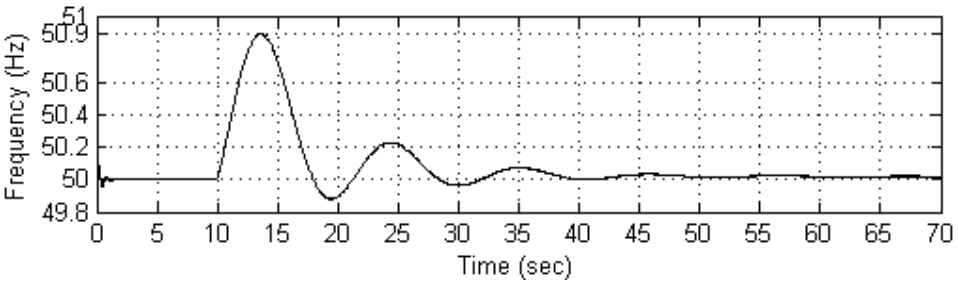

Figure 7.16: System frequency behaviour without participation of SSEG (load decrease)

7.4.2.2 Scenario2: System with SSEG networks with no Load-Frequency Control

This scenario investigates the system frequency behaviour of system with SSEG networks but with no load-frequency controller (LFC). The two types of system disturbance previously considered in scenario 1 have also been considered in this senario. As shown in Figure 7.17 and Figure 7.18 before the disturbance (0-10s period) the total generation in the system was 38.7 MW, the penetration of the SSEG networks was 22.6% (7.3 MW), the power from the main generators was 27.3 MW and 4MW from the interconnector. The total power generated by the system and the power supplied by the main grid are less than the power generated when there are no SSEG networks connected. This difference of active power generation in the system is due to the power generated by the SSEG networks being consumed locally without any transmission losses. Although as shown in Figure 7.17 and Figure 7.18 (10-70s period) there is no contribution of the SSEG networks during the change in the load, generally the results show that the system behaviour in these case studies is the same as for those presented for scenario 1 except for some small improvements on the system frequency response compared with the base case. As observed in Figure 7.19 the system frequency response in the under frequency test is 48.95 Hz (in the base case 48.8 Hz) and in Figure 7.20 the system frequency response in over frequency test is 50.84 Hz (in the base case 50.9 Hz).

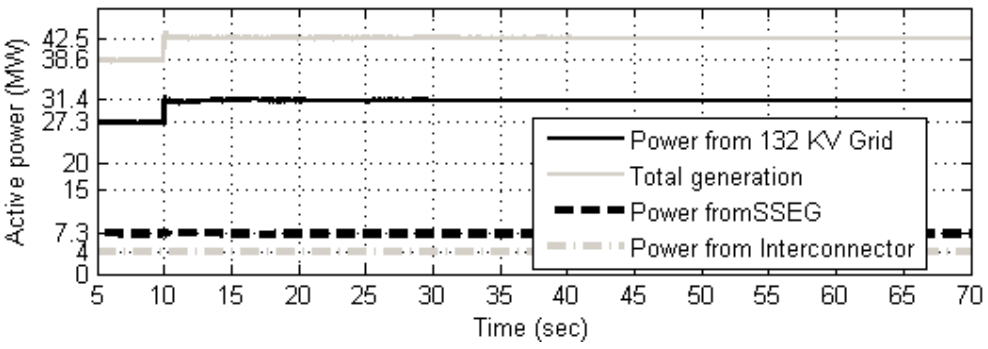

Figure 7.17: Active power generation in the system with no LFC (load increase)

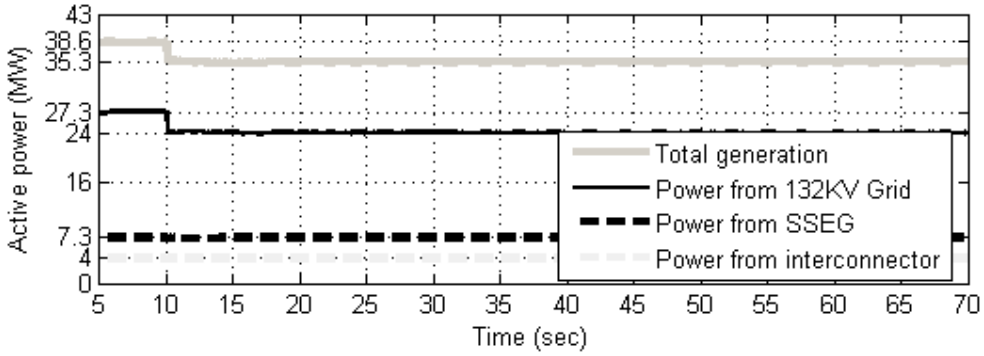

Figure7.18: Active power generation in the system with no LFC (load decrease)

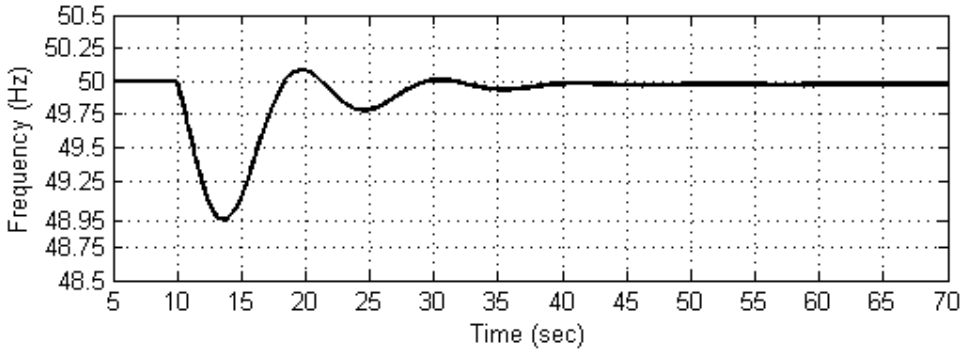

Figure 7.19: System frequency behaviour with SSEG networks with no LFC(load increase)

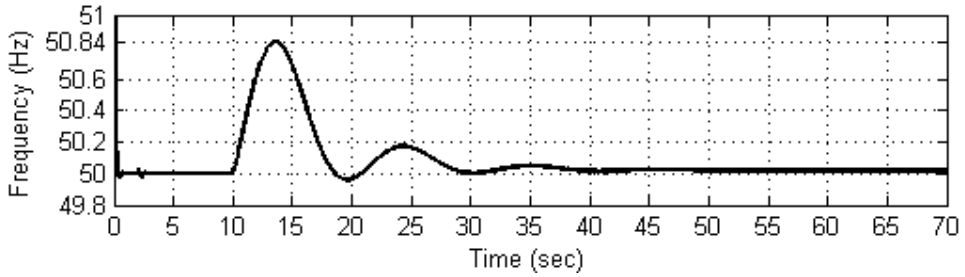

Figure 7.20: System frequency behaviour with of SSEG networks with no LFC (load decrease)

7.4.2.3 Scenario3: System with SSEG networks with Load-Frequency Control

In this scenario the participation of the SSEG networks with the proposed controller in a system frequency control has been tested for the same system disturbances considered in scenario 1 and 2. These types of testing are applied on the EHV1 33kV

rural network with different SSEG technologies; these units receive the reference active power set point from the central controller to change their outputs according to the type of disturbance to restore the system frequency to the normal operating limits.

A Under Frequency Test (load increase)

This type of test is same as the under frequency test in scenario 1 and 2. As shown in Figure 7.21 at t=10sec the load is increased by 10% from the total load (3.816MW). Once the disturbance is detected by the central controller, it sends signals to the SSEG networks to increase their output power. Then as shown in Figure 7.21 the total output power from the SSEG networks is increased to the maximum value during the first 3s after the disturbance to supply the change in the load which leads to the balance between electrical and mechanical torque of the main generators as observed in Figure 7.22. As a result the system frequency is controlled to value equal to 49.54 Hz which is in the limits of normal operation. However at t=15s, the main generators start increasing their output power and the SSEG networks start to reduce their output power until reach the actual operating condition before the disturbance at t= 20s.

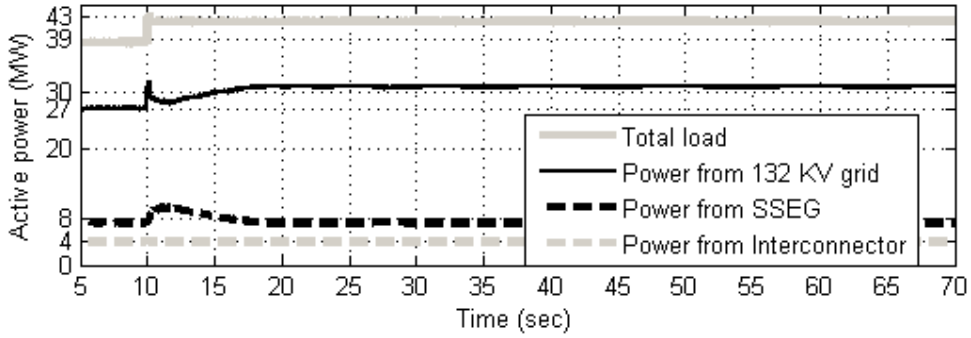

Figure 7.21: Active power generation in the system with LFC (load increase)

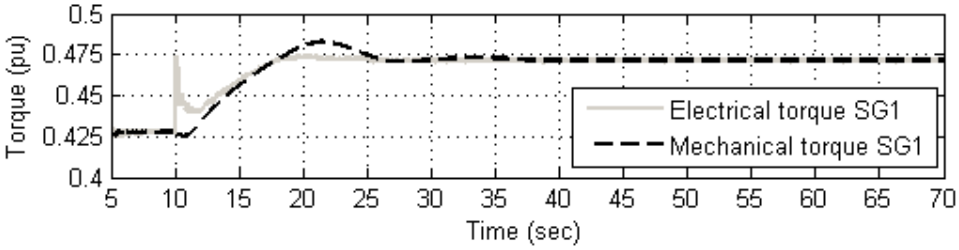

Figure 7.22: Torque for main synchronous generators with LFC (load increase)

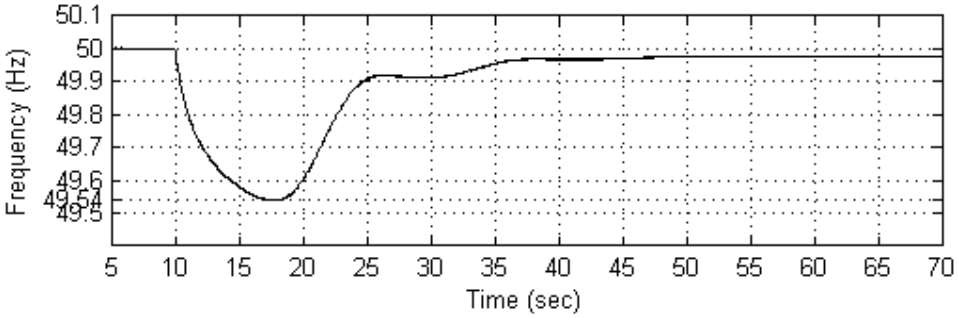

Figure 7.23: System frequency behaviour with SSEG networks with LFC (load increase)

a) Contribution of reciprocating engine driven synchronous generator in under frequency control

As illustrated from Figure 7.24(a), the reciprocating engine driven synchronous generator receives the reference power set point from the central controller to increase its output power. This increase is achieved by the unit local control system; the controller changes the input mechanical torque to the generator to change the output electrical power of the generator to the maximum value during the first 3s after the disturbance. However the increasing of electrical power output from the generator is combined by increasing in the load angle of synchronous generator as seen in Figure 7.24 (b). As shown in Figure 7.24 (c) the change in the system frequency has an impact on the speed of the synchronous generator (SG) due to the relationship between the system frequency ($\omega_s = 2\pi f$) and the speed of the generator. This results in a deceleration of the generator speed before the system settles in a new stable operating condition. In addition to using the synchronous generator, as

shown in Figure 7.24 (d) the reactive power and power factor can also be controlled. As the results show, the generator is working at 0.95 leading power factor.

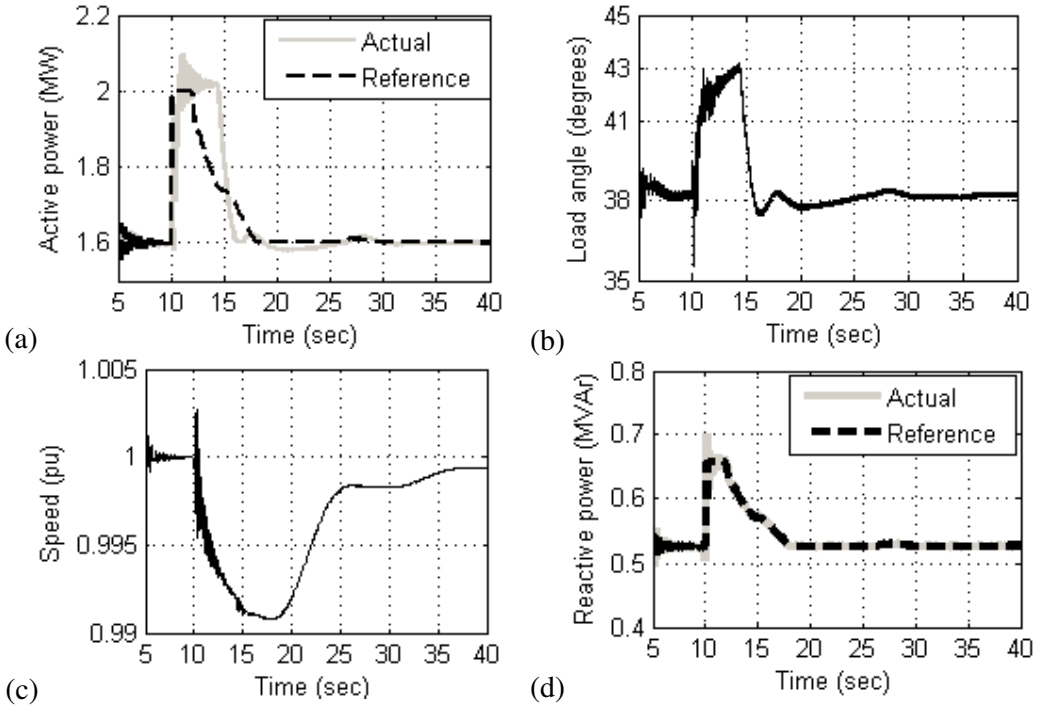

Figure 7.24: Response of reciprocating engine driven SG to load increase: (a) Active power output, (b) Load angle, (c) Rotor speed and (d) Reactive power output.

b) Contribution of small scale wind turbine driven induction generator in under frequency control

From the simulation results with a small-scale wind turbine unit shown in Figure 7.25 (a), the unit receives the reference power set point from the central controller to increase its output power. This increase of output power from the wind turbine is achieved by the pitch controller which decreases the pitch angle of the wind turbine to change the generator output power as illustrated in Figure 7.25(b). Also as shown in Figure 7.25 (c) the results show that the change in the system frequency has an impact on the speed of the generator due to the relationship between the system frequency ($\omega_s = 2\pi f$) and rotor speed of induction generator (ω_r)[$\omega_r = \omega_s * (1+s)$]. The induction generator injects power to the system only when the speed of the rotor

exceeds the synchronous speed of the electrical field of stator winding. However the result shows that the generator speed decelerates at the beginning and settles in a new stable operating condition following the system frequency.

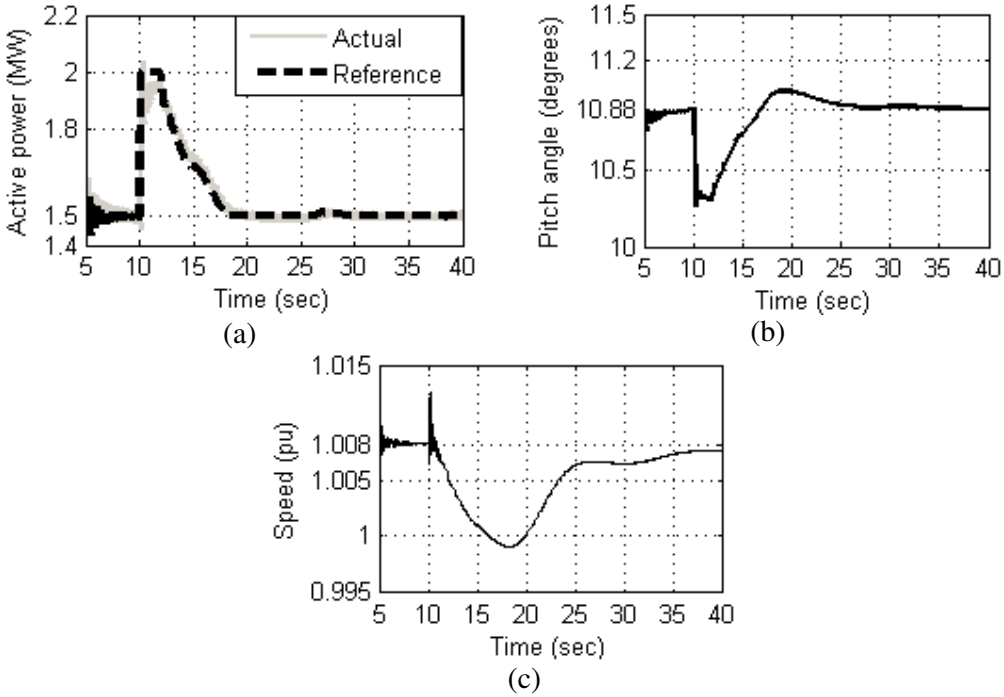

Figure 7.25: Response of small scale wind turbine driven IG to load increase: (a) Active power output, (b) pitch angle and (c) Rotor speed.

c) Contribution of stirling engine driven induction generator in under frequency control

Figure 7.26 (a), (b) and (c) show how the microCHP unit (Stirling engine SE) connected to an induction generator can contribute to under frequency control. As shown Figure 7.26 (a) the mechanical torque of the crank shaft of the striling engine increased according to reference value of the electrical power received by the local unit control system from the central controller as shown in Figure 7.26(b). This increase of the mechanical torque leads to increase the electrical power from the induction generator connected to the shaft of the stirling engine as shown in Figure 7.26 (b). Also Figure 7.26 (c) show that the change in the system frequency results in

a deceleration of the generator speed at the beginning before the system reaches a new stable operating condition.

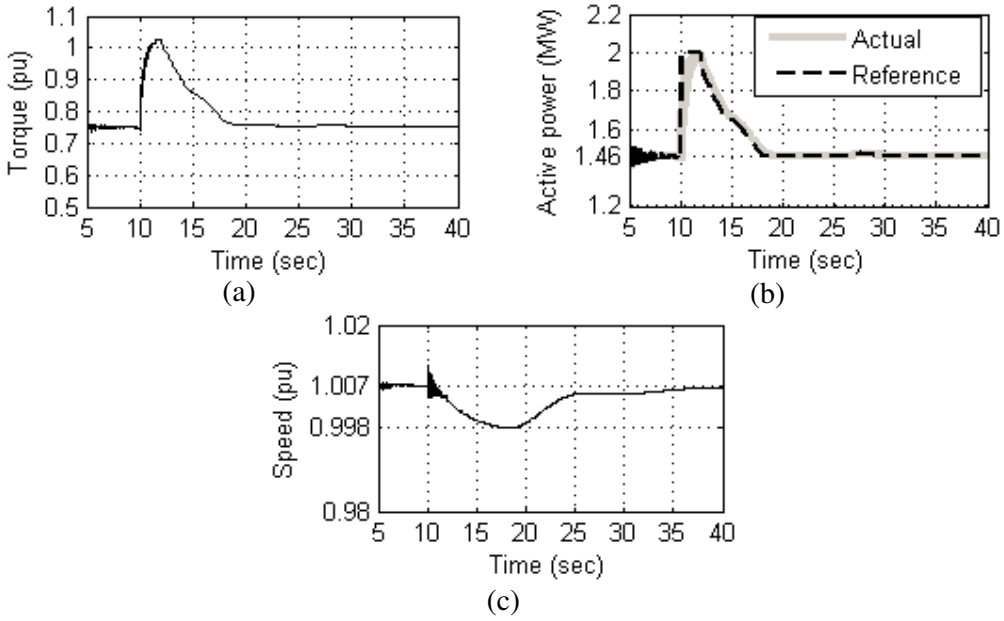

Figure 7.26: Response of stirling engine driven IG to load increase: (a) Active power output, (b) Mechanical torque and (c) Rotor speed.

d) Contribution of microCHP connected to permanent magnet synchronous generator in under frequency control

Figure 7.27(a), (b) and (c) show the performance of the microCHP connected to a permanent magnet synchronous generator (PMSG) for the contribution in the system frequency control. The results shown in Figure 7.27 (a) and (b) show that the response of the prim over is (mechanical torque and the electrical power reference value) same as the response of the prim over in case of the microCHP connected to induction generator (case b). Also, the change in the system frequency has an impact on the PMSG speed similar to that on a conventional synchronous generator (case a) as observed in Figure 7.27(c). However as illustrated in Figure 7.27(d) the

performance of PMSG differs from the performance of the conventional synchronous generator because, in the case of PMSG, the power factor cannot be controlled.

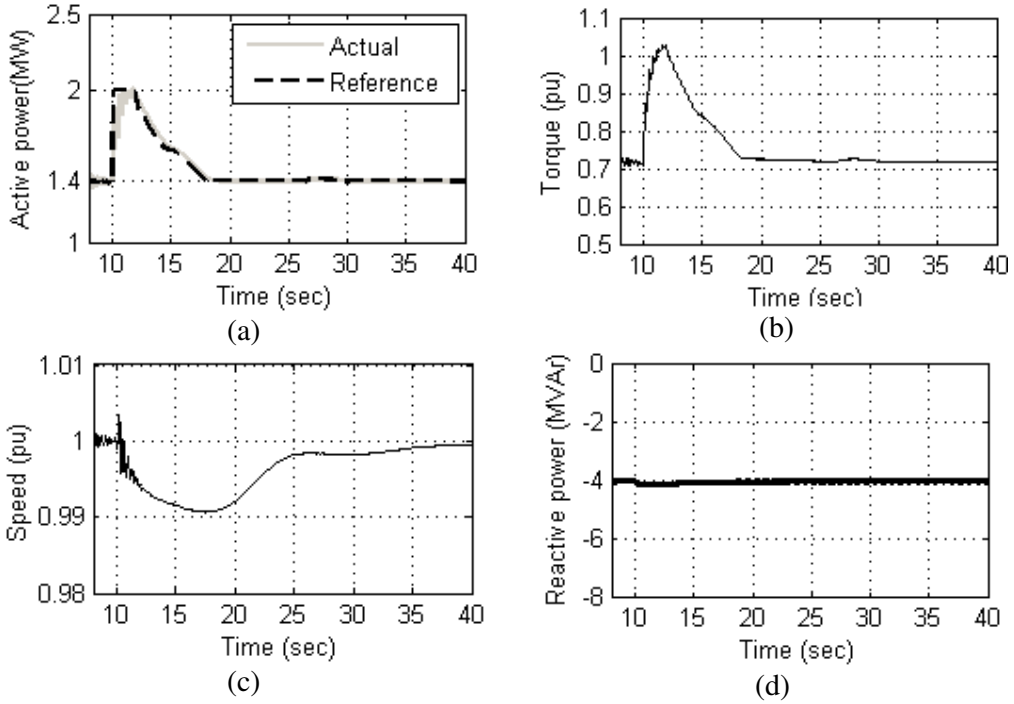

Figure 7.27: Response of reciprocating engine driven PMSG to load increase: (a) Active power output, (b) Mechanical torque, (c) Rotor speed and (d Reactive power absorbed).

e) Contribution of photovoltaic (PV) in under frequency control

Figure 7.28(a) illustrates the contribution of the PV unit in the power generated by the SSEG networks. The controller that controls the converter-connected PV increases the power angle of the converter as shown in Figure 7.28(b) in order to increase the output power from the PV unit, according to the reference power signal from the central controller as shown in Figure 7.28 (a).

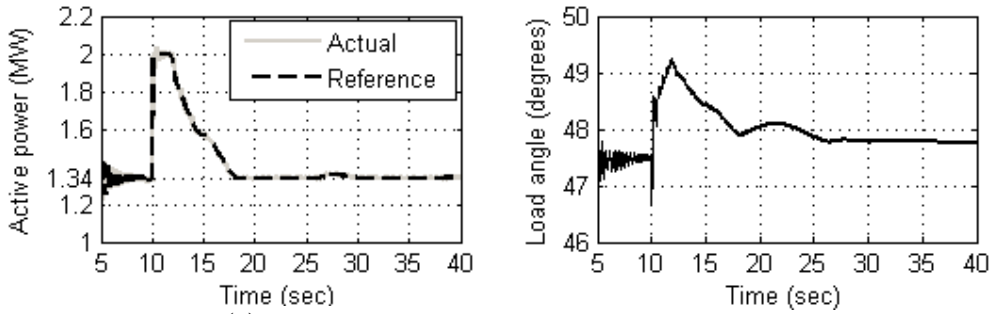

(a) (b)

Figure 7.28: Response of PV unit to load increase: (a) Active power output and (b) load angle.

B Over Frequency Test (load decrease)

As shown in Figure 7.29, similar to the over frequency test in scenario 1 and 2, 10% of the total load in the system (load 1105 is disconnected) is disconnected at t = 10s. Thus, as shown in Figure 7.30 this unbalance between consumption and generation leads to an unbalance between electrical and mechanical torque of the main generators. Therefore as shown in Figure 7.31 the system frequency increases as the mechanical torque is more than the electrical torque. However in this case the SSEG networks are combined with a load and frequency controller which detects the disturbance and sends signals to the SSEG networks to compensate the difference between the load and generation by decreasing their output power. As shown in Figure 7.29 the total output power from the SSEG units is reduced to half the total rated value within 3s of the disturbance. As a result, as shown in Figure 7.31 the frequency of the system is 50.395 Hz which is within the limits of normal operation. In addition, at t=15s the main generators start decreasing their output power and the SSEG units start to return to the actual operating condition as before the disturbance by t = 18s.

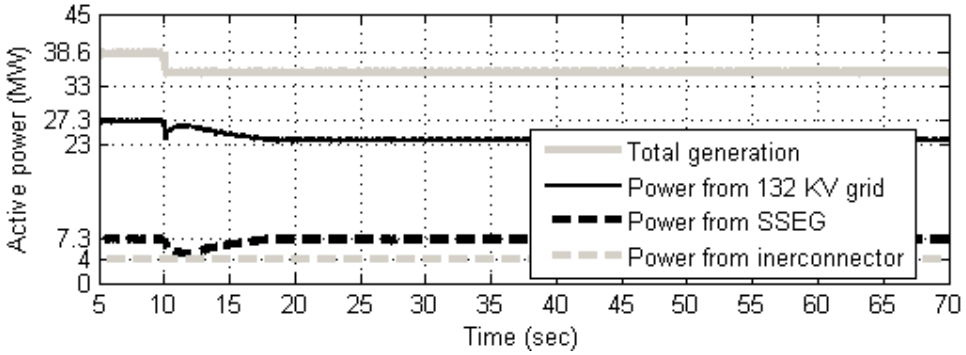

Figure 7.29: Active power generation in the system with LFC (load decrease).

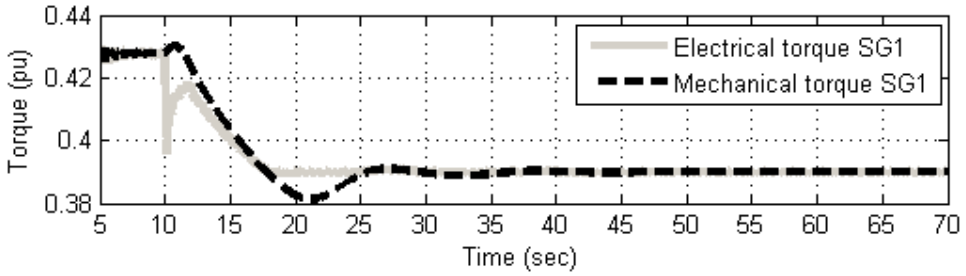

Figure 7.30: Torque for main synchronous generators with LFC (load decrease).

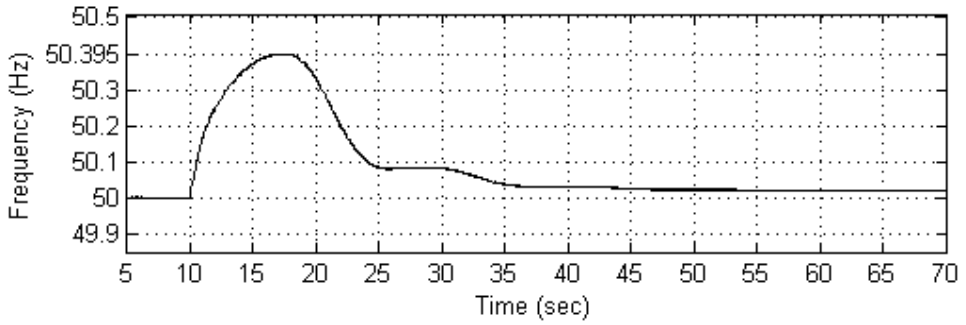

Figure 7.31: System frequency behaviour with SSEG networks with LFC (load decrease).

a) Contribution of reciprocating engine driven synchronous generator in over frequency control

Figure 7.32 (a), (b) and (c) illustrates the response of the reciprocating engine driven synchronous generator for the increasing of the system frequency. As shown in the Figure 7.32(a) once the unit receives signal from the central controller to change its output power after the disturbance detection, the unit control system starts decreasing the electrical output power of the generator by decreasing the input

mechanical torque input to the generator. As a result, the generator output power decreases during first 4s after disturbance. As shown in the Figure 7.32(b) the decrease in the electrical power output from the generator is combined with a decrease in the load angle of synchronous generator. As clearly observed in Figure 7.32 (c), the change in the system frequency has an impact on the speed of the synchronous generator that accelerates at the beginning before settling in a new stable operating condition.

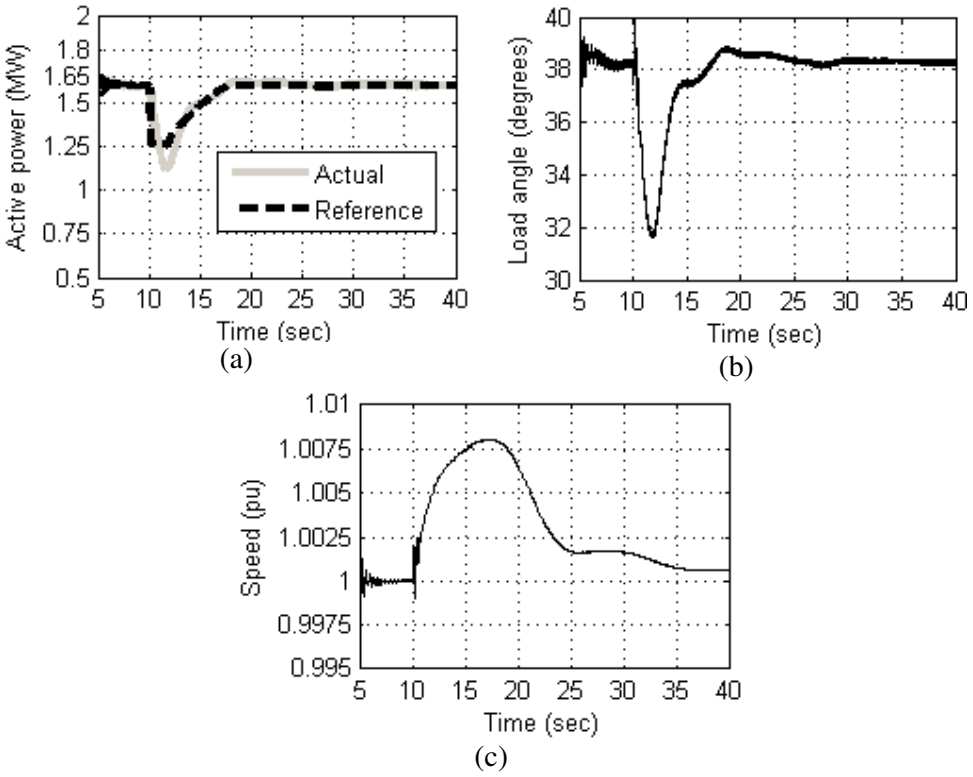

Figure 7.32: Response of reciprocating engine driven SG to load decrease: (a) Active power output, (b) Load angle and (c) Rotor speed.

b) Contribution of small-scale wind turbine driven induction generator in over frequency control

These simulation results show the contribution of the small-scale wind turbine unit (SSWT) in over frequency control. The over frequency control requires decreasing in

the output power of wind turbine. As shown in Figure 7.33(a) the small-scale wind turbine unit (SSWT) receives the reference power set point from the central controller to decrease its output power. This decreasing in the output power of the wind turbine is achieved by the pitch control system of the units, as shown Figure 7.33(b) in the results the pitch control increases the pitch angle of the wind turbine to change the generator output power.

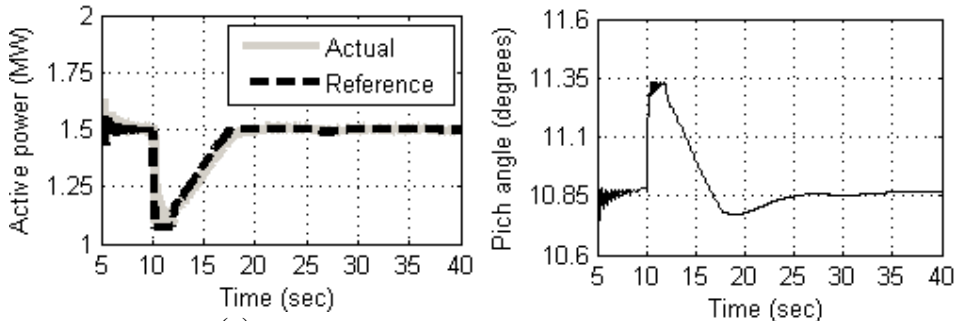

(a) (b)

Figure 7.33: Response of small scale wind turbine driven IG to load decrease: (a) Active power output and (b) Pitch angle.

c) Contribution of stirling engine driven induction generator in over frequency control

This part of the simulation results aims to show how the SSEG networks with microCHP (SE) technology driven induction generator can contribute in the regulation of the system frequency when the part of the load in the system is disconnected. The response of the SE to this event is illustrated in Figure 7.34(a) the unit control system decreases the unit electrical output power according to the signal received from the central controller. As shown in Figure 7.34(b), this decrease in electrical power is achieved by decreasing the input mechanical torque to the generator.

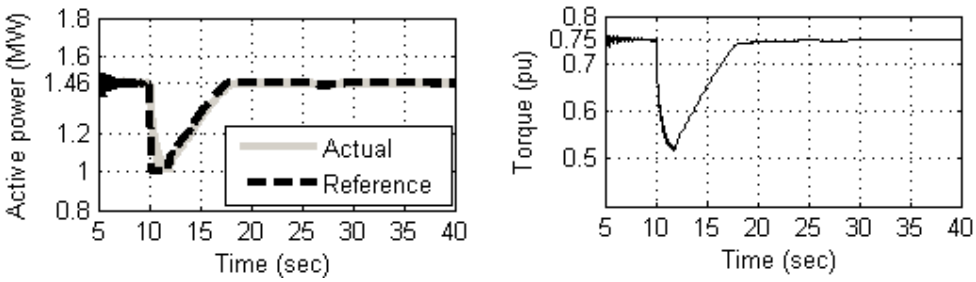

(a) (b)

Figure 7.34: Response of stirling engine driven IG to load decrease: (a) Active power output and (b) Mechanical torque.

d) Contribution of microCHP connected to permanent magnet synchronous in over frequency control

From the results shown in Figure 7.35(a) the microCHP connected to PMSG contributes to the frequency control by decreasing its output power, the output power from this unit decreased during first 3sec after disturbance according to the signal received from the central controller. This decreasing in the output power is achieved by the local microCHP unit control system; as shown in Figure 7.35(b) the controller reduces the mechanical torque of the generator to reduce the electrical output power. However when the system frequency returns to the normal operation condition the unit returns to the operation condition before the disturbance. Also as shown in Figure 7.35(c) the generator speed performs similar to the conventional synchronous generator which accelerates at the beginning before the system turns to new stable operating condition.

e) Contribution of photovoltaic (PV) in over frequency control

The contribution of the PV unit to prevent the system frequency to reach value above the standard operating limit is shown in Figure 7.36 (a). The output power from the PV unit is decreased by the unit control system depending on the reference value received from the central controller. As shown in Figure 7.36 (b) the control system decreases the power angle of the converter to change the output power from PV unit.

As a result the PV unit can participate in reducing the increase in the system frequency caused by the load increase.

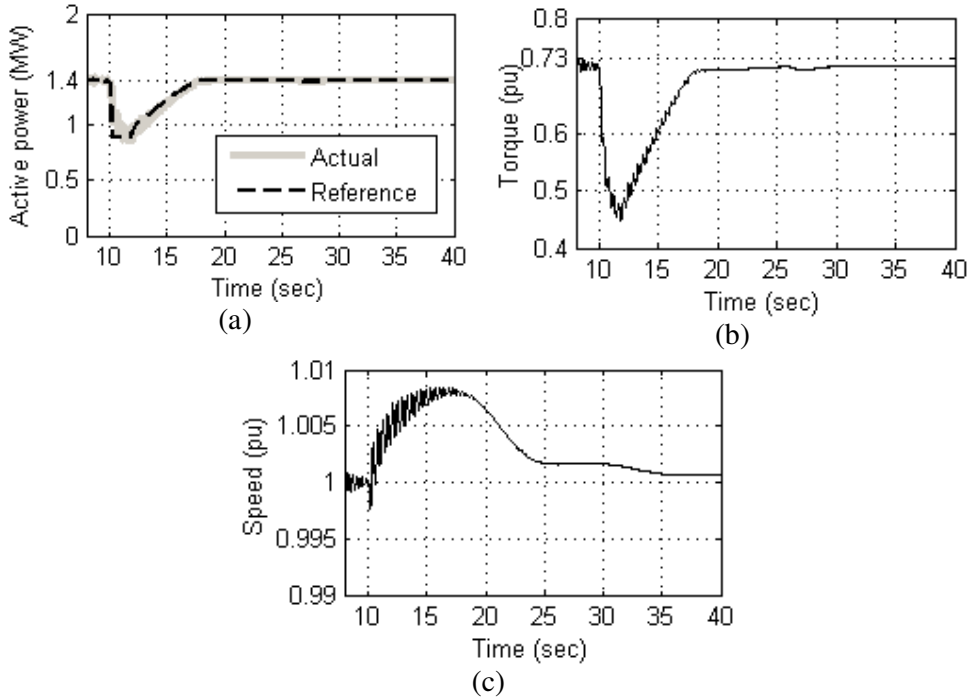

Figure 7.35: Response of reciprocating engine driven PMSG to load decrease: (a) Active power output, (b) Mechanical torque and(c) Rotor speed.

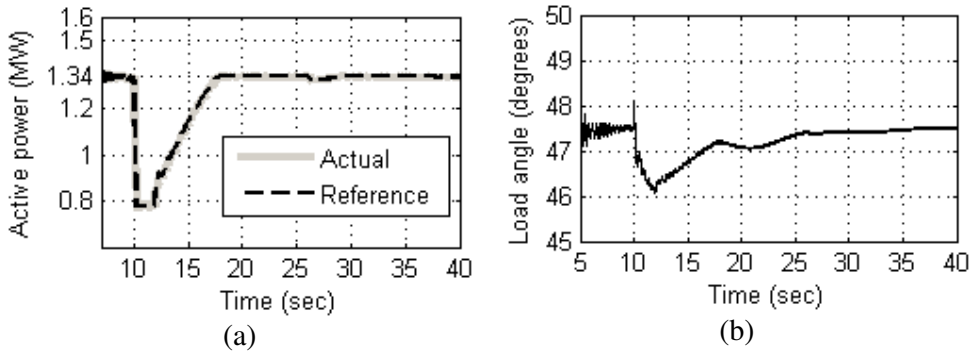

Figure 7.36: Response of PV to load decrease -(a) Active power output and (b) Load angle.

7.4.3 Comparison of System Frequency Response during Different Operating Conditions

In order to compare the system frequency behaviour with no participation of SSEG, with SSEG without load-frequency control and with SSEG with load-frequency control, the system frequency response of three cases are plotted together. Both under frequency and over frequency tests have been considered and are described in the following subsections.

7.4.3.1 Under Frequency Test (load increase)

Figure 7.37 illustrates the system frequency with participation of SSEGs both with and without load-frequency control. The results are also compared with the base case where there is no SSEGs connection in the system. These results illustrate that when a new load is connected (10% from the total load) to a system with no SSEGs, the frequency of the system decreases to value 48.8Hz which is below the threshold value (49.5Hz), potentially energizing under frequency protection and creating a blackout in the system. Using SSEGs without load and frequency control, the decrease in frequency is less (minimum value reached is 48.95Hz) than the base case, but this would also lead to under-frequency tripping. However, the study showed that by the connecting the SSEGs to the system with load and frequency controllers, an excellent response during steady state and disturbance were demonstrated. As shown in Figure 7.37, the frequency of the system is 49.54Hz which, is within in the limits of normal operation. Moreover using the proposed controller there are no oscillations in the system frequency before restoration to its initial condition.

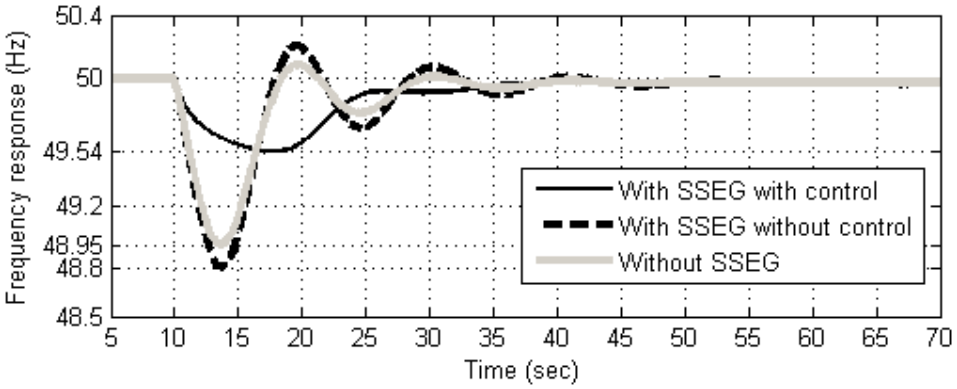

Figure 7.37: Comparison of system frequency response (load increase)

7.4.3.2 Over Frequency Test (load decrease)

The impact of using the SEEG networks with the proposed load-frequency control system on preventing the system frequency to reach value of over frequency (50.5 Hz) is compared with cases, the base case where there is no SSEG networks connection in the system and the SSEG networks connected but without load-frequency control. Figure 7.38 illustrates that the system frequency in both cases the base case and SSEG networks connected but without load-frequency control increases to values 50.9 Hz and 50.84 Hz, respectively. These values are above the threshold value (50.5Hz) which lead to over-frequency tripping. However, the study showed that by the connecting the SEEG networks to the system with load and frequency controllers, an excellent response during steady state and disturbance were demonstrated. As shown in Figure 7.38 the frequency of the system is 50.395Hz which, is within in the limits of normal operation. As a result connecting the SEEG networks with the proposed load-frequency control can restore the system frequency when a part of the load is disconnected.

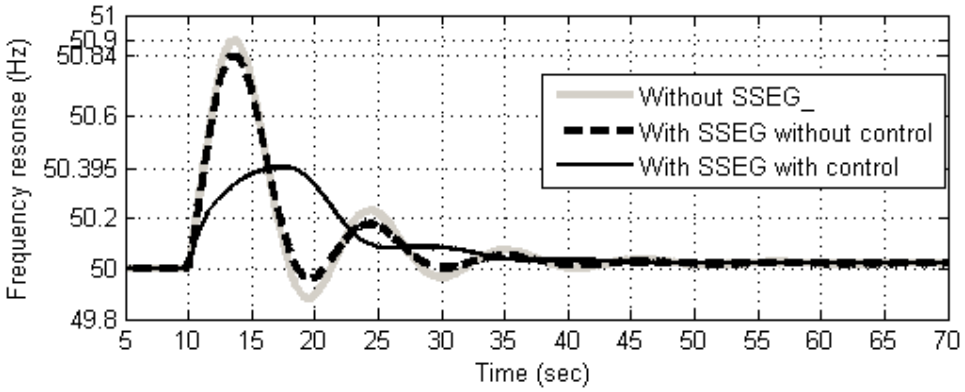

Figure 7.38: Comparison of system frequency response (load decrease)

7.5 Summary

The load-frequency controller has been successfully implemented and tested using PSCAD/EMTDC. The simulation results of primary frequency control studies are presented in this work. The impact of SSEGs with load and frequency control on

frequency stability is studied with the following different SSEG technologies: photovoltaic, reciprocating engine driven synchronous generator, stirling engine driven induction generator, small wind turbine driven induction generator, microCHP connected to permanent magnet synchronous generator. A real distribution system with a load scenario is used in the test. This study shows that large penetration of SSEG has a significant impact on the system frequency regulation when companied with central load and frequency control system. In both studies, with an assumed load increased and load loss, the results show that the SSEG units connected near the load area with load and frequency control cases strongly impact on the frequency stability of the system compared to the base case and the SSEG units without load and frequency control. The impact depends on the SSEG technology used. In most cases, the SSEG connected to the network through power electronic converter has a larger influence compared to the SSEG with rotating machines (induction generator or synchronous generator). Moreover using the proposed controller there are no oscillations in the system frequency before restoration to its initial condition. In addition the results show that it is necessary to coordinate between the central controller and the local controllers of SSEG units in order to maintain the system frequency within limits.

CHAPTER 8

Conclusions and Future Recommendation

8.1 General Conclusions

It is widely anticipated that the capacity of SSEG connected to distribution networks will greatly increase over the coming decade through newly built properties and the large-scale refurbishment of municipal or housing association properties. SSEG offers environmental, economic and social benefits. However, before introducing SSEG in large quantities a number of issues should be resolved in terms of connection to the distribution network: power quality problems, stability, voltage and frequency control, protection, reliability and safety.

Firstly this thesis has investigated the transient behaviour of a range of technologies in response to realistic network faults. From this investigation it has been found that the stability of the network may be endangered due to the small inertia of the SSEG. More care is required to ensure that the generator does not trip for remote network faults; otherwise, the heat energy from the building may be lost for short periods.

Secondly in this thesis the modelling, analysis and design of a PWM voltage source inverter (VSI) connected between a DC source and the AC grid was presented. Different control schemes were applied to the inverter in different operating conditions: when the SSEG worked with no connection to the grid and also when the SSEG was connected to the grid. The objective of this was to show that with appropriate control the converter can transfer the DC energy from SSEG improving the power factor and the voltage regulation of the electrical system.

Thirdly, the central controller that coordinates between multi SSEG networks connected to a 33 kV distribution network has been successfully implemented. The control system controls power flow in the grid-connected mode of operation and maintains the voltage and frequency of the SSEG networks within acceptable

operating limits when they island. When reconnecting them, the central controller resynchronizes SSEG networks with the MV distribution network demonstrating a smooth transition between the grid connection and islanded mode.

Fourthly, this thesis introduced techniques to control unified series-shunt compensators (USSC) connected between SSEG networks and a 33kV distribution network. Simulation results showed that the proposed control techniques for USSC ensure the fault ride-through capability of the SSEG networks and improve, even during steady state and transients, the voltage quality at the SSEG bus. During steady state, the power delivered to the grid is controlled improving the voltage of the SSEG. During a disturbance, the controllers maintain the voltage and frequency of SSEG networks at pre fault values. Moreover the technique can mitigate the voltage unbalance due to the asymmetrical grid faults and can reduce increasing in fault current levels in the electricity grid due to adding SSEGs.

Finally, a load-frequency control technique for a system with a high penetration of SSEGs was successfully implemented and tested using PSCAD/EMTDC. In this study, the impact of SSEGs on the frequency stability of the system was studied in detail implementing different SSEG technologies connected to a permanent magnet synchronous generator: photovoltaic, reciprocating engine driven synchronous generator, Stirling engine driven induction generator, small wind turbines driven induction generator, microCHP. The penetration of these SSEGs in the power of the network is 26.2% (10 MW). This study shows that a network with a large penetration of SSEG, with load and frequency controller, has a significant impact on the networks stability and security.

8.2 Future Research

Various aspects of networks with a high penetration of SSEGs need further investigation, these are:

- **Further research on the impact of SSEGs on the stability of the transmission network.**

As the level of the SSEGs will be high in the coming years there may be a scenario when surplus power in a part of the distribution network is transmitted through the transmission system. In this case the effect of the SSEGs on the transmission system has to be investigated.

- **Research on the protection systems of the distribution network.**
  Majority of the protection equipment in the LV distribution network are fuses or miniature circuit breakers. The installation of these small generators may requires a protection scheme to meet protection requirements.

- **Further research on the integration of energy storage devices.**
  As most of the energy sources are uncontrollable then to permit stable operation of SSEGs, the energy storage devices are required to be included within the devices themselves or as one central storage device within the network.

- **Further research on adding the optimiser on the proposed load-frequency controller.**
  Define the set point for every SSEG according to the speed response of the unit, the cost and availability of energy source.

References

[1] Robert Lasseter, “Microgrids,” IEEE Power Engineering Society Winter Meeting, vol. 1, pp. 305 - 308, Jan, 2002.

[2] Jenkins, R. Allan, P. Crossley, D. Kirschen, and G.Strbac, Embedded generation (book), England, The Institution of Electrical Engineers, 2000, pp. 1-20.

[3] P. Kundur, “Power System Stability and Control (book)”, McGraw-Hill Inc., (1994).

[4] The Grid Code,National Grid Electricity Transmission plc,Issue 3 Revision 28, 7th July 2008.

[5] T. Degner, A. Engler, B. Buchholz, "Distributed Generation with High Penetration of Renewable Energy Sources", Distribution Europe, Amsterdam, the Netherlands April 2004.

[6] D. Bayoumi, C. Haederli, D. Julian and M. Suter, “Network integration of distributed power generation,” Journal of Power Sources, vol. 106, Issues 1-2, pp. 1-9, April 2002.

[7] O. Rosli, A.Nasrudin, S.Marizan, “Modeling and simulation for voltage sags/swells mitigation using daynamic voltage restorer (DVR)," Journal of Theoretical and Applied Information Technology (JATIT), 2009.

[8] N. L. Soultanis, A. I. Tsouchnikas , N. D. Hatziargyriou and J. Mahseredjian , “Dynamic Analysis of Inverter Dominated Unbalanced LV Micro-Grids,” IPST 2007, Lyon, June, 2007.

[9] L.V.L Abreu, M.Shahidehpour,’’ Wind Energy and Power System Inertia,’’ IEEE Power Engineering Society General Meeting, Montreal, Que Oct.2006.

[10] C. N. Jardine, “Supergen HDPS Scenarios”, Supergen Consortium on Highly Distributed Power Systems, Oxford University, Nov. 2006.

[11] PSCAD was developed by the Manitoba HVDC Research Centre, https://pscad.com/home/

[12] R Lasseter, A. Akhil, C .Marnay, J. Stephens, J. Dagle, R. Guttromson, A.Meliopoulos,R. Yinger and J Eto,” The CERTS MicroGrid Concept,”

White Paper on Integration of Distributed Energy Resources,Office of Power Technologies of the US Department of Energy. Rep, April 2002

[13] M.A.A. Younis, N.A Rahim, S.Mekhilef,'' Distributed generation with parallel connected inverter,'' Industrial Electronics and Applications, 2009. ICIEA 2009. 4th IEEE Conference, pp.2935–2940, Xian, China, May 2009.

[14] R. Lasseter and P. Piagi, "Providing premium power through distributed resources," in Proc. 33rd Annu. Hawaii Int. Conf. System Sciences, Jan. 2000, pp. 1437–1445.

[15] S. Massoud Amin B.F, Wollenberg,'' Toward a smart grid'', Power and Energy Magazine, IEEE Vol.3 , Issue: 5 , pp. 34 – 41, 2005.

[16] A. Engler, C. Hardt J. Jimeno J. Ruela J. Oyarzabal, "Agent based Micro Grid Management System," International Conference on Future Power Systems, Amsterdam, Nov.2005.

[17] H. Jiayi, J. Chuanwen and X. Rong, "A review on distributed energy resources and MicroGrid," Renewable and Sustainable Energy Reviews, June 2007.

[18] Lasseter, R.H. '' Certs Microgrid'', International Conference on System of Systems Engineering, pp.1- 5, San Antonio, April, 2007.

[19] Hiromu Kobayashi and Ikuo Kurihara," Research and Development of Grid Integration of Distributed Generation in Japan,"IEEE Power Engineering Society General Meeting, Canada, July 2009.

[20] A. A. Salam, A. Mohamed and M. A. Hannan,'' Technical challenges on micro grids'', ARPN Journal of Engineering and Applied Sciences, vol. 3,no.6, Dec. 2008.

[21] EPSRC Supergen III: Highly Distributed Power Systems ,System Level Concept Definition, Nov. 2008

[22] Available from: the website for the Department of Energy and Climate Change.F:\Microgeneration - Department of Energy and Climate Change.mht

[23] G. Ault, I. Elders, J. McDonald, G. Burt, R. Tumilty, "Electricity Network Scenarios for 2020", July 2006. Available online from: www.supergen-networks.org.uk.

[24] Available from DTI website: http://www.dti.gov.uk/energy/whitepaper/page39534.html

[25] G. R. Simader, R. Krawinkler and G. Trnka, "Micro CHP systems state-of-the-art," Final Report, Vienna, Tech. Rep. March 2006.

[26] US Department of Energy Office of Energy Efficiency and Renewable Energy , "Advanced Micro turbine systems Program Plan for Fiscal Years 2000 Through 2006'', Tech .Rep, 2006.

[27] EA Technology, "Micro CHP-Review of emerging technologies, products, applications & markets", June 2000.

[28] I. Obernberger, H. Carlsen andF. Biedermann State Of the Art and Future Devlopments regarding Small-small Biomass CHP system with A special Focus On ORC and Stirling Engine Technologies, International Nordic Bioenergy, 2003

[29] H.Nehrir, W .Caisheng and S.R Shaw, "Fuel cells: promising devices for distributed generation'', Power and Energy Magazine, IEEE, vol. 4, Issue 1, pp 47 – 53,Feb. 2006

[30] The Hongkong Electric Co., Ltd,Project Profile : Renewable Energy by a Wind Turbine System on Lamma Island, March 2004.

[31] K.Brenden, Rubyna, W. Hallaj, G.Subramanian and S. Katoch,'' Wind energy roadmap,'' Management of Engineering & Technology, 2009. PICMET 2009. Portland International Conference, pp.2548-2562, Aug. 2009.

[32] Available from DTI website: http://superecoltd.com/wind_turbines.htm

[33] A.D. Peacock, D. Jenkins, M. Ahadzi, A. Berry and S. Turan, "Micro wind turbines in the UK domestic sector," Sciencedirect, Energy and Buildings, 40, pp. 1324–1333, 2008.

[34] Available: http://www.segen.co.uk/eng/wind/faq/index.htm

[35] A. Mellita, M. Benghanemb and S.A. Kalogirouc, "Modeling and simulation of a stand-alone photovoltaic system using an adaptive artificial neural network," Renewable Energy, vol.32, pp.285–313, 2007.

[36] Available: http://www.solaruk.net/index.asp

[37] Available: http://www.thegreenelectrician.co.uk/about

[38] C.L Moreira, J.A PecasLopes,'' MicroGrids Dynamic Security Assessment'', Clean Electrical Power, 2007.ICCEP '07. International Conference, pp 26-32, Capri, Italy, 21-23 May 2007.

[39] Piagi, P. Lasseter, R.H, "Autonomous control of microgrids," IEEE Power Engineering Society General Meeting, Montreal, Que, June 2006.

[40] Eric M. Fleming Ian A. Hiskens,'' Dynamics of a Microgrid Supplied by Solid Oxide Fuel Cells,'' Bulk Power System Dynamics and Control, vol.2, Charleston, South Carolina, USA, August, 2007.

[41] P.J.Binduhewa,A.C.Renfrew,M.Barnes,''ultracapacitor energy storage for micro grid micro generation," in *Proc.* PEMD 2008, York, UK,2 April 2008.

[42] A.Engler, R.Geipel, M.Landau, P.Stau and M.Vandenbergh, "Interconnection Management in Micro grids," 3rd European PV-Hybrid and Mini-Grid Conference, Aixen Provence, France, May, 2006.

[43] J. Harrison and S.Redford, " Domestic CHP–what are the benefits?," EA Technology Ltd, July 2001.

[44] G. Pepermans, J. Driesen, D. Haeseldonckx, R. Belmans and W. Dhaeseleer," distributed generation: definition, benefits and issues Energy Policy,"vol. 33, Issue 6, pp.787-798, April 2005.

[45] H.B Puttgen, M.Gregor and P.R.Lambert, "Distributed generation is Semantic hype or the dawn of a new era?," Power and Energy Magazine, IEEE vol. 1, Issue 1, pp.22–29, Feb. 2003.

[46] Lopes, N. Hatziargyriou, J. Mutale, P. Djapic and N. Jenkins," Integrating distributed generation into electric power systems: A review of drivers, challenges and opportunities," Electric Power Systems Research, vol. 77, Issue 9, pp.1189-1203, July 2007.

[47] G.Strbac, N. Jenkins, T.Green, "Future Network Technologies," Tech .Rep DTI, April 2006.

[48] K. C. Divya and P. S. Nagendra Rao," Study of dynamic behaviour of grid connected induction generators," in Proc. IEEE Power Engineering Society General Meeting ,vol. 4,pp. 2200-2205, Denver, CO, June 2004.

[49] R. H. Lasseter and Paolo Piagi,"Control and Design of Microgrid Components," Final Project Report, PSERC Publication, Jan. 2006.

[50] Michael Angelo Pedrasa and Ted Spooner,''A Survey of Techniques Used to Control Microgrid Generation and Storage'', Australasian Universities Power Engineering Conference, December 2006.

[51] J.A. Pecas Lopes, etal, "Defining Control Strategies for MicroGrids Islanded Operation," IEEE Transactions on Power Systems, vol.21, no.2, pp.916-924, May 2006.

[52] J.A. Peças Lopes, etal, "Control Strategies for MicroGrids Emergency Operation." International Conference on Future Power Systems, Nov. 2005.

[53] A. Engler, and N. Soultanis ," Droop Control in LV Grids," in Proc. International Conference on Future Power Systems, The Netherlands, Nov. 2005.

[54] N.Hatziargyiou, N.Jenkins, G.Strbac, J.Peacas Lopes, J.Ruela, A.Engler J.Oyarzabal, G.kariniotakis and A.Amorim," Microgrids-Large Scale Integration of Microgeneration to Low Voltage Grids, "CIGRE 2006.

[55] D. Georgakis, etal, "Operation of a Prototype Microgrid System Based on Microsources Equipped with Fast-acting Power Electronics Interfaces." in *Proc* 35th Annual IEEE Power Electronics Specialists Conference, 2004, vol.4, pp.2521-2526, June 2004.

[56] R. Majumder, A. Ghosh, G. Ledwich and F. Zare '' Power System Stability and Load Sharing in Distributed Generation', Power System Technology and IEEE Power India Conference,POWERCON2008. New Delhi, India, Oct. 2008.

[57] W. Lin and R.Cheuwng, "Model Adaptive Stability Control of DG Connected Distribution Systems", Large Engineering Systems Conference on Power Engineering, pp.67 - 72, Montreal, Que. Oct. 2007.

[58] J. A. Peças Lopes, C. L. Moreira and F. O. Resende, "Control Strategies for Micro-grids Black Start and Islanded Operation", 15th Power Systems Computation Conference (PSCC), Liege Belgium, August 2005.

[59] J. Oyarzabal, etal," Agent-based Micro Grid Management System," International Conference on Future Power Systems, Nov.2005

[60] Y.Dai , P.Zhaoand S.Chang, "Primary frequency control characteristic of a grid," Industrial Electronics and Applications, ICIEA2008, 3rd IEEE Conference, pp.1493 –1497, June, 2008.

[61] R. Oba, G. Shirai, , R. Yokoyama, T. Niimura, and G. Fujita,"Suppression of Short Term Disturbances from Renewable Resources by Load Frequency Control Considering Different Characteristics of Power Plants," in *Proc.* IEEE Power Engineering Society General Meeting**,** PES 2009, Canada, July, 2009.

[62] Brendan Fox, Damian Flynn, Leslie Bryans Nick Jenkins, David Milborrow, Mark O'Malley, Rick Watson and Olimpo Anaya-Lara,"Wind Power Integration Connection and System Operational Aspects(book)", The Institution of Engineering and Technology, London, UK,2007.

[63] S.Voller, A.-R Al-Awaad, and J.F Verstege ,''Wind farms with energy storages integrated at the control power market,'' Integration of Wide-Scale Renewable Resources Into the Power Delivery System, 2009 CIGRE/IEEE PES Joint Symposium, pp.1–13,July 2009.

[64] G.Lalor, J.Ritchie, S .Rourke, D. Flynn and M.O'Malley, "dynamic frequency control with increasing wind generation", IEEE Power Engineering Society General Meeting, vol.2, pp.1715 - 1720, June 2004.

[65] Rogério G. de Almeida ,J. A. Peças Lopes, Primary frequency control participation provided by double fed induction wind generators, 15th PSCC, Liege, 22-26 Aug. 2005.

[66] Michael Hughes, Olimpo Anaya-Lara, Nicholas Jenkins, and Goran Strbac, "Control of DFIG-Based Wind Generation for Power Network Support," IEEE transactions on power systems vol.20, no. 4, Nov. 2005.

[67] D. Boëda, A. Teninge, D. Roye, S. Bacha and R. Belhomme, "contribution of wind farms to frequency control and network stability," European Wind Energy Conference & Exhibition, Milan, Italy, May 2007.

[68] Van Thong, V.Vandenbrande, E.Soens, J.Van Dommelen, D.Driesen and J.Belmans, "Influences of large penetration of distributed generation on N-1 safety operation," IEEE Power Engineering Society General Meeting, vol.2, pp.2177-2181, June 2004.

[69] S. Abu-Sharkh, R.J. Arnold, J. Kohler, R. Li, T. Markvart, J.N. Ross, K. Steemers, P. Wilson and R. Yao, " Can microgrids make a major contribution to UK energy supply? ," Renewable and Sustainable Energy Reviews, vol.10, Issue 2, pp.78-127, April 2006.

[70] Electricity Safety, Quality and Continuity Regulations (ESQCR) 2002-Statutory Instrument Number 2665-HMSO ISBN 0-11-042920-6

[71] S. Ingram, S. Probert, K. Jackson, "The Impact of Small Scale Embedded Generation on the Operating Parameters of Distribution Networks", Contractor PB Power, DTI Renewable Energy Programme, Report number K/EL/00303/04/01, 2003.

[72] Engineering Recommendation P28, "Planning Limits for Voltage Fluctuations Caused by Industrial, Commercial and Domestic Equipment in the United Kingdom", London 1989.

[73] Engineering RecommendationNo.10 of the Electricity Distribution Code, Limits for Voltage Unbalance in the Electricity Supply System, Version 1.0, Prepared by:Abu Dhabi Distribution Company, Nov. 2005.

[74] D. Mahinda Vilathgamuwa and Poh Chiang Loh," Protection of Micro grids During Utility Voltage Sags," IEEE Transactions on Industrial Electronics, vol. 53, no. 5, pp.1427,Oct. 2006.

[75] C. J. Gajanayake, D. M. Vilathgamuwa and P. C. Loh, F. Blaabjerg and R. Teodorescu," Z-source inverter based power quality compensator with enhanced ride-through capability," Industry Applications Conference, 2007. 42nd IAS Annual Meeting, pp.955–962, Sept, 2007.

[76] M. A. Hannan and Azah Mohamed, "PSCAD/EMTDC Simulation of Unified Series-Shunt Compensator for Power Quality Improvement, "IEEE Transactions on Power Delivery," vol. 20, NO. 2, April 2005.

[77] Z.Anwar, B. Chen and M. Osman," Transient Studies of Custom Power Equipments and Static Var Compensator Using PSCAD, "International Journal of Electrical Power and Energy Systems Engineering, summer 2008.

[78] Poriya Fajri, Saeed Afsharnia, "A PSCAD/EMTDC Model for Distributed Static Series Compensator (DSSC),"Second International Conference on

Electrical Engineering University of Engineering and Technology, Lahore (Pakistan) , pp.25-26 March 2008.

[79] L. Qi, J.Langston and M. Steurer ,"Applying a STATCOM for Stability Improvement to an Existing Wind Farm with Fixed-Speed Induction Generators," IEEE Power and Energy Society General Meeting - Conversion and Delivery of Electrical Energy in the 21st Century, pp.1 – 6, 20-24 July 2008.

[80] A. Goikoetxea, M. Rodríguez, H. Bindner and A. Milo," Design of control strategies to improve grid integration in fixed speed wind energy systems with battery storage," in ICREPQ 08 Santander, 2008.

[81] M. Tarafdar Hagh, A. Roshan Milani, A. Lafzi ,"Dynamic Stability Improvement of a Wind Farm Connected to Grid Using STATCOM," in Proc. ECTI-CON 2008.

[82] Z. Chen, Y. Hu and F. Blaabjerg," Stability improvement of induction generator-based wind turbine systems," IET Renew. Power Gener. vol.1, pp. 81–93, 2007.

[83] Ashwin Kumar Sahoo and Dr. T. Thyagarajan," Transient Studies of FACTS and Custom Power Equipment," International Journal of Recent Trends in Engineering, vol.1, No. 3, May 2009.

[84] T. Sato, M. Yamaguchi, T. Terashima, S. Fukui, J. Ogawa and H. Shimizu," Study on the Effect of Fault Current Limiter in Power System With Dispersed Generators," IEEE Transactions on Applied Superconductivity, vol.17,no 2, June 2007.

[85] I.Vajda, A.Gyore, A.Szalay, V.Sokolovsky and W. Gawalek," Improved design and system approach of a three phase inductive HTS fault current limiter for a 12kVA synchronous generator," IEEE Transactions on Applied Superconductivity vol. 13, Issue 2, pp.2000–2003,June 2003.

[86] Chong H. Ng, Li Ran and Jim Bumby, "Unbalanced-Grid-Fault Ride-Through Control for a Wind Turbine Inverter," IEEE Transactions on Industry Applications," vol. 44, No. 3, June 2008.

[87] B. Renders, W.R. Ryckaert, K. De Gusseme, K. Stockman and L. Vandevelde ," Improving the voltage dip immunity of converter-connected

distributed generation units," Renewable Energy vol .33 pp 1011–1018 ,2008.

[88] Smart P., Dinning, A., Maloyd, A., Causebrook, A., Cowdroy, S, "Accommodating Distributed Generation", Econnect project Report No: 1672, prepared for: The Department of Trade and Industry 2006

[89] Azmy and I. Erlich, "Impact of Distributed Generation on the Stability of Electrical Power Systems," IEEE, Power Engineering Society General Meeting, Vol. 2, pp.1056-1063, June 2005.

[90] C. Marnay, R. Blanco, K S. Hamachi, Cornelia P. Kawaan, J. G. Osborn and F. J. Rubio, "Integrated Assessment of DER Deployment,"June 2000.

[91] A.Vladislav and K.Hans "Large penetration of wind and dispersed generation into Danish power grid," Electric Power Systems Research, vol.77 pp.1228–1238, 2007.

[92] S. Ko, S. R. Lee, H. Dehbonei and V. N.Chemmangot " Application of Voltage and Current-Controlled Voltage Source Inverters for Distributed Generation Systems," IEEE Trans. on Energy Conversion , vol .21, No.3, September 2006.

[93] Energy Networks Association, "Engineering Recommendation G83/1 - Recommendations for the connection of small scale embedded generators (up to 16A per phase) in parallel with public low-voltage distribution networks", London 2002

[94] Available from The United Kingdom Generic Distribution System (UKGDS) website: http://monaco.eee.strath.ac.uk/ukgds/

[95] Mohamed E. El-Hawary, Electrical Energy Systems(book), Dalhousie University, CRC Press LCC, Boca Raton London ,New York and Washington, D.C.,2000.

[96] J. Thomas Overbye, Duncan Glover, Mulukutla S. Sarma, Power Systems Analysis and Design (book), 4th ed ,CL-Engineering,2007.

[97] Stephen J.Chapman, Electric Machinery and Power System Fundamentals (book), McGraw-Hill, Inc., International Edition, 2002.

[98] J. Harrison, "Micro Combined Heat & Power (CHP) for housing," presented at the 3rd International Conference on Sustainable Energy Technologies, Nottingham, UK, June, 2004.

[99] M .Kazerani, **"**Naturally-commutated cycloconverter versus rectifier-inverter pair grid-connected distributed power generation based on high-speed microturbines**,"** The 29th Annual Conference of the IEEE Industrial Electronics Society, IECON '03**,** Nov. 2003.

[100] H. Nikkhajoei, and M. Reza Iravani, " A Matrix Converter Based Micro-Turbine Distributed Generation System," IEEE Transactions on Power Delivery, vol. 20, no. 3, July 2005.

[101] L. Ralph, R. Hendriks ,Völzke Wil L. Kling,'' Fault Ride-Through Strategies forVSC-Connected Wind Parks,''Europe's premier wind energy event (ewec), Parc Chanot, Marseille, France, 16-19 March 2009.

[102] T.C.Green and M. Prodanović ,''Control of inverter-based micro-grids,' Electric Power Systems Research, vol.77, Issue 9, pp.1204-1213, July 2007.

[103] Muhammad H. Rashid,''Power electronics circuits, devices, and applications (book)", Prentice Hall, Upper Saddle River, New Jersey, 1993.

[104] Katsuhiko Ogata, "Modern control engineering (book)", Upper Saddle River, NJ Prentice Hall, 4th Edition (2002).

[105] Robert Lasseter, Kevin Tomsovic and Paolo Piagi, "Scenarios for Distributed Technology Applications with Steady State and Dynamic Models of Loads and Micro-Sources," Univ.of Wisconsin, Madison, Tech. Rep. April 2000.

[106] N. L Soultanis and N. D. Hatziargyriou,**''** Control issues of inverters in the formation of L. V. micro-grids,'' Power Engineering Society General Meeting, 2007**.** pp.1 – 7, 24-28 June 2007.

[107] Engineering Recommendation G83/1, Recommendation for Connection of Small-Scale Embedded Generators in Parallel with Public Low-Voltage Distribution Networks, September 2003.

[108] P. Piagi, R. Lasseter, "Autonomous control of microgrids," in *Proc* IEEE Power Engineering Society General Meeting, June 2006.

[109] F.Katiraei, R. Iravani, N. Hatziargyriou and Dimeas, “Controls and operation aspects of microgrids,” IEEE Power and Energy Magazine, vol. 6, Issue 3, pp.54 – 65 June 2008.

[110] Nuno José Gil, and J. A. Peças Lopes, “ Hierarchical Frequency Control Scheme for Islanded Multi-Microgrids Operation’’, in *Proc.* Power Tech, 2007 IEEE Lausanne, pp.473 – 478, July 2007.

[111] F. Katiraei and M. Iravani, “Power management strategies for a microgrid with multiple distributed generation units,” IEEE Transactions on Power Systems, vol. 21, no. 4, pp. 1821–1831, May 2006.

[112] Y. Li, and D. Mahinda Vilathgamuwa, “Design, Analysis, and Real-Time Testing of a Controller for Multibus Microgrid System,” IEEE transaction on power electronics, vol. 19, no. 5, pp.1195, September 2004.

[113] M. A. Kashem and G. Ledwich,’’Multiple Distributed Generators for Distribution Feeder Voltage Support,’’ IEEE transaction on power energy conversion, vol.20, Issue3, pp.676 – 684, Sep. 2005.

[114] A. Creighton, M. Kay, J. Welsh and W. Hung ,Review of ER G59/1 G75 protection settings,19 September 2006.

[115] Faias, S.; Santos, P.; Matos, F.; Sousa, J.; Castro, R.’’ Evaluation of energy storage devices for renewable energies integration: Application to a Portuguese wind farm,’’ Electricity Market, 2008. EEM 2008. 5th International Conference on European , 2008 , pp. 1– 7

[116] Smith, S.C.; Sen, P.K.; Kroposki, B.;’’ Advancement of energy storage devices and applications in electrical power system ,’’ Power and Energy Society General Meeting - Conversion and Delivery of Electrical Energy in the 21st Century, 2008 IEEE, 2008 , pp.1 – 8

[117] Lone, S.A.; Mufti, M.-u-D., ‘’Integrating a Redox Flow Battery System with a Wind-Diesel Power System,’’ Power Electronics, Drives and Energy Systems, 2006. PEDES '06. International Conference on, 2006 , pp. 1 – 6

[118] Farias, M.F.; Cendoya, M.G.; Battaiotto, P.E,’’Wind farms in weak grids enhancement of ride-through capability using custom power systems,’’ Transmission and Distribution Conference and Exposition: Latin America, 2008 IEEE/PES,13-15, pp1 – 5, Latin America, Aug. 2008.

[119] M.A. Hannan, A. Mohamed, A. Hussain and Majid al Dabbay,'' Development of the unified series-shunt compensator for power quality mitigation,'' American Journal of Applied Sciences 6 (5),pp978-986, 2009

[120] Xiao-Ping Zhang, Christian Rehtanz, Bikash Pal,' Flexible AC Transmission Systems; Modelling and Control, Springer-Verlag Berlin Heidelberg Germany, 2006

[121] S. Abbas Taher and S. Mohammad,'' A multi-objective HPSO algorithm approach for optimally location of UPFC in deregulated power systems'', American Journal of Applied Sciences 5 (7), pp 835-843, 2008.

[122] Nashiren.F. Mailah, and Senan M. Bashi,"Single Phase Unified Power Flow Controller (UPFC): Simulation and Construction," European Journal of Scientific Research ISSN, vol.30 No.4, pp.677-684, 2009.

[123] S. Elyas Mubeen, R. K. Nema, and Gayatri Agnihotri,"Power Flow Control with UPFC in Power Transmission System," International Journal of Electrical Power and Energy Systems Engineering, Fall 2008.

[124] S. Tara Kalyani and G. Tulasiram Das," Simulation of real and reactive power flow control with UPFC connected to a transmission line," Journal of Theoretical and Applied Information Technology (JATIT), 2008.

[125] B. Geethalakshmi and P. Dananjayan," Investigation of performance of UPFC without DC link capacitor," Electric Power Systems Research, vol.78, pp.736–746, 2008.

[126] S. Tara Kalyan and G. Tulasiram Das," Simulation of d-q control system for a unfied power flow controller," ARPN Journal of Engineering and Applied Sciences, vol. 2, No. 6, December 2007.

[127] X.-P. Zhang," Comprehensive modelling of the unified power flow controller for power system control," Electrical Engineering vol.88, pp. 241–246, 2006.

[128] H. K. Al-Hadidi, A. M. Gole, and David A. Jacobson," Minimum Power Operation of Cascade Inverter-Based Dynamic Voltage Restorer," IEEE Transctions on Power Delivery, vol.23, No. 2, April 2008.

[129] R.A. Adams, C. Essex: Calculus - A complete course (7th ed.) (book), Pearson. Toronto, Ont. : Pearson/Addison Wesley, cop. 2006

[130] N. Mithulananthan, A. Sode-yome and N. Acharya, “Application of FACTS Controllers in Thailand Power Systems,” School of Environment, Resources and Development Asian Institute of Technology, Pathumthani, Thailand, Tech. Rep., January 2005.

[131] SimPower Systems, information available from the MathWorks website: http://www.mathworks.com/products/simpower/

[132] Hendri Masdi , Norman Mariun S.M. Bashi, Azah Mohamed, Sallehhudin Yusuf,’’ Construction of a Prototype D-Statcom for Voltage Sag Mitigation,’’ European Journal of Scientific Research , Vol.30 No.1 (2009), pp.112-127

[133] M. Brucoli, T. C. Green and J. D. F. McDonald,” Modelling and Analysis of Fault Behaviour of Inverter Micro grids to Aid Future Fault Detection," System of Systems Engineering, SoSE '07, IEEE International Conference, 2007.

[134] Nadarajah Mithulananthan, Mr. Arthit Sode-yome and Mr. Naresh Acharya,’’Application of FACTS Controllers in Thailand Power Systems,’’School of Environment, Resources and Development,Asian Institute of Technology,Pathumthani, Thailand,RTG Budget-Joint Research Project, January 2005

[135] John Kueck, Brendan Kirby, Tom Rizy, Fangxing Li and Ndeye Fall, “Reactive Power from Distributed Energy”, the Elecricity Jornal December 2006, Vol. 19, Issue 10.

[136] B. Kirby and E. Hirst, Ancillary-Service Details: Voltage Control, ORNL/CON-453, Oak Ridge National Laboratory, Oak Ridge, Tenn., December 1997.

[137] Jayanti, N.G.; Basu, M.; Conlon, M.F.; Gaughan, K,’’ Rating requirements of the unified power quality conditioner to integrate the fixed speed induction generator-type wind generation to the grid,’’ Renewable Power Generation, IET, Vol. 3, Issue 2, June 2009 ,pp133 – 143.

[138] A. Kehrli, M. Ross, “Understanding grid integration issues at wind farms andsolution using voltage source converter FACTS technology”, IEEE

Power Engineering Society General Meeting, July 2003, Vol. 3, pp 1822-1828.

[139] Pievatolo, A.; Tironi, E.; Valade, I.; Ubezio, G,''UPQC reliability analysis,'' Harmonics and Quality of Power, 10th International Conference Vol.1, 2002, pp390 – 397, 2002.

[140] V.Ravi Kumar, S,Siva Nagaraju,'' power quality improvement using D-statcom and DVR'', International Journal of Electrical and Power Engineering,1 (3),pp 368-376, 2007.

[141] A.Lashkar, S. Ali,'' comparison of the FACTS equipment operation in transmission and distribution systems,'' CIRED, 17th International Conference on Electricity Distribution Barcelona, 12-15 May 2003.

[142] Anaya-Lara O, Acha E., "Modeling and analysis of custom power systems by PSCAD/EMTDC", IEEE Transactions on Power Delivery, Vol.17, Issue1, Jan. 2002, pp266 – 272.

[143] H. Hatami, F. Shahnia, A. Pashaei, S.H. Hosseini,'' Investigation on D-STATCOM and DVR operation for voltage control in distribution networks with a new control strategy,'' Power Tech, 2007 IEEE Lausanne**,** 1-5 July 2007.

[144] Pal, Y.; Swarup, A.; Singh, B.,''A review of compensating type custom power devices for power quality improvement,'' Power System Technology and IEEE Power India Conference, 2008. POWERCON 2008. Joint International Conference, pp1-8, Oct. 2008.

[145] Yun Wei Li; Mahinda Vilathgamuwa, D.; Poh Chiang Loh; Blaabjerg, F.;A dual-functional medium voltage level DVR to limit downstream fault currents,'' Power Electronics, IEEE Transactions on Vol.22, Issue 4, pp1330–1340, July 2007.

[146] T.Masood, Abdel-Aty Edris, RK Aggarwal,'' Static synchronous compensator (STATCOM) modelling and analysis, techniques by MATLAB & SAT/FAT acceptance tests in the light of commissioning& installation scenarios,'' PSC 2006, November, 2006, Tehran, Iran.

[147] Hojo, M.; Funabashi, T,'' Unified power quality conditioner for dynamic voltage restoration and fault current limitation,'' Harmonics and Quality of

Power, 2008. ICHQP 2008. 13th International Conference, pp1 – 5, Sept. 2008.

[148] Baghaee, H.R.; Mirsalim, M.; Sanjari, M.J.; Gharehpetian, G.B.;Fault current limiting in distribution systems with distributed generation units by a new dual functional series compensator Power pp 537 – 542,1-3 Dec. 2008

[149] G. Beck, W. Breuer, D. Povh, D.Retzmann and E. Teltsch, ''Use of FACTS and HVDC for Power System Interconnection and Grid Enhancement,'' Siemens Power Transmission and Distribution, Abu Dhabi United Arab Emirates, Feb. 2006.

[150] J.M Andres, J.D, D.Retzmann, D.Soerangr and A. Zenkner,'' prospects of SVC converters for transmission system enhancement,'' power grid Europe, Madrid, Spain, June 2007.

[151] Review of ER G59/1 & ER G75/1 Briefing to Generators from Distribution Code ,Review Panel, Working Group, Nov. 2006.

[152] Paul M. Anderson, A. A. Fouad , "Power System Control and Stability (book)," 2nd Edition,Wiley-IEEE Press, October 2002.

[153] Available at: www.newage-avkseg.com.

[154] G. Qui˜nonez-Varela and A. Cruden, "Development of a Small-Scale Generator Set Model for Local Network Voltage and Frequency Stability Analysis," IEEE Transaction on energy conversion, vol.22, no.2, June 2007.

[155] Ju-chirl Park, , "modelling and simulation of selected distributed generation sources and their assessment", Thesis submitted to the College of Engineering and Mineral Resources at West Virginia University, Master of Science In Electrical Engineering,1999.

[156] "IEEE Recommended Practice for Excitation System Models for Power System Stability Studies," IEEE Std 421.5-1992.

Appendix A

Main Distribution Network (11kVand 132kV) Supply and Load Models.

Appendix-A.1 Main Distribution supply model

In this work two representations of a main distribution network have been used. The first is where an infinite bus has been modeled and the second is where synchronous generator model has been used.

A. 1.1: Description Of infinite bus model

This appendix describes the infinite bus model which has been used to represent the main distribution network (11kVand 132kV).

The infinite bus is modelled by a 3-phase AC voltage source, where the source impedance may be specified as ideal. This source can be controlled through either fixed internal parameters or variable external parameters. The external parameters are:

- V: Line-to-Ground, Peak Voltage Magnitude [kV]
- f: Frequency [Hz] [11]

A. 1.2: The main 3-Phase synchronous Generators

Three main synchronous generators (G1, G2 and G3) have similar ratings and which represent the main system providing 38.2MW connected to 132kV bus (bus 100). The Prime Mover is controlled by a V2 Compatible Hydro Governor (HGOV18) and a V2 Compatible Solid State Exciter (SCRX19). Fuller descriptions of the governor and exciters (SCRX19) are available in Appendices D and E. The synchronous generator, governor and exciter models have been used in the frequency control study. The parameters for the models where obtained from [152]:

Table A.1: The main 3-Phase synchronous machines parameters (28MVA) [152].

Rating (MVA)	28	X_d'' (pu)	0.280
V_{LL} (KV)	11	X_d'' (pu)	0.280
I (KA)	2.36	T_{d0}'(s)	6.55
N (RPM)	3000	T_{d0}''(s)	0.039
Ta (s)	0.278	X_q (pu)	0.770
H (s)	3.117	$X_{q''}$ (pu)	0.375
X_d (pu)	1.014	T_{q0}''(s)	0.071
X_d' (pu)	0.314	Xl (pu)	0.054

Appendix-A.2: Load Model

The loads used are represented by a fixed PQ load component model. This component models the load characteristics as a function of voltage magnitude and frequency. The loads real and reactive powers are considered separately defined by equations (C.1) and (C.2)

$$P = P_0\left(\frac{V}{V_0}\right)^{NP}\left(1 + K_{PF}.dF\right) \quad \text{(C.1)}$$

$$Q = Q_0\left(\frac{V}{V_0}\right)^{NQ}\left(1 + K_{QF}.dF\right) \quad \text{(C.2)}$$

Where: P= Equivalent load real power and P0=Rated real power per phase

V=Load voltage and V0=Rated load voltage (RMS, L-G)

NP=dP/dV Voltage index for real power

K_{PF}=dP/dF Frequency index for real power

Q=Load reactive power and Q_0=Rated reactive power (+inductive) per phase.

NQ=dQ/dV Voltage index for reactive power

K_{QF}=dQ/dF Frequency index for reactive power

The values of dQ, dP, dV and dF are in all per-unit quantities.

Appendix B

Modelling of Small Scale Embedded Generators

In this appendix the transient models of the rotating AC machines, static DC sources and prime mover technologies are described.

Appendix B.1: Three -Phase Asynchronous Generator

A complete electromagnetic transient model of a three-phase induction machine has been used which was based on a synchronously rotating reference frame. The type of induction machine that used in this work is the squirrel cage induction machine. The squirrel cage induction machine can be operated in either 'speed control' or 'torque control' modes.. Normally, the machine is started in speed control mode with the input speed(W) set to a rated per-unit speed (say 1.01 pu) and then switched over to torque control after the initial transients of the machine die out (i.e. the machine reaches steady-state). All stator and rotor parameters for the induction generator used in this work are listed in Table B.2 this data was obtained from [11, 48].

Table B.2:3-Phase asynchronous machine parameters [11,48].

Rating (kW)	**VN (V)**	**R_s (pu)**	**X_s (pu)**	**R_r(pu)**	**X_r (pu)**	**X_m (pu)**	**H(s)**	**p**
11	250	0. 05824	0. 05824	0. 0363	0. 078	2	0.2	4

For the machine rated 2MW (1492 HP) the generic values for machine parameters, have been used. Using this method the machine parameters are determined automatically.

Appendix B.2: Three-Phase Synchronous Generator

The full dynamic model of the synchronous generator includes an option to model two damper windings in the q-axis; it can therefore be used as either a round rotor machine or a salient pole machine. The speed of the machine may be controlled directly by inputting a positive value into the W (speed) input of the machine, or a mechanical torque may be applied to the Tm (torque) input. The electrically excited generator is controlled through an automatic voltage regulator (AVR) to control the reactive power with limited excitation current and a governor to control the active power. The impedance and time constants for the synchronous generators used in this work are listed in Table B.3. The data was obtained from Newage Stamford industrial generators data sheets [153].

Table B.3: 3-Phase synchronous machine parameters [153]

Rating (kVA)	28	Rating (kVA)	11	Rating (MVA)	2
V_N (V)	230	V_N (V)	240	V_{L-L} (KV)	11
I_N(A)	24.65	I_N(A)	14.66	I_N(KA)	0.105
N (RPM)	3000	N (RPM)	3000	N (RPM)	3000
Ta (s)	0.0049	Ta (s)	0.0049	Ta (s)	0.0049
H (s)	1 & 1.5	H (s)	1 & 1.5	H (s)	1.5
X_d (pu)	2.637	X_d (pu)	1.651	X_d (pu)	2.637
X_d' (pu)	0.269	X_d' (pu)	0.168	X_d' (pu)	0.3
X_d'' (pu)	0.172	X_d'' (pu)	0.105	X_d'' (pu)	0.172
T_{d0}'(s)	0.338	T_{d0}'(s)	0.25	T_{d0}'(s)	0.338
T_{d0}''(s)	0.0307	T_{d0}''(s)	0.00562	T_{d0}''(s)	0.0307
X_q (pu)	1.335	X_q (pu)	0.82	X_q (pu)	1.335
$X_{q''}$ (pu)	0.301	$X_{q''}$ (pu)	0.189	$X_{q''}$ (pu)	0.301
T_{q0}''(s)	0.041	T_{q0}''(s)	0.041	T_{q0}''(s)	0.041
Xl (pu)	0.054	Xl (pu)	0.066	Xl (pu)	0.054

Appendix-B.3: Three-Phase Permanent Magnet Synchronous Machine

The permanent magnet synchronous machine model contains, in addition to the three stator windings, two additional short-circuited windings which are included to model the effects of electromagnetic damping. The speed of the machine may be controlled directly by inputting a positive value into the W input of the machine. Figure B.1 shows the machine control system. The machine parameters are listed in TableB. 4.

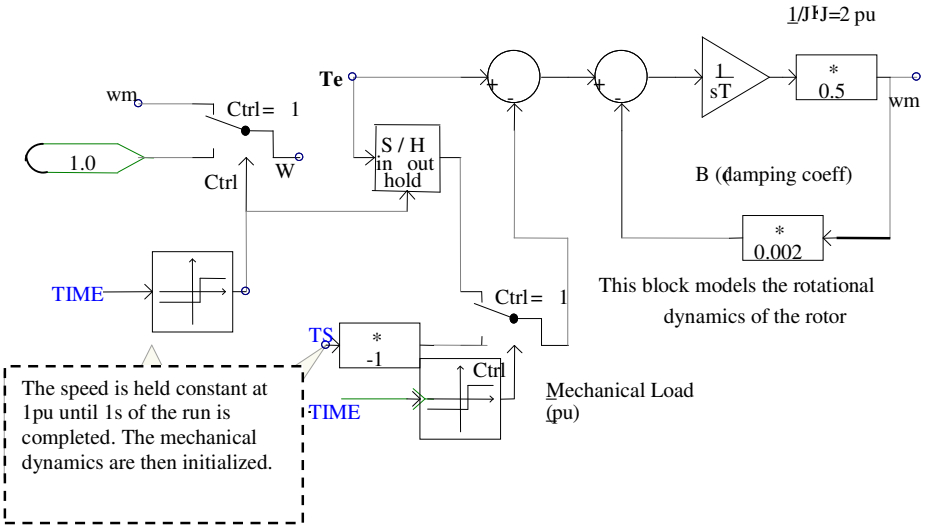

Figure B.1: Permanent magnet synchronous machine control system [11].

TableB. 4: 3-Phase Permanent Magnet Synchronous Machine Parameters [11].

Rated MVA	2
Rated Voltage (L-L) [kV]	11
Rated Frequency[Hz]	50.0
Stator Winding Resistance[pu]	0.017
Stator Leakage Reactance[pu]	0.064
D: Unsaturated Reactance [Xd] [pu]	0.55
Q: Unsaturated Reactance [Xq] [pu]	1.11
D: Damper Winding Resistance [Rkd] [pu]	0.055
D: Damper Winding Reactance [Xkd] [pu]	0.62
Q: Damper Winding Resistance [Rkq] [pu]	0.183
Q: Damper Winding Reactance [Xkq] [pu]	1.175
Magnetic Strength[pu].	1.0

Appendix-B.4: Small Scale Wind Energy Generator Model

The block diagram of the complete wind energy generator model is given in Figure B.2. The model consists of wind governor, wind turbine and induction generator.

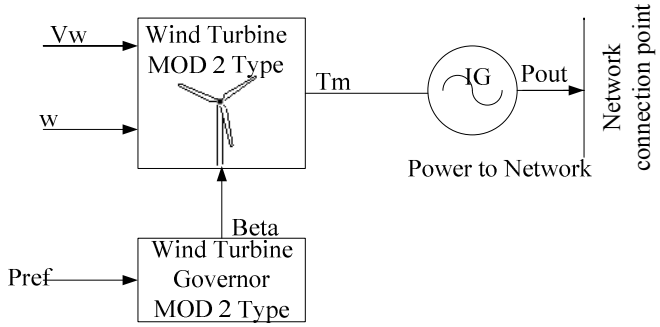

Figure B.2: Wind turbine driven induction generator block diagram [11]

Appendix-B.4.1Wind Governor Transfer Function

The block diagram of the Wind Governor is shown in Figure B.3. The function of the governor is to control the wind turbine by determining an appropriate pitch angle, Beta, depending on the power demand (P_{ref}), this signal is received from the central controller.

Appendix-B.4.2 Wind Turbine

As shown in Figure B.2, the function of wind turbine is to generate output torque; this is dependent on the pitch angle Beta. This output torque, in turn, will be an input of the induction generator. The wind turbine model inputs consist of wind speed, Vw, (which must be a positive value) [m/s] and the mechanical speed of the machine connected to the turbine, w [rad/s]. Beta is the pitch angle of the turbine blades and is measured in degrees [°]. Tm is the output torque in per-unit [pu], and is based on the machines rating. The output torque from wind turbine rotates the induction generator to produce electrical power which is then injected into a low voltage distribution network.

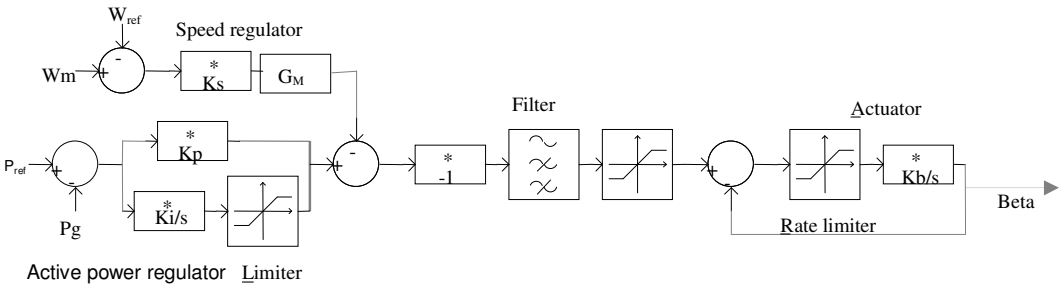

Figure B.3: The block diagram of the wind governor [11].

Where,

W_m =Mechanical speed of the machine [rad/s]
W_{ref}=Reference speed [rad/s]
P_{ref}= Power Demand [MW]
P_g = Power output of the machine based on the machine rating [pu]
K_s=Gain [pu]
K_p=Proportional gain [pu]
K_i=Integral gain [pu]
G_M=Gain multiplier [pu]
K_4=Blade actuator integral gain [s].

Appendix-B.5: MicroCHP (Stirling Engine (SE)) Model

Figure.B.4 shows the simplified model of the microCHP with the induction machine which is used in this study. The power output is compared with a reference value the difference is passed into a PI controller and the output of the PI controller adjusts the mechanical torque of the induction machine.

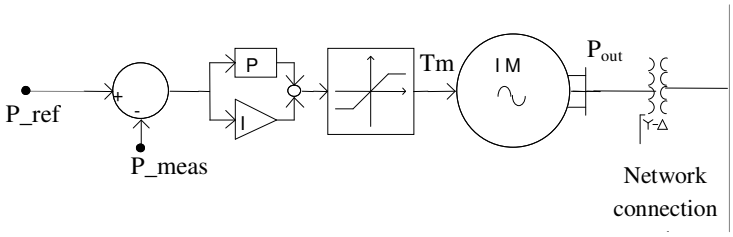

Figure.B.4: Simplified CHP model

Appendix-B.5.1: MicroCHP (Reciprocating Engine) Model

A complete electromagnetic transient model of a three-phase induction machine has been used based on a synchronously rotating reference frame. The block diagram of the complete diesel generator is given in Figure.B.5 and shows the real power loop that controls the output of the induction machine.

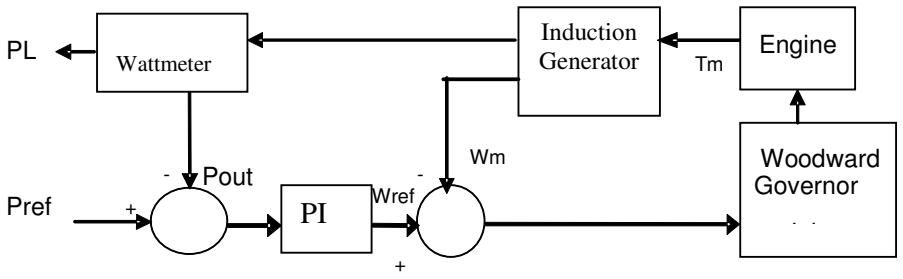

Figure.B.5: Diesel engine driven 3-phase induction generator block diagram

A reciprocating engine has been used for the prime mover and is shown schematically in Figure B.6 .The widely applied Woodward governor model is used to control a diesel engine approximated by a delay, expressed as an s-domain exponential function [143]. Parameters for the model are given in [11,154,155].

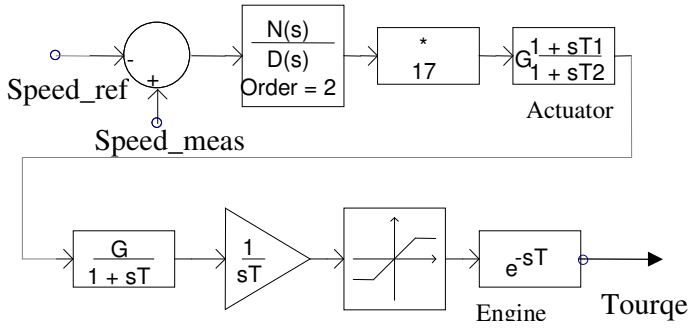

Figure B.6: Reciprocating engine Woodward governor model [11]

Appendix-B.6: 3-Phase Synchronous Generator with Reciprocating Engine Prime Mover

A complete electromagnetic transient model of a three-phase synchronous machine has been used based on a synchronously rotating reference frame. The block diagram of the complete diesel generator is given in Figure B.7; it shows the real and reactive power outer loops that control the output of the machine, these allow operation with a power factor of 0.95 lagging.

A Static Excitation System model of the solid state exciter (SCRX19) is used to provide field control to the generator and is described in Appendix G.

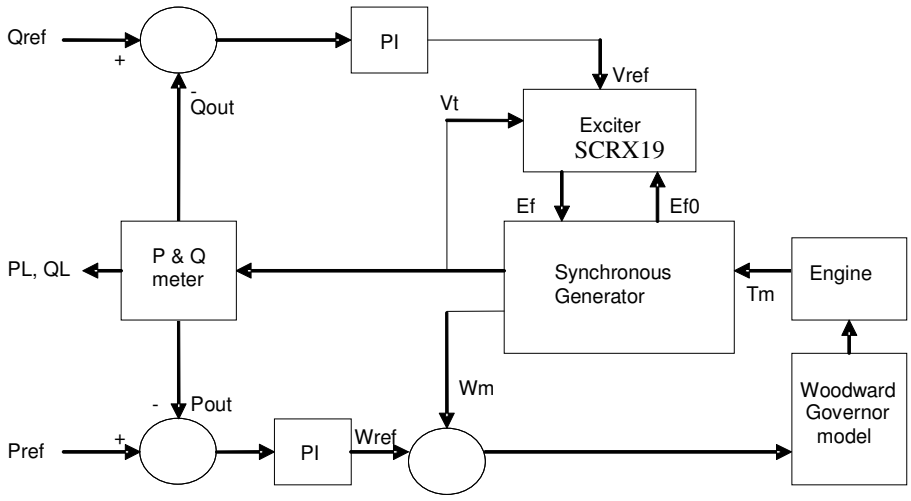

Figure B.7: Diesel engine driven 3-phase synchronous generator block diagram

Appendix-B.7: Single-Phase Inverter Interfaced Photovoltaic (PV) Model

In the transient studies the PV module, the maximum power point tracker and the link capacitor were represented as an ideal voltage sources. A block diagram is given in Figure B.8 and includes the controller, an IGBT bridge, an output filter (2^{nd} order LC) and an isolation transformer.

The control strategy, for the PV module, is shown in Figure B.9 and is intended to allow for operation at a constant power factor. The control system is based on an active power controller and a power factor controller. The function of the active controller is to generate the proper value for power angle of the sinusoidal voltage of the PWM bridge which depends on the active power reference value. The active power reference is set as a constant value based on the aforementioned DC side simplification (in practice this would be derived from the maximum power point tracking unit). To ensure a constant power factor the power factor controller is used to generate the desired value for the output voltage magnitude of the PWM bridge, this is dependent on the power factor reference value.

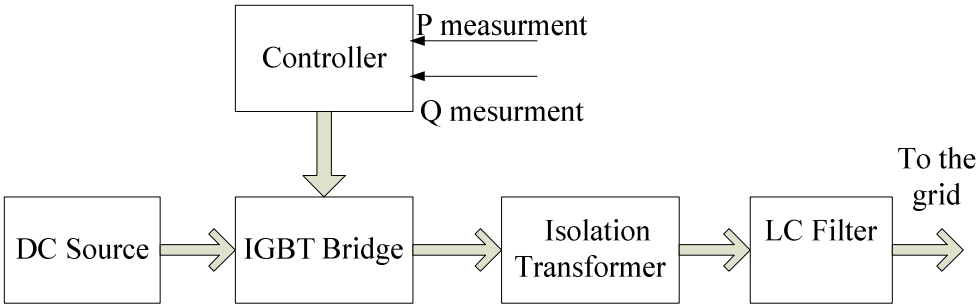

Figure B.8: PV module block diagram [35]

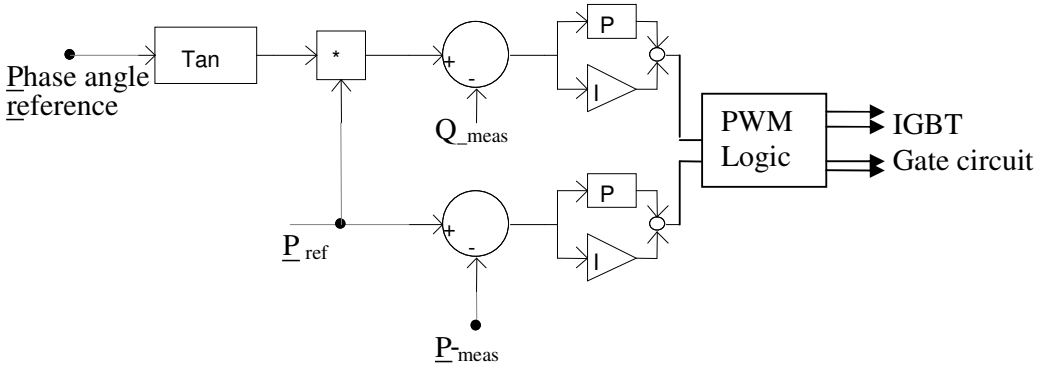

Figure B.9: PV module inverter control

Appendix-B.8: Fuel Cell

In the case of a SSEG is fuel cell there is a portion of the requested power that is provided instantaneously. This portion of power that the unit can instantaneously provide depends on the design of the fuel cell. It takes a longer period of time to reach its thermal equilibrium, which may be about 10 seconds, after this time it is then possible to obtain an increase in power. The fuel cell model is be represented by the model shown in Figure B.10[14].

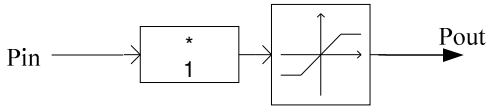

Figure B.10: Fuel cell model without Storage

When a new load comes on-line the fuel cell can maintain the instantaneous power balance without voltage reduction. Storage can take place in different forms, but the most practical is when the DC battery placed in parallel to the existing DC bus terminals of the sources [14].

Appendix C

Power Electronic Converter Model

This appendix mainly presents the main components of SPWM inverter and the operation principle of single-phase and three-phase SPWM inverter, some simulation results have been done to satisfy is the inverter switching model working properly. Also the description of PSCAD ideal voltage source inverter model has been shown.

C.1 Operation Principles of Single Phase Voltage Source Inverter

As an example to explain the operation of voltage source inverter the full-bridge single-phase inverter shown in Figure C.1a was used. Figure.1b shows the complete block diagram of single-phase inverter which was implemented in PSCAD. It consists of SPWM control unit, full-bridge single-phase inverter, and the load. As shown in Fig.1a single phase full-bridge inverter consists of four-power switches device (IGBT) with anti-parallel diodes and a DC source. The principle of the operation of the inverter is to convert DC to AC by turning the power switches ON and OFF at a certain time. Each two transistors should be on at the same time for a half cycle, which can be done by the use of PWM technique. IGBT power transistors have been selected in this work due to its high capabilities of high frequency switching and less loss compared to the thyristor [103].

C.1.1 SPWM Control Unit

The purpose of using PWM (Pulse Width Modulation) controller is to control the switching action of the power switches, therefore the magnitude and phase of the output of the inverter may be controlled. There are several types of PWM such as multiple PWM and sinusoidal PWM. SPWM was implemented in this work due to its ability to reduce the distortion factor and lower the order of harmonic. Referring to the theory of full-bridge single-phase inverter only two switches must be ON at

the same time therefore, generated PWM applied to inverting operation amplifier with gain one. As shown in Figure C.1 transistors 1, 2 conduct together and 3, 4 conduct together.

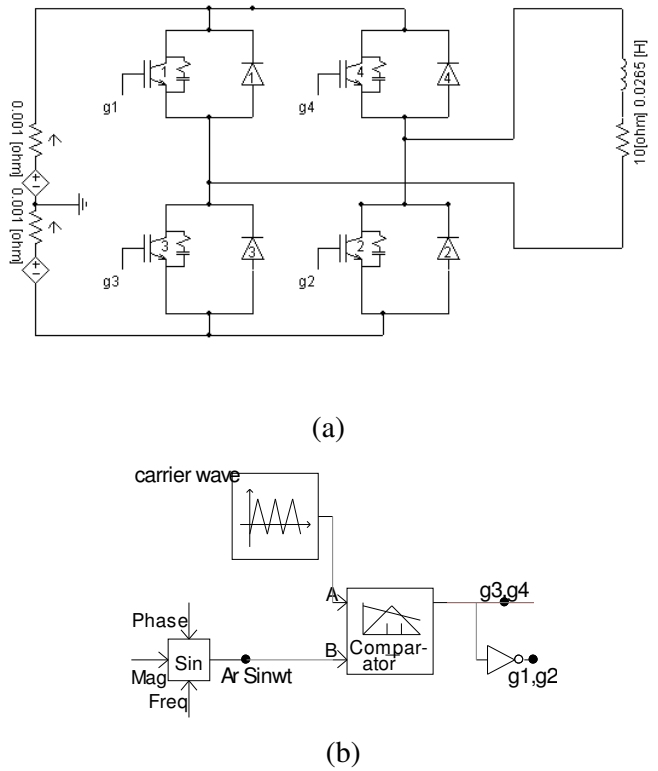

(a)

(b)

Figure C.11: (a) Full-bridge single-phase SPWM inverter and the load. (b)PWM control unit

C.1.1.1 Operation of SPWM

The operation begins from SPWM control unit that provides pulses to perform the switching sequence of the full-bridge inverter. In this operation compare two signals triangle wave and sine wave, the output of the comparator goes to the transistors gate terminal to turn ON and OFF the transistors. Control the output of the inverter by changing the modulation index of the control. The amplitude modulation index, M_a,

is the ratio of the amplitude of the fundamental sine wave, V_1, to the amplitude of the carrier triangle wave, V_C

$$M_a = \frac{V_1}{V_C} \tag{1}$$

The frequency modulation index, M_f is the ratio of the frequency of the carrier triangle wave, f_c, to the frequency of the fundamental sine wave,

$$M_f = \frac{f_c}{f_1} \tag{2}$$

The modulation index, M_a, usually is less than or equal to one, which means that the amplitude of the carrier wave is greater than or equal to the amplitude of the sine wave. As illustrated in Figure.F.2 the modulation is achieved by comparing a sinusoidal reference signal of frequency f_r and amplitude A_r with a triangular carrier wave of frequency f_c and amplitude A_c.The frequency of the reference signal determines the inverter output frequency, f_0, and its peak amplitude A_r ,controls the modulation index, M_a ,and then in turn the RMS output voltage V_0 [103].

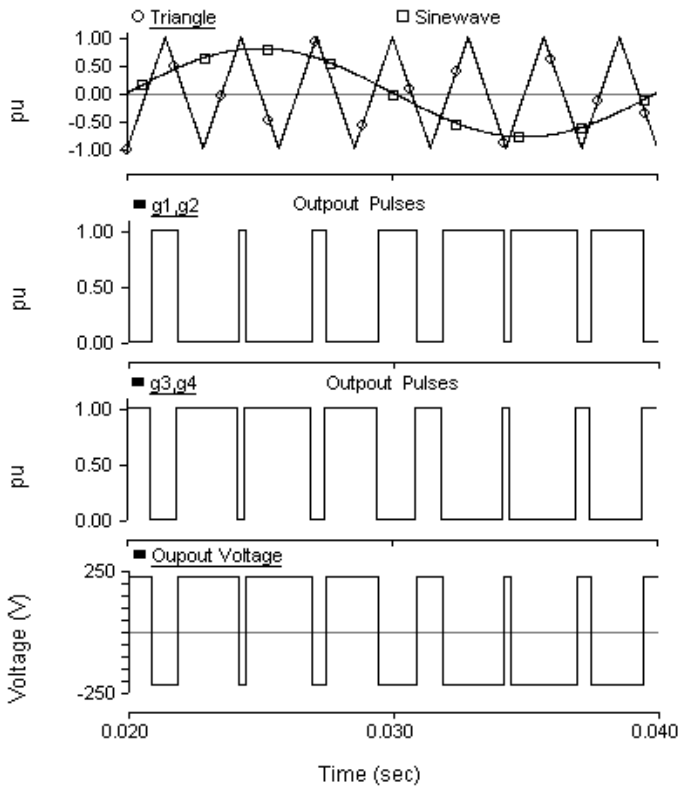

Figure C.12: Sinusoidal pulse-width modulation for single phase inverter

C.2 Operation Principles of Three-Phase Voltage Source Inverter

A three–phase inverter may be considered as three single–phase inverters and the output of each single-phase inverter is shifted by 120º[103]. As shown Figure.C.3 there are three sinusoidal reference waves each shifted by 120º. A carrier wave is compared with the reference signal corresponding to a phase to generate the gating signals for that phase, also the output voltage between phase A and B is shown in Figure C.4.

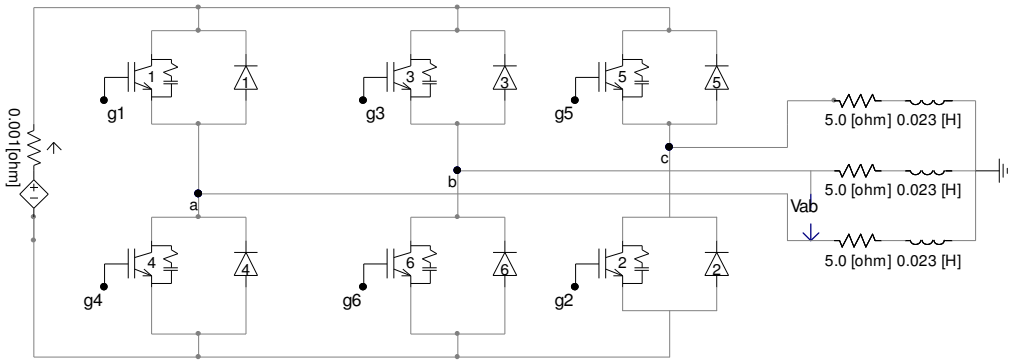

(a)

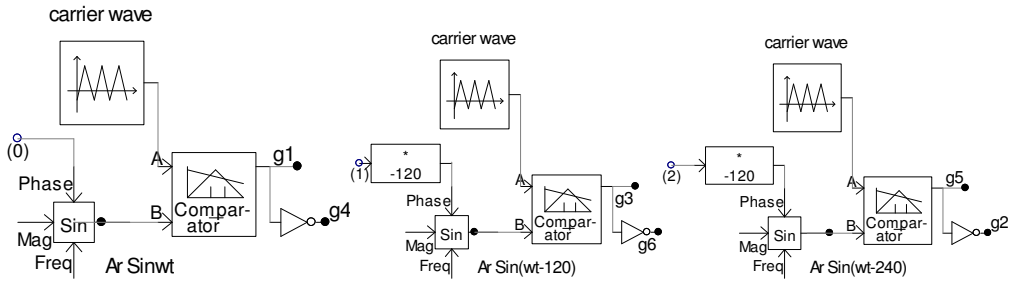

(b)

Figure C.13: (a) Three-phase inverter and the load& (b) Three-phase inverter PWM control units

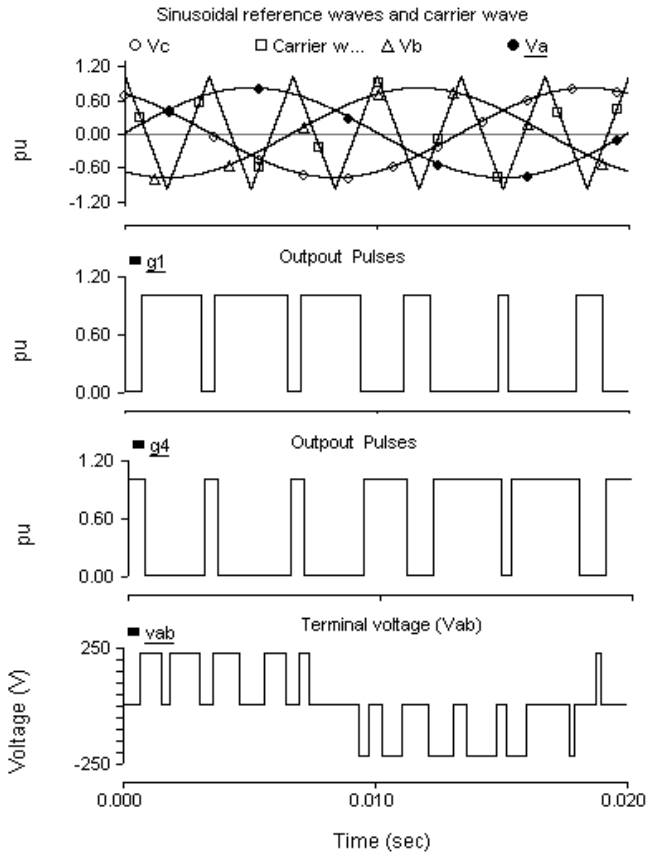

Figure C.14: Sinusoidal pulse-width modulation for three-phase inverter

C.3 Ideal Voltage Source Inverter Model

An ideal model is used to represent the inverter by means of three controlled sinusoidal voltage sources defined as:

$$v_a = \sqrt{2} \cdot V \cdot \sin(\omega t + \delta_v) \tag{3}$$

$$v_b = \sqrt{2} \cdot V \cdot \sin(\omega t + \delta_v - 2\pi/3) \tag{4}$$

$$v_c = \sqrt{2} \cdot V \cdot \sin(\omega t + \delta_v + 2\pi/3) \tag{5}$$

Where the control variables are V and δ. A full representation of the inverter using a switching model was considered not required to observe the performance of the controllers. Also, if a switching model is used the result would be just slower computer simulation.

C.3.1 Description of PSCAD Voltage Source Model

This component models a 3-phase AC voltage source. This source may be controlled through either fixed, internal parameters or variable external signals. The external inputs are described as follows [11]:

- V: Line-to-Line, RMS Voltage Magnitude [kV]
- F: Frequency [Hz]
- Ph: Phase angle [°] or [rad]

Table C.5:3-Phase Inverter parameters

KVA	11
Power factor(leading)	0.95
Switching frequency	2KHz

Table C.6**:**1-Phase Inverter parameters

KVA	3.3
ower factor(leading)	0.95
Switching frequency	2KHz

Appendix D

Description of the Small 33kV Rural Network with A sub-Sea Cable

The basic power system model of the small rural network with a sub-sea cable is shown in Figure D15 [93], has been used in this work. The EHV1 model is a 33kV rural network fed from a 132kV supply point. The network has long lines, including a sub-sea cable between buses 318 and 304, leading to voltage problems at the extremities of the network. The network includes generator (G1) which represents the main 132kV system (system slack bus) connected to 132kV bus (bus 100) and one interconnected generator works as PV bus 4MW connected to the network at bus 336. The following tables describe the buses, the loads, the generators, the branches and the transformers for all system. The system MVA base is the base value for all per unit impedances except for generator impedances.

Table D.7 System Description

Buses	132 kV	1
	33 kV	42
	11 kV	18
	Total	61
Loads	Number of loads	18
	Total P	38.16
	Total Q	7.74
	Average P	2.12
	Average Q	0.43
Generators	Number of generators	2
Branches	Number of branches	43
	Total length	244.62
	Average length	5.688837
	Average CR1	0.192512
	Average CX1	0.185512
	Average Rating CM1	18.72093
Transformers	Number of transformers	23
	Average TR1	0.769596
	Average TX1	6.030139
	Average Rating	7.391304

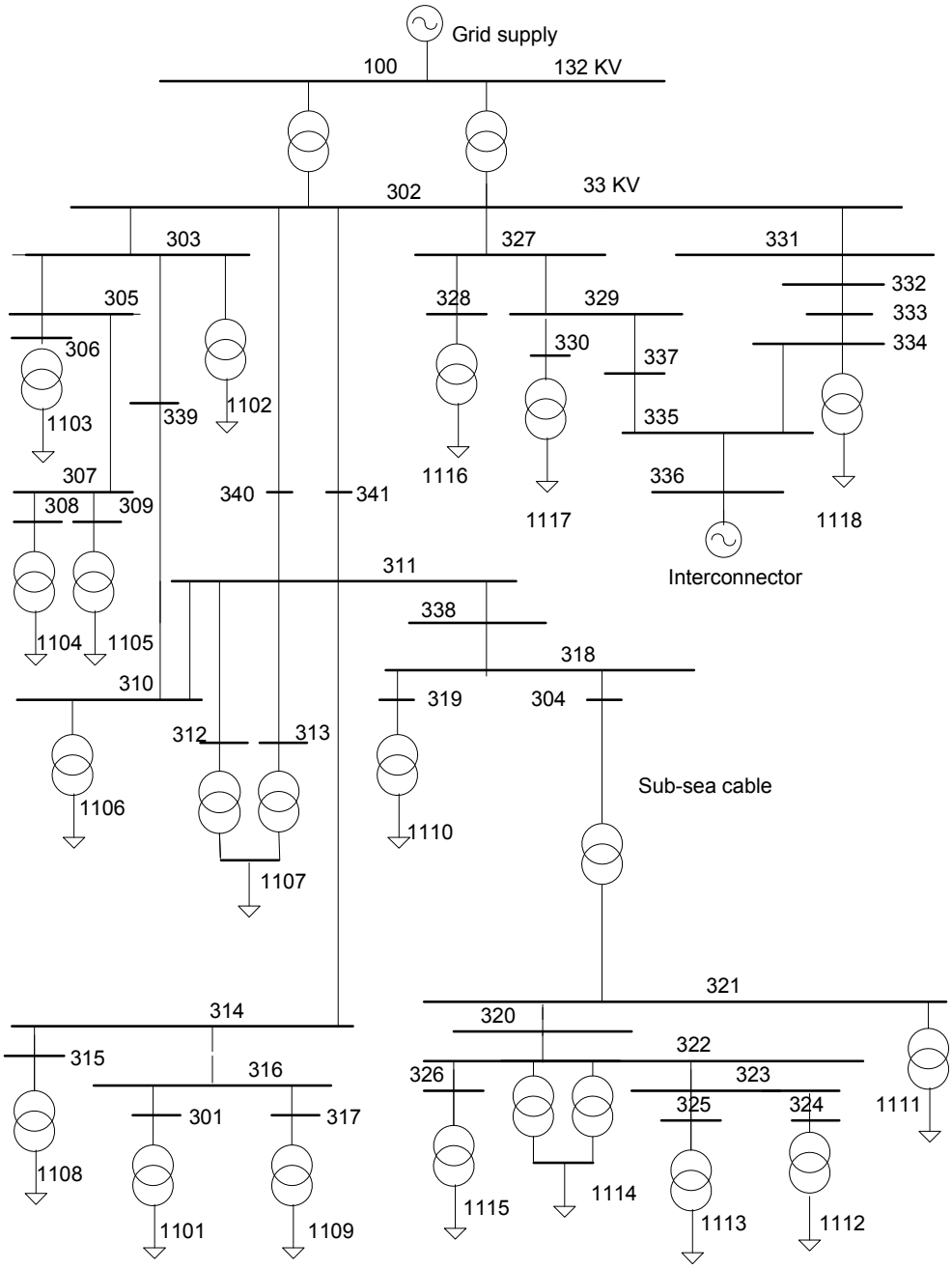

Figure D15: 33kV Network Model [93]

Table D.8 Buses description

Parameter	bus Number	Base Voltage	Bus Type	Target Voltage Magnitude	Minimum Voltage	Maximum Voltage
Values	100	132	Slack	1	0.97	1.03
	301	33	PQ	1	0.97	1.03
	302	33	PQ	1	1.01	1.03
	303	33	PQ	1	0.97	1.03
	304	33	PQ	1	0.97	1.03
	305	33	PQ	1	0.97	1.03
	306	33	PQ	1	0.97	1.03
	307	33	PQ	1	0.97	1.03
	308	33	PQ	1	0.97	1.03
	309	33	PQ	1	0.97	1.03
	310	33	PQ	1	0.97	1.03
	311	33	PQ	1	0.97	1.03
	312	33	PQ	1	0.97	1.03
	313	33	PQ	1	0.97	1.03
	314	33	PQ	1	0.97	1.03
	315	33	PQ	1	0.97	1.03
	316	33	PQ	1	0.97	1.03
	317	33	PQ	1	0.97	1.03
	318	33	PQ	1	0.97	1.03
	319	33	PQ	1	0.97	1.03
	320	33	PQ	1	0.97	1.03
	321	33	PQ	1	0.97	1.03
	322	33	PQ	1	0.97	1.03
	323	33	PQ	1	0.97	1.03
	324	33	PQ	1	0.97	1.03
	325	33	PQ	1	0.97	1.03
	326	33	PQ	1	0.97	1.03
	327	33	PQ	1	0.97	1.03
	328	33	PQ	1	0.97	1.03
	329	33	PQ	1	0.97	1.03
	330	33	PQ	1	0.97	1.03
	331	33	PQ	1	0.97	1.03
	332	33	PQ	1	0.97	1.03
	333	33	PQ	1	0.97	1.03
	334	33	PQ	1	0.97	1.03
	335	33	PQ	1	0.97	1.03
	336	33	PV	1	0.97	1.03
	337	33	PQ	1	0.97	1.03
	338	33	PQ	1	0.97	1.03
	339	33	PQ	1	0.97	1.03
	340	33	PQ	1	0.97	1.03
	341	33	PQ	1	0.97	1.03
	342	33	PQ	1	0.97	1.03

	1101	11	PQ	1	0.97	1.03
	1102	11	PQ	1	0.97	1.03
	1103	11	PQ	1	0.97	1.03
	1104	11	PQ	1	0.97	1.03
	1105	11	PQ	1	0.97	1.03
	1106	11	PQ	1	0.97	1.03
	1107	11	PQ	1	0.97	1.03
	1108	11	PQ	1	0.97	1.03
	1109	11	PQ	1	0.97	1.03
	1110	11	PQ	1	0.97	1.03
	1111	11	PQ	1	0.97	1.03
	1112	11	PQ	1	0.97	1.03
	1113	11	PQ	1	0.97	1.03
	1114	11	PQ	1	0.97	1.03
	1115	11	PQ	1	0.97	1.03
	1116	11	PQ	1	0.97	1.03
	1117	11	PQ	1	0.97	1.03
	1118	11	PQ	1	0.97	1.03

Table D.9 load data

Parameter	**Load Bus Number**	**Real Power** MW	**Reactive Power** MVAr.
Values	1101	1.9	0.39
	1102	1.5	0.3
	1103	0.28	0.06
	1104	0.32	0.06
	1105	3.31	0.67
	1106	1.93	0.39
	1107	18.4	3.74
	1108	1.9	0.39
	1109	0.06	0.01
	1110	0.06	0.01
	1111	0.55	0.11
	1112	0.04	0.01
	1113	0.77	0.15
	1114	2.7	0.55
	1115	2.85	0.58
	1116	0.8	0.16
	1117	0.21	0.04
	1118	0.58	0.12

Table D.10 Generators data

Parameter	Bus .N0	GPO	GPX	GPN	GQA
Values	100	30	60	-60	10
	336	0	15	-15	0
Parameter	Bus .N0	GQX	GQN	GMB	GR1
Values	100	60	-60	100	0
	336	15	-15	100	0

Table D.11 branches parameters

Symbol	From Bus	To Bus	CR1	CX1	CB1	CR0	CX0	CB0	CLE
Values	302	303	0	0.001	0	0.001	0.001	0	0.08
	302	327	0.213	0.284	0	0.64	0.852	0	8.69
	302	331	0.091	0.121	0	0.273	0.364	0	3.71
	302	340	0.227	0.302	0	0.681	0.907	0	9.24
	302	341	0.104	0.199	0	0.311	0.596	0	6.3
	303	305	0.128	0.094	0	0.379	0.28	0	2.75
	303	339	0.1	0.225	0	0.299	0.674	0	6.1
	305	306	0	0.001	0	0.001	0.001	0	1.03
	305	307	0.056	0.041	0	0.168	0.124	0	1.14
	307	308	0.002	0.001	0	0.006	0.004	0	0.04
	307	309	0.507	0.374	0	1.521	1.123	0	10.34
	310	311	0.216	0.287	0	0.648	0.862	0	8.79
	311	312	0.03	0.026	0.002	0.047	0.049	0.002	2.14
	311	313	0.031	0.032	0.001	0.064	0.075	0.001	1.97
	311	314	0.517	0.376	0	1.55	1.126	0	10.53
	311	338	0.079	0.106	0	0.238	0.317	0	3.23
	314	315	0.009	0.007	0	0.027	0.02	0	0.18
	314	316	0.166	0.121	0	0.499	0.363	0	3.39
	316	301	0.228	0.227	0	0.685	0.682	0	6.76
	316	317	0	0.001	0	0.001	0.001	0	0.92
	318	304	0.336	0.27	0.006	0.572	0.584	0.006	12.32
	318	319	0	0.001	0	0.001	0.001	0	0.93
	320	321	0	0.001	0	0.001	0.001	0	0.91
	320	322	0.538	0.733	0	1.613	2.198	0	22.28
	322	323	1.126	0.873	0.001	3.33	2.477	0.001	23.33

	322	326	0.944	0.657	0	2.833	1.971	0	19.05
	323	324	0.045	0.02	0	0.134	0.059	0	0.46
	323	342	0.238	0.173	0	0.715	0.519	0	4.86
	327	328	0.053	0.023	0	0.158	0.069	0	0.54
	327	329	0.094	0.11	0.001	0.247	0.31	0.001	3.69
	329	330	0.039	0.039	0	0.117	0.117	0	1.16
	329	337	0.083	0.083	0	0.249	0.248	0	2.46
	331	332	0.113	0.1	0.002	0.234	0.261	0.002	4.22
	332	333	0.153	0.203	0	0.457	0.609	0	6.21
	334	333	0.149	0.108	0	0.446	0.325	0	3.04
	335	334	0.4	0.291	0	1.2	0.872	0	8.16
	335	336	0.401	0.292	0	1.204	0.875	0	8.19
	337	335	0.088	0.088	0	0.264	0.263	0	2.61
	338	318	0.026	0.016	0.001	0.033	0.025	0.001	0.9
	339	310	0.098	0.221	0	0.294	0.663	0	5.95
	340	311	0.216	0.287	0	0.648	0.862	0	8.79
	341	311	0.208	0.398	0	0.624	1.195	0	12.63
	342	325	0.226	0.164	0	0.677	0.492	0	4.6

GPO= Real Power (MW.)	CX1 =Positive and Negative Sequence
GPX= Maximum Real Power	Reactance
GPN= Minimum Real Power	CB1= Positive and Negative Sequence
GQA= Reactive Power (MVAr)	Susceptance
GQX= Maximum Reactive Power	CR0 =Zero Sequence Resistance
GQN= Minimum Reactive Power	CX0= Zero Sequence Reactance
GMB= Generator MVA Base	CB0 =Zero Sequence Susceptance
CR1=Positive and Negative	GX0 =Zero Sequence Reactance
Sequence Resistance	CLE = The length of the branch in kilometres.

Table D.12 Transformers data

Parameter	TFB	TTB	TID	TR1	TX1	TR0	TX0	TRE	TXE
Values	100	302	1	0	0.25	0	0.25	50	0
	100	302	2	0	0.25	0	0.25	50	0
	301	1101	1	0.3813	2.9777	0	1.9858	0	0
	303	1102	1	0.5172	4.0186	0	2.8895	0	0
	304	321	1	0.0728	0.1039	0	0	0	0
	306	1103	1	1.579	12.1204	0	10.1004	0	0
	308	1104	1	1.579	12.1204	0	10.1004	0	0
	309	1105	1	0.1514	1.6144	0	1.6144	20.0261	0
	310	1106	1	0.0917	1.0553	0	1.0553	20.0261	0
	312	1107	1	0.0343	0.8925	0	0.8925	19.7758	0
	313	1107	1	0.0343	0.8925	0	0.8925	19.7758	0
	315	1108	1	0.3837	2.9969	0	1.9986	0	0
	317	1109	1	2.7139	20.7808	0	17.3173	0	0
	319	1110	1	2.7139	20.7808	0	17.3173	0	0
	321	1111	1	0.7967	6.1753	0	5.1461	0	0
	322	1114	1	0.3837	2.9969	0	1.9986	0	0
	322	1114	2	0.3837	2.9969	0	1.9986	0	0
	324	1112	1	2.7139	20.7808	0	17.3173	0	0
	325	1113	1	0.7431	5.7596	0	4.7997	0	0
	326	1115	1	0.0944	1.0869	0	1.0869	39.7037	0
	328	1116	1	0.7431	5.7596	0	4.7997	0	0
	330	1117	1	0.5795	4.4919	0	3.5703	0	0
	334	1118	1	1.0101	7.7911	0	6.4926	0	0

Parameter	From Bus	To Bus	TIL	TM1	TM2	TM3	TST	TTR	TTX
Values	100	302		30	33	15	1	1	1.05
	100	302		30	33	15	1	1	1.05
	301	1101	0	2.5	2.75	1.25	1	1	1.05
	303	1102	0	2	2.2	1	1	1	1.05
	304	321	0	15	16.5	7.5	1	1	1.05
	306	1103	0	0.5	0.55	0.25	1	1	1.05
	308	1104	0	0.5	0.55	0.25	1	1	1.05
	309	1105	0	5	5.5	2.5	1	1	1.05
	310	1106	0	10	11	5	1	1	1.05
	312	1107	0	25	27.5	12.5	1	1	1.05
	313	1107	0	25	27.5	12.5	1	1	1.05
	315	1108	0	2.5	2.75	1.25	1	1	1.05
	317	1109	0	0.5	0.55	0.25	1	1	1.05
	319	1110	0	0.5	0.55	0.25	1	1	1.05
	321	1111	0	1	1.1	0.5	1	1	1.05
	322	1114	0	2.5	2.75	1.25	1	1	1.05
	322	1114	0	2.5	2.75	1.25	1	1	1.05
	324	1112	0	0.5	0.55	0.25	1	1	1.05
	325	1113	0	1	1.1	0.5	1	1	1.05
	326	1115	0	10	11	5	1	1	1.05
	328	1116	0	1	1.1	0.5	1	1	1.05
	330	1117	0	1.5	1.65	0.75	1	1	1.05
	334	1118	0	1	1.1	0.5	1	1	1.05

Parameter	From Bus	To Bus	TTN	TTP	TWC	TPS	TCB
Values	100	302	0.85	21	DY	-30	302
	100	302	0.85	21	DY	-30	302
	301	1101	0.85	21	DY	-30	1101
	303	1102	0.85	21	DY	-30	1102
	304	321	0.85	21	DD	0	321
	306	1103	0.85	21	DY	-30	1103
	308	1104	0.85	21	DY	-30	1104
	309	1105	0.85	21	DY	-30	1105
	310	1106	0.85	21	DY	-30	1106
	312	1107	0.85	21	DY	-30	1107
	313	1107	0.85	21	DY	-30	1107
	315	1108	0.85	21	DY	-30	1108
	317	1109	0.85	21	DY	-30	1109
	319	1110	0.85	21	DY	-30	1110
	321	1111	0.85	21	DY	-30	1111
	322	1114	0.85	21	DY	-30	1114
	322	1114	0.85	21	DY	-30	1114
	324	1112	0.85	21	DY	-30	1112
	325	1113	0.85	21	DY	-30	1113
	326	1115	0.85	21	DY	-30	1115
	328	1116	0.85	21	DY	-30	1116
	330	1117	0.85	21	DY	-30	1117
	334	1118	0.85	21	DY	-30	1118

Appendix E

Three-Phase PI-Controlled Phase Locked Loop (PLL)

Three-Phase PI-Controlled Phase Locked Loop (PLL) measures the system frequency .The input of the Three-Phase PI-Controlled Phase Locked Loop is three phase voltage. This three phase voltage measurement is converted to three single phase voltages measurements using data signal array tap which extracts a specified range of elements from the data signal array it is connected to. Then Three-Phase PI-Controlled Phase Locked Loop (PLL) generates a ramp signal theta that varies between 0 and 360°, synchronized or locked in phase, to the input voltage Va**.** The ramp is generated by the phase vector technique. This technique exploits trigonometric multiplication identities to form an error signal that speeds up and slows down the phase-locked oscillator, to match the phase of the input. The phase error is passed as an output variable after conversion to degrees. The frequency of the input is computed and returned as an internal output parameter called name for tracked frequency.

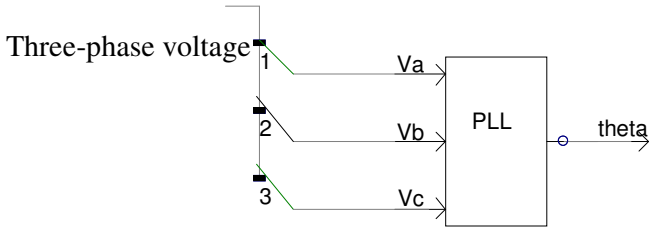

Figure E.16: Three-Phase PI-Controlled Phase Locked Loop (PLL)

Appendix F

Low Pass Filter

The transfer function of the low pass filter is 2nd order as described below:

$$Y(t) = L^{-1}\left[\frac{G.X(t)}{1+2\cdot\zeta\cdot\left(\frac{s}{\omega_c}\right)+\left(\frac{s}{\omega_c}\right)^2}\right] \qquad [11] \qquad (3)$$

Where,

G=Gain

ω_c = Characteristic frequency

ζ=Damping Ratio

s=Laplace operator

L^{-1}=Inverse Laplace transform

Frequencies below the characteristic frequency are referred to as low frequencies.

Appendix G

IEEE Excitation System Model

This exciter is based on an IEEE type SCRX solid state exciter (SCRX19). The output field voltage is varied by a control system to maintain the system voltage at Vref**.**

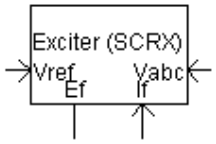

Figure G.17: SCRX solid state exciter

Inputs:

- Vref**:** The reference voltage in per-unit, which the exciter acts to control.
- If**:** The field current received from the machine in per-unit.
- Vabc: Receives input from the Node Loop component.

Outputs:

- Ef**:** This output is the computed field voltage applied directly to synchronous machine.

  The schematic diagram of the transfer function of3-phase IEEE type SCRX solid state exciter is given in Figure G.18

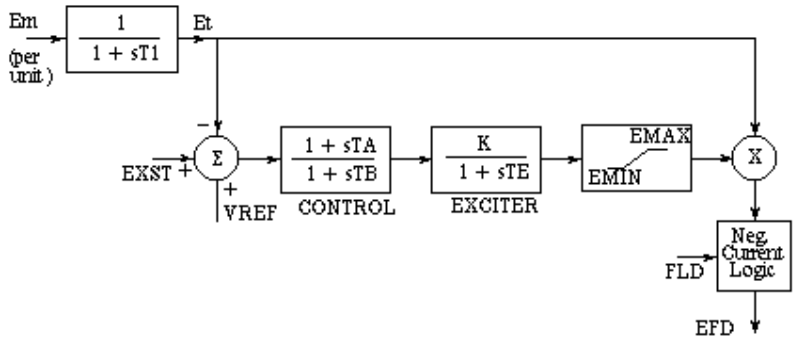

Figure G.18: 3-phase IEEE type SCRX solid state exciter [11,156].

T_1 =Rectifier Smoothing Time Constant[s]

T_A =Controller Lead Time Constant[s]

T_B =Controller Lag Time Constant[s]

T_E =Exciter Time Constant [s]

K= Exciter Gain [pu]

EMAX= Maximum Field Voltage [pu]

EMIN =Minimum Field Voltage [pu]

Appendix H

V2 Compatible Hydro Governor (HGOV18)

This component models an IEEE type 2 hydro governor and turbine has been used in this work is shown in

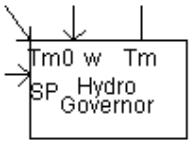

Figure H.19: Hydro Governor (HGOV18)

The schematic diagram of the transfer function of Hydraulic governor is given in Figure H.1.

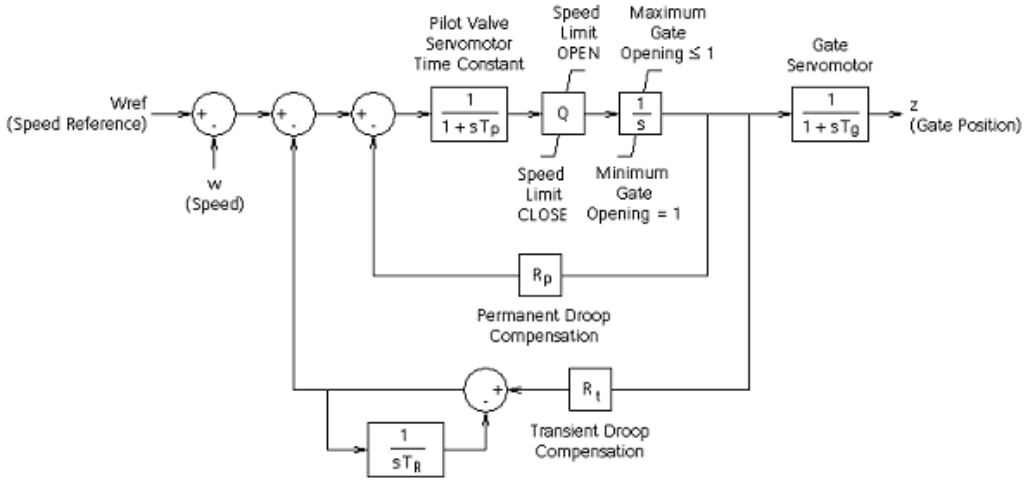

Figure H.20: Transfer function of Hydraulic governor [11]

Inputs :

SP: The reference speed [pu].

Tm0: Mechanical torque from the machine [pu].

w: Machine rotor speed [rad/s].

Outputs:

Tm: Mechanical torque output [pu].

Where

Q= Servo gain [pu]

R_p = Permanent Droop [pu]

R_t=Temporary Droop [pu]

T_g= Main Servo Time Constant [s]

T_p = Pilot valve and servo motor time constant [s]

T_R = Reset or Dashpot Time Constant [s]

Appendix I

Additional Test Results for SSEG Contribution to the Frequency Control

The appendix provides additional test results which have not been presented in chapter 7.

I.1 Results for System with no Participation of SSEG

This section of the appendix provides additional test results for system with no participation of SSEG (base case) which have not been presented in chapter 7.

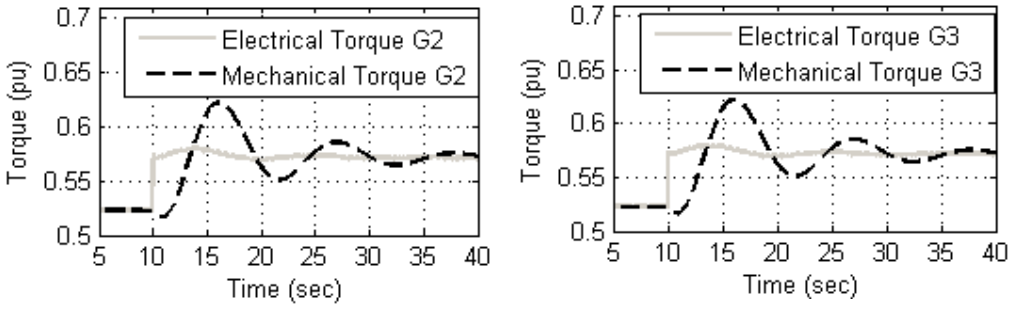

Figure I-21: Torque for main synchronous generator with no SSEG (load increase)

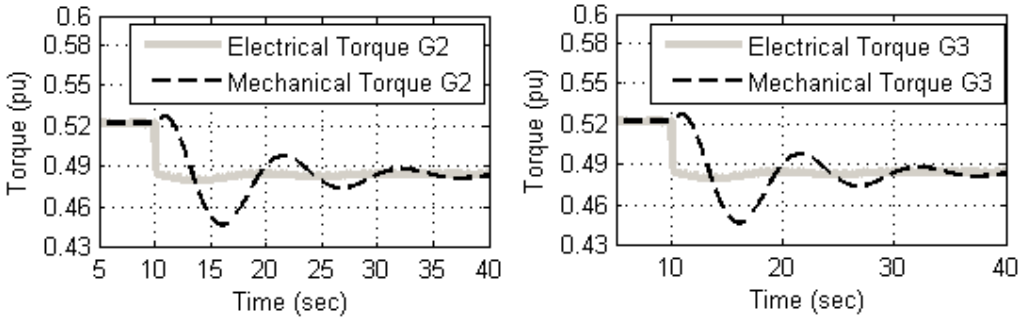

Figure I-22: Torque for main synchronous generator with no SEGG (load decrease)

I.2 System with SSEG with no Load-Frequency Control

This section of the appendix provides additional test results which have not been presented in chapter 7.

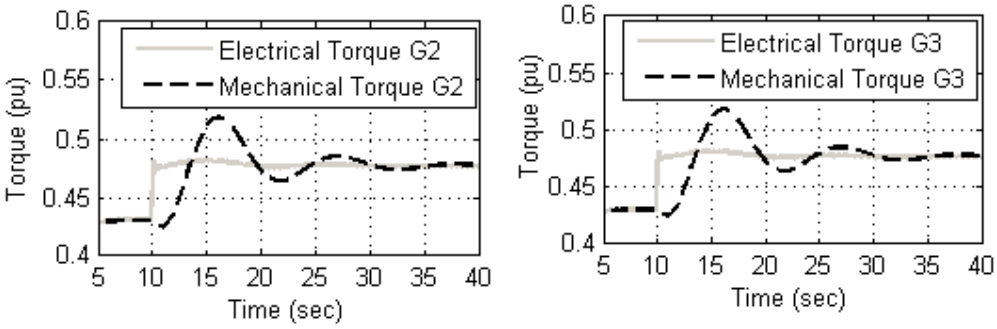

Figure I-23: Torque for main synchronous generators with no LFC (load increase)

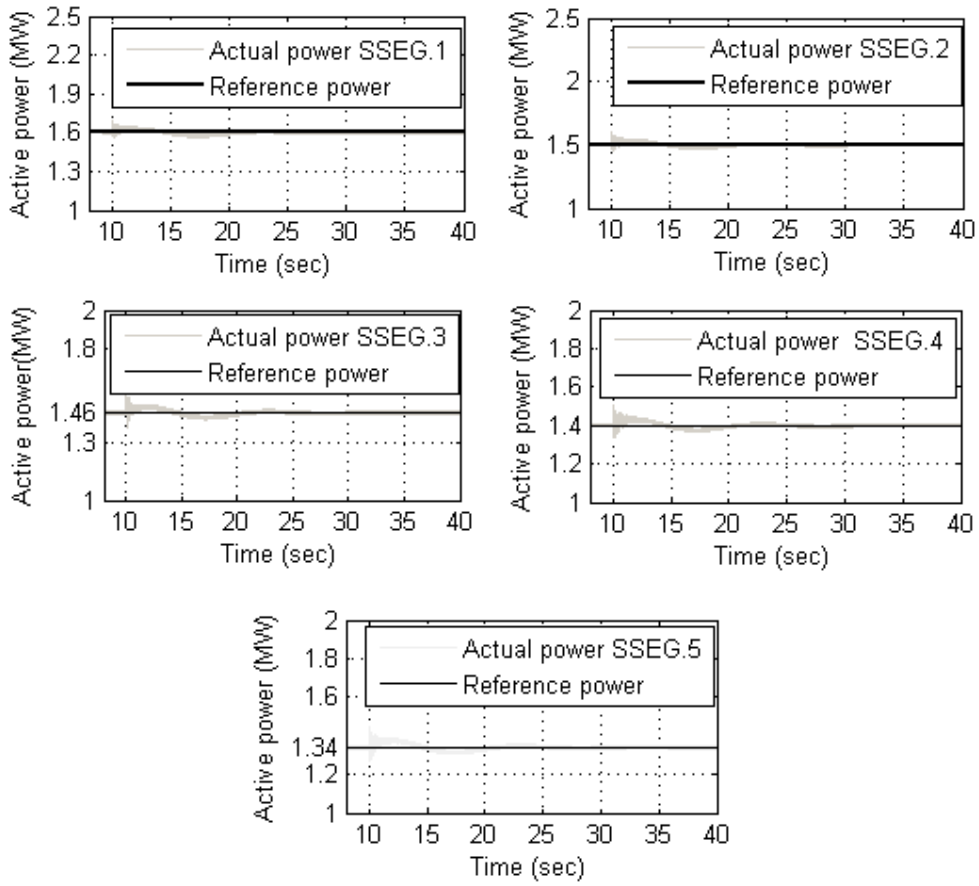

Figure I-24: Active power output from SSEGs with no LFC (load increase).

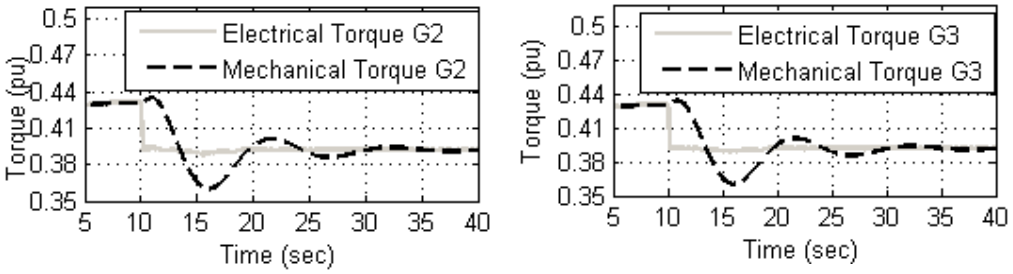

Figure I-25: Torque for main synchronous generators with no LFC (load decrease)

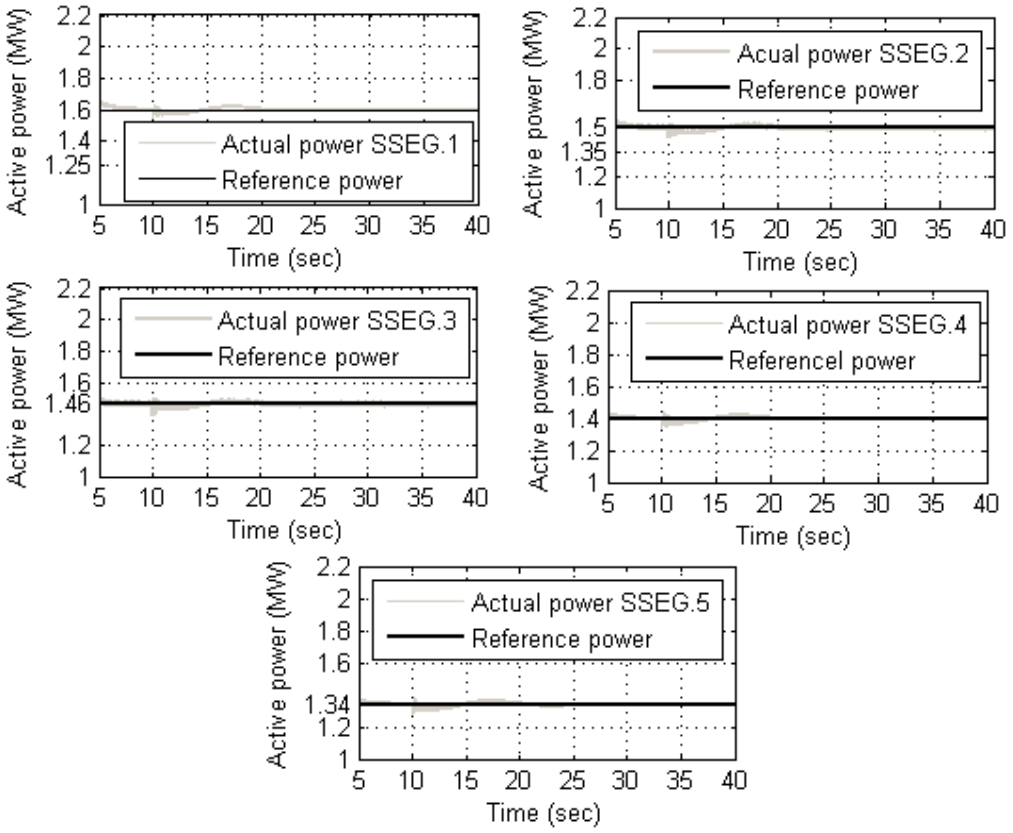

Figure I-26: Active power output from SSEGs with no LFC (load decrease).

I.3 Mixed SSEG Technologies Contribution to the Frequency Control

This appendix provides additional test results which have not been presented in chapter 7.

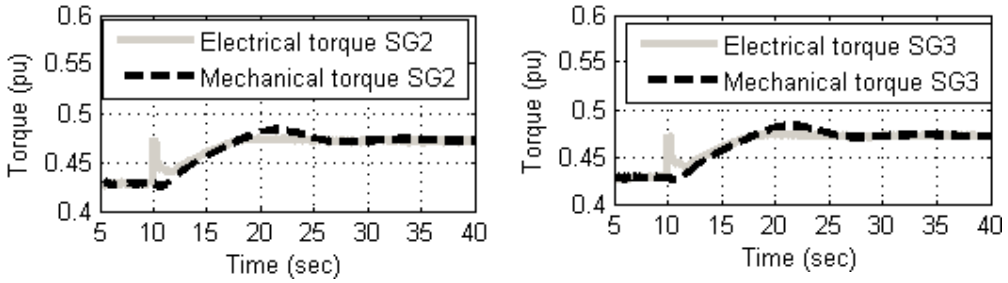

Figure I-27: Torque of main synchronous generators with mixed SSEGs (load increase)

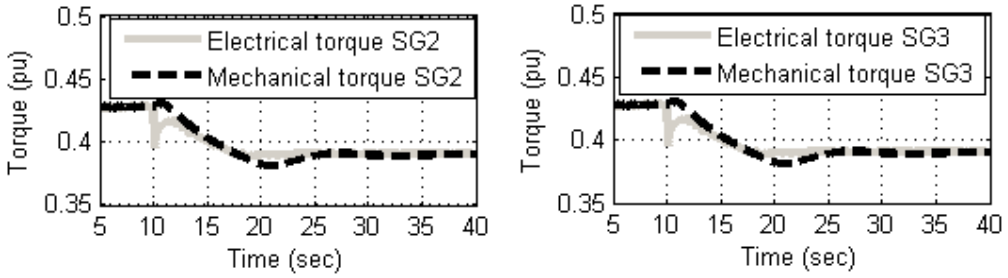

Figure I-28: Torque of main synchronous generators with mixed SSEGs (load decrease)

VITA

Adel Hamad Rafa was born on 17th October 1968 in Benghazi, Libya. He Graduated from Garuonise University in Electrical Engineering, Libya (1991), 1991-1993 worked as Electric Engineering in Tobruk Power Station, 1994-1995 A chef of Electrical Maintenance Department in Tobruk Power Station and joint with Faculty of Engineering Omar Almkutahr University since 1995-2000 as a lecturer assistance. In 2002 He had Master of Science in Electrical power engineering at University Putra Malaysia, Malaysia. From 2003 to 2006 he was a lecturer in Electrical Engineering Department Omar Al-Mukhtar University, Libya,

Mr. Adel Hamad Rafa left to UK in 2006 and Continued PhD degree in Electrical Engineering at University of Strathclyde, Glasgow.